



The
University
Of
Sheffield.

Design and Synthesis of Efficient Polymers for Photovoltaic Applications

Ali S Alkorbi

A Thesis submitted for the Degree of Doctor of Philosophy

Department of Chemistry, University of Sheffield

March 2020

Declaration

I hereby declare that the dissertation entitled “Design and Synthesis of Efficient Polymers for Photovoltaic Applications” is submitted for the degree of doctorate of philosophy (PhD) at the University of Sheffield. It records the research carried out from January 2016 to January 2020. I further declare that all work reported was carried out under the supervision of Dr. Ahmed Iraqi, who also helped with the editing of this dissertation.

All results presented in this dissertation were undertaken myself, unless where referenced.

Signed:.....

Acknowledgments

I would like to express my appreciation to my supervisor Dr Ahmed Iraqi, for his guidance and help whilst I was under his supervision during my PhD studies. His patience, encouragement and generous help with research time in the laboratory and the writing up of my thesis have been invaluable and much appreciated. In addition, I would like to thank all the staff in the Department of Chemistry and the Iraqi group for their support and for creating such a friendly environment to work in.

My special thanks go to Najran University for sponsoring me and giving me this golden opportunity in my life. I would also like to thank the Saudi Arabian cultural bureau in London for their financial support.

Finally, I would like to thank my father, mother, wife, children and all of my family for helping me and supporting me during this period.

Abstract

Harvesting energy directly from sunlight is an environmentally friendly method of converting energy from one type to another. Indeed, inorganic solar cells have been commonly used over the last few decades and are now evidencing good power conversion efficiencies, but the cost of this type of solar cells is high. The cheaper alternative to inorganic solar cells is organic conjugated polymers. These are basic materials which take advantage of the single-double bond alternation along the polymer's backbone. Electronic transitions occur within the electronic levels of the different species of the conjugated polymers, especially between the HOMO (highest occupied molecular orbital) and the LUMO (lowest unoccupied molecular orbital). These transitions represent the basic work of the conjugated polymer-based solar cells.

In this project, we present our work on the preparation of furan based donor-acceptor (D-A) conjugated polymers based on benzothiadiazole (BTD) with alkoxy substitution as an acceptor with donor moieties of fluorene and carbazole using Suzuki cross coupling reaction polymerisation. In addition, conjugated polymers based on benzothiadiazole (BTD) with fluorine atoms substituents as an acceptor with donor moieties of fluorene and carbazole were copolymerised *via* direct hetero arylation (DHA). Also in this project, we synthesised acceptor-donor-acceptor (A-D-A) conjugated polymers based on (IDIC-C16) as an acceptor with donor units of benzothiadiazole flanked by thiophenes, bithiophene and fullerene through the Stille cross coupling reaction. Impressively, the results from UV-visible and cyclic voltammetry both achieved low bandgap polymers regardless of the type of donor units used in the conjugated polymers synthesised.

Chapter 2 in this thesis presents work synthesising three novel conjugated polymers **P1**, **P2** and **P3** based on 4, 7- bis (5-bromofuran-2-yl)-5, 6-bis (octyloxy)benzo[c][1,2,5] thiadiazole (as an acceptor) with fluorene, fluorene flanked by furan, and carbazole respectively. The optical studies presented bandgaps of **P1** and **P3** which were slightly above 2.01 eV and 2.04 eV. **P2** had a lower bandgap than those of **P1** and **P3** (1.93 eV), which was attributed to the extra furan in the backbone of the polymer.

In chapter 3, two novel polymers were synthesised and characterised (**P4** and **P5**) based on benzothiadiazole with fluorine atoms at the 5,6-positions flanked by furan as an acceptor, with fluorene and carbazole as donors respectively. The optical properties displayed

bandgaps of 1.91 and 1.92 eV for **P4** and **P5** respectively. The electrochemical bandgaps were slightly higher due to barriers to oxidation and reduction between polymer films and electrodes.

In the last chapter, three novel polymers (A-D-A) were prepared and characterised (**P6**, **P7** and **P8**) based on (IDIC-C16) as an acceptor with donor units such as benzothiadiazole flanked by thiophenes, bithiophene and fluorene through the Stille cross coupling reaction. The optical properties showed bandgaps of 1.55, 1.54 and 1.65 eV for **P6**, **P7** and **P8** respectively. The electrochemical bandgaps were higher at 1.58, 1.78 and 1.82 eV for **P6**, **P8** and **P8** respectively.

All polymers were characterised by Proton Nuclear Magnetic Resonance (^1H NMR) and Gel Permeation Chromatography (GPC). The results showed each polymer had a different molecular weight depending on factors such as the chemical structure of the repeat moiety, the solubility in organic solvents, and the fraction in which the polymer was collected using the Soxhlet extraction method. In addition, UV-visible absorption spectroscopy, Cyclic Voltammetry (CV), Thermal Gravimetric Analysis (TGA) and powder X-Ray diffraction were also used to analyse the properties of the polymers. The optical bandgaps were in the range of 1.54 eV to 2.07 eV. Thermal Gravimetric Analysis revealed that all the polymers possessed excellent thermal stability. Finally, powder X-Ray diffraction showed that all polymers were, in general, amorphous.

Table of Contents

Chapter 1 - Introduction.....	1
1.1 Resolving energy demand issues.....	1
1.2 Solar power	1
1.3 Conjugated polymers.....	2
1.4 The semiconducting properties of conjugated polymers.....	2
1.5 Conduction process	4
1.6 Conductivity in conjugated polymers	5
1.7 Engineering of the band gap.....	7
1.8 Polymerisation methods of conjugated polymers	11
1.8.1 Metal-catalysed cross-coupling polymerisation routes.....	11
1.8.1.1 Suzuki cross-coupling reaction	11
1.8.1.2 Stille cross-coupling	12
1.8.1.3 Direct (Hetero) arylation DHA.	13
1.9 Conjugated polymer solubility	14
1.10 Applications of conjugated polymers	15
1.10.1 Polymer Light-Emitting Diodes (PLEDs)	15
1.10.2 Organic Field-Effect Transistors (OFETs)	17
1.10.3 Organic solar cells (OSCs).....	18
1.11 Architecture of polymer solar cells	19
1.11.1 Single layer device	19
1.11.2 Bilayer devices.....	20
1.11.3 Bulk heterojunction devices.....	21
1.12 Principle of operation of photovoltaic cells.....	22
1.13 Conjugated polymers as donors with fullerenes as acceptors	23
1.14 Conjugated polymers as donors with non-fullerenes as acceptors	24

1.15	Characteristics of organic solar cell devices.....	25
1.15.1	Open circuit voltage (Voc).....	26
1.15.2	Short current circuit (Jsc).....	26
1.15.3	Fill factor (FF).....	26
1.16	Perovskite solar cell as a competing technology to bulk heterojunction solar cells 27	
1.17	Aims of the thesis	28
1.18	References	31
Chapter 2 - Design and synthesis of furan-based polymers for photovoltaic applications...45		
2.1	Introduction	45
2.2	Results and discussion.....	48
2.2.1	Synthesis of monomers	48
2.2.2	Synthesis of polymers	59
2.2.3	Analysis of polymer properties	61
2.2.3.1	Gel permeation chromatography (GPC) analysis.....	61
2.2.3.2	Optical properties of the polymers	62
2.2.3.3	Electrochemical properties of the polymers	64
2.2.3.4	Thermal gravimetric analysis (TGA) studies	67
2.2.3.5	Polymers' X-ray diffraction (XRD) studies	67
2.3	Conclusion.....	68
2.4	References	70
Chapter 3 - Design and synthesis of furan-based polymers with alternating fluorinated benzothiadiazole units for photovoltaic applications.....75		
3.1	Introduction	75
3.2	Results and discussion.....	77
3.2.1	Synthesis of monomers	77
3.2.2	Synthesis of polymers	79
3.2.3	Analysis of polymers' properties	80
3.2.3.1	Optical properties of the polymers	81

3.2.3.2	Electrochemical properties of the polymers.....	84
3.2.3.3	Thermal Gravimetric Analysis (TGA).....	86
3.2.3.4	Powder X-ray diffraction (XRD) analysis	87
3.3	Conclusion.....	87
3.4	References	90
Chapter 4 - Design and synthesis of A-D_A polymers with narrow bandgaps for photovoltaic applications.		
		94
4.1	Introduction	94
4.2	Results and discussion.....	96
4.2.1	Synthesis of monomers	96
4.2.2	Synthesis of polymers	106
4.2.3	Analysis of polymers' properties	107
4.2.3.1	GPC analysis	107
4.2.3.2	Optical properties of the polymers	108
4.2.3.3	Electrochemical properties of the polymers.....	111
4.2.3.4	Thermal Gravimetric Analysis (TGA).....	113
4.2.3.5	Polymers' XRD	114
4.3	Conclusion.....	115
4.4	References	117
Chapter 5 - Conclusions and future works.....		
		121
5.1	Conclusions	121
5.2	Future work	124
Chapter 6 - Experimental.....		
		128
6.1	Materials.....	128
6.2	Synthesis of monomers and polymers for chapter 2	129
6.2.1	1, 2-Bis (octyloxy) benzene (2) ¹	129
6.2.2	1,2-Dinitro-4,5-bis(octyloxy)benzene (3) ²	130
6.2.3	4,5-Bis(octyloxy)benzene-1,2-diammonium chloride (4) ³	130
6.2.4	5,6-Bis(octyloxy)benzo[c][1,2,5] thiadiazole (5) ⁴	131

6.2.5	4,7-Dibromo-5,6-bis(octyloxy)benzo[c][1,2,5]thiadiazole (6) ⁴	132
6.2.6	Tributyl(furan-2-yl)stannane (7) ⁵	132
6.2.7	5,6 Bis(octyloxy)-4,7-di(furan-2-yl)benzo [c][1,2,5]thiadiazole. (8) ⁶	133
6.2.8	4, 7- Bis (5-bromofuran-2-yl)-5, 6-bis (octyloxy)benzo[c][1,2,5] thiadiazole. (M1) ⁶	134
6.2.9	2,7-Bis(furan-2-yl)-9,9-dioctyl-9 <i>H</i> -fluorene (M2) ⁷	135
6.2.10	Poly[9,9-dioctyl-9 <i>H</i> -fluorene-2,7-diyl- <i>alt</i> -(5,6-bis(octyloxy)-4,7-di-2-furanyl- 2,1,3-benzothiadiazole)-5,5-diyl] (P1).....	135
6.2.11	Poly[9,9-dioctyl-9 <i>H</i> -fluorene-2,7-diyl- <i>alt</i> -(5,6-bis(octyloxy)-4,7-di(2,2'- bifuran-5-yl)benzo[c][1,2,5] thiadiazole)-5,5-diyl] (P2)	137
6.2.12	Poly[9-(heptadecan-9-yl)-9 <i>H</i> -carbazole-2,7-diyl- <i>alt</i> -(5,6-bis(octyloxy)-4,7-di- 2-furanyl-2,1,3-benzothiadiazole)-5,5-diyl] (P3)	138
6.3	Synthesis of monomers and polymers for chapter 3	139
6.3.1	5,6-Difluoro-4,7-diiodobenzo[c][1,2,5]thiadiazole (9). ⁸	139
6.3.2	5,6-Difluoro-4,7-di(furan-2-yl)benzo[c][1, 2, 5] thiadiazole(M4) ⁹	140
6.3.3	Poly[9,9-dioctyl-9 <i>H</i> -fluorene-2,7-diyl- <i>alt</i> -(5,6-difluoro-4,7-di-2-furanyl-2,1,3- benzothiadiazole)-5,5-diyl] (P4)	140
6.3.4	Poly[9-(heptadecan-9-yl)-9 <i>H</i> -carbazole-2,7-diyl- <i>alt</i> -(5,6-difluoro-4,7-di-2- furanyl-2,1,3-benzothiadiazole)-5,5-diyl] (P5).....	141
6.4	Synthesis of monomers and polymers for chapter 4	142
6.4.1	2,5- Dithien-2-yl terephthalic acid diethyl ester (10) ¹⁰	142
6.4.2	2,5-Di(thien-2-yl)terephthalic acid (11) ¹¹	143
6.4.3	4, 9-Dihydro-s-indaceno [1, 2-b: 5, 6-b']-dithiophene-4, 9-dione (12) ¹²	143
6.4.4	4,9-Dihydro-s-indaceno[1,2-b:5,6-b']-dithiophene (13) ¹³	144
6.4.5	4,9-Dihydro-4,4,9,9-tetrahexadecyl-s-indaceno[1,2-b:5,6-b']-dithiophene (14) ¹¹ 145	
6.4.6	4,4,9,9-Tetrahexadecyl-4,9-dihydro-s-indaceno[1,2-b:5,6-b'] dithiophene-2,7- dicarbaldehyde (15) ¹⁴	145
6.4.7	5-Bromo-1,3-indanedione (16) ¹⁵	146

6.4.8	2-(6-Bromo-2,3-dihydro-3-oxo-1-inden-1-ylidene)-propanedinitrile (17) ¹⁶ ...	147
6.4.9	2-Bis[(6-bromo-2,3-dihydro-3-oxo-1-inden-1-ylidene)-propanedinitrile]- 4,4,9,9-tetrahexadecyl-4,9-dihydro-s-indaceno[1,2-b:5,6-b'] dithiophene-2,7-diethylene. IDIC-C16-Br (M5) ¹⁷	147
6.4.10	4,7-Dibromobenzo[c][1,2,5]thiadiazol (18) ¹⁸	148
6.4.11	4,7-Di (thiophene-2-yl)benzo[c] thiadiazole (19) ¹⁹	149
6.4.12	4,7-bis(5-(trimethylstannyl)thien-2-yl)benzo[c][1,2,5] thiadiazole (M6) ²⁰	149
6.4.13	5,5' –Bis (trimethyl stannyl)-2,2' – bithiophene.(M7) ⁵	150
6.4.14	2,7-Bis(trimethyltin)-9,9-dioctylfluorene (M8) ⁵	151
6.4.15	Polymer 6 (P6)	152
6.4.16	Polymer 7 (P7)	153
6.4.17	Polymer 8 (P8)	154
6.5	References	155

Table of figures

Figure 1.1: Molecular structures of some common conjugated polymers.....	2
Figure 1.2: Bandgap forming during polymerisation method of π -conjugated polymers.....	3
Figure 1.3: Diagram illustration of the three types of materials according to their bandgaps.....	4
Figure 1.4: Possible neutral, polaron and bipolaron thiophene trimer transitions.....	5
Figure 1.5: Two degenerate cases of trans-polyacetylene.....	5
Figure 1.6: Diagram showing the addition of electrons to the conduction band (n-type doping) and removal of electrons from the valence band (p-type doping).....	6
Figure 1.7: Aromatic and quinoid resonance forms of some polymers. The diameter of the blue and red circles signify the proportional contribution of the mesomeric structures.....	8
Figure 1.8: The chemical structure of poly(thieno[3,4-b] pyrazine) P1 and poly(thieno[3,4-b]thiophene) P2	9
Figure 1.9: Illustration of the interaction of orbitals for donor and acceptor units important to a reduced band gap in a D-A conjugated polymer.....	10
Figure 1.10: Structures of monomers using the Suzuki cross-coupling reaction.....	11
Figure 1.11: Soluble conjugated polymers in common organic solvents.....	15
Figure 1.12: Basic structural diagram of a PLED.....	16
Figure 1.13: The simple structure of OFET.....	18
Figure 1.14: Sunlight spectrum.....	19
Figure 1.15: Structural diagram of a single layer device polymer solar cell.....	20
Figure 1.16: Structural diagram of the bilayer device polymer solar cell.....	21

Figure 1.17: Structural diagram of the bulk heterojunction device polymer solar cell.....	22
Figure 1.18: Schematic illustration of the working principle of photovoltaic cells.....	22
Figure 1.19: Fullerene derivatives used in the manufacture of OPV devices.....	23
Figure 1.20: Molecular structure of (PM6) and (Y6).....	25
Figure 1.21: Curve of current-voltage <i>J-V</i> characteristics in dark and illuminated environments.....	26
Figure 1.22: Polymer structure of P1 , P2 , P3 , P4 and P5	29
Figure 1.23: Polymer structure of PZ1 , P6 , P7 and P8	30
Figure 2.1: The structures of PFDTBT-8 , PFDT2BT-8 and PCDTBT-8	47
Figure 2.2. ¹ H-NMR spectrum of compound (M1) in CDCl ₃	56
Figure 2.3. ¹ H-NMR spectrum of compound (M2) in CDCl ₃	59
Figure 2.4: The UV-visible wavelengths of P1 , P2 and P3 (a) in chloroform solutions and (b) in thin films.....	64
Figure 2.5: Cyclic voltammetry curves for P1 , P2 and P3	66
Figure 2.6: TGA curves for P1 , P2 and P3	67
Figure 2.7: Powder X-Ray diffraction curves for P1 , P2 and P3	68
Figure 3.1: The structure of PFO-DFFBT and PCDTBT-F	77
Figure 3.2. ¹ H-NMR spectrum of compound (M4) in CDCl ₃	79
Figure 3.3: The UV-visible wavelengths of P4 and P5 (a) in chloroform solutions (b) in thin films.....	83
Figure 3.4: Cyclic voltammetry curves for P4 and P5	85
Figure 3.5: TGA curves for P4 and P5	86
Figure 3.6: Powder X-Ray diffraction curves for P4 and P5	87

Figure 4.1: The structures of IDIC-C16 , IDIC-Br , PZ1 and IC , ICBr	95
Figure 4.2. ¹ H-NMR spectrum of compound (M5) in CDCl ₃	104
Figure 4.3: The UV-visible wavelengths of P6 , P7 and P8 (a) in chloroform solutions (b) in thin films.....	110
Figure 4.4: Cyclic voltammetry curves for P6 , P7 and P8	113
Figure 4.5: TGA curves for P6 , P7 and P8	114
Figure 4.6: Powder X-Ray diffraction curves for P6 , P7 and P8	115
Figure 5.1: Chemical structure of suggested conjugated polymers.....	125
Figure 5.2: Chemical structure of suggested conjugated polymers.....	125
Figure 5.3: Chemical structure of suggested conjugated polymers.....	126
Figure 6.1: Commercially purchased materials.....	128
Figure 6.2: Materials synthesised by Iraqi group.....	129

Table of schemes

Scheme 1.1: The suggested catalytic cycle for Suzuki coupling.....	12
Scheme 1.2: Process diagram of Stille cross-coupling reaction.....	13
Scheme 1.3: Process diagram of direct arylation cross-coupling reaction.....	14
Scheme 2.1: Synthesis of M1 acceptor.....	48
Scheme 2.2: Synthesis of 1,2-bis(octyloxy)benzene.....	49
Scheme 2.3: The mechanism of alkylation reaction <i>via</i> nucleophilic substitution.....	50
Scheme 2.4: Mechanism of the nitration reaction.....	51
Scheme 2.5: The mechanism of ring closure reaction of synthesis (5)	53
Scheme 2.6: The mechanism of bromination of 5 to synthesis (6)	54
Scheme 2.7: The mechanism of synthesis of (7)	55
Scheme 2.8: The Stille coupling cycle to synthesise (8)	55
Scheme 2.9: The mechanism of synthesis of (M1)	57
Scheme 2.10: Synthesis of M2 donor.....	58
Scheme 2.11: Synthetic routes to P1 , P2 and P3	60
Scheme 3.1: Synthesis of M4 acceptor.....	77
Scheme 3.2: Methods of synthesis of P4 and P5	80
Scheme 4.1: Synthesis of M5	97
Scheme 4.2: Synthesis of M6 , M7 and M8	97
Scheme 4.3: Mechanism for the hydrolysis of ester for compound (11)	99
Scheme 4.4: The mechanism of reduction reaction of compound (12) to afford (13)	101

Scheme 4.5: The mechanism of alkylation reaction <i>via</i> nucleophilic substitution to afford compound (14).....	102
Scheme 4.6: The suggested mechanism of synthesis of compound (15).....	103
Scheme 4.7: The mechanism of synthesis of (M6).....	105
Scheme 4.8: Synthetic routes to P6 , P7 and P8	107

Table of tables

Table 2.1: GPC data for P1 , P2 , P3 and their analogous polymers.....	61
Table 2.2: The UV-visible data of P1 , P2 , P3 and their analogous polymers.....	62
Table 2.3: The HOMO and LUMO data of P1 , P2 , P3 and their analogous polymers....	66
Table 3.1: GPC data for P4 , P5 , PFO-DFFBT and PCDTBT-F	81
Table 3.2: The UV-visible data of P4 , P5 , PFO-DFFBT and PCDTBT-F	82
Table 3.3: Cyclic voltammetry for P4 , P5 , PFO-DFFBT and PCDTBT-F	85
Table 4.1: GPC data for P6 , P7 , P8 and their analogous polymer PZI	108
Table 4.2: UV-visible data for P6 , P7 and P8	109
Table 4.3: Cyclic voltammetry results for P6 , P7 , P8 and PZI	112

Abbreviations

A	Acceptor
A-D-A	Acceptor-Donor-Acceptor
BHJ	Bulk heterojunction
BTD	Benzothiadiazole
CB	Conduction band
CV	Cyclic voltammetry
^{13}C NMR	Carbon Nuclear Magnetic Resonance
D	Donor
d	Doublet (NMR)
D-A	Donor-Acceptor
DCM	Dichloromethane
dd	Doublet of doublet (NMR)
DHA	Direct (Hetero) arylation
$E_{\text{g}}^{\text{elec}}$	Electrochemical bandgap
$E_{\text{g}}^{\text{opt}}$	Optical bandgap
^{19}F NMR	Fluorine Nuclear Magnetic Resonance
FF	Fill factor
GPC	Gel permeation chromatography
^1H NMR	Proton Nuclear Magnetic Resonance
HOMO	Highest occupied molecule orbital

ICT	Intramolecular charge transfer
J _{sc}	Short current circuit
LUMO	Lowest unoccupied molecule orbital
M	Molar
M _n	Number-average molecular weight
M _w	Weight-average molecular weight
NBS	N-bromosuccinimide
OFETs	Organic Field-Effect Transistors
OPV	Organic photovoltaic
OSCs	Organic solar cells
PCE	Power conversion efficiency
PDI	Polydispersity index
PLEDs	Polymer Light-Emitting Diodes
ppm	Part per million
s	Singlet (NMR)
t	Triplet (NMR)
TGA	Thermal gravimetric analysis
UV-visible	Ultraviolet-visible spectroscopy
VB	Valance band
V _{oc}	Open circuit voltage
XRD	X-ray diffraction
λ _{max}	Maximum absorption wavelength

Chapter 1:-

Introduction

Chapter 1 - Introduction

1.1 Resolving energy demand issues

Global warming issues and high prices of traditional energy production systems which convert coal, crude oil, natural gas and fossil fuel into electricity have led to a significant increase in scientific studies that focus on renewable energy solutions¹⁻³. In terms of the former issue, greenhouse gas emissions are decreased by harnessing sources of clean energy, such as wind, hydro and solar power, all of which are considered environmentally friendly energy systems⁴⁻⁶. Thus, the most important aspect of renewable energy systems is that the materials used do not produce adverse environmental effects as a result of their working^{7,8}. Yet despite their importance in alleviating the issues arising due to climate change, there are problems which must be considered by engineers. The principle amongst these is that their operation is based on climatic situations, which are currently not predictable nor constant. This means that levels of efficiency (certainly of wind and solar power at least) are not stable^{5,9-11}. The solution of this issue is the production of hybrid systems to improve the efficiency of the systems and fulfil the total energy demand¹².

1.2 Solar power

In 1839, Becquerel discovered the operating principle of photovoltaic devices. He observed that the illumination of silver bromide / silver chloride-coated platinum electrodes in acid solutions can create photocurrent¹³⁻¹⁵. This discovery has since led to great leaps forward in our understanding of how to harness solar power, the most abundant energy source known at 3.86×10^{26} Joules per second¹⁶. One of the earliest developments came in 1954, when Chapin *et al.* reported the creation of a novel solar cell with a silicon-based p-n junction. They found that it had a power conversion efficiency (PCE) of 6%¹⁷. By 2009, improvements to the PCE of silicon-based solar cells had been increased to 25% by Martin¹⁵. Indeed, the best feature of the silicon-based solar cells is their superior power conversion efficiency; however, the main reason to search for alternative materials is the high price of silicon-based solar cells¹⁸. Thus, scientists have recently shifted their attention to increasing the structural complexity of solar cell models with the aim of allowing more efficient conversion of solar energy. In short, organic photovoltaic material has become more commonly used than inorganic due to its inexpensive fabrication and low thermal budget process, which leads to the materials' flexibility and light weight¹⁹⁻²³.

1.3 Conjugated polymers

Conjugated polymers are macromolecules containing single and double bonds in an alternating pattern. This leads to wide delocalisation of π -electrons with a network of bonding and anti-bonding orbitals over the polymer's main chain that are in control of their semiconducting features²⁴. Natta *et al.* produced poly(acetylene) as a black and insoluble powder in 1958. This was the earliest and simplest formula of a conjugated polymer²⁵. However, significant improvement was not attained until a thin film of poly(acetylene) was produced by accident in 1974 by Ito and Shirakawa²⁶. Soon after, in 1976, Shirakawa *et al.* discovered that the conductivity of poly(acetylene) could reach approximately 1 S cm^{-1} when doped oxidatively or reductively²⁷. Rather belatedly, in 2000, Shirakawa and his co-workers gained the Nobel Prize recognition for this discovery. Unsurprisingly, since 1976 conjugated polymers have received great scientific and commercial attention²⁷. This is because they possess a unique combination of features of both plastics and metals. These features include easy processing, flexibility, optical activity and conductivity²⁸.

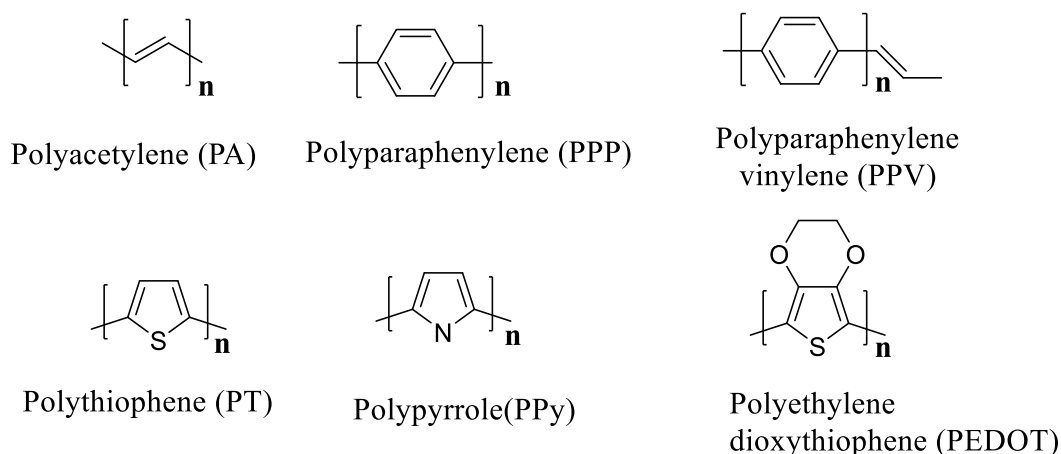


Figure 1.1: Molecular structures of some common conjugated polymers.

1.4 The semiconducting properties of conjugated polymers

Conjugated polymers are semiconducting materials that have low electronic conductivity. However, the conductivity of these materials can be enhanced along the polymer chain upon oxidation. Moreover, electronic delocalisation is affected depending on the structural make-up of the conjugated polymer, and the creation of alternating carbon-carbon single bonds and

carbon-carbon double bonds along the conjugated polymer to form a system of π -bonds. This can occur due to overlapping of the Pz-orbitals on adjacent carbons.

It is possible to start with the monomer ethylene, which has π -orbitals. The electronic structures of ethylene and the conjugated oligomers of polyacetylene are shown in figure (1.2). The highest occupied molecule orbital (HOMO) corresponds to the π -bonding orbital (valence band), and the lowest unoccupied molecule orbital (LUMO) corresponds to the π^* -antibonding orbital (conduction band). For example, in ethylene, a large energy gap separates the HOMO and LUMO orbitals. However, if the length of the conjugated chain is increased, meaning more π -bonds are added to the system, this leads to the creation of energy bands rather than levels of energy, and the energy gap consequently falls²⁹.

ΔE is the distance between the HOMO and LUMO, and the electronic and optical properties of conjugated polymers are controlled by ΔE . Therefore, controlling the HOMO-LUMO gap by structural adjustment is an important consideration when designing low band gap energy polymers. There are two very important factors to consider; the bandgap (E_g) based on these (ΔE) and the band width W (β), which symbolises a hybridisation function (β) of monomer levels in the polymer. Polymers with low bandgap have to be designed to absorb electromagnetic radiation in the visible light range as well as the long wavelength infrared region as we know that $E_g = 1240/\lambda_{\max}$ ³⁰.

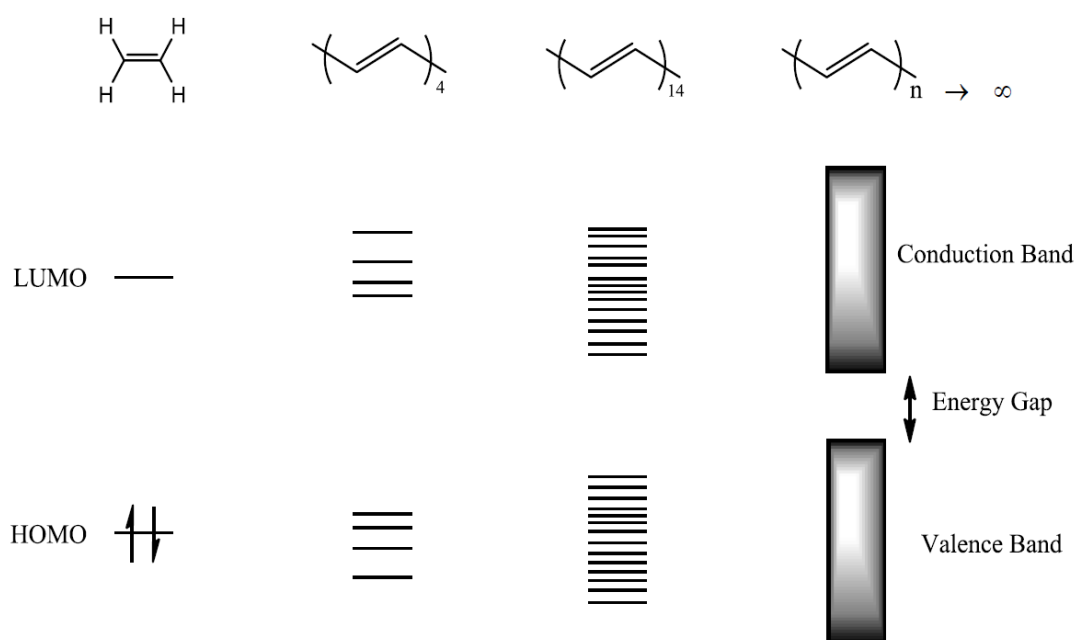


Figure 1.2: Bandgap forming during polymerisation method of π -conjugated polymers³⁰.

1.5 Conduction process

In terms of conductivity, materials can be divided into the following three major types: insulators, semiconductors and conductors. One of the key criteria used to differentiate between these material types is the energy difference between the HOMO and LUMO levels in each; in other words, the band gap, which is equivalent to the energy required for an electron to be freed from the outer shell to give a mobile charge carrier. Figure (1.3) illustrates the bandgaps of materials depending on their conductivity. Due to the overlap between the valance band and the conduction band, if the bandgap is equivalent to 0 eV, the material is a conductor. Semiconductors have a bandgap smaller than 3.0 eV whereas the bandgap of insulators is greater than 3.0 eV³¹.

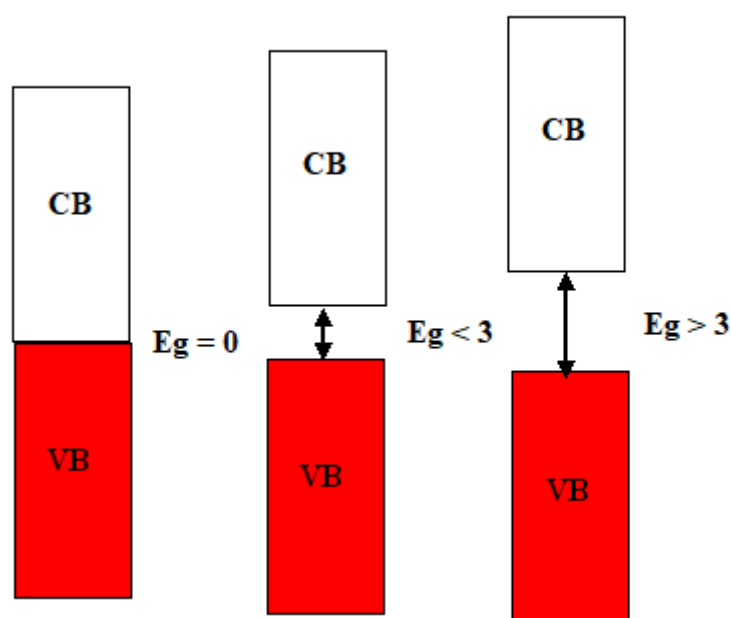


Figure 1.3: Diagram illustration of the three types of materials according to their bandgaps.

Doping methods, which can be divided into p doping and n doping, can be used in the modification of conjugated polymers to reduce the bandgap and therefore increase power conversion efficiency. Modification of the band structure of polymers is done by lowering energy transition formation and the creation of charge carriers (e.g. polarons and bipolarons), as presented in figure (1.4) below. Importantly, charge carriers control the conductivity in polymers³². λ max characterises π - π^* transitions in conjugated polymers; the transition π - π^* in neutral polymers determines the bandgap of conjugated polymers²⁷.

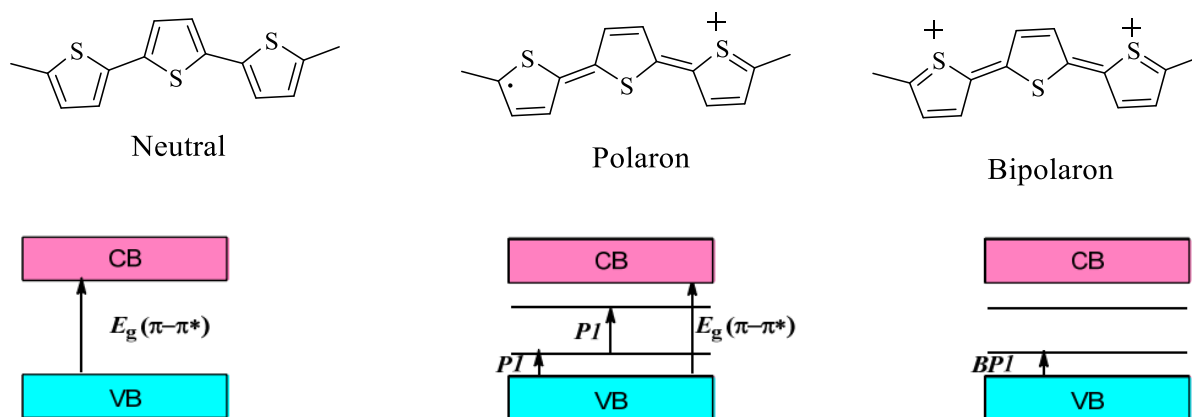


Figure 1.4: Possible neutral, polaron and bipolaron thiophene trimer transitions.

1.6 Conductivity in conjugated polymers

A conjugated polymer's backbone does not have full delocalisation of electrons due to the difference in the length of the σ -bond and π -bond. As every carbon atom contains an electron that is unpaired, this creates a delocalisation state. This fact is key to our ability to improve the stability of conjugated systems³³. Polymers can change between two main cases³⁴, as illustrated in figure (1.5). For example, these cases in polyacetylene can be degenerate, whereby all single and double bonds are of the same length. This allows delocalisation of electrons along the polymer's backbone. In non-degenerate cases in conjugated aromatic systems, there are two resonance forms for the ground state with non-degenerate energy³⁵.

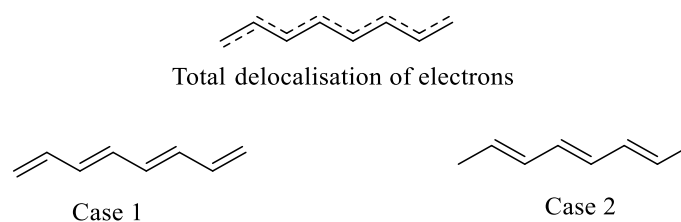


Figure 1.5: Two degenerate cases of trans-polyacetylene.

Narrowing the bandgap in conjugated polymers can be done by relaxing the length of bonds between σ - π bonds alternation through the inclusion of aromatic rings in the polymer chains. This strategy also effectively increases delocalisation of electrons as a consequence of the π -electron network extension, thus resisting the Peierls effect³⁶. The supporting of charge carriers and semiconducting properties in conjugated polymers arises from the delocalisation of π -electrons. In recent studies, new conjugated polymers have been prepared to harvest more energy from the solar spectrum – between 1.4 and 1.9 eV³⁷. In terms of band theory,

removing electrons from the valence band (VB) with an oxidising agent or donating electrons with reducing agents to the empty conduction band (CB) is the reason that conductivity increases^{38,39}. These two methods are examples of n-type doping and p-type doping, as shown in figure (1.6): (n-type doping) is the excitation of electrons from the impurity level to the conduction band whereas (p-type doping) involves excitation of electrons from the valence band to the empty impurity level⁴⁰.

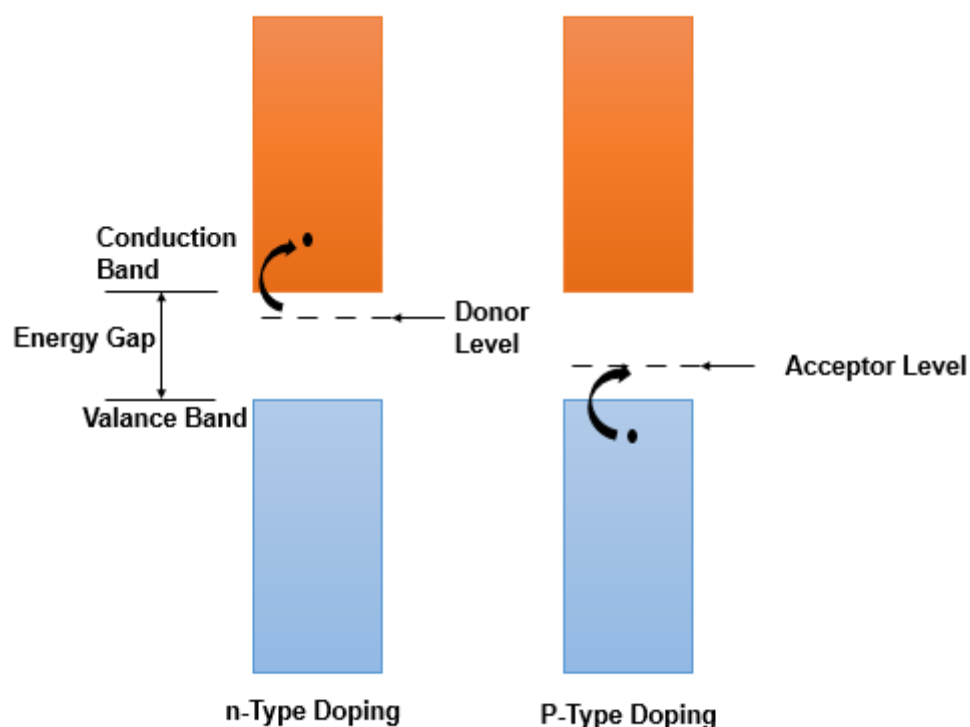


Figure 1.6: Diagram showing the addition of electrons to the conduction band (n-type doping) and removal of electrons from the valence band (p-type doping).

In these two types of doping, the free spin movement of the unpaired electrons is thought to cause the conductivity of the polymer; the valence (oxidation) band and conduction (reduction) band already have these free spins. In addition, n-type and p-type doping both create occupied donor levels and cause a lowering of the conduction band.

Another important aspect to these processes is polarons, which are radical cations or anions generated by reduction or oxidation methods in conjugated polymer doping. With the reduction method, a negative polaron is created due to the existence of an unpaired electron

alongside paired electrons that are in the high-energy negative polaron state. The oxidation method causes a single electron to jump to the newly created energy level in the gap between the valence and conduction bands. In another case termed bipolaron, a dianion or dication is created by the transfer of another electron⁴⁰.

1.7 Engineering of the band gap

Due to their importance in establishing the limits of power conversion efficiency, band gaps are a key consideration for any conjugated polymer used in photovoltaic applications. Therefore, it is useful to establish the best strategies of design for controlling these band gaps^{41,42,43}.

In terms of its structure, the definition of the skeleton of a conjugated polymer, for example polyphenylene or polythiophene, can be cited as “a series of consecutive carbon-carbon double bonds linked together by carbon-carbon single bonds”⁴⁴. The energy of the ground state of a non-degenerate case is likely to be one of two resonance structures, as shown in figure (1.7): the aromatic form and the quinoid form. Firstly, the aromatic form is any unit of benzene or thiophene upholding its aromaticity with restricted π -electrons. The quinoid form is a resonance structure that merges the delocalisation of electrons along the chain of a conjugated polymer. This simultaneously changes double bonds into single bonds and vice versa. It should be noted that the band gap of the quinoid form is smaller than the band gap of the aromatic form. This is due to the destruction of the aromaticity that is needed before adopting a quinoid, thus causing a loss of the energy of stabilisation. Geometric parameters, such as bond length alternation (BLA), defined as “the average of the difference in length between adjacent carbon-carbon bonds in a polyene chain”⁴⁴, can be used to explain the proportion of the aromatic to quinoid inhabitants in a polyaromatic conjugated structure. In the ground state, as a result of the additional stability provided, the aromatic form dominates. Due to this, it has been shown that a larger BLA value is achieved⁴⁵.

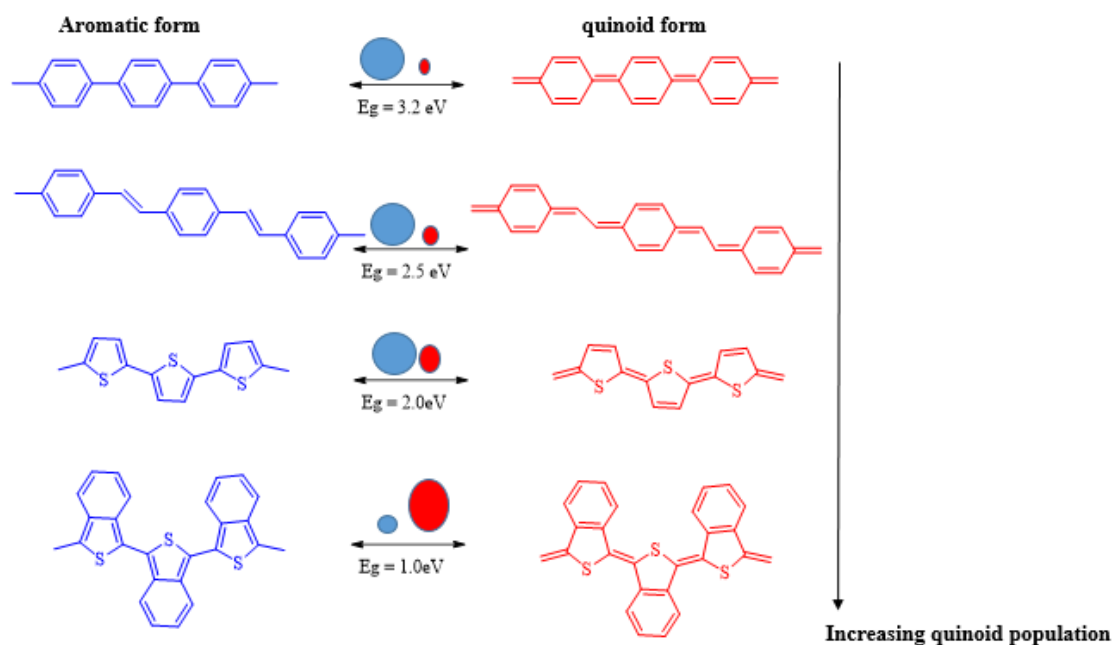


Figure 1.7: Aromatic and quinoid resonance forms of some polymers. The diameter of the blue and red circles signify the proportional contribution of the mesomeric structures⁴⁴.

As the amount of quinoid contribution is increased, the carbon-carbon single bonds between two end-to-end rings foster more double bonds and the BLA begins to decline. Generally, when the quinoid character increases, the value of BLA decreases and the band gap of HOMO-LUMO declines linearly. It is important to note that the aromatic stabilisation resonance energy of the aromatic unit affects the value of BLA. The quinoid form adopted by the delocalisation of π electrons is due to the decreasing aromaticity of the aromatic units in the conjugated main chain. Polyphenylene has a large band gap of around 3.2 eV and this is due to the high level of aromaticity in the rings of benzene. That said, it is possible to reduce the band gap of poly(phenylenevinylene) to around 2.4 eV. This can be achieved by decreasing the aromaticity by introducing a double bond in order to reduce the influence of the benzene rings. Moreover, the aromaticity of benzene is more than that of thiophene, but the band gap of polythiophene is low at 2.0 eV, so the likelihood of it adopting a quinoid form is increased. Polyisothianaphthene (PITN) explains the increasing effect of the quinoid character of polythiophene in an inventive way⁴⁶. Once more, this is due to the higher energy of aromatic resonance for benzene compared to thiophene (1.56 vs 1.26 eV respectively). Another point to note is that the quinoid form adopted by the main chain of PITN allows the aromaticity of benzene to be retained. Thus, PITN represents the first time a conjugated polymer has been discovered with a band gap as narrow as 1 eV^{47,48}. In terms of methods to

achieve quinoidisation, aromatic exchange has been shown to be effective. Using this method, poly(thieno[3,4-*b*]pyrazine) **P1**⁴⁹ and poly(thieno[3,4-*b*]-thiophene) **P2**⁵⁰ have been produced. These polymers have rings of primary thiophene attached with a different aromatic pyrazine or thiophene ring at the β -position. This is to encourage quinoid population and reach conjugated polymers with low band gaps (see figure (1.8) below).

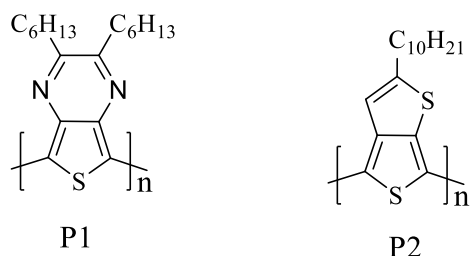


Figure 1.8: The chemical structure of poly(thieno[3,4-*b*] pyrazine) **P1** and poly(thieno[3,4-*b*]thiophene) **P2**⁴⁴.

Moreover, the molecular structure can be modified so that steric or electronic effects are forced onto the main chains of conjugated polymers. This provides a diverse method for lowering the band gap. In order to broaden conjugation and encourage delocalisation, the interactions of p-orbitals should be parallel. This is achieved by planarisation of adjacent aromatic units, which allows the BLA to decrease and causes a reduction of the band gap. Rotational disorder caused by steric hindrance was first demonstrated by Roncali *et al.*^{51,52}.

Generally, there is a reduction in the energy difference between the HOMO and LUMO with an increase in the conjugation length. However, there is a specific value of saturation of effective conjugation length. After this value, if extra units of monomer are added, the band gap is not significantly affected. Consequently, restricted decreasing of the band gap causes unrestricted extension of the conjugation length. One of the most common methods of decreasing the band gap is by incorporating electron-donating groups, such as the alkoxy group, or electron-withdrawing groups, such as the nitro group, into the aromatic unit of the main chain. In general, the raising of the HOMO energy is caused by electron-donating groups while the decreasing of the LUMO energy is caused by electron-withdrawing groups. For example, the band gap of poly[3, 4-(ethylenedioxy)thiophene] is 1.5 eV whereas the band gap of the parent polythiophene is higher. This is due to the alkoxy group in poly[3, 4-(ethylenedioxy)thiophene] being electron-donating⁵³. Actually though, a more useful approach when creating low band gap conjugated polymers is to have both a conjugated

electron-rich donor (D) unit and a conjugated electron-deficient acceptor (A) unit contained in the backbone of the polymer⁵⁴. This creates push-pull driving forces, simplifying electron delocalisation. It also allows the configuration of quinoid mesomeric structures ($D-A \rightarrow D^+=A^-$) along the conjugated main chain. Using this approach, an impressive reduction of the BLA can be achieved⁴⁴.

Reduction of the optical band gap can be accounted for by photo-induced intramolecular charge transfer (ICT) linked with the high-lying HOMO of the donor unit and the low-lying LUMO of the acceptor unit. This can be simplified using the idea of hybridisation of the molecular orbitals between the donor and acceptor in the D-A polymer⁵⁵. As presented in figure (1.9), according to the basics of perturbation view, there is interaction between the HOMO of both the donor and acceptor. This produces two new HOMOs for the donor-acceptor polymer. Likewise, there is interaction between the LUMO of both the donor and acceptor that produces two new LUMOs for the donor-acceptor polymer. The reason for the narrow optical band gap is due to the electrons moving from their initial orbitals that do not interact with the new hybridised orbitals of the polymer. Commonly, when the polarity of a solvent increases, there is a decrease in the energy needed for absorption⁴⁴.

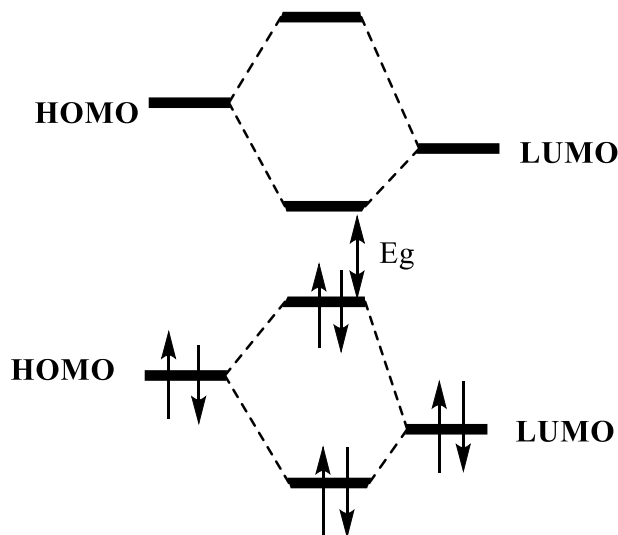


Figure 1.9: Illustration of the interaction of orbitals for donor and acceptor units important for a reduced band gap in a D-A conjugated polymer.

1.8 Polymerisation methods of conjugated polymers

There are many methods of synthesis used to produce conjugated polymers. These methods can be divided into the following types: metal-catalysed cross-coupling reactions, oxidative polymerisations and condensation polymerisations. An explanation of these methods is provided below.

1.8.1 Metal-catalysed cross-coupling polymerisation routes

The majority of conjugated polymers are easily synthesised using metal-catalysed methods and this is commonly done with organic solvents. There are three polymerisation methods using metal-catalysed cross-coupling: Suzuki cross-coupling, Stille cross-coupling and direct (Hetero) arylation (DHA).

1.8.1.1 Suzuki cross-coupling reaction

This method of polymerisation is tolerant of functional groups on the monomer⁵⁶⁻⁵⁸. Due to this feature, this reaction is widely used for the synthesis of a diversity of polymers. In terms of the procedure, aryl halides and boronic acid derivatives⁵⁹ or aryl boronic esters are reacted together in the presence of palladium Pd(0) as a catalyst and a mineral base^{60,61}. Figure (1.10) shows the structures of monomers using *via* Suzuki cross-coupling reaction.

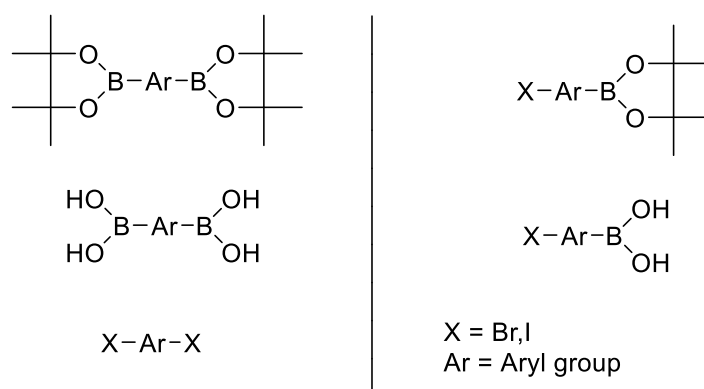
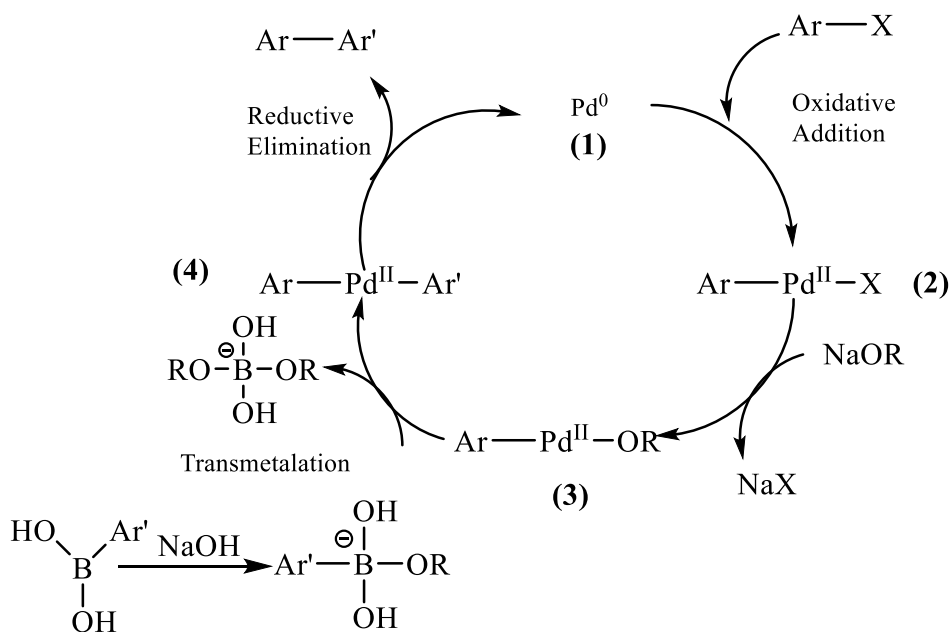


Figure 1.10: Structures of monomers using the Suzuki cross-coupling reaction.

There are four steps in the catalytic cycle of the Suzuki cross-coupling reaction. Scheme (1.1) below illustrates these.



Scheme 1.1: The suggested catalytic cycle for Suzuki coupling.

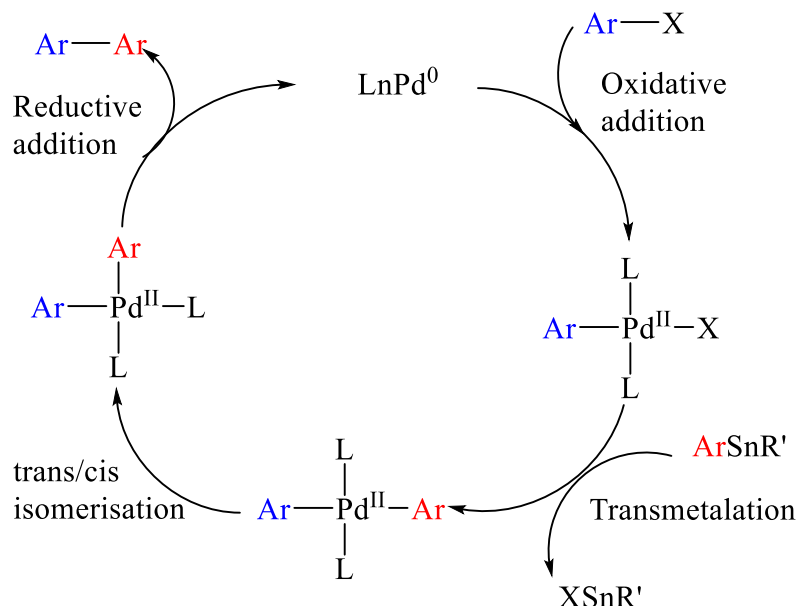
As shown in the scheme, the initial phase involves the oxidative addition of the palladium $\text{Pd}(0)$ to the halide to produce an organopalladium species (2)⁶². In general, the rate of the catalytic cycle is determined by this step⁶². As a result of this process, $\text{Pd}(0)$ changes to $\text{Pd}(\text{II})$. The organopalladium species created by the oxidative addition reacts with the base. This is then followed by transmetalation to yield (3)⁶³. The $\text{Pd}(\text{II})$ complex (4) is yielded by transferring the ligands from the activated organoboronic species that are produced during transmetalation. The last stage involves reductive elimination whereby the product is eliminated by $\text{Pd}(\text{II})$. At this point, the $\text{Pd}(0)$ catalytic species (1) is created⁶².

1.8.1.2 Stille cross-coupling

For this type of polymerisation, the monomers have to consist of organotin- and/or halofunctionalities to react together. Palladium is used as a catalyst. This method has been used widely for different polymers and copolymers because it can deal with a diversity of different functional groups on the monomers, such as amine, esters, ethers and alcohols, and possesses good stabilisation to air and humidity. The main disadvantage of this reaction is that organotin reagents are highly toxic⁶³⁻⁶⁵.

There are four steps in the catalytic cycle of Stille cross-coupling, illustrated in scheme (1.2) below. First, the oxidative addition occurs when the palladium catalyst ($\text{Pd}(0)\text{L}_2$) forms an organopalladium (II) complex through reaction with an aryl hydride. Second, transmetalation

occurs on the aryltin to create a biarylated palladium unit. Third, the created biarylated palladium is trans/cis isomerised. Finally, reductive elimination of the product biaryl (Ar-Ar') and the palladium (0) species occurs to close the catalytic cycle^{63,64}.



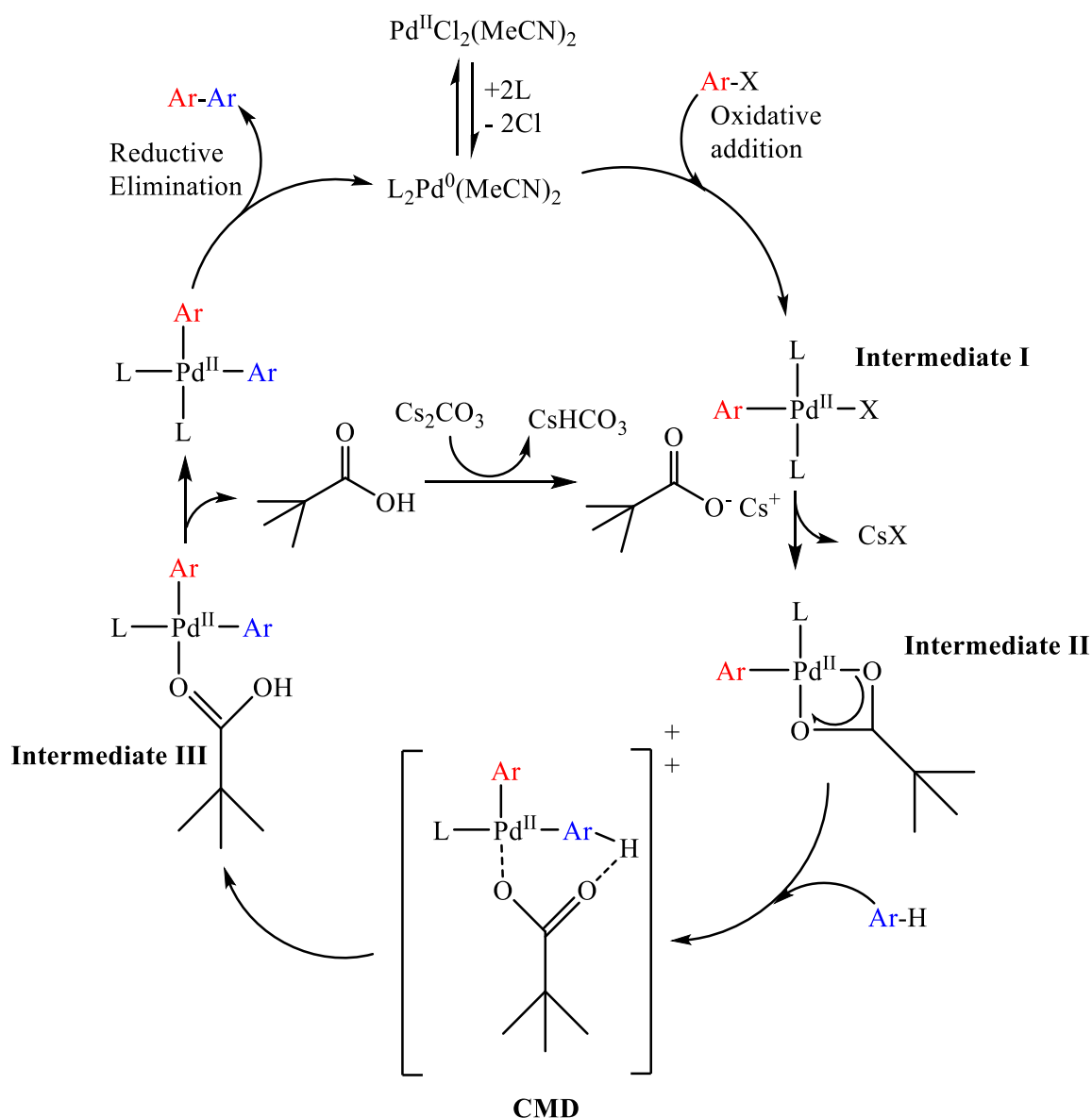
Scheme 1.2: Process diagram of Stille cross-coupling reaction.

1.8.1.3 Direct (Hetero) arylation DHA.

A great number of polymer chemists use direct C-H heteroarylation in the synthesis of π -conjugated organic polymers. They prefer direct arylation than other methods, including Stille and Suzuki cross-coupling reactions, due to it being non-toxic when creating a new C-C bond, the reduced amount of harmful chemical by-products, and the fact that it eliminates the need to use a large amount of toxic organometallic reagents⁶⁶⁻⁶⁹. Palladium can be used as a catalyst, caesium carbonate (Cs_2CO_3) or potassium carbonate (K_2CO_3) as a base, and pivalic acid (trimethyl acetic acid) as a source of carboxylate^{66,70,71}.

The proposed catalytic cycle of this type of polymerisation is illustrated in scheme (1.3). In this mechanism, the palladium (0) complex is produced through the activation of a palladium (II) complex. Then an oxidative addition forms **Intermediate I** and creates the palladium (II) complex *via* incorporation of the aryl bromide (Ar-Br) into the palladium (0). After this, **Intermediate II** forms through the exchange of bromide ligand, which is caused by interaction of the pivalate anion with the palladium intermediate. After this, deprotonation of

the aryl substrate (Ar-H) occurs, creating **Intermediate III** through a concerted metalation-deprotonation (CMD) transition state. Lastly, pivalic acid separates from **Intermediate III** then enables the process of reductive elimination. This creates Aryl-Aryl products and regenerates the catalyst⁷²⁻⁷⁴.



Scheme 1.3: Process diagram of direct arylation cross-coupling reaction.

1.9 Conjugated polymer solubility

There are six different causes of the solubility of conjugated polymers. These are; the length of the side chain on the aliphatic group, the degree of polymerisation, the substituent polarity, the rigidity of the backbone of the polymer, the forces of the interaction between species in

the same polymer, and the polymer's regioregularity⁴⁴. The issue of insoluble conjugated polymers due to rigidity can be solved through the introduction of functional side groups to the structure of polymers such as alkyl or alkoxy groups⁷⁵.

Changing of soluble conjugated polymers into thin film can be achieved using different techniques; roll-to-roll printing⁷⁶, spin-coating^{77,78}, ink-jet printing⁷⁹⁻⁸¹ and the screen-printing technique⁸²⁻⁸⁴. The modification of the bandgap of conjugated polymers can be achieved through adjusting the molecular structure of the repeated moiety^{85,86}.

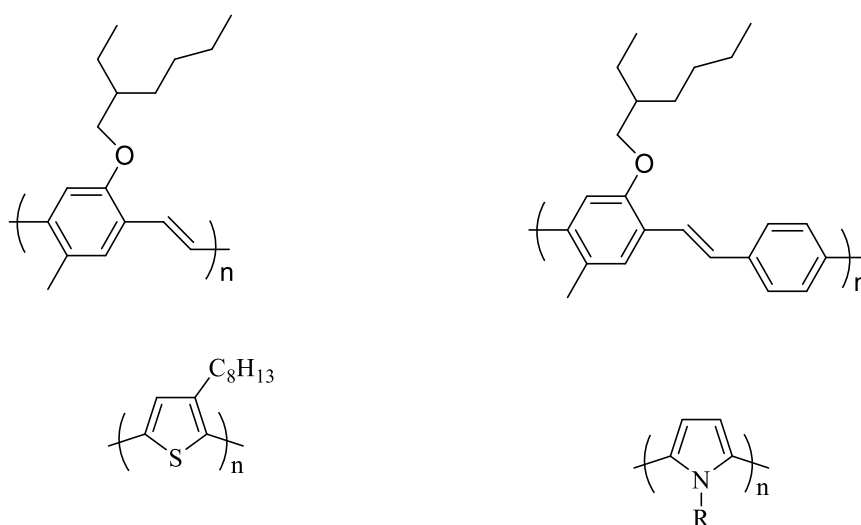


Figure 1.11: Soluble conjugated polymers in common organic solvents.

1.10 Applications of conjugated polymers

Semi-conducting properties of conjugated polymers have opened up broad prospects for this research to be used in novel and varied applications. Indeed, conjugated polymers are used in several areas due to ease of processing. Some common applications of conjugated polymers are summarised in this section, including in polymer light-emitting diodes (PLED), organic field-effect transistors (OFETs) and organic solar cells (OSCs).

1.10.1 Polymer Light-Emitting Diodes (PLEDs)

In 1963, Pope *et al.* discovered electroluminescence in organic materials⁸⁷, and in 1990 Burroughes *et al.* first discovered electroluminescence from conjugated polymers. In this later research, polyphenylene vinylene (PPV) was used⁸⁸. All organic electronic devices, such as PLEDs, OFETs and solar cells, have been investigated since electroluminescence in conjugated polymers was discovered.

The principle behind the function of PLED is that first, a voltage is applied to the conjugated polymer. Under this voltage, electrons and holes are inserted into the polymer from the cathode and anode respectively. These negative and positive charges meet and recombine to create a short-lived excited state known as an exciton. Thereafter, the excited state (exciton) decays, leading to the emission of energy in the form of light or photons in a process named photoluminescence (PL)^{89,90}.

PLED has two structures – a single and a multi-layer. The fundamental structure is a single layer thin film of a conjugated polymer sandwiched between two electrodes. The anode is typically constructed from ITO, due to it having a high work function. On the other hand, the cathode has to be fashioned from a low-work-function material, for example Al, Ca or Mg⁹⁰. Electrons and holes are transported from their electrodes when the device is under the influence of electricity. The valance band (HOMO) accepts holes that are transported from the anode while the conductive band (LUMO) accepts electrons that are transported from the cathode. This causes the formation of positive and negative polarons that carry the holes and electrons along the conjugated polymer chains and between chains. When these polarons meet and recombine, an exciton is formed and radiative decay can occur. It has been shown that by avoiding decay of the exciton near the electrodes, which could lead to the flow of current without emission, the efficiency of LEDs can be raised^{91,92}. See figure (1.12) below for an illustration of the basic structure of a PLED.

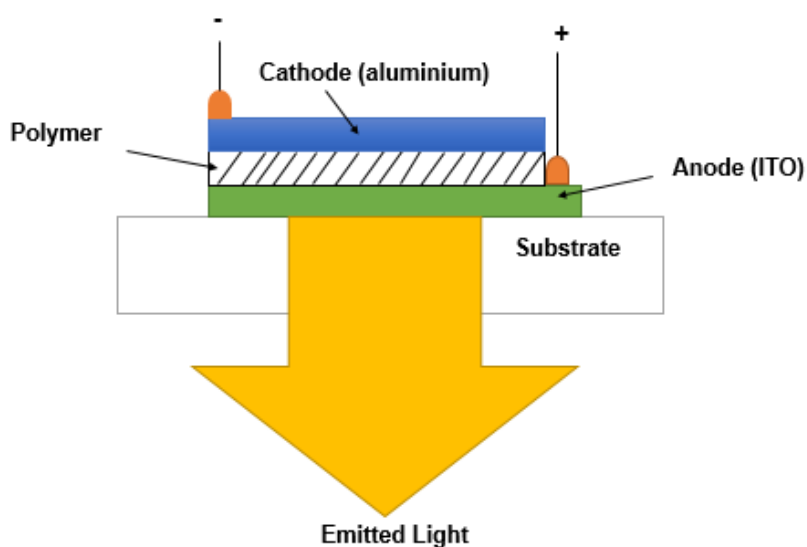


Figure 1.12: Basic structural diagram of a PLED.

The organic layer can be used to avoid the exciton decay from the electrodes by sandwiching the organic layer between two layers: electron transporting materials (ETL) alongside the cathode and hole-transporting materials (HTL) alongside the anode. Examples of electron transport materials include PBD, PDPyDP and Alq3. Hole-transporting materials include, for example, PPV, TPD, PMPS, TPTE and PVK. The transport of charges can be improved using these two layers and the energy barriers for electron or hole injection can be decreased⁹³.

1.10.2 Organic Field-Effect Transistors (OFETs)

A common type of semiconductor device is the field-effect transistor, which can be defined as a device that switches electrical signals. These transistors are integral components of electronic circuits, for example in the chips of a computer. FETs are also used in other electronic devices such as switches for controlling and in amplifiers^{94,95}. Lilienfeld suggested the basic concept of the FET towards the beginning of 1930s⁹⁶. Ever since, various FETs have been manufactured using a silicon base; for example, the metal-oxide-semiconductor and metal-insulator-semiconductor.

Now the focus has switched to the enormous potential of organic semiconductors for OFET. There are some important advantages of OFETs over traditional FETs such as flexibility and a decrease in the cost. Due to these advantages they have been significantly improved over time. In 1986, the first OFET was fabricated from polythiophene, which is a conjugated polymer. It was found that the mobility of this device was $10^{-5} \text{ cm}^2/\text{Vs}$ ⁹⁷⁻⁹⁹. Generally speaking, an OFET consists of the following: a drain, source and gate, an organic semiconducting layer and a dielectric layer, as illustrated in figure (1.13)¹⁰⁰. In terms of its operating principle, current passes between the source (S) and the drain (D) electrodes. To manage this flow, two independent influences are applied: one is (V_{SD}), which is placed between the source and the drain, and the other is (V_{SG}), which is placed between the source and the gate (G); (V_{SG}) controls the charge carriers on the FET. Subsequently, if the voltage of V_{SG} is equal to zero, either the conductivity of the charge carrier density will be greatly reduced or the current flow will be absent. In the latter case, the device is switched off. On the other hand, if the V_{SG} is greater than zero, the density of charge carrier will be high, which means the device is switched on¹⁰¹.

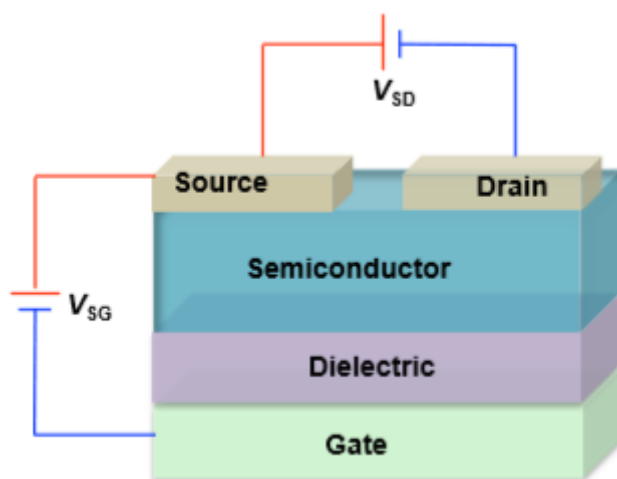


Figure 1.13: The simple structure of an OFET.

1.10.3 Organic solar cells (OSCs)

As noted at the beginning of this chapter, the first scientist to discover photocurrent in inorganic materials was Becquerel. From that time, solar cells have been constructed using these materials. Solar cells have traditionally used silicon, which is an inorganic semiconductor with about 25% efficiency¹⁵. Unfortunately, between 1980 to 1990, OSCs were found to lack efficiency and possessed relatively short lifetimes¹⁰². Over the last 20 years, however, there have obviously been clear improvements in the power conversion efficiency, which recently exceeded 16%¹⁰³⁻¹⁰⁶. In addition, OSCs have distinct characteristics such as flexibility of substrate, high speed of processing, low cost and zero emissions when activated. Researchers have specifically focused on polymers with a wavelength of absorption higher than 600 nm for OSCs due to this range of wavelengths allowing for the best absorption of light. In order to increase power conversion efficiency, solar cells must be able to absorb a high proportion of the solar photon flux, as shown in figure (1.14).

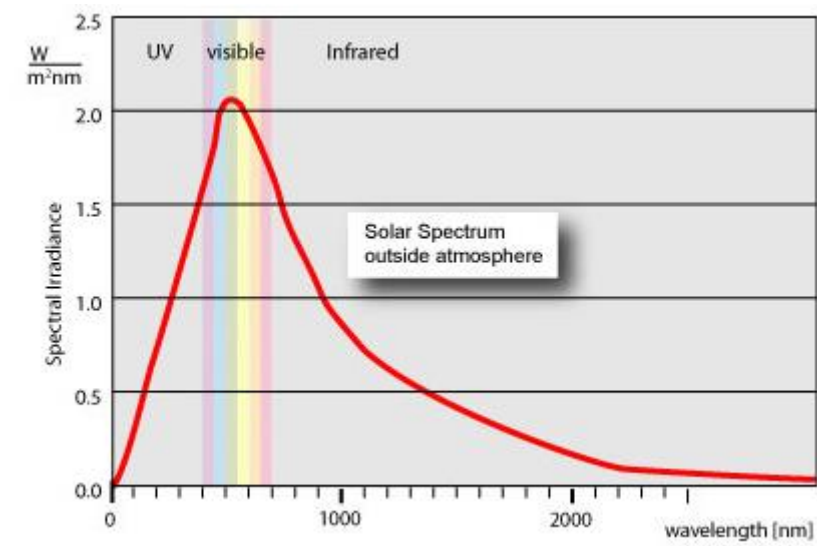


Figure 1.14: Sunlight spectrum.

Polymers with low bandgap that have the ability to harvest long wavelength light are necessary for increased PCE. Thus, numerous studies have been conducted to lengthen the electronic conjugation in polymers and produce materials which have a low bandgap that absorbs longer wavelengths of light. The energy bandgap can be controlled through modifying the structure of the polymer, and these modifications can be controlled using polymerisation to produce quinoid structures along the backbone of polymer. Low bandgaps with more electronic conjugated systems are caused by the planarity of quinoid^{107,108}.

1.11 Architecture of polymer solar cells

There are two main properties that organic compounds must possess to be used in solar cells. Firstly, they must have ability to produce charge carriers *via* absorption of sunlight. Secondly, they must have the ability to transfer these charges to generate electrical current. Actually, these properties are linked to the delocalisation system of the π -bonds in the organic semiconductor. This link produces the semiconducting properties of the organic material. In terms of variety, there are different structures in organic solar cells with the main difference being the active layer. The following sections detail the different types.

1.11.1 Single layer device

Organic solar cells in their simplest form are single layer devices. These consist of two electrodes and an organic semiconductor layer in which the organic semiconductor layer is placed between the anode and cathode electrodes. The anode is usually formed from indium-

tin-oxide(ITO)-coated glass or quartz substrate, and the cathode is formed from Al or Ca, as illustrated in figure (1.15)^{109,110}. The first use of single-layer devices was polyacetylene or polythiophene sandwiched between two diverse direct connects in the 1980s¹¹¹. However, there are some drawbacks in the devices that use a single layer. First, power conversion efficiencies are low, with the lowest efficiency being 0.1% due to a short exciton diffusion length of between 1 and 10 nm. Secondly, there is a decrease in the generation of photocurrent because the absorption of the light is not total^{109,110,112,113}.

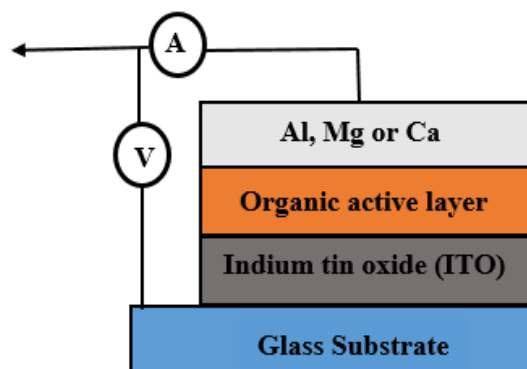


Figure 1.15: Structural diagram of a single layer device polymer solar cell.

1.11.2 Bilayer devices

Figure (1.16) illustrates the construction of an example bilayer device in which there is an organic active layer and acceptor layer arranged together and sandwiched between two electrodes. In a bilayer device, the separation of charge happens at the interface of the donor and acceptor layers^{114,115}. The dissociation of the exciton state at the interface between these two active layers becomes easier using this design compared to a single layer device. Therefore, the acceptor layer, which has larger electron affinity, accepts the electron; the donor layer, which has lower ionisation potential, accepts the hole²¹.

The distance of the excitons from the interface should be between 10 to 20 nm in this type of device. This means that only a tiny portion of excitons can travel the entire distance to the interface. As is widely known, quantum efficiencies decrease due to the separation of charge. However, if photons are absorbed far from the interface they will not have the ability to charge separately¹¹⁶. The range of diffusion length of excitons is usually around 10 nm in organic electronic materials. Therefore, to obtain highly efficient energy production, excitons should be created at a distance not further than the diffusion length of the interface. The

power conversion efficiency which has been achieved with bilayer devices is around 4.2%^{117,118}.

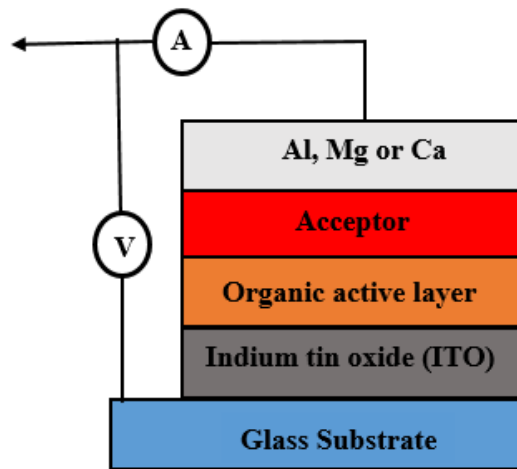


Figure 1.16: Structural diagram of the bilayer device polymer solar cell.

1.11.3 Bulk heterojunction devices

The invention of bulk heterojunction devices was achieved by Heeger *et al.* in the 1990s. In this type of device, the polymer donor and fullerene acceptor are combined in one layer. This means a large donor-acceptor interface is created. This interface is larger than that found in bilayer devices, helping to solve the issue of the inefficient generation of charges in the polymers. To attain this quality, the polymer donor and fullerene acceptor are mixed before being applied to the anode. This creates a network of interpenetrating nanoscale donor and acceptor regions¹¹⁹⁻¹²¹. Therefore, the distance travelled by excitons to reach the donor-acceptor interface is short, at around 10 to 20 nm, and the separation of charge is more efficient (see figure (1.17))¹²². The ratio between the donor and acceptor plays a major role in the equilibrium between absorption of light and transport of electrons¹²³.

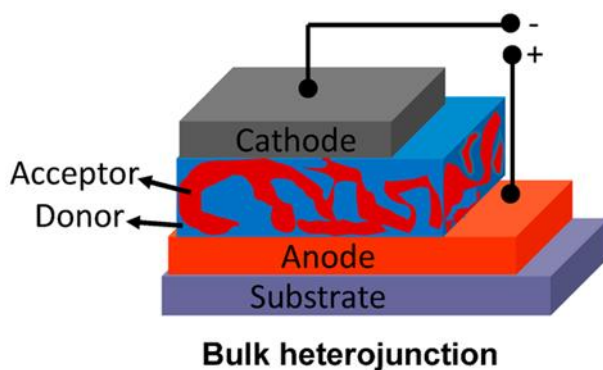


Figure 1.17: Structural diagram of the bulk heterojunction device polymer solar cell.

1.12 Principle of operation of photovoltaic cells

In polymer solar cells, there are four main steps to creating charge from incident photons¹²⁴ (see figure (1.18) below). (1) When photons are absorbed by the organic active layer, an exciton state is created by the promotion of electrons from the HOMO to the LUMO energy level of the donor. This leaves holes in the HOMO¹²⁵. (2) The excitons consequently diffuse to the interface of the donor-acceptor²². (3) The electrons are then transferred from the LUMO energy level of the donor to the LUMO energy level of the acceptor. The acceptor phase contains the electrons and the donor phase contains the holes, and these are still linked together as twin pairs¹²⁶. (4) Then, the twin pairs are separated and the free holes are moved to the anode through donors. The free electrons are then moved to the cathode *via* the acceptor where they are collected¹²⁷.

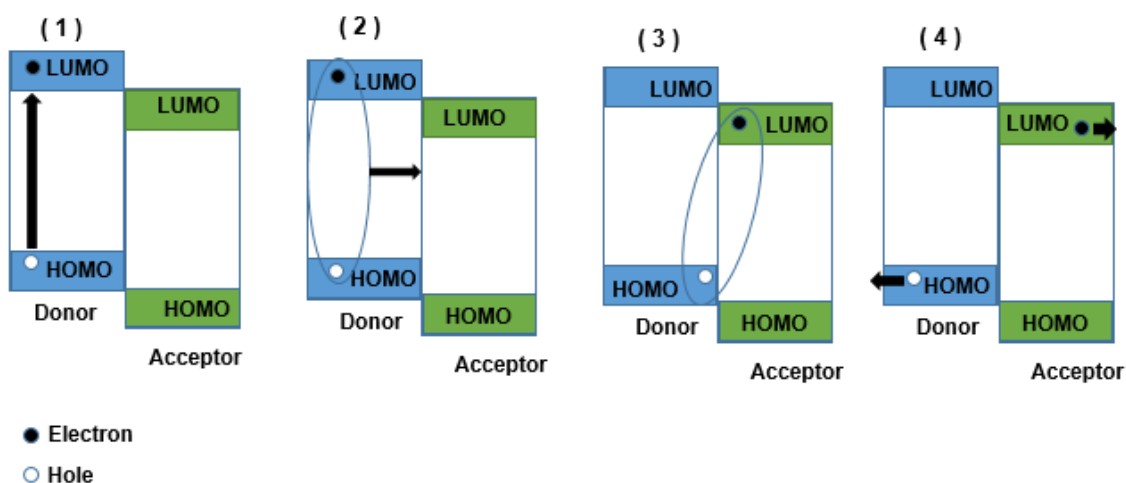


Figure 1.18: Schematic illustration of the working principle of photovoltaic cells⁴⁴.

1.13 Conjugated polymers as donors with fullerenes as acceptors

Scientists have focused on two important points when synthesising conjugated polymers for solar cells. First, the absorption of these materials has to be above 600 nm due to this range being particularly suited to the absorption of sunlight. Second, it has to be able to transfer these charges⁷⁷. These two points correspond to the delocalised system of π -bonds, which consequently causes the semiconducting behaviour in conjugated polymers. The efficiency of organic solar cell devices can be enhanced by merging conjugated polymer with fullerene derivatives such as PC71BM¹²⁸. Figure (1-19) displays two fullerene derivatives used in the production of organic solar cell devices.

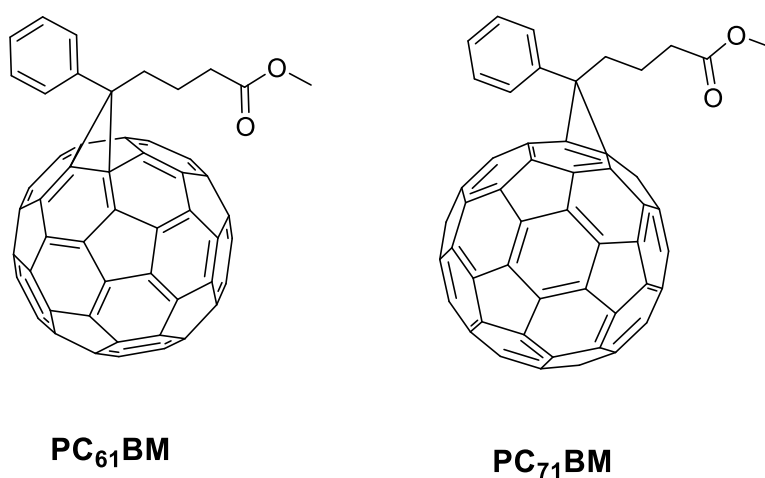


Figure 1.19: Fullerene derivatives used in the manufacture of OPV devices.

Unfortunately, fullerene derivatives are low in solubility. To combat this issue, a solubilising group can be added. The transfer of an electron from conjugated polymer (donor) to fullerene derivative (acceptor) occurs very rapidly – a matter of femtoseconds (fs). Due to the higher speed of electron transfer compared to the recombination process, the total PCE of organic solar cells is decreased. In addition, the rate of recombination method is slow due to the rapid movement of electrons from the fullerene molecules to the interfacial area¹²⁹. However, mixing of fullerene derivatives (acceptor) units with conjugated polymer (donor) units has been shown to improve of the total PCE¹³⁰⁻¹³². It has also been noted that blending of the fullerene derivative acceptor with the conjugated polymer (donor) not only narrows the bandgap of the conjugated polymer but also develops the charge carrier mobility by decreasing the distance of π - π interchain stacking¹³³⁻¹³⁵.

1.14 Conjugated polymers as donors with non-fullerenes as acceptors

Recently, researchers have focused on non-fullerene acceptors due to their enormous potential to achieve high PCE¹⁰⁴. For instance, bulk heterojunction (BHJ) organic photovoltaics based on a blend of a p-type donor and n-type acceptor have been developed¹²⁶. The length of the wavelength of the absorption materials play a major role in the bandgap, with most OPV materials absorbing light wavelengths shorter than 800 nm¹⁰³. In the last 2-3 years, rapid improvement of low bandgap non-fullerene acceptors has afforded effective methods to develop the performance of organic photovoltaics due to their tunable level of energy and strong absorption in the near infrared region^{132,136-141}. Appropriate non-fullerene acceptors (NFAs) should have HOMO and LUMO energy levels appropriately located in terms of the energy levels of the donor material used. For instance, Yuan *et al.* used PM6 (polymer) – as illustrated in figure (1.20) – as a donor with a HOMO energy level of -5.56 eV and LUMO level of -3.50 eV. To maximise the short-circuit current density (J_{sc}) and the open-circuit voltage (V_{oc}), the HOMO levels of non-fullerene acceptors should be near to those of the donor polymer. Suitable LUMO levels are also required to achieve the ideal optical bandgap¹⁰⁴. In addition, Yuan *et al.* used Y6 as an acceptor – see figure (1.20) – to achieve PCE above 15%¹⁰⁴.

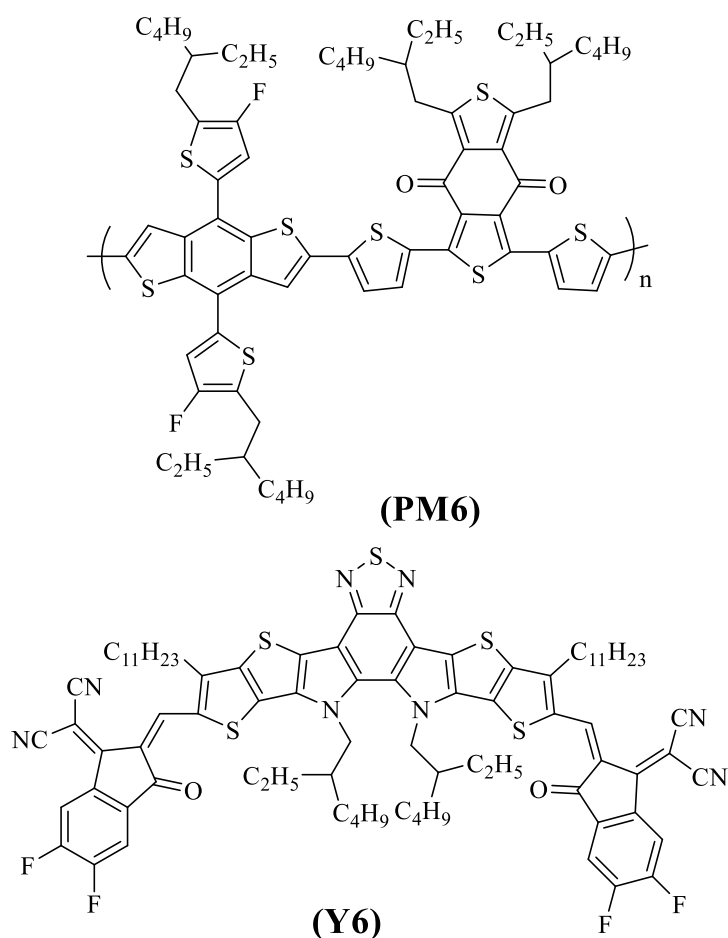


Figure 1.20: Molecular structure of (PM6) and (Y6).

1.15 Characteristics of organic solar cell devices

To establish the effectiveness of organic solar cells, we have to consider the power conversion efficiency (PCE), which is calculated using the following three variables: open circuit voltage (V_{oc}), short current circuit (J_{sc}) and fill factor (FF)^{128,142}. In addition, J-V characteristics, which explain the link between these parameters, must be fully known (see Figure (1.21)). It should be noted that the test of devices is always run under two conditions: illuminated and dark.

Power conversion efficiency (PCE) can be calculated easily after identification of the parameters:

$$PCE = (J_{sc} \times V_{oc} \times FF) / I_{light}$$

where J_{sc} is short current circuit, V_{oc} is open circuit voltage, FF is fill factor and I_{light} is the incident radiation intensity of solar light¹⁰².

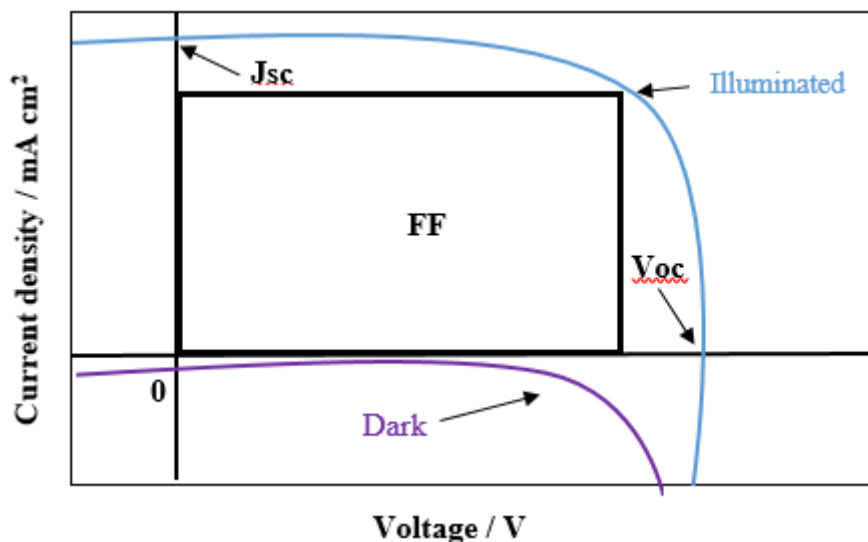


Figure 1.21: Curve of current-voltage J - V characteristics in dark and illuminated environments.

1.15.1 Open circuit voltage (V_{oc})

Open circuit voltage is the highest device voltage reached when the current flow in the organic solar cell devices is equal to zero¹⁴³. Numerous studies have demonstrated V_{oc} is based on the energy gap between the (HOMO) level of the donor and the (LUMO) level of the acceptor of the bulk heterojunction, establishing the basis for estimating the open circuit voltage in these devices. Worthy of note is that V_{oc} is affected by the morphology of an active layer¹⁴⁴. In addition, it is decreased when the temperature is increased due to the recombination methods and because the free charges are highly mobile^{144,145}.

1.15.2 Short current circuit (J_{sc})

Short current circuit is the highest current that can be harvested in organic solar cell devices when the voltage applied between the anode and cathode is equal to zero¹⁴³. It is based on the charge mobility of the blend used in organic solar cell device manufacture and is changed when the morphology of an active layer is changed. Choosing a suitable solvent is the main key in achieving desirable morphology of the active layer¹⁰².

1.15.3 Fill factor (FF)

Fill factor is the maximum gained power collected from the organic solar cell devices and denotes the degree to which charge carriers can be extracted from the solar cell device.

Another definition of (FF) is an oblongate area in the current-voltage J-V plot, which is at right angles on V_{oc} and J_{sc} in the plot¹⁴⁶⁻¹⁴⁸. There are many factors which affect the fill factor such as the thickness of an active layer, the area of the organic solar cell devices, and the efficiency of the electrode in its collection of free charges^{149,150}.

1.16 Perovskite solar cell as a competing technology to bulk heterojunction solar cells

The organometallic halide perovskite materials have gained considerable attention in the last few years due to their excellent optical and electrical properties. These materials demonstrated highly effective capability of converting light into electricity using cheap solution-processable methods in fabricating photovoltaic (PV) devices. Power conversion efficiency (PCE) of perovskite solar cells (PSCs) has remarkably jumped from 3.8% in 2009 to about 24% up to date with two types of typical PV device structures; i.e. based-on mesoporous structure and planar heterojunction structures¹⁵¹. The mesoporous structure of (PSCs) content of FTO/compact TiO₂/meso-TiO₂/ perovskite/spiro-OMeTAD/Ag while the planar heterojunction structure of (PSCs) content of ITO/PEDOT:PSS/perovskite/PCBM/Ag.

The rapid increase in the performance of perovskite based solar cells is caused by their distinctive features including a low energy direct bandgap (1.5 eV), high absorption coefficient, balanced electron-hole mobility, long range charge diffusion length (100–1000 nm), high dielectric constant, high carrier mobility and small exciton binding energies¹⁵².

Although the excellent progression in the performance of (PSCs) there are various challenges that request to be addressed before commercialization will be possible. Most importantly, (PSCs) have not yet showed the long-term stability that is required to compete with Si based solar cells. In addition, other main concerns related with potential environmental influences since perovskite material contain Lead (Pb) which is toxic material¹⁵³.

1.17 Aims of the thesis

Polymer solar cells (PSCs) as a renewable energy source have been studied in great detail due to their excellent features, which include the flexibility of devices, their light weight and solution processing abilities¹⁵⁴. Fortunately, the power conversion efficiency (PCE) of bulk heterojunction polymer solar cells, where the photoactive layer includes a blend of donor (D) and acceptor (A) molecules, has increased significantly. In order to achieve such high PCE with these devices, certain requirements must be met: a deep HOMO level in order to increase V_{oc} , a low energy bandgap to absorb the solar energy to lead to a higher J_{sc} , a high absorption coefficient, and excellent hole mobility¹⁵⁵. Currently the best strategy to obtain low-bandgap polymers is to use alternating donor-acceptor (D-A) or acceptor-donor-acceptor (A-D-A) units along the backbone of conjugated polymers. Indeed, certain types of (D-A) and (A-D-A) copolymers have provided devices with very good PCEs. Based on this knowledge, the aims of this project are to synthesise and study the properties of novel D-A and A-D-A copolymers using different donors – fluorene, fluorene flanked by furan rings, carbazole, benzothiadiazole flanked by thiophene rings, and bithiophene – in order to achieve excellent optical and electrochemical properties in the resulting materials. The main goal is to narrow the bandgaps of the resulting polymers to achieve high power conversion efficiencies (PCEs).

Benzothiadiazole (BTD) is one of the most common acceptor units that has been used in this research area, with good efficiencies reported in bulk heterojunction solar cells. One of the aims in this thesis is to synthesise novel D-A polymers based on BTD with alkoxy groups or with fluorine atoms at the 5,6-positions flanked by furan rings as an acceptor with the following different donors of fluorene, fluorene flanked with furan rings, and carbazole units all copolymerised with an acceptor. In this research, the BTD was linked with alkoxy chains in the 5,6-positions to enhance the solubility of the resulting polymers. The equivalent thiophene polymers that have been described in the literature showed good PCE in solar cells. We replaced the thiophenes with furans units because the furans have higher quantum yield of fluorescence than thiophene units. It was thus hoped that this would increase the quantum yield of fluorescence of the resulting materials. We will thus investigate and study the thermal, optical and electrochemical properties of the new polymers and the effect of replacing thiophene repeat units with furan repeat units in donor/acceptor conjugated polymers for applications in solar cells by comparing our polymers with those synthesised before. In addition, the effect of the addition of an extra furan ring in the backbone of the

conjugated polymer is to be explored. Finally, we are also interested in investigating the effect of the incorporation of fluorine atoms instead of alkoxy groups at the 5,6-positions of BTD units in order to probe the variation in the electron accepting properties of BTD. The target polymers are shown in figure 1.22.

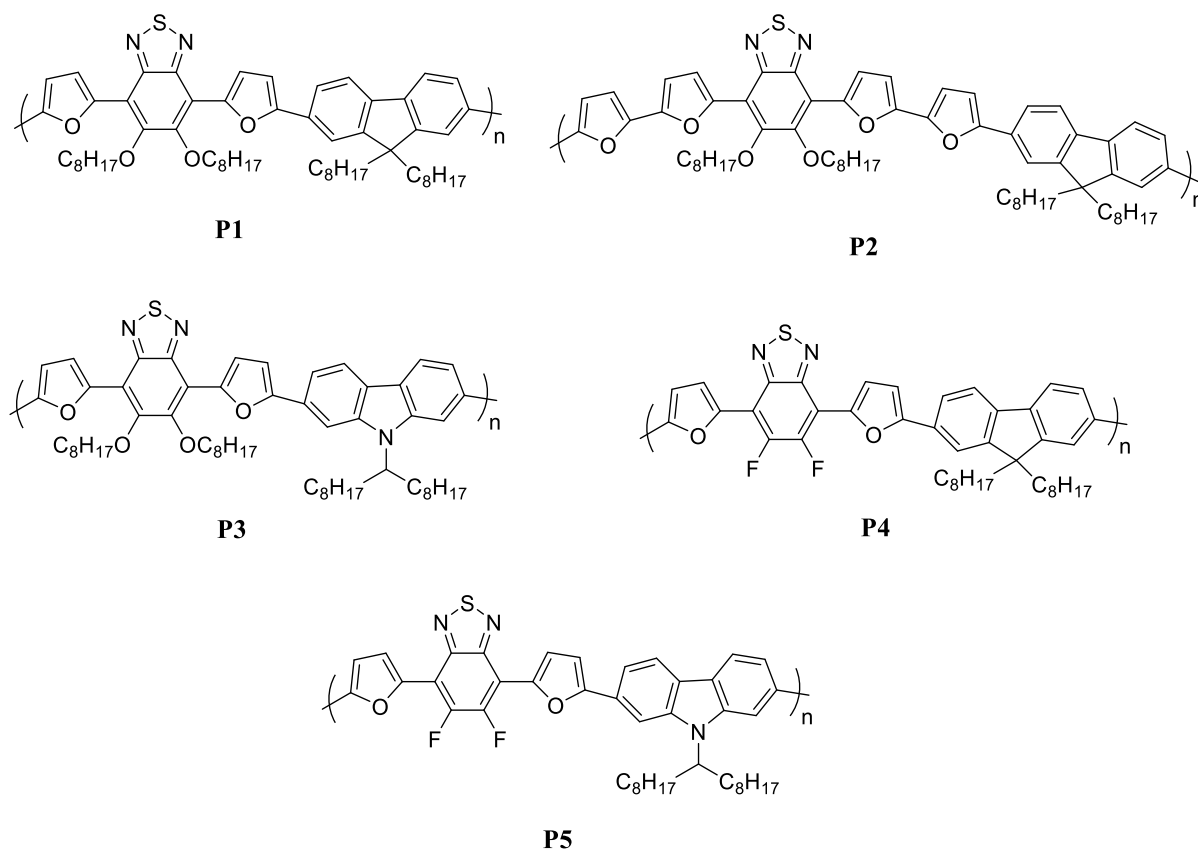


Figure 1.22: Polymer structure of **P1**, **P2**, **P3**, **P4** and **P5**.

In the second part of this project, we are also interested in the preparation of very low band gap polymers. Great attention is now placed on the synthesis of acceptor-donor-acceptor conjugated polymers with decreased bandgaps in order to achieve high PCEs in bulk heterojunction solar cells. The synthesis of novel A-D-A conjugated polymers that involve IDIC, which is a low band gap molecule, reacting with three different monomers: 4,7-bis(5-(trimethylstannyl)thien-2-yl)benzo[c][1,2,5]thiadiazole (**M6**); 5,5'-bis(trimethylstannyl)-2,2'-bithiophene (**M7**); and 2,7-bis(trimethyltin)-9,9-dioctylfluorene (**M8**) to obtain **P6**, **P7** and **P8**, respectively, is to be investigated in this work. In addition, the new A-D-A novel conjugated polymers **P6**, **P7** and **P8** will be compared with an analogous polymer (**PZI**) synthesised by Zhi-Guo *et al.* in 2017. Their research has shown good results, with the

polymer having an optical bandgap of 1.55 eV and an excellent PCE of 9.19%. The structure of these polymers and PZI are shown in figure 1.23.

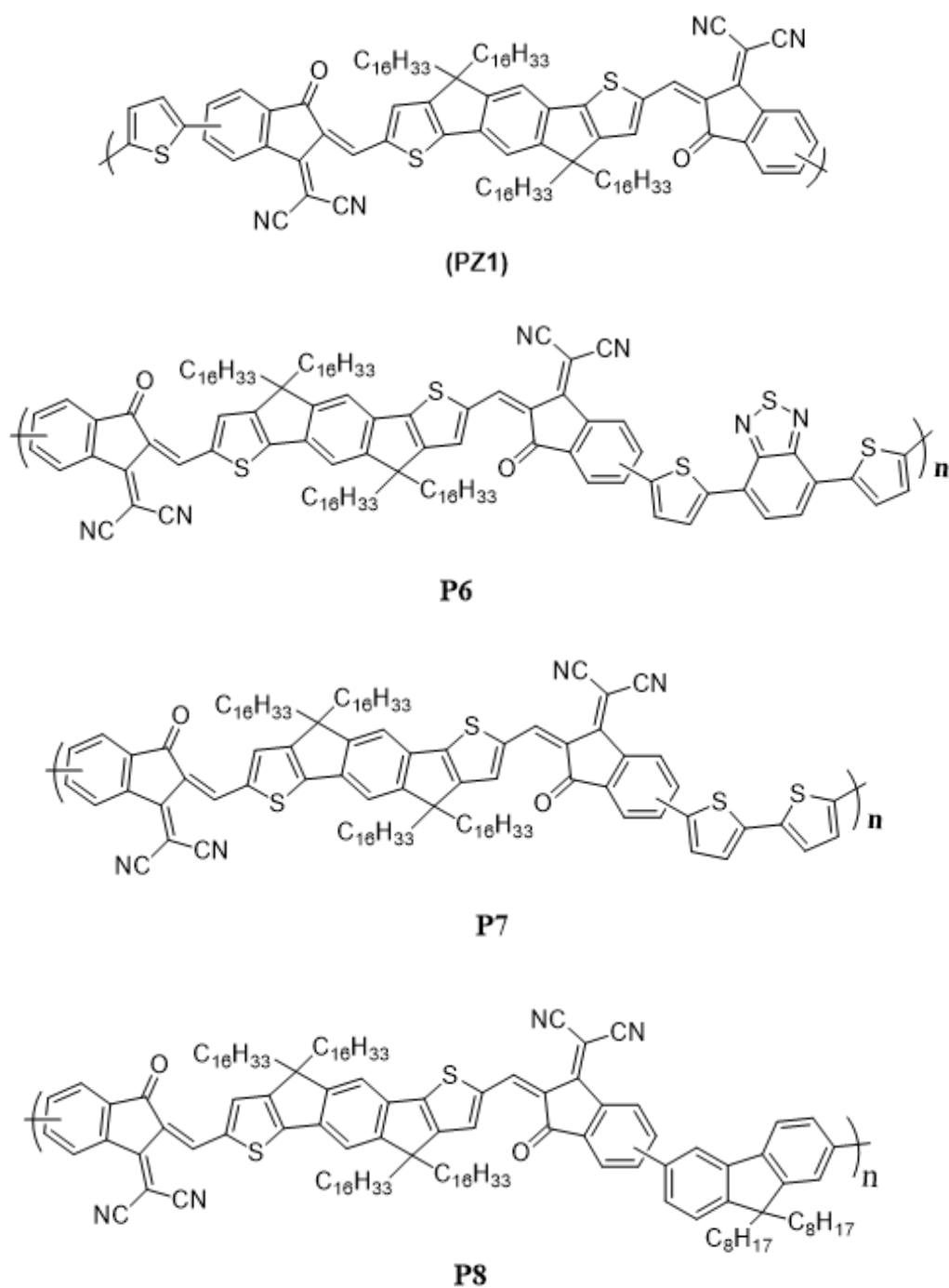


Figure 1.23: Polymer structure of **PZI**, **P6**, **P7** and **P8**.

1.18 References

- (1) Erdinc, O.; Uzunoglu, M. Optimum design of hybrid renewable energy systems: Overview of different approaches. *Renewable and Sustainable Energy Reviews* **2012**, *16* (3), 1412.
- (2) Goedecke, M.; Therdthianwong, S.; Gheewala, S. Life cycle cost analysis of alternative vehicles and fuels in Thailand. *Energy Policy* **2007**, *35* (6), 3236.
- (3) Straatman, P.; Van Sark, W. A new hybrid ocean thermal energy conversion–Offshore solar pond (OTEC–OSP) design: A cost optimization approach. *Solar Energy* **2008**, *82* (6), 520.
- (4) Shaahid, S.; Elhadidy, M. Technical and economic assessment of grid-independent hybrid photovoltaic–diesel–battery power systems for commercial loads in desert environments. *Renewable and sustainable energy reviews* **2007**, *11* (8), 1794.
- (5) Zhou, W.; Lou, C.; Li, Z.; Lu, L.; Yang, H. Current status of research on optimum sizing of stand-alone hybrid solar–wind power generation systems. *Applied Energy* **2010**, *87* (2), 380.
- (6) Kornelakis, A. Multiobjective particle swarm optimization for the optimal design of photovoltaic grid-connected systems. *Solar Energy* **2010**, *84* (12), 2022.
- (7) Nayar, C.; Islam, S.; Dehbonei, H.; Tan, K.; Sharma, H. ". *Power Electronics Handbook-Devices, Circuits and Applications*," in *Power Electronics for Renewable Energy Sources, USA, Elsevier* **2011**, 723.
- (8) Hepbasli, A. A key review on exergetic analysis and assessment of renewable energy resources for a sustainable future. *Renewable and Sustainable Energy Reviews* **2008**, *12* (3), 593.
- (9) Al-Alawi, A.; Al-Alawi, S. M.; Islam, S. Predictive control of an integrated PV-diesel water and power supply system using an artificial neural network. *Renewable Energy* **2007**, *32* (8), 1426.
- (10) Yang, H.; Lu, L.; Zhou, W. A novel optimization sizing model for hybrid solar-wind power generation system. *Solar Energy* **2007**, *81* (1), 76.
- (11) Chen, F.; Duic, N.; Alves, L. M.; da Graça Carvalho, M. Renewable energy solutions for islands. *Renewable and Sustainable Energy Reviews* **2007**, *11* (8), 1888.
- (12) Ekren, O.; Ekren, B. Size optimization of a PV/wind hybrid energy conversion system with battery storage using simulated annealing. *Applied Energy* **2010**, *87* (2), 592.

- (13) Kippelen, B.; Brédas, J.-.; Science, E. Organic photovoltaics. *Energy & Environmental Science* **2009**, *2* (3), 251.
- (14) Becquerel, M. Mémoire sur les effets électriques produits sous l'influence des rayons solaires. *Comptes rendus hebdomadaires des séances de l'Académie Des Sciences* **1839**, *9*, 561.
- (15) Bailey, S. G.; Raffaele, R.; Emery, K. Applications. Space and terrestrial photovoltaics: synergy and diversity. *Progress in Photovoltaics: Research and Applications* **2002**, *10* (6), 399.
- (16) Facchetti, A. π -Conjugated polymers for organic electronics and photovoltaic cell applications. *Chemistry of Materials* **2010**, *23* (3), 733.
- (17) Chapin, D. M.; Fuller, C.; Pearson, G. A new silicon p-n junction photocell for converting solar radiation into electrical power. *Journal of Applied Physics* **1954**, *25* (5), 676.
- (18) Goetzberger, A.; Knobloch, J.; Voss, B. Crystalline silicon solar cells. *New York* **1998**, *1*.
- (19) Köppe, R.; Bossart, O.; Calzaferri, G.; Sariciftci, N. cells, s. Advanced photon-harvesting concepts for low-energy gap organic solar cells. *Solar Energy Materials and Solar cells* **2007**, *91* (11), 986.
- (20) Gregg, B. A.; Hanna, M. Comparing organic to inorganic photovoltaic cells: Theory, experiment, and simulation. *Journal of Applied Physics* **2003**, *93* (6), 3605.
- (21) Spanggaard, H.; Krebs, F. C. A brief history of the development of organic and polymeric photovoltaics. *Solar Energy Materials and Solar Cells* **2004**, *83* (2), 125.
- (22) Brédas, J.-L.; Norton, J. E.; Cornil, J.; Coropceanu, V. Molecular understanding of organic solar cells: the challenges. *Accounts of Chemical Research* **2009**, *42* (11), 1691.
- (23) Liang, Y.; Xu, Z.; Xia, J.; Tsai, S. T.; Wu, Y.; Li, G.; Ray, C.; Yu, L. For the bright future—bulk heterojunction polymer solar cells with power conversion efficiency of 7.4%. *Advanced Materials* **2010**, *22* (20), E135.
- (24) Friend, R. Conjugated polymers. New materials for optoelectronic devices. *Pure and Applied Chemistry* **2001**, *73* (3), 425.
- (25) Natta, G.; Corradini, P.; Bassi, I. Atti accad. nazl. *Lincei Rend. Classe sci. fis. mat. e nat* **1958**, *25*, 3.

- (26) Ito, T.; Shirakawa, H.; Ikeda, S. Simultaneous polymerization and formation of polyacetylene film on the surface of concentrated soluble Ziegler-type catalyst solution. *Journal of Polymer Science: Polymer Chemistry Edition* **1974**, *12* (1), 11.
- (27) Skotheim, T. A.; Reynolds, J. *Handbook of Conducting Polymers, 2 Volume Set*; CRC press, 2007.
- (28) Heeger, A. J. Semiconducting and metallic polymers: the fourth generation of polymeric materials. *The Journal of Physical Chemistry B* **2001**, *105* (36), 8475.
- (29) Salzner, U.; Lagowski, J.; Pickup, P.; Poirier, R. Comparison of geometries and electronic structures of polyacetylene, polyborole, polycyclopentadiene, polypyrrole, polyfuran, polysilole, polyphosphole, polythiophene, polyselenophene and polytellurophene. *Synthetic Metals* **1998**, *96* (3), 177.
- (30) Ajayaghosh, A. Donor–acceptor type low band gap polymers: polysquaraines and related systems. *Chemical Society Reviews* **2003**, *32* (4), 181.
- (31) Thomas, C. A., University of Florida, 2002.
- (32) Argun, A. A.; Aubert, P.-H.; Thompson, B. C.; Schwendeman, I.; Gaupp, C. L.; Hwang, J.; Pinto, N. J.; Tanner, D. B.; MacDiarmid, A. G.; Reynolds, J. Multicolored electrochromism in polymers: structures and devices. *Chemistry of Materials* **2004**, *16* (23), 4401.
- (33) Singh, A. K.; Prakash, R. 2008 2nd National Workshop on Advanced Optoelectronic Materials and Devices, 2008; p 65.
- (34) Gustafsson, G.; Inganäs, O.; Nilsson, J.; Liedberg, B. Thermal undoping in poly (3-alkylthiophenes). *Synthetic Metals* **1988**, *26* (3), 297.
- (35) Naarmann, H.; Theophilou, N. New process for the production of metal-like, stable polyacetylene. *Synthetic Metals* **1987**, *22* (1), 1.
- (36) Admassie, S.; Inganäs, O.; Mammo, W.; Perzon, E.; Andersson, M. R. Electrochemical and optical studies of the band gaps of alternating polyfluorene copolymers. *Synthetic Metals* **2006**, *156* (7), 614.
- (37) Grigore, L.; Petty, M. Polyaniline films deposited by anodic polymerization: Properties and applications to chemical sensing. *Journal of Materials Science: Materials in Electronics* **2003**, *14* (5-7), 389.
- (38) Fukuda, M.; Sawada, K.; Yoshino, K. Synthesis of fusible and soluble conducting polyfluorene derivatives and their characteristics. *Journal of Polymer Science Part A: Polymer Chemistry* **1993**, *31* (10), 2465.

- (39) Longo, C.; De Paoli, M.-A. Dye-sensitized solar cells: a successful combination of materials. *Journal of the Brazilian Chemical Society* **2003**, *14* (6), 898.
- (40) Chance, R. R.; Bredas, J.; Silbey, R. Bipolaron transport in doped conjugated polymers. *Physical Review B* **1984**, *29* (8), 4491.
- (41) Roncali, J. Synthetic principles for bandgap control in linear π -conjugated systems. *Chemical Reviews* **1997**, *97* (1), 173.
- (42) Van Mullekom, H.; Vekemans, J.; Havinga, E.; Meijer, E. Developments in the chemistry and band gap engineering of donor-acceptor substituted conjugated polymers. *Materials Science and Engineering: R: Reports* **2001**, *32* (1), 1.
- (43) Roncali, J. Molecular engineering of the band gap of π -conjugated systems: Facing technological applications. *Macromolecular Rapid Communications* **2007**, *28* (17), 1761.
- (44) Brédas, J. Relationship between band gap and bond length alternation in organic conjugated polymers. *The Journal of Chemical Physics* **1985**, *82* (8), 3808.
- (45) Cheng, Y.-J.; Yang, S.-H.; Hsu, C.-S. Synthesis of conjugated polymers for organic solar cell applications. *Chemical Reviews* **2009**, *109* (11), 5868.
- (46) Wudl, F.; Kobayashi, M.; Heeger, A. Poly (isothianaphthene). *The Journal of Organic Chemistry* **1984**, *49* (18), 3382.
- (47) Brédas, J.; Heeger, A.; Wudl, F. Towards organic polymers with very small intrinsic band gaps. I. Electronic structure of polyisothianaphthene and derivatives. *The Journal of Chemical Physics* **1986**, *85* (8), 4673.
- (48) Hoogmartens, I.; Adriaensens, P.; Vanderzande, D.; Gelan, J.; Quattrocchi, C.; Lazzaroni, R.; Brédas, J. Low-bandgap conjugated polymers. A joint experimental and theoretical study of the structure of polyisothianaphthene. *Macromolecules* **1992**, *25* (26), 7347.
- (49) Wen, L.; Duck, B. C.; Dastoor, P. C.; Rasmussen, S. C. Poly (2, 3-dihexylthieno [3, 4-b] pyrazine) via GRIM polymerization: simple preparation of a solution processable, low-band-gap conjugated polymer. *Macromolecules* **2008**, *41* (13), 4576.
- (50) Pomerantz, M.; Gu, X. Poly (2-decylthieno [3, 4-b] thiophene). A new soluble low-bandgap conducting polymer. *Synthetic Metals* **1997**, *84* (1), 243.
- (51) Payne, A.-J.; McCahill, J. S.; Welch, G. C. Indoloquinoline as a terminal building block for the construction of π -conjugated small molecules relevant to organic electronics. *Dyes and Pigments* **2015**, *123*, 139.

- (52) Orti, E.; Sanchis, M.; Viruela, P.; Viruela, R. Effects of Carbon-sp³ Bridging on the Electronic Properties of Oligothiophenes. *Synthetic Metals* **1999**, *101* (1), 602.
- (53) Pei, Q.; Zuccarello, G.; Ahlskog, M.; Inganäs, O. Electrochromic and highly stable poly (3, 4-ethylenedioxythiophene) switches between opaque blue-black and transparent sky blue. *Polymer* **1994**, *35* (7), 1347.
- (54) Kitamura, C.; Tanaka, S.; Yamashita, Y. Design of narrow-bandgap polymers. Syntheses and properties of monomers and polymers containing aromatic-donor and o-quinoid-acceptor units. *Chemistry of Materials* **1996**, *8* (2), 570.
- (55) Brocks, G.; Tol, A. Small band gap semiconducting polymers made from dye molecules: polysquaraines. *The Journal of Physical Chemistry* **1996**, *100* (5), 1838.
- (56) Miyaura, N.; Suzuki, A. Palladium-catalyzed cross-coupling reactions of organoboron compounds. *Chemical Reviews* **1995**, *95* (7), 2457.
- (57) Miura, Y.; Oka, H.; Morita, M. Syntheses and Characterization of Poly (1, 3-phenylene-2-amino-1, 3-phenylene) s and Dimer and Tetramer Model Compounds. *Macromolecules* **1998**, *31* (7), 2041.
- (58) Ding, J.; Tao, Y.; Day, M.; Roovers, J.; D'Iorio, M.; Optics, A. Electrochemical and fluorescent properties of alternating copolymers of 9, 9-dioctylfluorene and oxadiazole as blue electroluminescent and electron transport materials. *Journal of Optics A: Pure and Applied Optics* **2002**, *4* (6), S267.
- (59) Morin, J.-F.; Leclerc, M. 2, 7-Carbazole-based conjugated polymers for blue, green, and red light emission. *Macromolecules* **2002**, *35* (22), 8413.
- (60) Yu, W.-L.; Cao, Y.; Pei, J.; Huang, W.; Heeger, A. Blue polymer light-emitting diodes from poly (9, 9-dihexylfluorene-alt-co-2, 5-didecyloxy-para-phenylene). *Applied Physics Letters* **1999**, *75* (21), 3270.
- (61) Liu, B.; Yu, W.-L.; Lai, Y.-H.; Huang, W. Blue-light-emitting fluorene-based polymers with tunable electronic properties. *Chemistry of Materials* **2001**, *13* (6), 1984.
- (62) Waldvogel, S. Strategic Applications of Named Reactions in Organic Synthesis. Background and Detailed Mechanisms. By Laszlo Kürti and Barbara Czako. *Angewandte Chemie International Edition* **2005**, *44* (32), 5005.
- (63) Matos, K.; Soderquist, J. Alkylboranes in the Suzuki–Miyaura coupling: Stereochemical and mechanistic studies. *The Journal of Organic Chemistry* **1998**, *63* (3), 461.

- (64) Hassan, J.; Sevignon, M.; Gozzi, C.; Schulz, E.; Lemaire, M. Aryl–aryl bond formation one century after the discovery of the Ullmann reaction. *Chemical Reviews* **2002**, *102* (5), 1359.
- (65) Stanforth, S. Catalytic cross-coupling reactions in biaryl synthesis. *Tetrahedron* **1998**, *54* (3-4), 263.
- (66) Matsidik, R.; Martin, J.; Schmidt, S.; Obermayer, J.; Lombeck, F.; Nübling, F.; Komber, H.; Fazzi, D.; Sommer, M. C–H Arylation of Unsubstituted Furan and Thiophene with Acceptor Bromides: Access to Donor–Acceptor–Donor-Type Building Blocks for Organic Electronics. *The Journal of Organic Chemistry* **2014**, *80* (2), 980.
- (67) Wang, K.; Wang, M. Direct arylation polymerization: a green, streamlining synthetic approach to π -conjugated polymers. *Current Organic Chemistry* **2013**, *17* (9), 999.
- (68) Schipper, D. J.; Fagnou, K. Direct arylation as a synthetic tool for the synthesis of thiophene-based organic electronic materials. *Chemistry of Materials* **2011**, *23* (6), 1594.
- (69) Facchetti, A.; Vaccaro, L.; Marrocchi, A. Semiconducting polymers prepared by direct arylation polycondensation. *Angewandte Chemie International Edition* **2012**, *51* (15), 3520.
- (70) Okamoto, K.; Zhang, J.; Housekeeper, J. B.; Marder, S. R.; Luscombe, C. C–H arylation reaction: atom efficient and greener syntheses of π -conjugated small molecules and macromolecules for organic electronic materials. *Macromolecules* **2013**, *46* (20), 8059.
- (71) Wakioka, M.; Ichihara, N.; Kitano, Y.; Ozawa, F. A highly efficient catalyst for the synthesis of alternating copolymers with thieno [3, 4-c] pyrrole-4, 6-dione units *via* direct arylation polymerization. *Macromolecules* **2014**, *47* (2), 626.
- (72) Alberico, D.; Scott, M. E.; Lautens, M. Aryl–aryl bond formation by transition-metal-catalyzed direct arylation. *Chemical Reviews* **2007**, *107* (1), 174.
- (73) Chang, S.-Y.; Lin, P.-H.; Liu, C. Pd-catalyzed direct C–H arylation of thieno [3, 4-c] pyrrole-4, 6-dione (TPD): a step-economical synthetic alternative to access TPD-centred symmetrical small molecules. *RSC Advances* **2014**, *4* (68), 35868.
- (74) Gorelsky, S. I.; Lapointe, D.; Fagnou, K. Analysis of the palladium-catalyzed (aromatic) C–H bond metalation–deprotonation mechanism spanning the entire spectrum of arenes. *The Journal of Organic Chemistry* **2011**, *77* (1), 658.

- (75) Mercier, L. G.; Leclerc, M. Direct (hetero) arylation: a new tool for polymer chemists. *Accounts of Chemical Research* **2013**, *46* (7), 1597.
- (76) Katz, E.; Gevorgyan, S.; Orynbayev, M.; Krebs, F. Out-door testing and long-term stability of plastic solar cells. *The European Physical Journal-Applied Physics* **2006**, *36* (3), 307.
- (77) Knobloch, A.; Manuelli, A.; Bernds, A.; Clemens, W. Fully printed integrated circuits from solution processable polymers. *Journal of Applied Physics* **2004**, *96* (4), 2286.
- (78) Wang, G.; Moses, D.; Heeger, A. J.; Zhang, H.-M.; Narasimhan, M.; Demaray, R. Poly (3-hexylthiophene) field-effect transistors with high dielectric constant gate insulator. *Journal of Applied Physics* **2004**, *95* (1), 316.
- (79) Friend, R.; Gymer, R.; Holmes, A.; Burroughes, J.; Marks, R.; Taliani, C.; Bradley, D.; Dos Santos, D.; Bredas, J.; Lögdlund, M. Electroluminescence in conjugated polymers. *Nature* **1999**, *397* (6715), 121.
- (80) Chang, S.-C.; Bharathan, J.; Yang, Y.; Helgeson, R.; Wudl, F.; Ramey, M. B.; Reynolds, J. Dual-color polymer light-emitting pixels processed by hybrid inkjet printing. *Applied Physics Letters* **1998**, *73* (18), 2561.
- (81) Hebner, T.; Wu, C.; Marcy, D.; Lu, M.; Sturm, J. Ink-jet printing of doped polymers for organic light emitting devices. *Applied Physics Letters* **1998**, *72* (5), 519.
- (82) Chang, S. C.; Liu, J.; Bharathan, J.; Yang, Y.; Onohara, J.; Kido, J. Multicolor organic light-emitting diodes processed by hybrid inkjet printing. *Advanced Materials* **1999**, *11* (9), 734.
- (83) Pschenitzka, F.; Sturm, J. Three-color organic light-emitting diodes patterned by masked dye diffusion. *Applied physics letters* **1999**, *74* (13), 1913.
- (84) Rogers, J. A.; Bao, Z.; Raju, V. J. A. p. I. Nonphotolithographic fabrication of organic transistors with micron feature sizes. *Applied Physics Letters* **1998**, *72* (21), 2716.
- (85) Shaheen, S. E.; Radspinner, R.; Peyghambarian, N.; Jabbour, G. Fabrication of bulk heterojunction plastic solar cells by screen printing. *Applied Physics Letters* **2001**, *79* (18), 2996.
- (86) Reyes-Reyes, M.; Kim, K.; Dewald, J.; López-Sandoval, R.; Avadhanula, A.; Curran, S.; Carroll, D. Meso-structure formation for enhanced organic photovoltaic cells. *Organic Letters* **2005**, *7* (26), 5749.
- (87) Lu, H.-H.; Liu, C.-Y.; Jen, T.-H.; Liao, J.-L.; Tseng, H.-E.; Huang, C.-W.; Hung, M.-C.; Chen, S. Excimer formation by electric field induction and side chain motion assistance in polyfluorenes. *Macromolecules* **2005**, *38* (26), 10829.

- (88) Pope, M.; Kallmann, H.; Magnante, P. Electroluminescence in organic crystals. *The Journal of Chemical Physics* **1963**, *38* (8), 2042.
- (89) Burroughes, J.; Bradley, D.; Brown, A.; Marks, R.; Mackay, K.; Friend, R.; Burns, P.; Holmes, A. Light-emitting diodes based on conjugated polymers. *Nature* **1990**, *347* (6293), 539.
- (90) Brütting, W.; Frischeisen, J.; Schmidt, T. D.; Scholz, B. J.; Mayr, C. Device efficiency of organic light-emitting diodes: Progress by improved light outcoupling. *Physica Status Solidi* **2013**, *210* (1), 44.
- (91) Kim, D.; Cho, H.; Kim, C. Blue light emitting polymers. *Progress in Polymer Science* **2000**, *25* (8), 1089.
- (92) Bolognesi, A.; Botta, C.; Facchinetti, D.; Jandke, M.; Kreger, K.; Strohmriegl, P.; Relini, A.; Rolandi, R.; Blumstengel, S. Polarized Electroluminescence in Double-Layer Light-Emitting Diodes with Perpendicularly Oriented Polymers. *Advanced Materials* **2001**, *13* (14), 1072.
- (93) Mitschke, U.; Bäuerle, P. The electroluminescence of organic materials. *Journal of Materials Chemistry* **2000**, *10* (7), 1471.
- (94) Zhang, Y.; Huang, F.; Jen, A. K.; Chi, Y. High-efficiency and solution processible multilayer white polymer light-emitting diodes using neutral conjugated surfactant as an electron injection layer. *Applied Physics Letters* **2008**, *92* (6), 63303.
- (95) Mei, J.; Diao, Y.; Appleton, A. L.; Fang, L.; Bao, Z. Integrated materials design of organic semiconductors for field-effect transistors. *Journal of the American Chemical Society* **2013**, *135* (18), 6724.
- (96) Zaumseil, J.; Sirringhaus, H. Electron and ambipolar transport in organic field-effect transistors. *Chemical Reviews* **2007**, *107* (4), 1296.
- (97) Fortunato, E.; Barquinha, P.; Pimentel, A.; Goncalves, A.; Marques, A.; Pereira, L.; Martins, R. Recent advances in ZnO transparent thin film transistors. *Thin Solid Films* **2005**, *487* (1-2), 205.
- (98) Tsumura, A.; Koezuka, H.; Ando, T. Macromolecular electronic device: Field-effect transistor with a polythiophene thin film. *Applied Physics Letters* **1986**, *49* (18), 1210.
- (99) Koezuka, H.; Tsumura, A.; Ando, T. Field-effect transistor with polythiophene thin film. *Synthetic Metals* **1987**, *18* (1-3), 699.
- (100) Drummond, J. T.; Johnson, G. Selective method for the preparation of isomeric N-alkyl and N-aryl-3 (5)-amino-5 (3)-hydroxy-1H-pyrazole-1-carboxamides. *Journal of Heterocyclic Chemistry* **1988**, *25* (4), 1123.

- (101) Facchetti, A.; Yoon, M. H.; Marks, T. Gate dielectrics for organic field-effect transistors: new opportunities for organic electronics. *Advanced Materials* **2005**, *17* (14), 1705.
- (102) De Boer, B.; Facchetti, A. Semiconducting polymeric materials. *Polymer Reviews* **2008**, *48* (3), 423.
- (103) Brabec, C. J. Organic photovoltaics: technology and market. *Solar Energy Materials and Solar Cells* **2004**, *83* (2-3), 273.
- (104) Zhao, W.; Li, S.; Yao, H.; Zhang, S.; Zhang, Y.; Yang, B.; Hou, J. Molecular optimization enables over 13% efficiency in organic solar cells. *Journal of the American Chemical Society* **2017**, *139* (21), 7148.
- (105) Yuan, J.; Zhang, Y.; Zhou, L.; Zhang, G.; Yip, H.-L.; Lau, T.-K.; Lu, X.; Zhu, C.; Peng, H.; Johnson, P. Single-junction organic solar cell with over 15% efficiency using fused-ring acceptor with electron-deficient core. *Joule* **2019**.
- (106) Cui, Y.; Yao, H.; Zhang, J.; Zhang, T.; Wang, Y.; Hong, L.; Xian, K.; Xu, B.; Zhang, S.; Peng, J. Over 16% efficiency organic photovoltaic cells enabled by a chlorinated acceptor with increased open-circuit voltages. *Nature Communications* **2019**, *10* (1), 2515.
- (107) An, Q.; Ma, X.; Gao, J.; Zhang, F. Solvent additive-free ternary polymer solar cells with 16.27% efficiency. *Science Bulletin* **2019**, *64*, 504.
- (108) Secades, C.; O'Connor, B.; Brown, C.; Walpole, M.; Skidmore, A.; Wang, T. Review of the use of remotely-sensed data for monitoring biodiversity change and tracking progress towards the Aichi Biodiversity Targets: e-book. **2013**.
- (109) Firouzi, R.; Zahedi, M. Polyacenes electronic properties and their dependence on molecular size. *Journal of Molecular Structure* **2008**, *862* (1-3), 7.
- (110) Petritsch, K. *Organic Solar Cell Architectures*; na, 2000.
- (111) Brabec, C. J.; Shaheen, S. E.; Winder, C.; Sariciftci, N. S.; Denk, P. Effect of LiF/metal electrodes on the performance of plastic solar cells. *Applied Physics Letters* **2002**, *80* (7), 1288.
- (112) Glenis, S.; Tourillon, G.; Garnier, F. Influence of the doping on the photovoltaic properties of thin films of poly-3-methylthiophene. *Thin Solid Films* **1986**, *139* (3), 221.
- (113) Glenis, S.; Tourillon, G.; Garnier, F. Influence of the doping on the photovoltaic properties of thin films of poly-3-methylthiophene. *Thin Solid Films* **1986**, *139* (3), 221.

- (114) Karg, S.; Riess, W.; Dyakonov, V.; Schwoerer, M. Electrical and optical characterization of poly (phenylene-vinylene) light emitting diodes. *Synthetic Metals* **1993**, *54* (1-3), 427.
- (115) Peumans, P.; Yakimov, A.; Forrest, S. R. Small molecular weight organic thin-film photodetectors and solar cells. *Journal of Applied Physics* **2003**, *93* (7), 3693.
- (116) Tang, C. W. Two-layer organic photovoltaic cell. *Applied Physics Letters* **1986**, *48* (2), 183.
- (117) Günes, S.; Neugebauer, H.; Sariciftci, N. S. Conjugated polymer-based organic solar cells. *Chemical Reviews* **2007**, *107* (4), 1324.
- (118) Peumans, P.; Forrest, S. Very-high-efficiency double-heterostructure copper phthalocyanine/C60 photovoltaic cells. *Applied Physics Letters* **2001**, *79* (1), 126.
- (119) Xue, J.; Uchida, S.; Rand, B. P.; Forrest, S. R. Asymmetric tandem organic photovoltaic cells with hybrid planar-mixed molecular heterojunctions. *Applied Physics Letters* **2004**, *85* (23), 5757.
- (120) Halls, J.; Walsh, C.; Greenham, N.; Marseglia, E.; Friend, R.; Moratti, S.; Holmes, A. Efficient photodiodes from interpenetrating polymer networks. *Nature* **1995**.
- (121) Geens, W.; Aernouts, T.; Poortmans, J.; Hadziioannou, G. Organic co-evaporated films of a PPV-pentamer and C60: model systems for donor/acceptor polymer blends. *Thin Solid Films* **2002**, *403*, 438.
- (122) Yu, G.; Gao, J.; Hummelen, J. C.; Wudl, F.; Heeger, A. J. Polymer photovoltaic cells: Enhanced efficiencies via a network of internal donor-acceptor heterojunctions. *Science* **1995**, *270* (5243), 1789.
- (123) Boudreault, P.-L. T.; Najari, A.; Leclerc, M. Processable low-bandgap polymers for photovoltaic applications†. *Chemistry of Materials* **2010**, *23* (3), 456.
- (124) Gebeyehu, D.; Maennig, B.; Drechsel, J.; Leo, K.; Pfeiffer, M. Bulk-heterojunction photovoltaic devices based on donor–acceptor organic small molecule blends. *Solar Energy Materials and Solar Cells* **2003**, *79* (1), 81.
- (125) Cai, W.; Gong, X.; Cao, Y. cells, s. Polymer solar cells: recent development and possible routes for improvement in the performance. *Solar Energy Materials and Solar Cells* **2010**, *94* (2), 114.
- (126) Son, H. J.; He, F.; Carsten, B.; Yu, L. Are we there yet? Design of better conjugated polymers for polymer solar cells. *Journal of Materials Chemistry* **2011**, *21* (47), 18934.

- (127) Thompson, B. C.; Fréchet, J. Polymer–fullerene composite solar cells. *Angewandte Chemie International Edition* **2008**, *47* (1), 58.
- (128) Yeh, N.; Yeh, P. Organic solar cells: Their developments and potentials. *Renewable and Sustainable Energy Reviews* **2013**, *21*, 421.
- (129) Chen, S.; Du, X.; Ye, G.; Cao, J.; Sun, H.; Xiao, Z.; Ding, L. Thermo-cleavable fullerene materials as buffer layers for efficient polymer solar cells. *Journal of Materials Chemistry A* **2013**, *1* (37), 11170.
- (130) Wang, G.; Swensen, J.; Moses, D.; Heeger, A. Increased mobility from regioregular poly (3-hexylthiophene) field-effect transistors. *Journal of Applied Physics* **2003**, *93* (10), 6137.
- (131) He, Z.; Zhong, C.; Su, S.; Xu, M.; Wu, H.; Cao, Y. Enhanced power-conversion efficiency in polymer solar cells using an inverted device structure. *Nature Photonics* **2012**, *6* (9), 591.
- (132) You, J.; Dou, L.; Yoshimura, K.; Kato, T.; Ohya, K.; Moriarty, T.; Emery, K.; Chen, C.-C.; Gao, J.; Li, G. J. N. c. A polymer tandem solar cell with 10.6% power conversion efficiency. *Nature Communications* **2013**, *4*, 1446.
- (133) Lin, Y.; Wang, J.; Zhang, Z. G.; Bai, H.; Li, Y.; Zhu, D.; Zhan, X. An electron acceptor challenging fullerenes for efficient polymer solar cells. *Advanced Materials* **2015**, *27* (7), 1170.
- (134) Li, Y.; Singh, S. P.; Sonar, P. A High Mobility P-Type DPP-Thieno [3, 2-b] thiophene Copolymer for Organic Thin-Film Transistors. *Advanced Materials* **2010**, *22* (43), 4862.
- (135) Tsao, H. N.; Cho, D. M.; Park, I.; Hansen, M. R.; Mavrinskiy, A.; Yoon, D. Y.; Graf, R.; Pisula, W.; Spiess, H. W.; Müllen, K. Ultrahigh mobility in polymer field-effect transistors by design. *Journal of the American Chemical Society* **2011**, *133* (8), 2605.
- (136) Bürgi, L.; Turbiez, M.; Pfeiffer, R.; Bienewald, F.; Kirner, H. J.; Winnewisser, C. High-mobility ambipolar near-infrared light-emitting polymer field-effect transistors. *Advanced Materials* **2008**, *20* (11), 2217.
- (137) Luo, Z.; Bin, H.; Liu, T.; Zhang, Z. G.; Yang, Y.; Zhong, C.; Qiu, B.; Li, G.; Gao, W.; Xie, D. Fine-Tuning of Molecular Packing and Energy Level through Methyl Substitution Enabling Excellent Small Molecule Acceptors for Nonfullerene Polymer Solar Cells with Efficiency up to 12.54%. *Advanced Materials* **2018**, *30* (9), 1706124.
- (138) Xu, X.; Bi, Z.; Ma, W.; Wang, Z.; Choy, W. C.; Wu, W.; Zhang, G.; Li, Y.; Peng, Q. Highly efficient ternary-blend polymer solar cells enabled by a nonfullerene acceptor

- and two polymer donors with a broad composition tolerance. *Advanced Materials* **2017**, *29* (46), 1704271.
- (139) Yao, Z.; Liao, X.; Gao, K.; Lin, F.; Xu, X.; Shi, X.; Zuo, L.; Liu, F.; Chen, Y.; Jen, A. Dithienopicenocarbazole-based acceptors for efficient organic solar cells with optoelectronic response over 1000 nm and an extremely low energy loss. *Journal of the American Chemical Society* **2018**, *140* (6), 2054.
- (140) Jiang, W.; Yu, R.; Liu, Z.; Peng, R.; Mi, D.; Hong, L.; Wei, Q.; Hou, J.; Kuang, Y.; Ge, Z. Ternary nonfullerene polymer solar cells with 12.16% efficiency by introducing one acceptor with cascading energy level and complementary absorption. *Advanced Materials* **2018**, *30* (1), 1703005.
- (141) Kan, B.; Zhang, J.; Liu, F.; Wan, X.; Li, C.; Ke, X.; Wang, Y.; Feng, H.; Zhang, Y.; Long, G. Fine-Tuning the Energy Levels of a Nonfullerene Small-Molecule Acceptor to Achieve a High Short-Circuit Current and a Power Conversion Efficiency over 12% in Organic Solar Cells. *Advanced Materials* **2018**, *30* (3), 1704904.
- (142) Cheng, P.; Li, G.; Zhan, X.; Yang, Y. Next-generation organic photovoltaics based on non-fullerene acceptors. *Nature Photonics* **2018**, *12* (3), 131.
- (143) Bian, L.; Zhu, E.; Tang, J.; Tang, W.; Zhang, F. Recent progress in the design of narrow bandgap conjugated polymers for high-efficiency organic solar cells. *Progress in Polymer Science* **2012**, *37* (9), 1292.
- (144) Haruk, A.; Mativetsky, J. Supramolecular approaches to nanoscale morphological control in organic solar cells. *International Journal of Molecular Sciences* **2015**, *16* (6), 13381.
- (145) Elumalai, N. K.; Uddin, A. Open circuit voltage of organic solar cells: an in-depth review. *Energy & Environmental Science* **2016**, *9* (2), 391.
- (146) Al-Khazzar, A. Behavior of Four Solar PV Modules with Temperature Variation. *International Journal of Renewable Energy Research (IJRER)* **2016**, *6* (3), 1091.
- (147) Qi, B.; Wang, J. Fill factor in organic solar cells. *Physical Chemistry Chemical Physics* **2013**, *15* (23), 8972.
- (148) Mihailetschi, V.; Wildeman, J.; Blom, P. Space-charge limited photocurrent. *Physical Review Letters* **2005**, *94* (12), 126602.
- (149) Dongaonkar, S.; Servaites, J. D.; Ford, G. M.; Loser, S.; Moore, J.; Gelfand, R. M.; Mohseni, H.; Hillhouse, H. W.; Agrawal, R.; Ratner, M. Universality of non-Ohmic shunt leakage in thin-film solar cells. *Journal of Applied Physics* **2010**, *108* (12), 124509.

- (150) Jeong, W. I.; Lee, J.; Park, S. Y.; Kang, J. W.; Kim, J. Reduction of collection efficiency of charge carriers with increasing cell size in polymer bulk heterojunction solar cells. *Advanced Functional Materials* **2011**, *21* (2), 343.
- (151) Frolova, L.A., Chang, Q., Luchkin, S.Y., Zhao, D., Akbulatov, A.F., Dremova, N.N., Ivanov, A.V., Chia, E.E., Stevenson, K.J. and Troshin, P.A., 2019. Efficient and stable all-inorganic perovskite solar cells based on nonstoichiometric Cs_xPbI₂Br_x (x > 1) alloys. *Journal of Materials Chemistry C*, *7*(18), pp.5314-5323.
- (152) Dubey, A., Adhikari, N., Mabrouk, S., Wu, F., Chen, K., Yang, S. and Qiao, Q., 2018. A strategic review on processing routes towards highly efficient perovskite solar cells. *Journal of Materials Chemistry A*, *6*(6), pp.2406-2431.
- (153) Song, Z., Wathage, S.C., Phillips, A.B. and Heben, M.J., 2016. Pathways toward high-performance perovskite solar cells: review of recent advances in organo-metal halide perovskites for photovoltaic applications. *Journal of Photonics for Energy*, *6*(2), p.022001.
- (154) Gupta, D.; Bag, M.; Narayan, K. Area dependent efficiency of organic solar cells. *Applied Physics Letters* **2008**, *93* (16), 384.
- (155) Duan, C.; Huang, F.; Cao, Y. Recent development of push-pull conjugated polymers for bulk-heterojunction photovoltaics: rational design and fine tailoring of molecular structures. *Journal of Materials Chemistry* **2012**, *22* (21), 10416.
- (156) Cartwright, L.; Iraqi, A.; Zhang, Y.; Wang, T.; Lidzey, D. Impact of fluorine substitution upon the photovoltaic properties of benzothiadiazole-fluorene alternate copolymers. *RSC Advances* **2015**, *5* (57), 46386.

Chapter 2:-

Design and synthesis of furan-based polymers for photovoltaic applications

Chapter 2 - Design and synthesis of furan-based polymers for photovoltaic applications

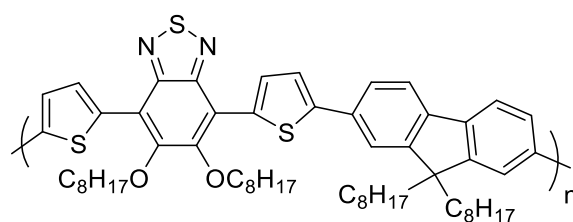
2.1 Introduction

In the last few decades, researchers have focused significant attention on polymer photovoltaics – those which have an active layer of conjugated polymer. This is due to their various features that have opened promising avenues for application. These include the fact that they are lightweight, flexible and cheaper than the more commonly used inorganic materials typically found in solar cells. In order to choose appropriate polymers to be applied in the manufacture of solar cells, excellent electronic and physical properties must be found. These include the extent of sunlight absorption and the HOMO and LUMO energy levels. In solar cell devices that blend a polymer as donor and fullerene derivative as acceptor, close attention must be paid to their morphology to attain the highest possible charge mobility and effective exciton dissociation¹⁻³.

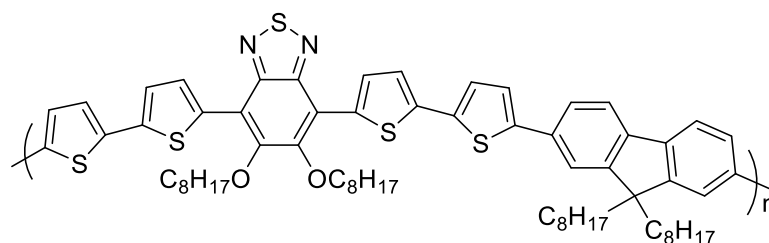
One key consideration with such novel photovoltaics is the band gap of the components in blends due to their role in enhancing power conversion efficiency (PCE%). To date, researchers have enhanced organic solar cells and the engineering of their band gap so that power conversion efficiency has exceeded 11%⁴. It has also been discovered that there is an inverse relationship between the band gap of polymers and their PCE%. In other words, when the polymer has a low band gap, it absorbs more sunlight, leading to improvements in the power conversion efficiency⁵⁻⁸. To this end, the band gap of certain polymers can be adjusted over the visible range if the structure allows it, as with D-A copolymers⁹, or by changing the side-chains of polymers¹⁰. Moreover, conjugated polymers with alternating donor-acceptor monomers can be used to adjust the polymer's bandgap by governing the intramolecular charge transfer (ICT)¹¹⁻¹³. As has been previously noted, to achieve the best PCE%, the band gap and the HOMO and LUMO energy levels of the polymer should be developed^{14,15}.

Researchers have attempted to prepare low-band-gap-conjugated polymers able to absorb a broad range of the spectrum of light using a wide variety of methods. A significant number of conjugated polymers contain benzothiadiazole (BTD) moiety due to the thiadiazole units. These allow withdrawal of the electrons to the conjugated polymer's backbone¹⁶. Studies have also shown that polymers possessing good features, such as low band gaps and excellent charge transfer, can be created by linking the BTD unit as a strong electron acceptor with a

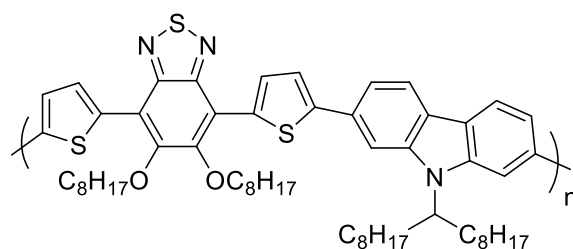
suitable electron donor¹⁷⁻²⁰. In fact, the majority of research has focused on thiophene-based conjugated polymers to create high-performance devices with a much lesser amount focusing on nonthiophene-based conjugated polymers²¹. Specific examples of the former include the conjugated polymer **PFDTBT-8**, which has the structure of alternating fluorene units flanked by thiophene units and benzothiadiazole units. Its band gap is 2.12 eV with a HOMO level of -5.44 eV and LUMO level of -3.32 eV²². As a comparison, with alternating fluorene units flanked by bithiophene units and benzothiadiazole units in **PFDT2BT-8**, a band gap of 1.99 eV with a HOMO level of -5.33 eV and LUMO level of -3.34 eV was noted. It should also be noted that the addition of an extra thiophene ring along the polymer backbone caused the bandgap value to reduce by compared with having only one thiophene ring²³. **PCDTBT-8**, which has the same acceptor as the **PFDTBT-8** but with carbazole instead of fluorene, has shown a band gap of 2.13 eV with a HOMO level of -5.40 eV and LUMO level of -3.27 eV²⁴. See Figure 2.1 for diagrams of each of the polymer's structures.



PFDTBT-8



PFDT2BT-8



PCDTBT-8

Figure 2.1: The structures of **PFDTBT-8**, **PFDT2BT-8** and **PCDTBT-8**²²⁻²⁴.

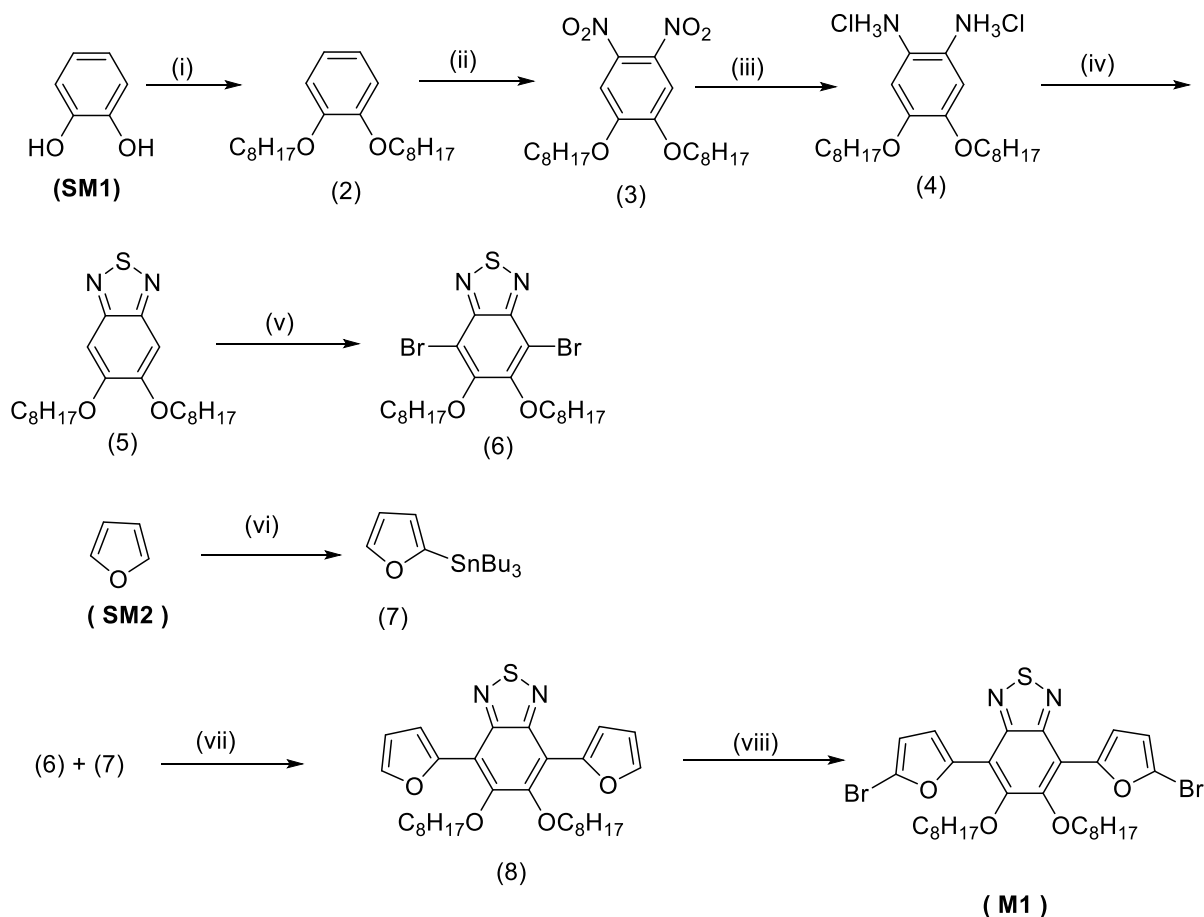
In other research, Woo *et al.* used furan instead of thiophene to create conjugated polymer solar cells²⁵. They found that polymers with furan displayed electronic and optical properties that were similar to those of their thiophene analogous polymers²⁵⁻²⁷. One of the key reasons for the use of furan units to create such polymers is the electronegativity of oxygen atoms being stronger than that of sulfur atoms. This leads to the probability that the HOMO level of polymers can be decreased through the addition of furan units. In addition, furan derivatives can be prepared from natural products. This translates into polymer synthesis being simpler, cheaper and more sustainable than when using thiophene. Indeed, the functions and properties of furans in conjugated polymers have encouraged researchers to synthesise more furan-containing polymers, and this is an ongoing area of interest.

The synthesis and analysis of three novel polymers are reported in this chapter. These are fluorene-*alt*- benzothiadiazole and carbazole-*alt*-benzothiadiazole D-A copolymers, poly[9,9-dioctyl-9*H*-fluorene-2,7-diyl-*alt*-(5,6-bis(octyloxy)-4,7-di-2-furanyl-2,1,3-benzothiadiazole)-5,5-diyl] (**P1**) , poly[9,9-dioctyl-9*H*-fluorene-2,7-diyl-*alt*-(5,6-bis(octyloxy)-4,7-di(2,2'-bifuran-5-yl)benzo[c][1,2,5] thiadiazole)-5,5-diyl] (**P2**), and poly[9-(heptadecan-9-yl)-9*H*-carbazole-2,7-diyl-*alt*-(5,6-bis(octyloxy)-4,7-di-2-furanyl-2,1,3-benzothiadiazole)-5,5-diyl] (**P3**). The solubility of these was enhanced by introducing octyloxy chains at the 5, 6-positions of the BT moieties. This in turn increased the planarity of the polymers' backbone, as discovered in previous literature²⁸. The synthesised polymers **P1**, **P2** and **P3** were analysed using GPC, UV-vis absorption, TGA, CV and XRD and the results of the various analyses are compared with analogous polymers **PFDTBT-8**, **PFDT2BT-8** and **PCDTBT-8**, respectively, all of which contained thiophene units instead of furan units.

2.2 Results and discussion

2.2.1 Synthesis of monomers

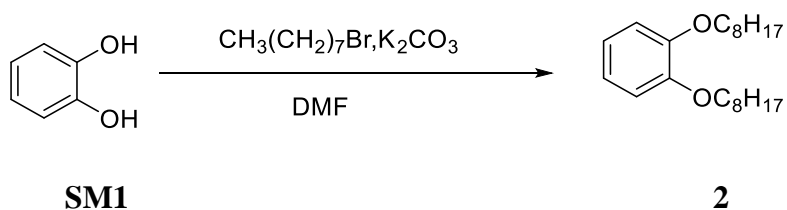
The methods of synthesising the acceptor and donors presented in this chapter are shown in the scheme below.



(i) 1-Bromooctane, K_2CO_3 , dry DMF, $100^\circ C$. (ii) Solution of acetic acid, DCM, $10^\circ C$, 65% nitric acid, fuming nitric acid, r.t 40 h. (iii) Tin (II) chloride, conc.HCl, ethanol, $85^\circ C$ overnight. (iv) Et_3N , $SOCl_2$, DCM, reflux at $45^\circ C$ overnight. (v) Br_2 , acetic acid, DCM, dark r.t 48h.(vi) n-BuLi, Dry THF, $-78^\circ C$ for 2h, $40^\circ C$, Bu_3SnCl , r.t overnight. (vii) $Pd(OAc)_2$, tri-*o*-tolylphosphine, dry Toluene, $115^\circ C$ for 48h. (viii) NBS, dry $CHCl_3$, glacial acetic acid, dark at $60^\circ C$ for 24h.

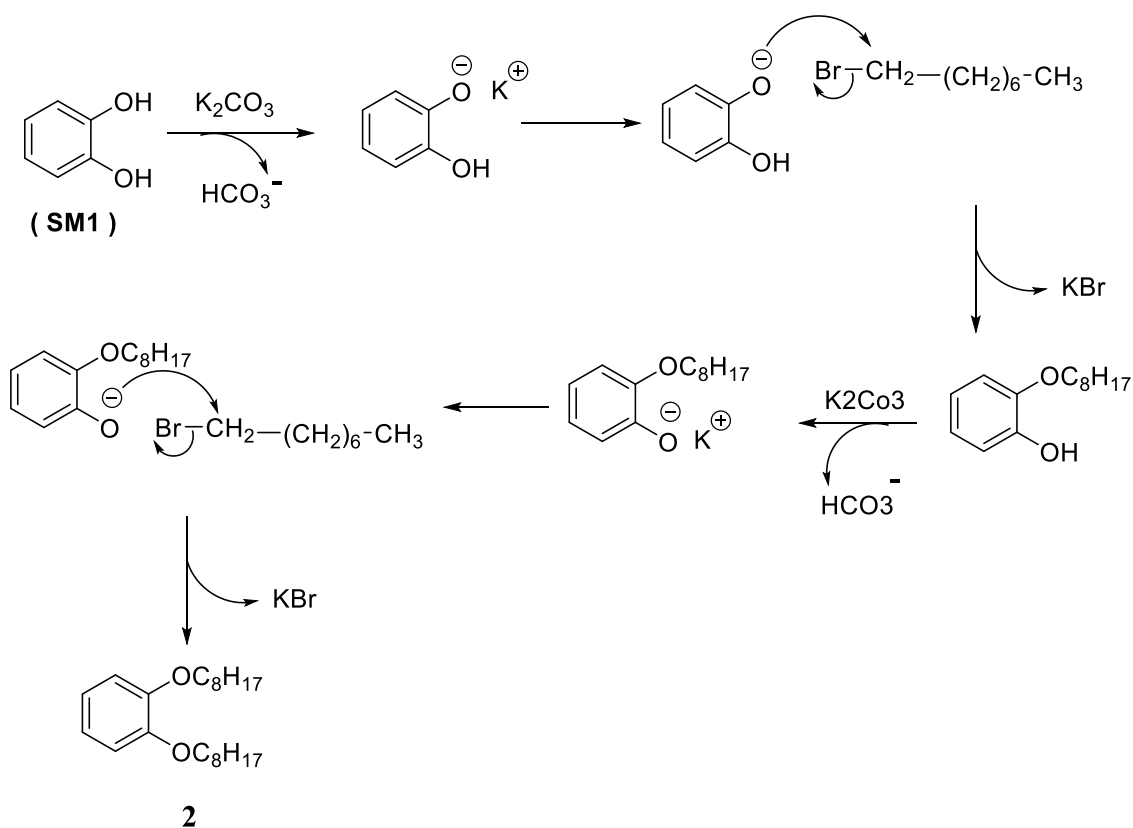
Scheme 2.1: Synthesis of M1 acceptor.

1,2-Bis(octyloxy)benzene (**2**) was prepared using the modified procedure reported by Zhang *et al.*²⁹. Using this method, synthesis starts with an alkylation reaction between catechol (**SM1**) and 1-bromooctane, and the base potassium carbonate. The reaction mixture was left at reflux at 100°C overnight. The subsequent purification procedure occurred *via* recrystallising of the product in methanol to obtain product (**2**) in a good yield (66%) as white needle-shaped crystals. The purity and the structure of the product (**2**) was confirmed by, ¹H NMR, ¹³C NMR, elemental analysis and mass spectrometry. The elemental analysis confirmed the structure of the product. The mass spectrum show the main integer mass at 334 (M⁺) which is in agreement with the proposed structure.



Scheme 2.2: Synthesis of 1,2-bis(octyloxy)benzene.

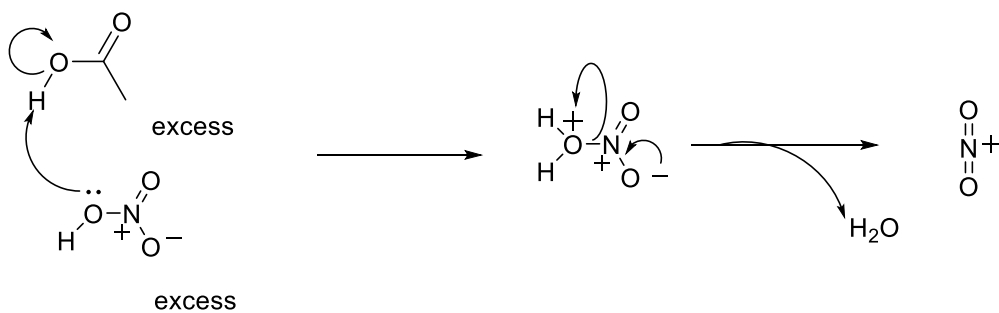
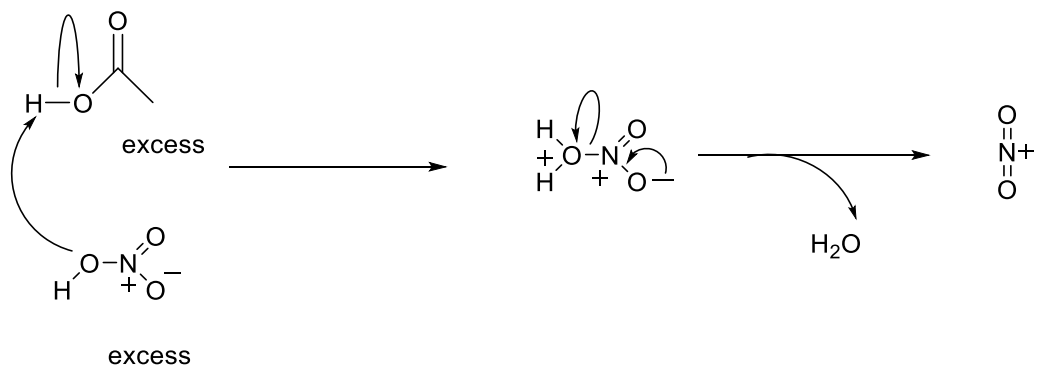
The mechanism of this reaction follows the bimolecular nucleophilic substitution (S_N2), as shown in Scheme 2.3. below. Initially the hydroxyl group was deprotonated by the base (K₂CO₃) to generate the phenoxide ion nucleophile. This attacked 1-bromooctane to give the desired product.



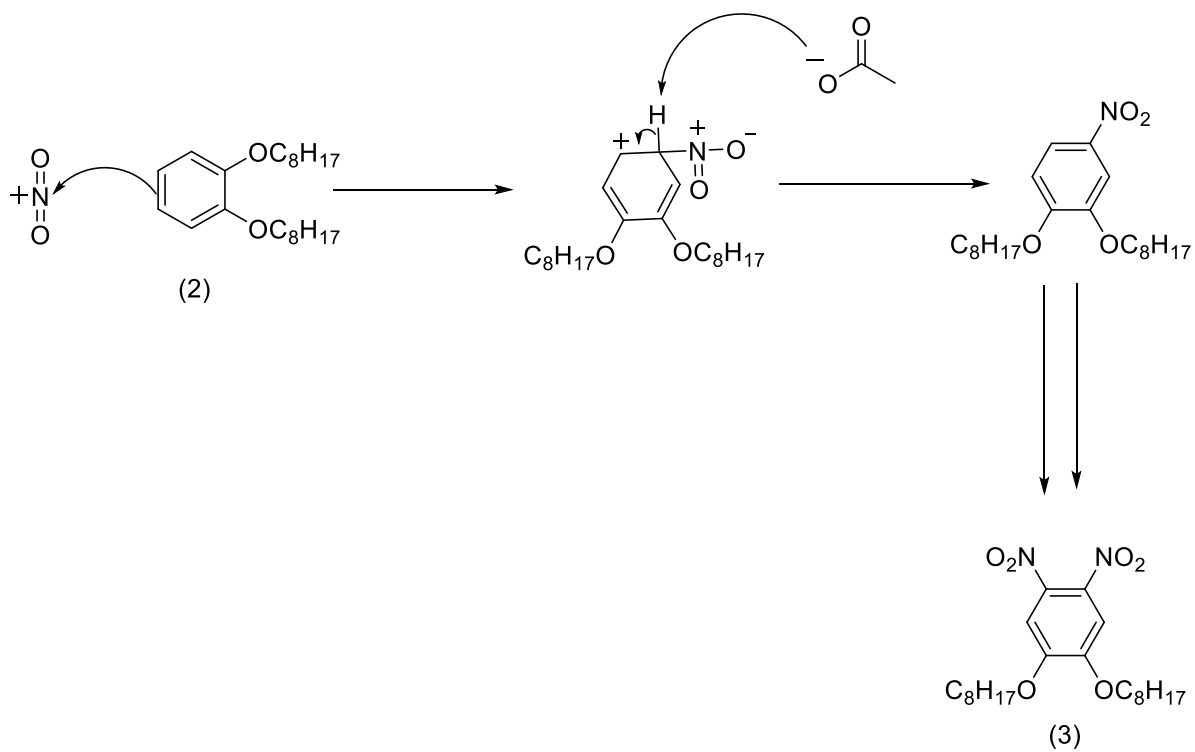
Scheme 2.3: The mechanism of alkylation reaction *via* nucleophilic substitution.

This step was followed by nitration of compound **(2)** by reacting nitric acid in acetic acid to yield compound **(3)**. The product was then separated as yellow crystals after purification of the mixture by recrystallising it in ethanol in yield (64%). The purity and the structure of the product **(3)** was confirmed by, ^1H NMR, ^{13}C NMR, elemental analysis and mass spectrometry. The elemental analysis confirmed the structure of the product. The mass spectrum show the main integer mass at 423 (M^+) which is in agreement with the proposed structure. The proposed mechanism of this nitration reaction is represented in Scheme 2.4. below and can be divided into two steps: firstly, production of the electrophile (nitronium ion) by reacting acetic acid with nitric acid; and secondly, electrophilic aromatic substitution.

Step 1: Formation of the electrophile:



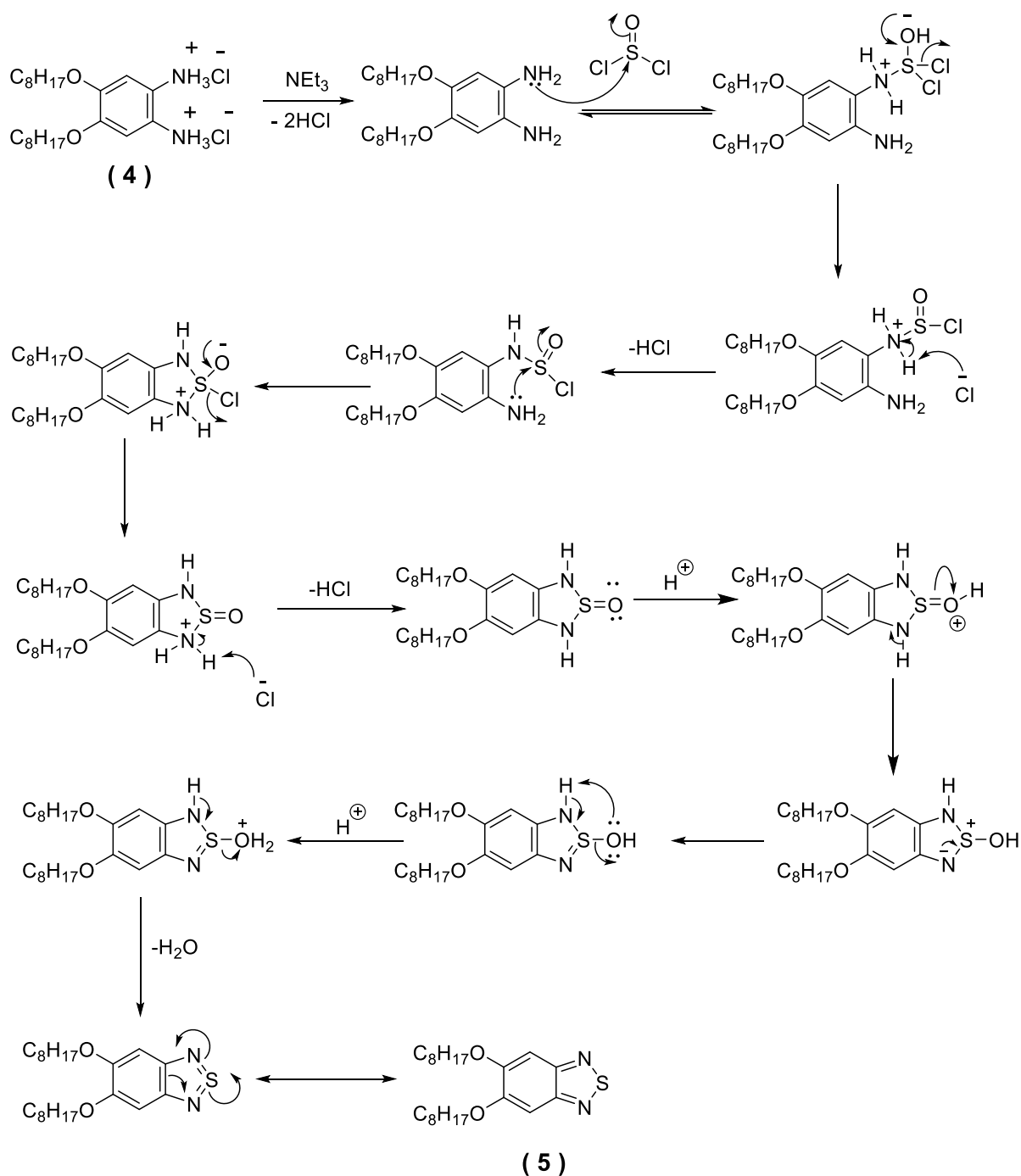
Step 2: Electrophilic aromatic substitution:



Scheme 2.4: Mechanism of the nitration reaction.

In the third step, tin (II) chloride and hydrochloric acid was used to reduce the two nitro groups in compound **(3)** to obtain 4,5-bis(octyloxy)benzene-1,2-diammonium chloride **(4)** as hydrochloride salt in the form of a white powder. Water was used to wash the precipitate that formed during the reaction. This removed any excess acid present in the reaction mixture. The product was then washed using ethanol. As a result of its unstable nature, the resulting product was obtained in a good yield (85%) then immediately used rather than first being purified.

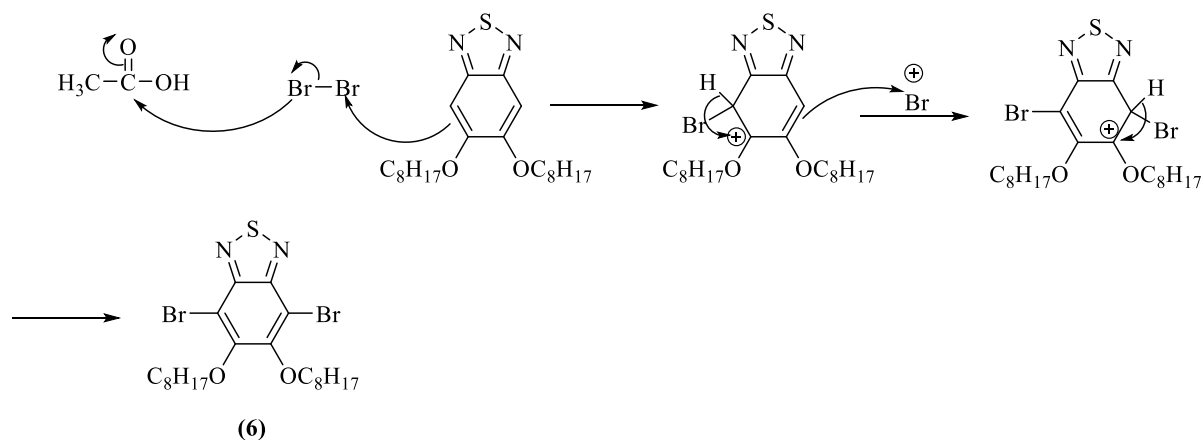
Compound **(4)** was reacted with thionyl chloride and triethylamine to produce 5,6-bis(octyloxy)benzo[c][1,2,5] thiadiazole **(5)** as a brown solid. The reaction was heated to 45°C overnight and then purified by recrystallising it in ethanol to yield it as a brown solid in yield (70%). The purity and the structure of the product **(5)** was confirmed by, ¹H NMR, ¹³C NMR, elemental analysis and mass spectrometry. The elemental analysis confirmed the structure of the product. The mass spectrum show the main integer mass at 392 (M⁺) which is in agreement with the proposed structure. The mechanism of the reaction proceeded in four steps. Firstly, the base triethylamine was used to remove any hydrogen chloride present in compound **(4)**. Secondly, nucleophilic attack by the amine groups on the highly electrophilic sulphur of thionyl chloride followed. Thirdly, a cyclisation reaction occurred to form the benzothiadiazole ring. Finally, water was removed to obtain product **(5)**. Scheme 2.5. illustrates the mechanism of this reaction.



Scheme 2.5: The mechanism of ring closure reaction of synthesis (5).

Compound (6) was prepared by bromination of compound (5) at the 4,7-positions using Br₂ in acetic acid and DCM. The electrophilicity of the bromine was increased using acetic acid and the product was yielded as a white solid in a good yield (84%) after being purified by recrystallisation using ethanol. The purity and the structure of the product (6) was confirmed by, ¹H NMR, ¹³C NMR, elemental analysis and mass spectrometry. The elemental analysis

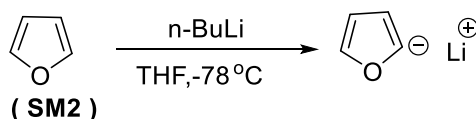
confirmed the structure of the product. The mass spectrum show the main integer mass at 550 (M^+) which is in agreement with the proposed structure.



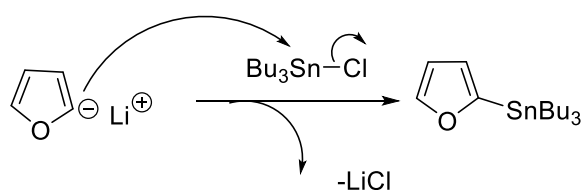
Scheme 2.6: The mechanism of bromination of (5) to synthesis (6).

Reaction of furan (**SM2**) with *n*-butyl lithium (2.5 M in hexane) in dry THF at -78°C occurred before tributyltin chloride was added to obtain tributyl(furan-2-yl)stannane (**7**) as a yellow liquid in a good yield (93%). The reaction mechanism comprised two steps. Firstly, the 5-position of furan was deprotonated using *n*-BuLi to generate the anion. Secondly, the anion carried out a nucleophilic substitution on Bu_3SnCl by displacing chloride to obtain the product. This is shown in Scheme 2.7. The purity and the structure of the product (**7**) was confirmed by, ^1H NMR, ^{13}C NMR, elemental analysis and mass spectrometry. The elemental analysis confirmed the structure of the product. The mass spectrum show the main integer mass at 357.8 (M^+) which is in agreement with the proposed structure.

First:

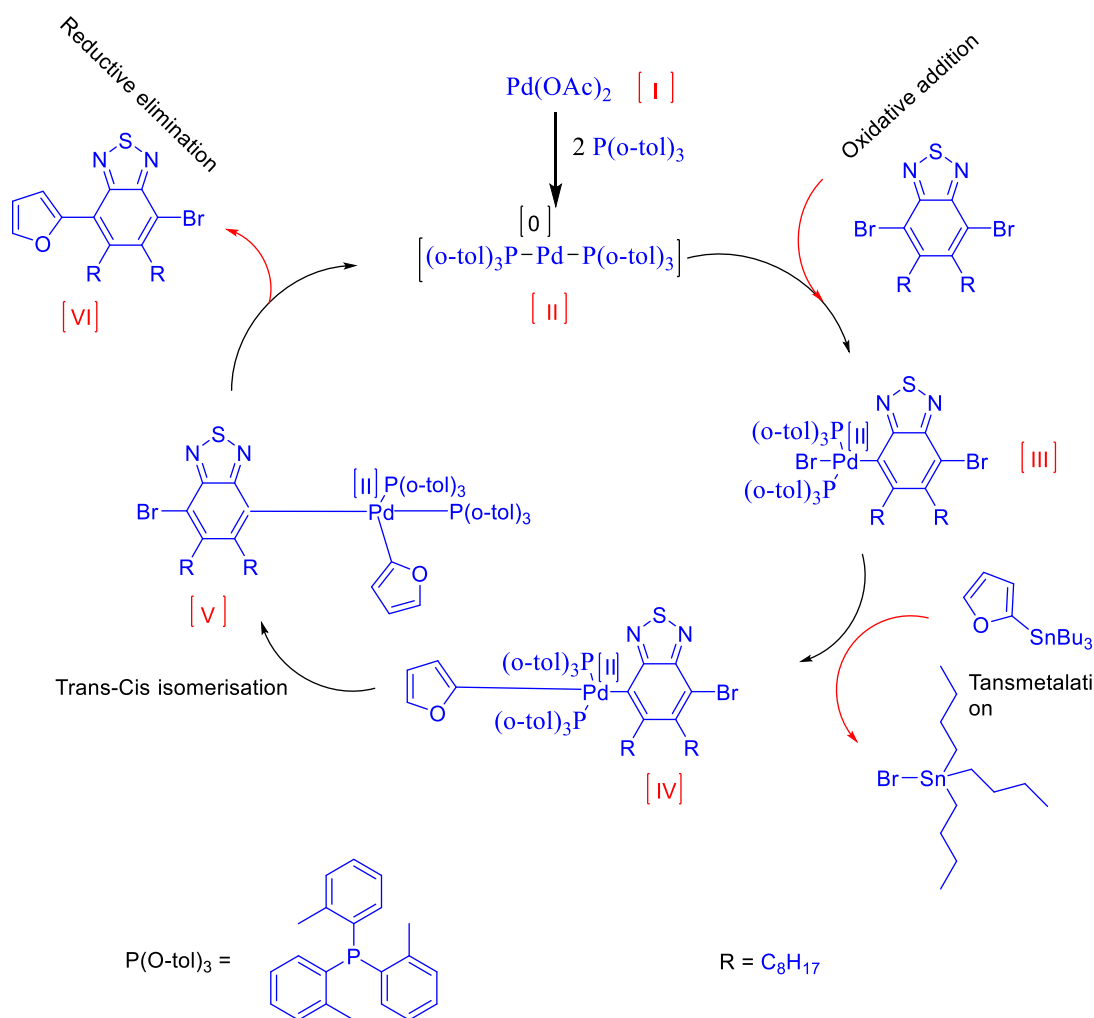


Second:



Scheme 2.7: The mechanism of synthesis of (7).

Product (8) was synthesised using the Stille coupling reaction³⁰. This coupling formed a C-C bond and occurred in the presence of a palladium catalyst between an arylstannanes and an aryl halide. The Stille coupling catalytic cycle comprises four steps: an oxidative addition, a transmetalation, a trans / cis isomerisation, and a reductive elimination, as shown in scheme 2.8. The ratio between compound (6) to compound (7) was 1:2.5. The compounds were reacted in dry toluene at a temperature of 115°C for 48 hours. Pd (OAc)₂ and tri-*o*-tolylphosphine were used to catalyse the reaction and the ratio between them was 1:2 respectively. 5,6 Bis(octyloxy)-4,7-di(furan-2-yl)benzo[*c*][1,2,5]thiadiazole (8) in the form of a dark brown liquid in an excellent yield (95%) was produced following purification by column chromatography (petroleum ether / DCM, gradient 4/1)³¹.



Scheme 2.8: The Stille coupling cycle to synthesise (8).

The purity and the structure of the product (**8**) was confirmed by, ^1H NMR, ^{13}C NMR, elemental analysis and mass spectrometry. The elemental analysis confirmed the structure of the product. The mass spectrum show the main integer mass at 524 (M^+) which is in agreement with the proposed structure.

The final step included the bromination of compound (**8**) with N-bromosuccinimide (NBS) in glacial acetic acid and CHCl_3 to produce 4, 7- bis (5-bromofuran-2-yl)-5, 6-bis (octyloxy) benzo [c] [1,2,5] thiadiazole (**M1**) as an orange solid in a yield (60%) after purification through column chromatography. The purity and the structure of (**M1**) was confirmed by, ^1H NMR, ^{13}C NMR, elemental analysis and mass spectrometry. The elemental analysis confirmed the structure of the product. The mass spectrum show the main integer mass at 682 (M^+) which is in agreement with the proposed structure. The ^1H NMR gave two different environments as expected in the aromatic region. In addition, ^1H NMR gave different peaks as expected in aliphatic area as shown in Figure 2.2.

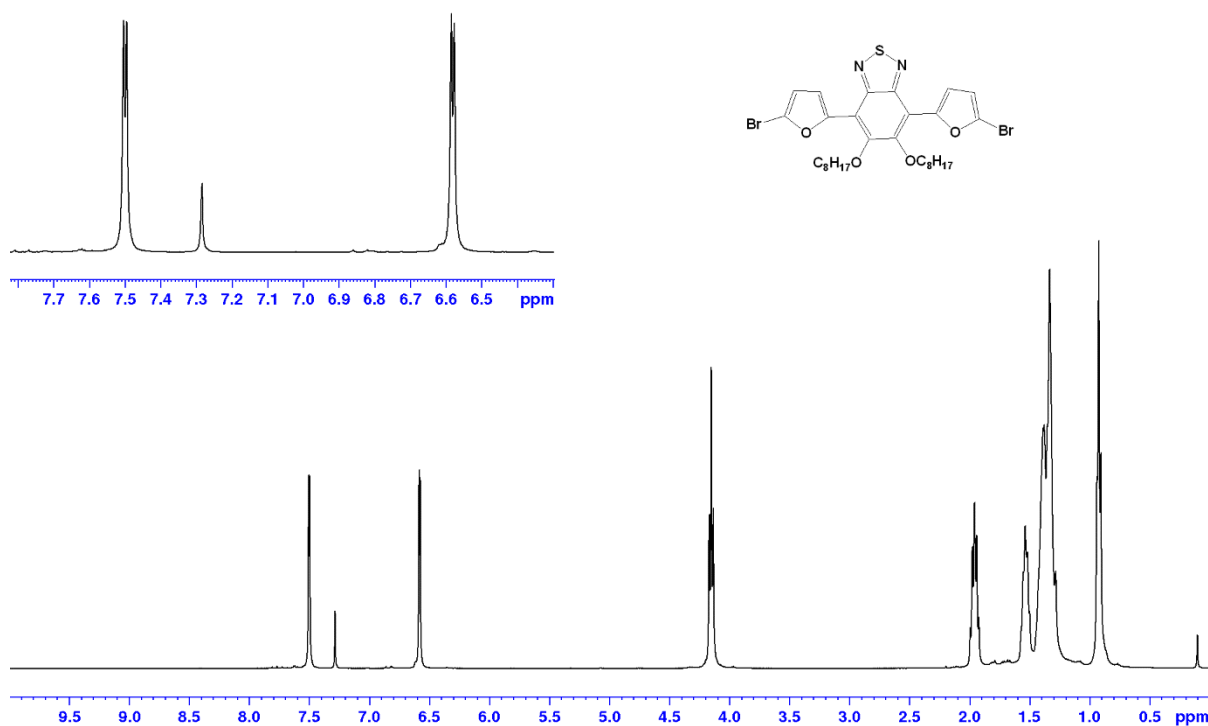
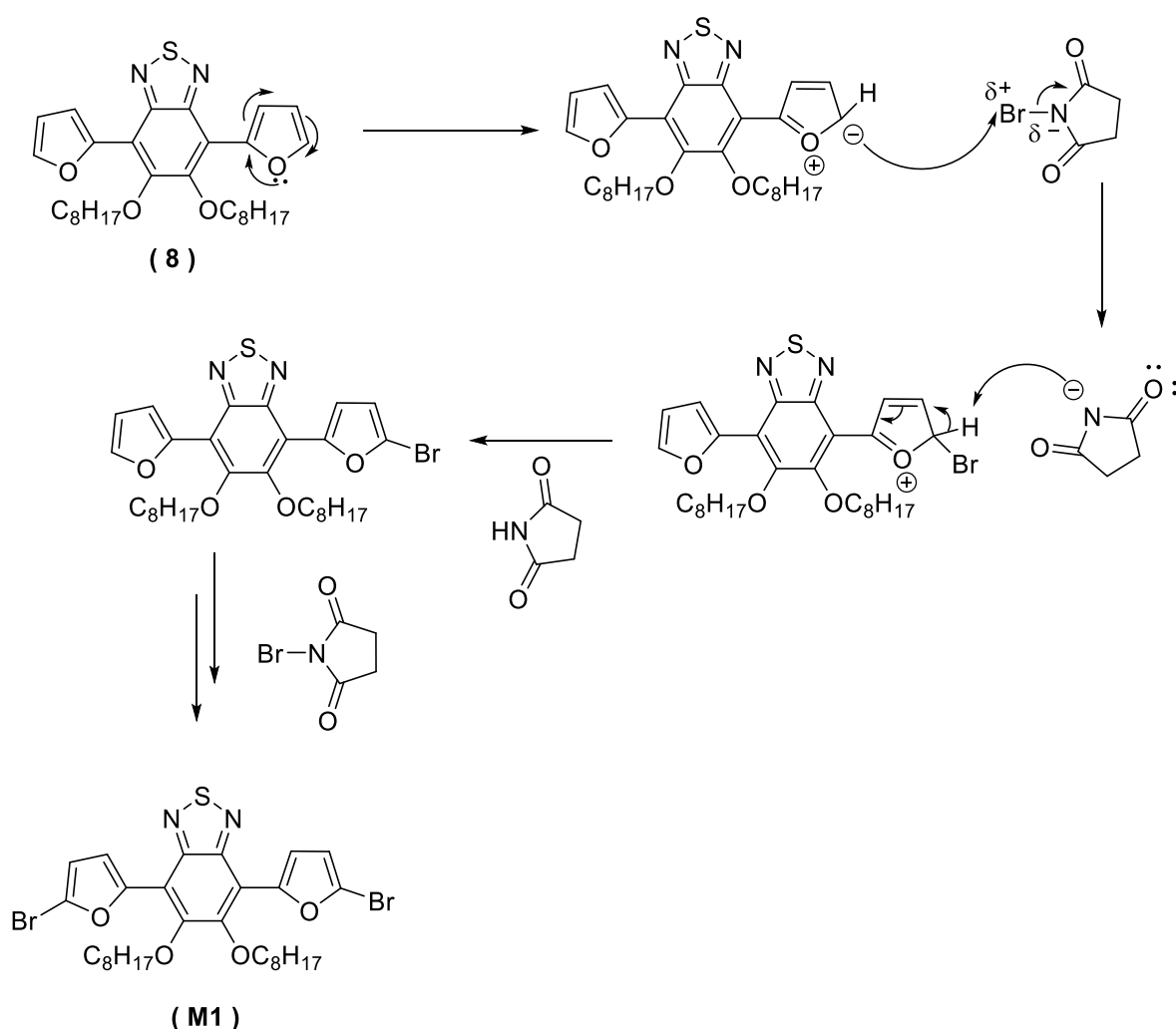


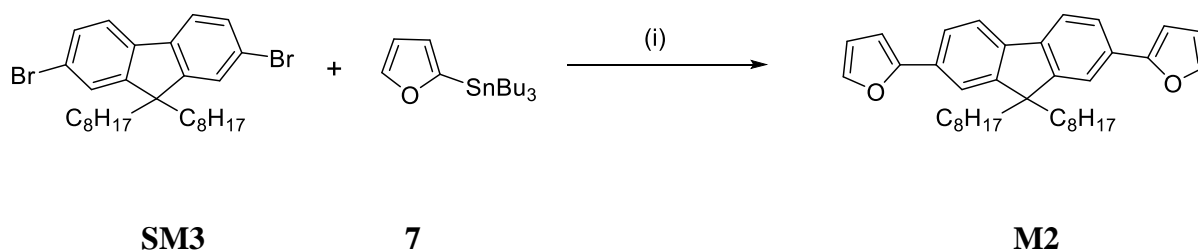
Figure 2.2. ^1H -NMR spectrum of compound (**M1**) in CDCl_3 .

The suggested mechanism is shown in Scheme 2.9 below. In terms of its chemistry, the oxygen atom of furan has a lone pair that donates electron density into the aromatic ring, making it more reactive toward electrophilic substitution. The 5-position is associated with the highest electron density, therefore making it more nucleophilic. In addition, the nitrogen atom is more electronegative than bromine, causing the bromine to have a partial positive charge in NBS, which is attacked by the furan ring. The proton on the furan ring is attracted towards the succinimide anion to harvest the brominated ring. This same process is repeated for another furan ring to form the desired product.



Scheme 2.9: The mechanism of synthesis of (M1).

The donor moiety (**M2**) was synthesised by Stille coupling of fluorene derivative (**SM3**) with tributyl(furan-2-yl) stannane (**7**) using palladium(II) acetate and tri(o-tolyl)phosphine in dry toluene at 115°C .



(i) Palladium(II) acetate and tri(o-tolyl)phosphine in dry toluene at 115°C.

Scheme 2.10: Synthesis of **M2** donor.

The product (**M2**) was yielded as a dark yellow to green oil with yield (60%). The purity and the structure of the product (**M2**) was confirmed by, ^1H NMR, ^{13}C NMR, elemental analysis and mass spectrometry. The elemental analysis confirmed the structure of the product. The mass spectrum show the main integer mass at 522 (M^+) which is in agreement with the proposed structure. The ^1H NMR gave six different environments as expected in the aromatic region. In addition, ^1H NMR gave different peaks as expected in aliphatic area as shown in Figure 2.3.

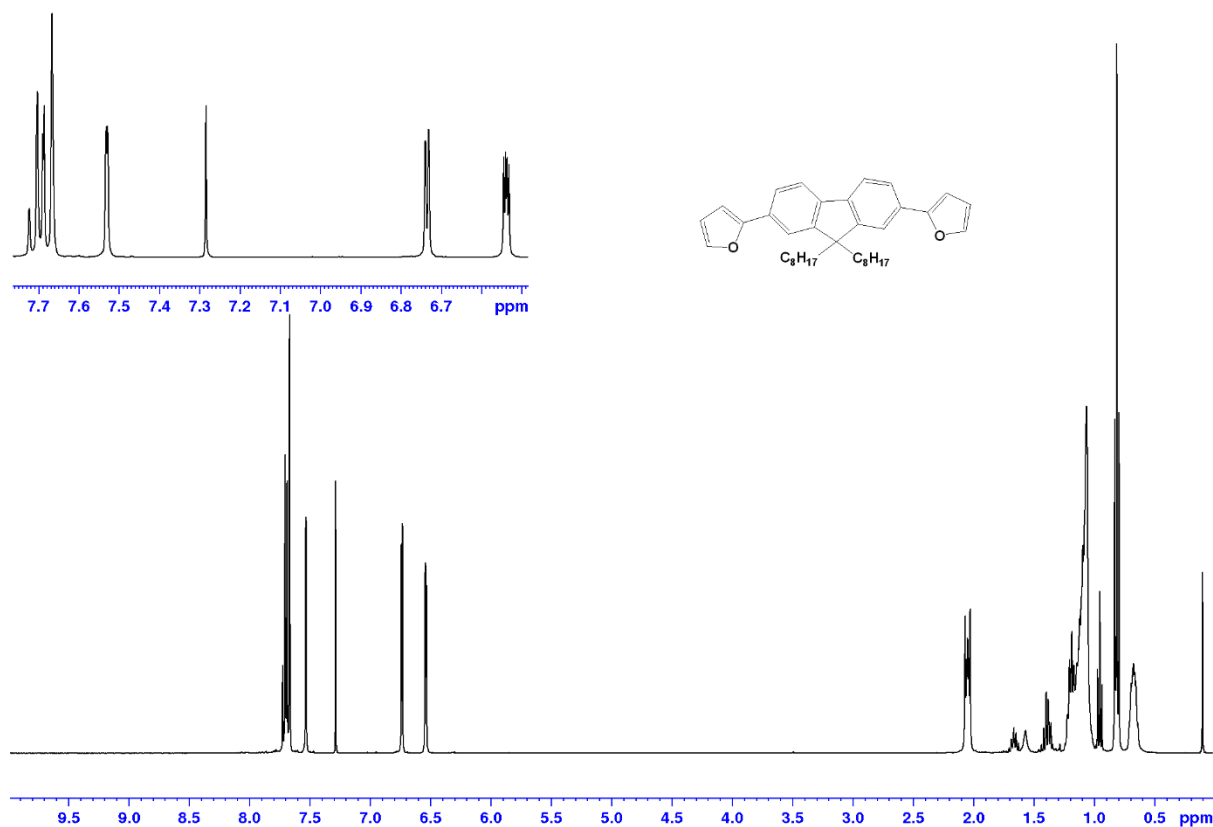
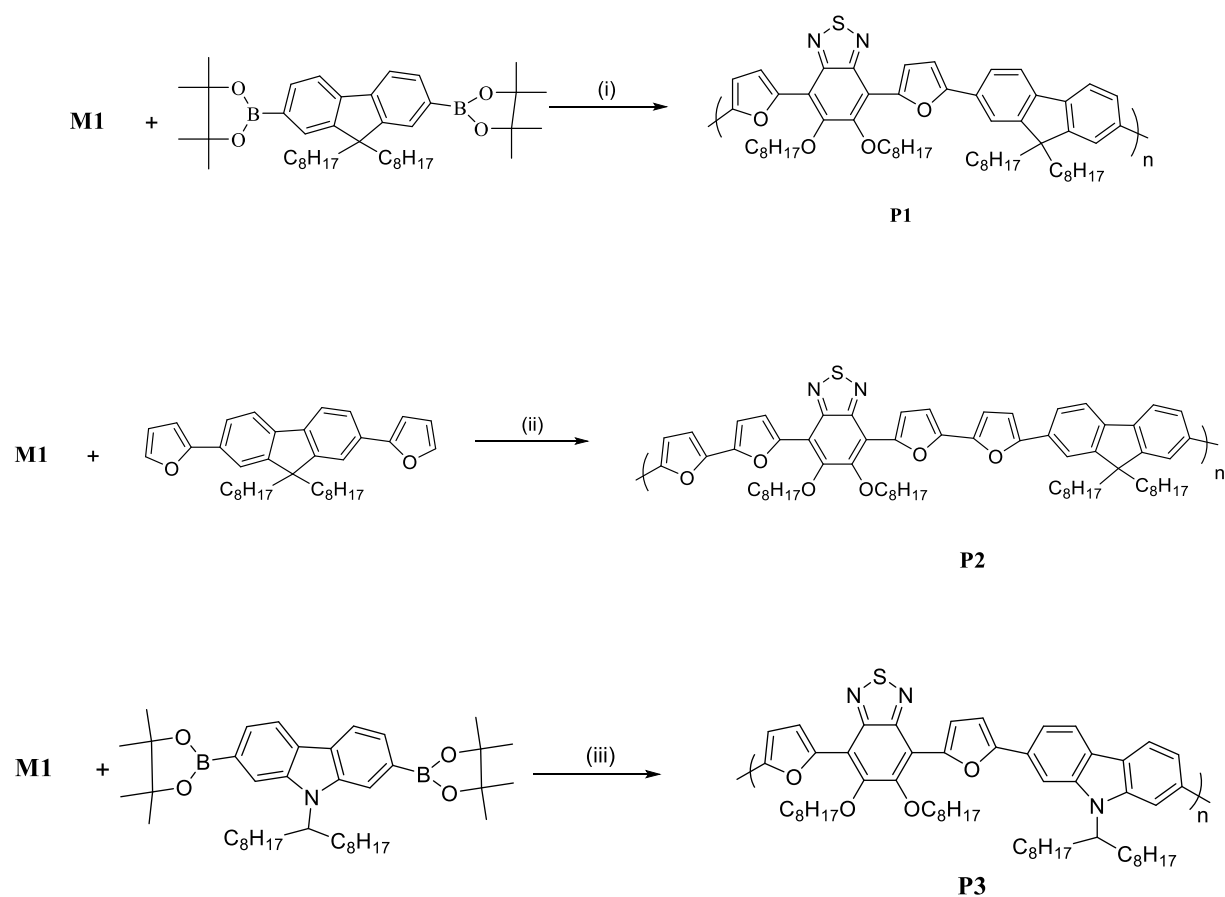


Figure 2.3. ^1H -NMR spectrum of compound (**M2**) in CDCl_3 .

2.2.2 Synthesis of polymers

The following three monomers were reacted with the final acceptor monomer **M1**: 9,9-dioctyl-2,7-bis(4,4,5,5-tetramethyl-1,3,2-dioxaborolan-2-yl)-9*H*-fluorene (**SM4**), 2,7-bis(furan-2-yl)-9,9-dioctyl-9*H*-fluorene (**M2**), and 9-(heptadecan-9-yl)-2,7-bis(4,4,5,5-tetramethyl-1,3,2-dioxaborolan-2-yl)-9*H*-carbazole (**SM11**). **P1** and **P3** were prepared *via* Suzuki cross-coupling polymerisation in the presence of $\text{Pd}(\text{OAc})_2$ as a catalyst and tri(*o*-tolyl)phosphine as a ligand under argon, according to the procedure outlined in previous research³². Dry THF and a saturated aqueous solution of NaHCO_3 were used in the polymerisations of **P1** and **P3**. The polymerisation reaction was maintained for 2 hours and 40 minutes for **P1** and 5 hours for **P3**. The timing was dependent on duration over which precipitation formed in the flask. **P2** was synthesised *via* direct arylation polymerisation using $\text{PdCl}_2(\text{MeCN})_2$ as a catalyst, $\text{P}(\text{O-MeOPh})_3$ as a ligand, caesium carbonate as the base, and pivalic acid as the source of carboxylate, which is important in direct arylation reactions³³. Dry THF was used as a solvent in this polymerisation process in a sealed tube under an

argon atmosphere and polymerisation occurred for 72 hours. **P1**, **P2** and **P3** were purified by Soxhlet extraction using different solvents – methanol, acetone, hexane, toluene and chloroform – after removal of the remaining catalysts by washing these with NH_4OH solution. The portions of toluene, chloroform and hexane were collected. The next step was to precipitate the polymers through drop-wise addition into methanol. The solubility of these polymers is excellent in common organic solvents. Proton Nuclear Magnetic Resonance (^1H NMR) was used to confirm the chemical structures of **P1**, **P2** and **P3** and gel permeation chromatography (GPC) was used to identify the number average molecular weight and the weight average molecular weight. The methods of synthesising polymers **P1**, **P2**, and **P3** are shown in Scheme 2.11.



- (i) $\text{Pd}(\text{OAc})_2$, tri(o-tolyl)phosphine, (4ml) dry THF, saturated NaHCO_3 (1ml), 90°C .
 (ii) $\text{Pd}_2(\text{MeCN})_2$, P(o-MeOPh) $_3$, CsCO_3 , pivalic acid, (1 ml) dry THF, 120°C .
 (iii) $\text{Pd}(\text{OAc})_2$, tri(o-tolyl)phosphine, (4ml) dry THF, saturated NaHCO_3 (1 ml), 90°C .

Scheme 2.11: Synthetic routes to **P1**, **P2** and **P3**.

2.2.3 Analysis of polymer properties

2.2.3.1 Gel permeation chromatography (GPC) analysis

GPC was performed using polystyrene standards and chloroform as the eluent at 40 °C. Polymer **P2**, which had been collected in the hexane fraction, evidenced the highest molecular weight and number-average molecular weight values of all three polymers. Analysis of polymers **P1** and **P3** provided values of Mn and Mw that were almost identical in both polymers. The increase of Mn and Mw in **P2** can be attributed to the presence of bifuran moiety flanked with the acceptor units, which led to a decrease in the steric hindrance between the groups linked to the acceptor and donor units through the reaction. **P1**, **P2** and **P3** showed lesser values of Mn and Mw than analogous polymers **PFDTBT-8**, **PFDT2BT-8** and **PCDTBT-8** that comprised thiophene units instead of furan units, as shown in Table 2.1. This is believed to be due to the increase in the electronegativity of oxygen present in the furan ring, which increased the π - π staking and led to the precipitation of the polymer to be faster than with thiophene-based polymers and prevented the increase of Mn and Mw.

Table 2.1: GPC data for **P1**, **P2**, **P3** and their analogous polymers.

Polymers	Soxhlet fraction	Mn(Da) ^a	Mw(Da) ^a	PDI ^b
P1	Toluene	11500	29700	2.57
PFDTBT-8 ²²		77100	130500	1.69
P2	Hexane	16400	35500	2.16
PFDT2BT-8 ²³		62300	91600	1.47
P3	Chloroform	10500	25800	2.44
PCDTBT-8 ²⁴		14700	34800	2.36

^a denotes the detection using differential refractive index (DRI) of the toluene, hexane and chloroform fractions of the polymer. ^b is the polydispersity index.

2.2.3.2 Optical properties of the polymers

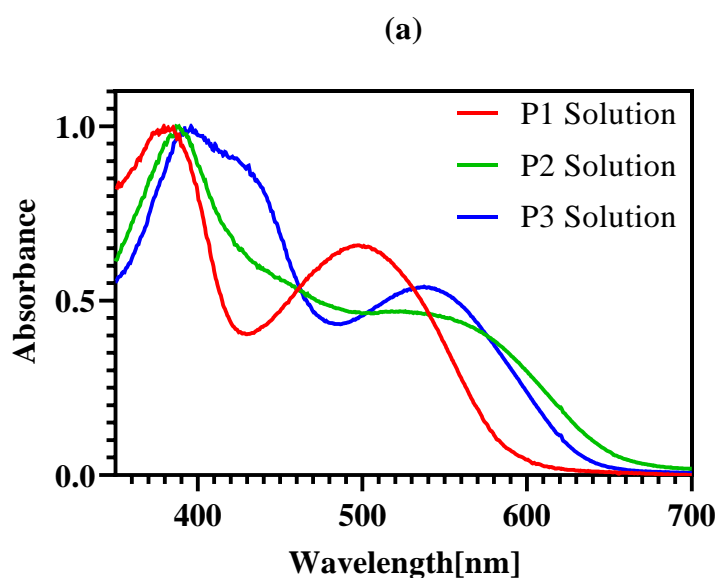
UV-vis spectroscopy in dilute chloroform solutions are shown in Figure 2.4 (a) and those for films in Figure 2.4 (b). They were used to investigate the optical properties of the synthesised polymers. Absorption maxima values in both solutions and films, absorption maxima onset values in films used in calculation of optical band gaps, and optical band gaps are all shown in Table 2.2 below.

Table 2.2: The UV-visible data of **P1**, **P2**, **P3** and their analogous polymers.

Polymer	λ_{max} solution (nm)	λ_{max} film (nm)	$\lambda_{\text{max onset}}$ film (nm)	E_{g opt} (eV)
P1	498	512	616	2.01 (+/- 0.02)
PFDTBT-8 ²²	530	550	616	2.01
P2	487	490	642	1.93 (+/- 0.04)
PFDT2BT-8 ²³	420	550	655	1.89
P3	490	494	607	2.04 (+/- 0.05)
PCDTBT-8 ²⁴	513	536	626	1.98

The absorption bands of the three polymers formed two distinct groupings for both solutions and thin films. When the bands formed into shorter wavelengths, this shows the π - π^* transitions from the monomer repeat units. On the other hand, when the bands formed into longer wavelengths, this is when intramolecular charge transfer (ICT) occurred between fluorene or carbazole units flanked by furan or bifuran groups as the electron donor moieties, and benzothiadiazole as the electron deficient units. The ICT bands of solutions of **P1**, **P2** and **P3** have maxima located at 498, 487 and 490 respectively. It can be clearly seen that the absorption peak of **P1** is slightly red-shifted compared to those of **P2** and **P3**, and that the absorption peak of **P3** is slightly red-shifted compared to that of **P2**. Compared to the

absorption spectra of their solutions, the UV-visible spectra of films are red-shifted in the absorption band. This is a result of the aggregation of polymer chains when the polymers are in their solid state³⁴. The synthesised polymers **P1**, **P2** and **P3** have optical band gaps of 2.01 eV, 1.93 eV and 2.04 eV with errors from an average (+/- 0.02, +/- 0.04, +/- 0.05) respectively. It should also be noted that **P2** show a reduced optical band gap compared to **P1** and **P3** by approximately 0.08 and 0.11 eV respectively. This can be attributed to the higher molecular weight caused by the introduction of an extra furan in the former, which then led to more electronic delocalisation along the backbone of the polymer, increasing the conjugation, and consequently increasing the ICT along the backbone of the polymer. Analogous polymers **PFDTBT-8**, **PFDT2BT-8** and **PCDTBT-8** show evidence of red shift of the absorption, indicating that the **PFDTBT-8**, **PFDT2BT-8** and **PCDTBT-8** polymer chains are highly aggregated due to the larger heteroatoms of the thiophene units. Consequently, the optical band gaps as estimated from the absorption onset of films are 2.01 eV, 1.89 eV and 1.98 eV. It is clear from the data in the above Table that the optical band gaps of **P1** and **PFDTBT-8** are similar. This implies that changing the thiophene units to furan units does not cause any difference in the optical band gap. However, the optical band gap of **P2** is slightly higher than the optical band gaps of **PFDT2BT-8** by 0.04 eV, and the optical band gap of **P3** is slightly larger than the optical band gaps of **PCDTBT-8** by 0.06 eV. Finally, the corresponding polymers **PFDTBT-8**, **PFDT2BT-8** and **PCDTBT-8** with thiophene units instead of the furan units have the same optical band gap or slightly higher.



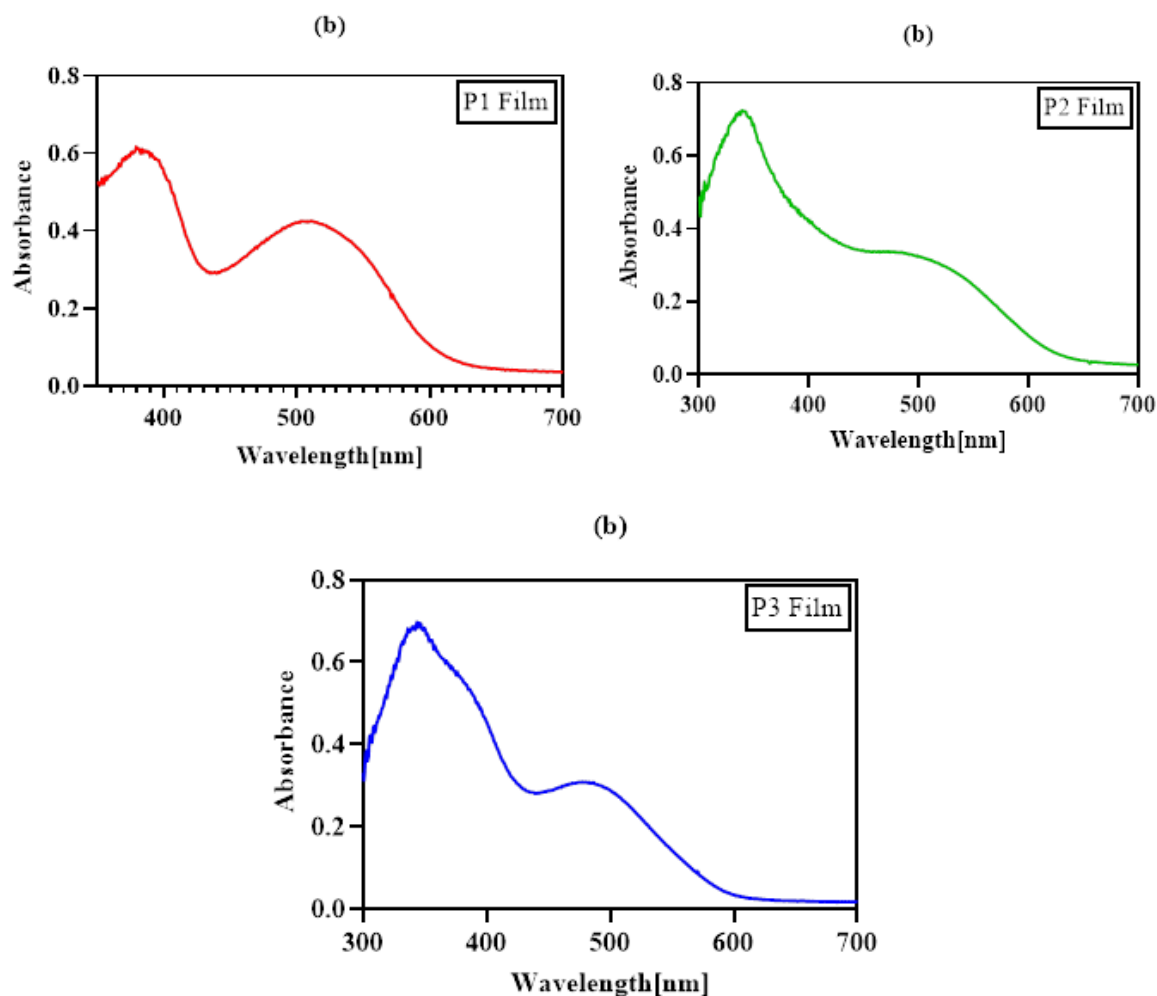


Figure 2.4: The UV-visible wavelengths of **P1**, **P2** and **P3** (a) in chloroform solutions and (b) in thin films.

2.2.3.3 Electrochemical properties of the polymers

Determination of the HOMO and LUMO energy levels (vs vacuum) was done by cyclic voltammetry using drop-cast polymer films in acetonitrile with tetrabutylammonium perchlorate as the electrolyte. The HOMO levels of the prepared polymers were calculated from the onsets of the oxidation potential whereas the onsets of the reduction potential were used to calculate the LUMO levels in each polymer. As the data in Table 2.3 reveals, the HOMO levels of all synthesised polymers **P1**, **P2** and **P3** are the same, at -5.31 eV, which meant they all have the same ionisation potential. It can be noted that the donors are different in all polymers; fluorene flanked by furan in **P1**, fluorene flanked by bifuran rings in **P2**, and carbazole flanked by furan, which is more electron donating than fluorene in **P3**. We

expected the HOMO level of **P2** to be shallower than **P1** due to the increase of intramolecular charge transfer along the backbone of polymer as result of incorporating bifuran spacer-units. In addition, **P3** should have been shallower than **P1** due to carbazole being more electron donating than fluorene but this was not observed. The analogous polymers, however, are different. To be more specific, the HOMO level of **PFDT2BT-8** is equal to -5.33 eV, and is shallower than **PFDTBT-8** and **PCDTBT-8**. This could have been caused by the higher electron donation of the bithiophene moieties³⁵. It is clear that the HOMO levels of the analogous polymers based on thiophene, **PFDTBT-8**, **PFDT2BT-8** and **PCDTBT-8** are deeper than the corresponding furan based polymers, **P1**, **P2** and **P3**, with differences never higher than 0.13 eV. This is possibly due to the lesser electronegativity of sulphur in thiophene compared to oxygen in furan, which increases the electron-donating tendency and introduces more delocalisation, which then would have reduced the HOMO levels. Another explanation is the big difference in the molecular weights, which are much higher than **P1**, **P2** and **P3**. The LUMO levels of **P1**, **P2** and **P3** are -3.39 eV, -3.12 eV and -3.07, respectively: **P3** is shallower than **P1** and **P2** due to the lower molecular weight of **P3** or the greater propensity of carbazole to donate, causing higher electronic conjugation. The LUMO levels of analogous polymers **PFDTBT-8**, **PFDT2BT-8** and **PCDTBT-8** are generally deeper than **P1**, **P2** and **P3** due to the increase in molecular weight. As reported in previous literature, increasing the molecular weight leads to a decrease in the LUMO level of the polymer³⁶.

The comparison between electrochemical band gaps of the synthesised polymers in our work and those in the work published by other groups is presented in Table 2.3. The E_g (eV) of **P1**, **P2** and **P3** were estimated to be 1.92 eV, 2.19 eV and 2.24 eV with errors average (+/- 0.07, +/- 0.05, +/- 0.06) respectively, whereas **PFDTBT-8**, **PFDT2BT-8** and **PCDTBT-8** were estimated to be 2.12 eV, 1.99 eV and 2.13 eV respectively. Thus, the band gaps of polymers with furan rings are bigger than those of the analogous polymers with thiophene rings because the analogous polymers have deeper HOMO levels, leading to reduced electrochemical band gaps such as those mentioned above that decreased the HOMO levels.

Table 2.3: The HOMO and LUMO data of **P1**, **P2**, **P3** and their analogous polymers.

Polymer	HOMO (eV) ^a	LUMO (eV) ^b	Eg(eV) ^c
P1	-5.31	-3.39	1.92 (+/- 0.07)
PFDTBT-8 ²²	-5.44	-3.32	2.12
P2	-5.31	-3.12	2.19 (+/- 0.05)
PFDT2BT-8 ²³	-5.33	-3.34	1.99
P3	-5.31	-3.07	2.24 (+/- 0.06)
PCDTBT-8 ²⁴	-5.40	-3.27	2.13

^aHOMO level of the polymer determined from the onset of the oxidation potential, ^bLUMO level of the polymer determined from the onset of the reduction potential, ^celectrochemical band gap.

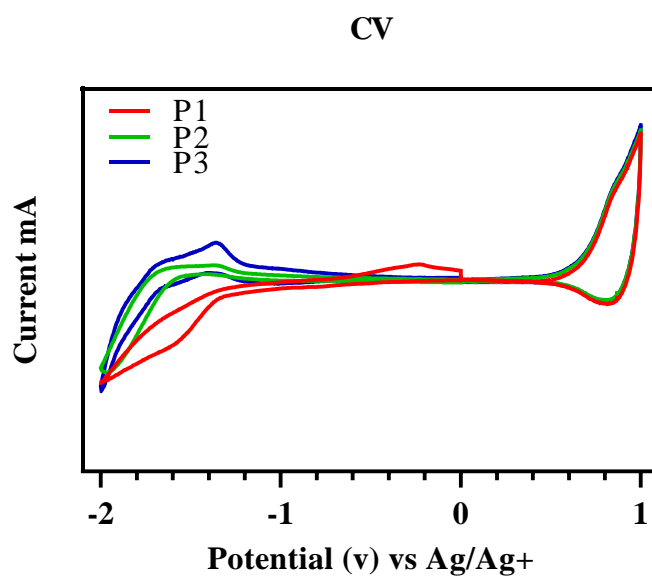


Figure 2.5: Cyclic voltammetry curves for **P1**, **P2** and **P3**.

2.2.3.4 Thermal gravimetric analysis (TGA) studies

The thermal stability of polymers was measured using thermogravimetric analysis. The polymers prepared were exposed to temperatures ramped up from room temperature to 800 °C at a heating rate of 10 °C / min under a nitrogen atmosphere in order to ascertain the temperature of the onset of decomposition (Td). The polymers **P1**, **P2** and **P3** presented, respectively, a Td of 341 °C, 200 °C and 328 °C. **P1** and **P3** showed good thermal stability above 300 °C whereas **P2** decomposed at approximately 100 °C less, possibly due to the fraction of the polymer collected in hexane or the addition of furan units attached with the benzothiadiazide. All polymers, **P1**, **P2** and **P3**, degraded until 45%, 42% and 45% of the mass remained, respectively, which can be attributed to the fact that during decomposition, a burnt residue of significant thickness is formed on the polymers, which insulates the polymer from the heat flux because of its low conductivity. This method delays the thermal decomposition of the polymer. The Td of analogous polymers **PFDTBT-8**, **PFDT2BT-8** and **PCDTBT-8** are 310°C, 340°C and 328°C respectively²²⁻²⁴.

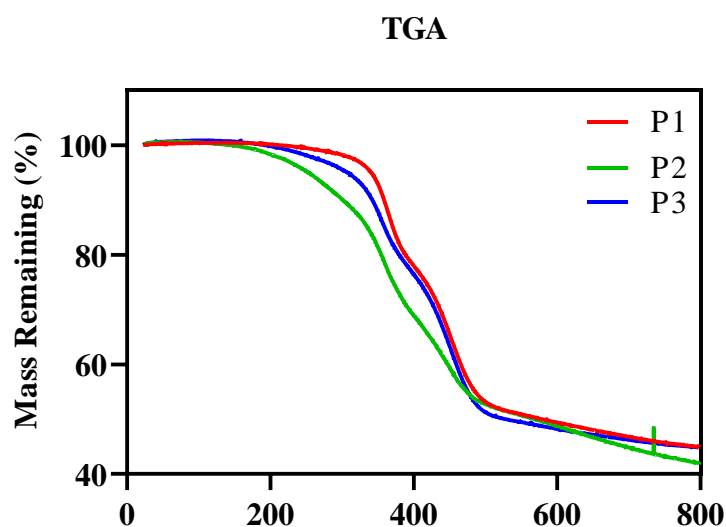


Figure 2.6: TGA curves for **P1**, **P2** and **P3**.

2.2.3.5 Polymers' X-ray diffraction (XRD) studies

The morphology of synthesised polymers **P1**, **P2** and **P3** was investigated using powder X-ray diffraction. As shown in Figure 2.7, there is a wide-angle broad peak at 2θ value at 20.40° for **P1**. This value is connected to π - π stacking of 4.34 Å distance. In addition, **P2** has a wide angle broad peak at 2θ value at 21.20° which corresponds to 4.18 Å. This is due to the addition of more furan units in the backbone of the polymer. **P3** also has a wide peak at

2θ value of 20.26° , which coincides with π - π stacking at a distance of 4.37 \AA . Expectedly, **P2** displays less stacking distance than **P1** and **P3**, a result of the increased planar backbone in the **P2**. The small angle region at 2θ shows values of 3.87° and 4.66° for **P2** and **P3**, respectively, which are connected to stacking distances of 22.80 \AA and 18.94 \AA respectively. These coincide with the distance of side-chains between lamella-packed polymer backbones. In sum, the synthesised polymers **P1**, **P2** and **P3** all have broad peaks in XRD, a result indicative of amorphous shapes³⁷.

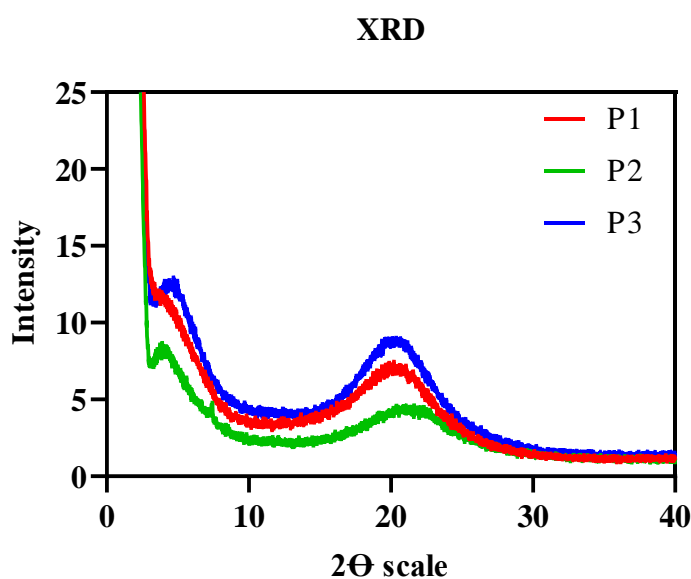


Figure 2.7: Powder X-Ray diffraction curves for **P1**, **P2** and **P3**.

2.3 Conclusion

In this study, we have presented the method of synthesis of donor-acceptor low-energy-band-gap polymers using Suzuki coupling and direct arylation procedures. A 2,7-linked fluorene unit as a donor copolymerised with benzothiadiazole, with alkoxy substituents flanked by furan rings as acceptor repeat moieties was used to afford **P1** by Suzuki coupling. Direct arylation was used to afford **P2** by copolymerisation of benzothiadiazole units with alkoxy substituents flanked by furan rings as acceptor repeat units with fluorene flanked by furan rings as donor moieties. Synthesis of **P3** was conducted using the same method as with **P1** apart from the use of carbazole instead of fluorene as a donor. All polymers have shown good solubility in common organic solvents. This feature can be explained by the alkoxy substituents in their benzothiadiazole repeat moieties²⁶.

The characterisations of the polymers were studied using GPC, UV-vis absorption, cyclic voltammetry, TGA and XRD. GPC determined the molecular weight (Mn) of **P1**, **P2** and **P3** as 11500 Da, 16400 Da and 10500 Da, respectively, and showed that **P2** has the highest molecular weight of all three polymers due to the incorporation of bifuran units, which increased the planarity of its backbone. The fact that the optical band gap of **P2** (1.93 eV) is narrower than **P1** (2.01 eV) and **P3** (2.04 eV) is possibly due to the extension of conjugation of the backbone of the polymer with additional of furan units. The thermal gravimetric analysis (TGA) shows that **P1** and **P3** have good thermal stability above 300°C whereas **P2** only maintains stability at 200 °C and degrades when exposed to higher temperature. Finally, **P1**, **P2** and **P3** have shown broad peaks in XRD, which is indicative of amorphous shapes. In comparison with **P1**, **P2** and **P3**, the analogous polymers **PFDTBT-8**, **PFDT2BT-8** and **PCDTBT-8** have a higher molecular weight. Moreover, the optical band gap of **PFDTBT-8** is the same as that of **P1** whereas **PFDT2BT-8** and **PCDTBT-8** have narrower gaps than **P2** and **P3** respectively. The Td of analogous polymers **PFDTBT-8**, **PFDT2BT-8** and **PCDTBT-8** determined by TGA are 310 °C, 340 °C and 328 °C, respectively, evidencing very good thermal stability.

In general, it can be concluded that exchanging of thiophene units by furan units flanked with benzothiadiazole with alkoxy substituents units does not allow the narrowing of the band gap. At best, these conjugated polymers have a band gap which is the same or slightly wider than that of polymers with thiophene units. The results obtained in this work are consistent with the information published by Woo *et al.*³⁸ in terms of the effect of replacing thiophene by furan on the optical properties: polymers containing furan displayed similar electronic and optical properties relative to their thiophene analogous polymers²⁵.

2.4 References

- (1) Brabec, C. J. Organic photovoltaics: technology and market. *Solar Energy Materials and Solar Cells* **2004**, *83* (2-3), 273.
- (2) Banerji, A.; Tausch, M. W.; Scherf, U. Classroom experiments and teaching materials on OLEDs with semiconducting polymers. *Educación Química* **2013**, *24* (1), 17.
- (3) Tipnis, R.; Laird, D.; Mathai, M. Polymer-based materials for printed electronics: enabling high efficiency solar power and lighting. *Material Matters* **2008**, *3* (4), 92.
- (4) Wu, Z.; Sun, C.; Dong, S.; Jiang, X.-F.; Wu, S.; Wu, H.; Yip, H.-L.; Huang, F.; Cao, Y. n-Type water/alcohol-soluble naphthalene diimide-based conjugated polymers for high-performance polymer solar cells. *Journal of the American Chemical Society*, **2016**, *138* (6), 2004.
- (5) Brabec, C. J.; Winder, C.; Sariciftci, N. S.; Hummelen, J. C.; Dhanabalan, A.; van Hal, P. A.; Janssen, R. A low-bandgap semiconducting polymer for photovoltaic devices and infrared emitting diodes. *Advanced Functional Materials* **2002**, *12* (10), 709.
- (6) Dhanabalan, A.; van Duren, J. K.; van Hal, P. A.; van Dongen, J. L.; Janssen, R. Synthesis and characterization of a low bandgap conjugated polymer for bulk heterojunction photovoltaic cells. *Advanced Functional Materials* **2001**, *11* (4), 255.
- (7) Van Duren, J.; Dhanabalan, A.; Van Hal, P.; Janssen, R. Low-bandgap polymer photovoltaic cells. *Synthetic Metals* **2001**, *121* (1-3), 1587.
- (8) Winder, C.; Sariciftci, N. Low bandgap polymers for photon harvesting in bulk heterojunction solar cells. *Journal of Materials Chemistry* **2004**, *14* (7), 1077.
- (9) Meyers, F.; Heeger, A.; Brédas, J. Fine tuning of the band gap in conjugated polymers via control of block copolymer sequences. *The Journal of Chemical Physics* **1992**, *97* (4), 2750.
- (10) Van Mullekom, H.; Vekemans, J.; Havinga, E.; Meijer, E. Developments in the chemistry and band gap engineering of donor–acceptor substituted conjugated polymers. *Materials Science and Engineering: R: Reports* **2001**, *32* (1), 1.
- (11) Beaujuge, P. M.; Reynolds, J. R. Color control in π -conjugated organic polymers for use in electrochromic devices. *Chemical Reviews* **2010**, *110* (1), 268.
- (12) Ashraf, R. S.; Meager, I.; Nikolka, M.; Kirkus, M.; Planells, M.; Schroeder, B. C.; Holliday, S.; Hurhangee, M.; Nielsen, C. B.; Sirringhaus, H. Chalcogenophene comonomer comparison in small band gap diketopyrrolopyrrole-based conjugated

- polymers for high-performing field-effect transistors and organic solar cells. *Journal of the American Chemical Society* **2015**, *137* (3), 1314.
- (13) Kim, J.; Yun, M. H.; Kim, G.-H.; Lee, J.; Lee, S. M.; Ko, S.-J.; Kim, Y.; Dutta, G. K.; Moon, M.; Park, S. Y. Synthesis of PCDTBT-based fluorinated polymers for high open-circuit voltage in organic photovoltaics: towards an understanding of relationships between polymer energy levels engineering and ideal morphology control. *ACS Applied Materials & Interfaces* **2014**, *6* (10), 7523.
- (14) Siddiki, M. K.; Li, J.; Galipeau, D.; Qiao, Q. A review of polymer multijunction solar cells. *Energy & Environmental Science* **2010**, *3* (7), 867.
- (15) Yassar, A.; Garnier, F.; Jaafari, H.; Rebiere-Galy, N.; Frigoli, M.; Moustrou, C.; Samat, A.; Guglielmetti, R. Light-triggered molecular devices based on photochromic oligothiophene substituted chromenes. *Applied Physics Letters* **2002**, *80* (23), 4297.
- (16) Efrem, A.; Lim, C.-J.; Lu, Y.; Ng, S. Synthesis and characterization of dithienobenzothiadiazole-based donor–acceptor conjugated polymers for organic solar cell applications. *Tetrahedron Letters* **2014**, *55* (35), 4849.
- (17) Boudreault, P.-L. T.; Najari, A.; Leclerc, M. Processable low-bandgap polymers for photovoltaic applications†. *Chemistry of Materials* **2010**, *23* (3), 456.
- (18) Chen, J.; Cao, Y. Development of novel conjugated donor polymers for high-efficiency bulk-heterojunction photovoltaic devices. *Accounts of Chemical Research* **2009**, *42* (11), 1709.
- (19) Inganaes, O.; Zhang, F.; Andersson, M. Alternating polyfluorenes collect solar light in polymer photovoltaics. *Accounts of Chemical Research* **2009**, *42* (11), 1731.
- (20) Peet, J.; Heeger, A. J.; Bazan, G. “Plastic” solar cells: self-assembly of bulk heterojunction nanomaterials by spontaneous phase separation. *Accounts of Chemical Research* **2009**, *42* (11), 1700.
- (21) Wang, X.; Chen, S.; Sun, Y.; Zhang, M.; Li, Y.; Li, X.; Wang, H. A furan-bridged D- π -A copolymer with deep HOMO level: synthesis and application in polymer solar cells. *Polymer Chemistry* **2011**, *2* (12), 2872.
- (22) Li, W.; Qin, R.; Zhou, Y.; Andersson, M.; Li, F.; Zhang, C.; Li, B.; Liu, Z.; Bo, Z.; Zhang, F. Tailoring side chains of low band gap polymers for high efficiency polymer solar cells. *Polymer* **2010**, *51* (14), 3031.
- (23) Watters, D. C.; Yi, H.; Pearson, A. J.; Kingsley, J.; Iraqi, A.; Lidzey, D. Fluorene-Based Co-polymer with High Hole Mobility and Device Performance in Bulk

- Heterojunction Organic Solar Cells. *Macromolecular Rapid Communications* **2013**, *34* (14), 1157.
- (24) Alghamdi, A. A.; Watters, D. C.; Yi, H.; Al-Faifi, S.; Almeataq, M. S.; Coles, D.; Kingsley, J.; Lidzey, D. G.; Iraqi, A. Selenophene vs. thiophene in benzothiadiazole-based low energy gap donor–acceptor polymers for photovoltaic applications. *Journal of Materials Chemistry A* **2013**, *1* (16), 5165.
- (25) Woo, C. H.; Beaujuge, P. M.; Holcombe, T. W.; Lee, O. P.; Fréchet, J. Incorporation of furan into low band-gap polymers for efficient solar cells. *Journal of the American Chemical Society* **2010**, *132* (44), 15547.
- (26) Bunz, U. α -oligofurans: molecules without a twist. *Angewandte Chemie International Edition* **2010**, *49* (30), 5037.
- (27) Chen, S.; Su, A.; Chen, S. Noncrystalline Phases in Poly (9, 9-di-n-octyl-2, 7-fluorene). *The Journal of Physical Chemistry B* **2005**, *109* (20), 10067.
- (28) Du, C.; Li, W.; Duan, Y.; Li, C.; Dong, H.; Zhu, J.; Hu, W.; Bo, Z. Conjugated polymers with 2, 7-linked 3, 6-difluorocarbazole as donor unit for high efficiency polymer solar cells. *Polymer Chemistry* **2013**, *4* (9), 2773.
- (29) Zhang, D.; Tessier, C. A.; Youngs, W. J. Synthesis of Tris (2, 5-dialkynylthieno) cyclotrienes, Tris (4, 5-dialkoxyphenyl) cyclotrienes, and Tetrakis (4, 5-dialkoxyphenyl) cyclo-tetraynes with Long-Chain Alkyl Substituents, and the Nickel and Cobalt Complexes of Tris [4, 5-(didodecyloxy) phenyl] cyclo-triyne. *Chemistry of Materials* **1999**, *11* (11), 3050.
- (30) Casado, A. L.; Espinet, P.; Gallego, A. M. Mechanism of the stille reaction. 2. Couplings of aryl triflates with vinyltributyltin. Observation of intermediates. A more comprehensive scheme. *Journal of the American Chemical Society* **2000**, *122* (48), 11771.
- (31) Santos, L. S.; Rosso, G. B.; Pilli, R. A.; Eberlin, M. The mechanism of the Stille reaction Investigated by electrospray ionization mass spectrometry. *The Journal of Organic Chemistry* **2007**, *72* (15), 5809.
- (32) Wakioka, M.; Ichihara, N.; Kitano, Y.; Ozawa, F. A highly efficient catalyst for the synthesis of alternating copolymers with thieno [3, 4-c] pyrrole-4, 6-dione units via direct arylation polymerization. *Macromolecules* **2014**, *47* (2), 626.
- (33) Cartwright, L.; Neal, T. J.; Rutland, N. J.; Iraqi, A. Anthracene-thieno [3, 4-c] pyrrole-4, 6-dione based donor–acceptor conjugated copolymers for applications in optoelectronic devices. *Polymers for Advanced Technologies* **2016**, *27* (4), 525.

- (34) Noriega, R.; Rivnay, J.; Vandewal, K.; Koch, F. P.; Stingelin, N.; Smith, P.; Toney, M. F.; Salleo, A. A general relationship between disorder, aggregation and charge transport in conjugated polymers. *Nature materials* **2013**, *12* (11), 1038.
- (35) Wang, N.; Chen, Z.; Wei, W.; Jiang, Z. Fluorinated benzothiadiazole-based conjugated polymers for high-performance polymer solar cells without any processing additives or post-treatments. *Journal of the American Chemical Society* **2013**, *135* (45), 17060.
- (36) Kim, B. G.; Ma, X.; Chen, C.; Ie, Y.; Coir, E. W.; Hashemi, H.; Aso, Y.; Green, P. F.; Kieffer, J.; Kim, J. Energy Level Modulation of HOMO, LUMO, and Band-Gap in Conjugated Polymers for Organic Photovoltaic Applications. *Advanced Functional Materials* **2013**, *23* (4), 439.
- (37) Cartwright, L.; Iraqi, A.; Zhang, Y.; Wang, T.; Lidzey, D. Impact of fluorine substitution upon the photovoltaic properties of benzothiadiazole-fluorene alternate copolymers. *RSC Advances* **2015**, *5* (57), 46386.
- (38) Yan, T.; Bin, H.; Yang, Y.; Xue, L.; Zhang, Z.-G.; Li, Y. Effect of furan π -bridge on the photovoltaic performance of DA copolymers based on bi (alkylthio-thienyl) benzodithiophene and fluorobenzotriazole. *Science China Chemistry* **2017**, *60* (4), 537.

Chapter 3:-

Design and synthesis of furan-based polymers with alternating fluorinated benzothiadiazole units for photovoltaic applications

Chapter 3 - Design and synthesis of furan-based polymers with alternating fluorinated benzothiadiazole units for photovoltaic applications.

3.1 Introduction

Of the many sources of clean energy on earth, the largest carbon-neutral energy source is solar energy produced by the sun, at a rate of 3.86×10^{26} J per second¹. In order to harness this abundant energy, Bell laboratories first manufactured commercial crystalline silicon p-n junction solar cells in 1954. Since that time, the conversion efficiency of these devices has steadily increased, and we have recently reached a point where researchers have been able to manufacture single junction crystalline silicon solar cells that are wafer-sized with an efficiency of approximately 25%^{2,3}. This means that the harvesting of the solar energy in the inorganic monocrystalline photovoltaic devices which presently exist is a viable energy generation method. However, there are many disadvantages with such devices: they are breakable, perform poorly in low light intensities and at extremes of temperature, and require manufacturing systems that are energy intensive. The third generation of PV devices (organic photovoltaic devices) have been developed as a result of research to find appropriate alternative devices to output solar energy. This newest generation has a number of advantages over its inorganic parallel: decreased embodied energy, increased flexibility, the abundance of materials for their manufacture, and their comparatively increased performance at lower light intensity^{3,4}.

In terms of the structure of the newest type of PV devices, a bulk heterojunction (BHJ) is usually used to mount the active layer of polymer solar cells. The active layer of BHJ cells is formed by blending a conjugated polymer as an electron donor and a fullerene derivative as an electron acceptor. The advantages of using conjugated polymers is that they can be designed with narrow band gaps, enlarged absorption in the visible and infrared area, high absorption coefficients, high molecular weights and high carrier mobilities to allow good energy conversion efficiencies in polymer solar cells. The solubility of the conjugated polymer in common organic solvents is affected by the length and flexibility of side chains that are attached to the backbone of the rigid polymer.

Past studies have shown that the best way to achieve the aforementioned benefits of conjugated polymers is to prepare them so that they are composed of alternating donor-acceptor repeat units along the chains of the polymer⁵⁻⁷. Moreover, it has been illustrated that

the band gap of a polymer can be controlled *via* the internal charge transfer between the donor and acceptor units⁸. In terms of adjusting the HOMO and LUMO levels of D-A polymers in order to decrease the band gap then improve the power conversion efficiency, different approaches have been suggested. For example, when a more electron-rich donor monomer is polymerised with a more electron-deficient acceptor monomer, this produces a small band gap⁹. Further tuning of the HOMO and LUMO levels can be attained by introducing electron withdrawing or electron donating substituents and attaching solubilising side chains^{7,10,11}.

Significant scholarly attention has been placed on the addition of substituents and their consequences to the studied polymer systems¹⁰⁻¹⁵. Arguably, fluorine is a very interesting substituent because it is the smallest electron withdrawing group with an electronegativity of 4.0⁷. To be more specific, Li *et al.* designed and prepared a polymer with a fluorine-functionalised benzothiadiazole-acceptor unit that was used with an electron rich alternate benzodithiophene moiety¹³. A parallel polymer with no fluorine substituent was also prepared to demonstrate the impact of fluorine substitution. Results reveal that the photovoltaic performance dramatically increased in the fluorinated polymer due to the deeper HOMO level and decreasing of the band gap of the resulting polymer. A number of other studies have also confirmed that the use of fluorinated-acceptors causes similar increases in performance^{11,15-17}. However, there is contradictory evidence from other research which has found that, by incorporating the fluorinated benzothiadiazole moiety, this does not necessarily enhance photovoltaic performance^{10,18}.

In this chapter, the process of incorporating fluorine substituent into the benzothiadiazole acceptor is described. This acceptor, flanked by two furan repeat units, was polymerised with two important electron rich monomers, 2,7-dibromo-9,9-dioctyl-9*H*-fluorene (**SM3**) and 2,7-dibromo-9-(heptadecan-9-yl)-9*H*-carbazole (**SM10**), to yield two polymers. The structure of fluorene is analogous to that of carbazole. However, an electron-donating nitrogen atom exists in the central fused pyrrole ring, which provides carbazole completely with aromaticity. This is dissimilar to fluorene¹⁹. Copolymerisation of the acceptor was then done with first the fluorene monomer to yield poly[9,9-dioctyl-9*H*-fluorene-2,7-diyl-*alt*-(5,6-difluoro-4,7-di-2-furanyl-2,1,3-benzothiadiazole)-5,5-diyl] (**P4**) and with the carbazole monomer to afford poly[9-(heptadecan-9-yl)-9*H*-carbazole-2,7-diyl-*alt*-(5,6-difluoro-4,7-di-2-furanyl-2,1,3-benzothiadiazole)-5,5-diyl] (**P5**). **P4** and **P5** were analysed using GPC, UV-vis absorption, TGA, CV and XRD and compared with their analogous polymers **PFO-DFFBT**²⁰ and **PCDTBT-F**¹⁰, as reported in previous literature. These contain thiophene

instead of furan respectively. The chapter concludes with a comparison of these results with those of **P1** and **P3** presented in the previous chapter.

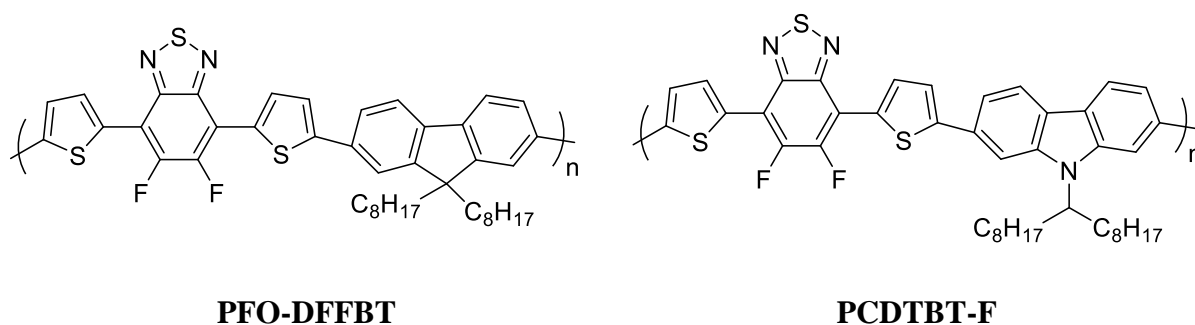
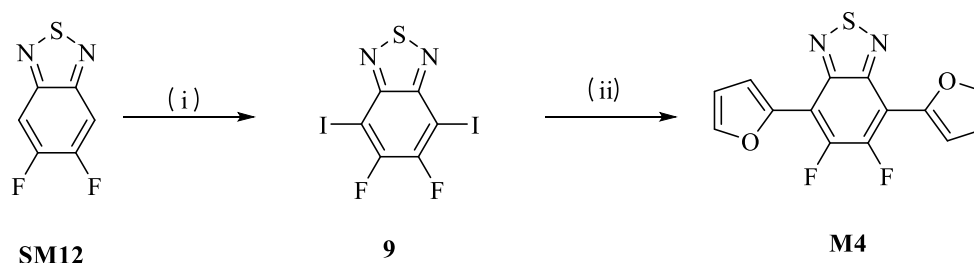


Figure 3.1: The structure of **PFO-DFFBT** and **PCDTBT-F**.

3.2 Results and discussion

3.2.1 Synthesis of monomers

The method of synthesising monomer **M4** is presented in scheme 3.1. below.



(i) Iodine, fuming H_2SO_4 , stirred at 60°C for 24 hours. (ii) Tributyl-2-furanyl-stannane, $\text{Pd}(\text{OAc})_2$, tri-*o*-tolyl phosphine, dry THF, refluxed at 70°C overnight.

Scheme 3.1: Synthesis of **M4** acceptor.

The first step was iodination of 5,6-difluorobenzo[*c*][1,2,5]thiadiazole (**SM12**) with iodine and fuming sulphuric acid to afford 5,6-difluoro-4,7-diiodobenzo[*c*][1,2,5]thiadiazole (**9**) in yield (70%) as a cream-yellow solid after it had been stirred at 60°C for 24 hours and extracted using water and chloroform. The main reason for good iodination of **SM12** is that

the oxidation reaction of iodine by SO₃ group in fuming sulphuric acid awarded an active iodine electrophile I₂⁺. The oxidation reaction of I₂ is shown in equation 3.1. The purity and the structure of the product (**9**) was confirmed by, ¹H NMR, ¹³C NMR, elemental analysis and mass spectrometry. The elemental analysis confirmed the structure of the product. The mass spectrum show the main integer mass at 423 (M⁺) which is in agreement with the proposed structure.



Equation 3.1: Oxidation reaction of I₂.

The second step in the process to afford 5,6-difluoro-4,7-di(furan-2-yl)benzo[c][1, 2, 5]thiadiazole (**M4**) was to react 5,6-difluoro-4,7-diiodobenzo[c][1,2,5]thiadiazole (**9**) with tributyl-2-furanyl-stannane (**7**) in the presence of Pd(OAc)₂ and tri-*o*-tolyl phosphine as catalysts, which were dissolved in dry THF and refluxed at 70 °C overnight. The ratio between (**9**) and (**7**) was 1:4 respectively. The Stille coupling reaction was the mechanism which enabled this process to occur, as described previously for compound (**8**) in Scheme 2.8. The product obtained in yield (93%). The purity and the structure of the (**M4**) was confirmed by, ¹H NMR, ¹³C NMR, elemental analysis and mass spectrometry. The elemental analysis confirmed the structure of the product. The mass spectrum show the main integer mass at 304 (M⁺) which is in agreement with the proposed structure. The ¹H NMR gave three different environments as expected in the aromatic region whereas in compound (**9**) there was not any proton which mean the compound of (**M4**) was done as shown in Figure 3.2.

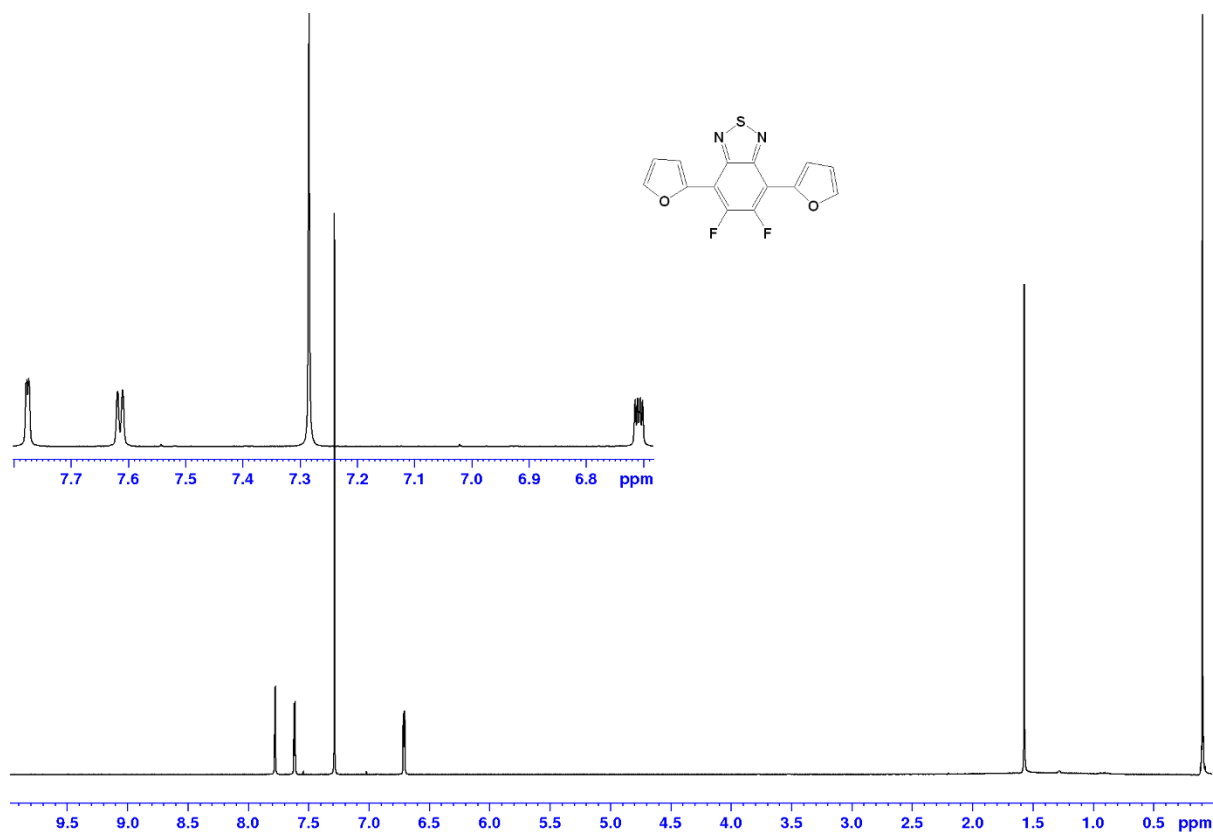
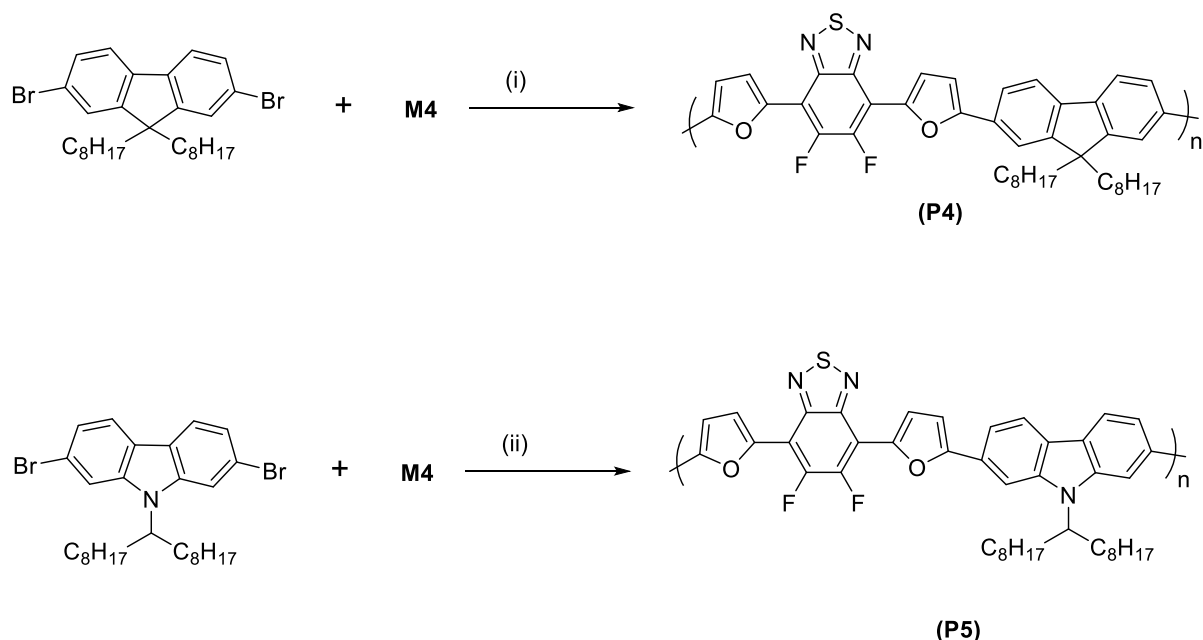


Figure 3.2. ¹H-NMR spectrum of compound (**M4**) in CDCl₃.

3.2.2 Synthesis of polymers

The final acceptor monomer **M4** was reacted with two different donors: 2,7-dibromo-9,9-dioctyl-9*H*-fluorene (**SM3**) and 2,7-dibromo-9-(heptadecan-9-yl)-9*H*-carbazole (**SM10**) by direct hetero arylation (DHA)²¹ polymerisation in the presence of Pd₂(dba)₃ as a catalyst, P(o-MeOPh)₃ as a ligand, Cs₂CO₃, and pivalic acid, to synthesise **P4** and **P5**. Polymerisation occurred in a sealed tube under an argon atmosphere, as recommended in the literature²¹. 1 ml of dry toluene was used in these polymerisation processes as a solvent. The length of polymerisation time varied between polymers: **P4** was 24 hours and **P5** 72 hours according to the formation of precipitates of polymer at the bottom of the polymerisation tube. Extraction of both polymers was done with a Soxhlet apparatus using different solvents – methanol, acetone, hexane, toluene and chloroform – after removal of the remaining catalysts by washing these with NH₄OH solution. The portions of chloroform were collected for the subsequent steps. The next step was to precipitate the polymers to yield them as solids through the addition of fractions of polymer solution in a drop-wise into methanol. The

solubility of both polymers was excellent in common organic solvents. ^1H NMR was then used to confirm the chemical structures of **P4** and **P5**, and GPC was used to identify the number and weight average molecular weight. The methods used to synthesise polymers **P4** and **P5** are shown in Scheme 3.2.



(i) and (ii) $\text{Pd}_2(\text{dba})_3$, $\text{P}(\text{o-MeOPh})_3$, Cs_2CO_3 , pivalic acid, 1ml dry toluene, 110°C .

Scheme 3.2: Methods of synthesis of **P4** and **P5**.

3.2.3 Analysis of polymers' properties

GPC analysis was conducted using polystyrene standard and chloroform as the eluent at 40°C . Both **P4** and **P5** were collected in chloroform fractions and these were measured at slightly different molecular weight values and number-average molecular weight values: those for **P5** were found to be slightly higher than for **P4**, as shown in Table 3.1. A comparison of the fluorine-substituted polymers **P4** and **P5** with **P1** and **P3**, which had alkoxy side-chains, showed that the number average molecular weight (M_n) and weight average molecular weight (M_w) of **P4** and **P5** was estimated at 2800 Da and 6400 Da and 2900 Da and 6500 Da, respectively, as shown in Table 3.1. As a comparison, (M_n) and (M_w) in **P1** and **P3** were estimated to be 11500 Da and 29700 Da, 10500 Da and 25800 Da respectively. This significant difference in the values of M_n and M_w in **P4** and **P5** compared with those of **P1** and **P3** can be attributed to the rigidity of the polymers and to the fluorine atoms incorporated on the benzothiadiazide unit, causing strong π - π stacking and the

aggregation of polymer chains. Therefore, the precipitation of the polymer occurred quickly and limited the molecular weight of the product. Incorporation of alkoxy side-chains in benzothiadiazide, such as those in **P1** and **P3**, disturbed the π - π staking and controlled the aggregation resulting in a higher molecular weight²⁰. Analogous polymers **PFO-DFFBT** and **PCDTBT-F** with thiophene rings instead of furan rings flanked with fluorinated benzothiadiazide were analysed as having higher values of Mn and Mw than **P4** and **P5**. The reason for this is possibly due to the decrease of electronegativity of sulfur in the thiophene ring compared to the oxygen in the furan ring leading to a decrease in the π - π staking of the compounds of thiophene. This then would have caused the precipitation of the polymer to take more time to occur, increasing the molecular weight compared to the polymers with furan rings.

Table 3.1: GPC data for **P4**, **P5**, **PFO-DFFBT** and **PCDTBT-F**.

Polymers	Soxhlet fraction	Mn(Da)^a	Mw(Da)^a	PDI^b
P4	Chloroform	2800	6400	2.29
PFO-DFFBT²⁰	Toluene	6800	9600	1.41
P5	Chloroform	2900	6500	2.24
PCDTBT-F¹⁰		4000	6000	1.5

^a Detected by differential refractive index (DRI) of the toluene and chloroform fractions of the polymer. ^b is the polydispersity index.

3.2.3.1 Optical properties of the polymers

UV-vis spectroscopy in dilute chloroform solutions [see Figure 3.3 (a)] and film states [see Figure 3.3 (b)] was used to investigate the optical properties of the synthesised polymers. The absorption maxima values in both solutions and films, and the absorption maxima onset values in films that were used in calculating the optical band gaps are shown in table 3.2. below.

Table 3.2: The UV-visible data of **P4**, **P5**, **PFO-DFFBT** and **PCDTBT-F**.

Polymer	λ_{max} solution (nm)	λ_{max} film (nm)	λ_{max} onset film (nm)	E_g opt (eV)
P4	515	524	648	1.91 (+/- 0.05)
PFO-DFFBT ²⁰	518	549	649	1.91
P5	513	502	646	1.92 (+/- 0.03)
PCDTBT-F ¹⁰	500	519	633	1.96

The absorption bands of the two polymers form two distinct groupings for both solutions and thin films. When the bands are formed into shorter wavelengths, this shows the π - π^* transitions from the monomer repeat units. On the other hand, when the bands form into longer wavelengths, this is when intramolecular charge transfer (ICT) occurs between fluorene or carbazole units as the electron donor moieties, and 5,6-difluorobenzothiadiazide flanked by furan groups as the electron deficient units. The ICT bands for solutions of **P4** and **P5** are located at 515 and 513, respectively. This difference of 2 nm is negligible, but **P4** is very slightly red-shifted. The optical band gaps of **P4** and **P5** are 1.91 eV and 1.92 eV with errors average (+/- 0.05 and +/- 0.03) respectively, and thus it can be concluded that there are no notable differences between these polymers when changing fluorene or carbazole units. It was noticed that in the majority of polymers, the UV-visible spectra of films are red-shifted in the absorption band compared to the absorption spectra of their solutions. This can be hypothesised as having occurred due to the polymer chains' aggregation in their solid state. Analogous polymers **PFO-DFFBT** and **PCDTBT-F** show optical band gaps of 1.91 eV and 1.96 eV respectively. Therefore, the optical band gaps of **P4** and **PFO-DFFBT** are similar, and so changing thiophene units with furan units does not cause any difference in the optical band gap. However, the optical band gap of **P5** is slightly lower than the optical band gaps of **PCDTBT-F** by 0.04 eV, which can be attributed to the increasing of conjugation along the backbone of **P5** compared with **PCDTBT-F**. The optical band gaps of **P4** and **P5** were measured as 1.91 eV and 1.92 eV, respectively, while those of the analogous polymers **P1**

and **P3** with alkoxy chains attached to benzothiadiazide units were measured as 2.01 eV and 2.04 eV respectively. It is clear then that the band gaps of **P4** and **P5** are lower than those of **P1** and **P3** by 0.1 eV and 0.08 eV, respectively, due to the two fluorine atoms attached at the 5,6-positions of the benzothiadiazide units providing stronger electron accepting properties and higher ICT on the backbone of the resulting polymers.

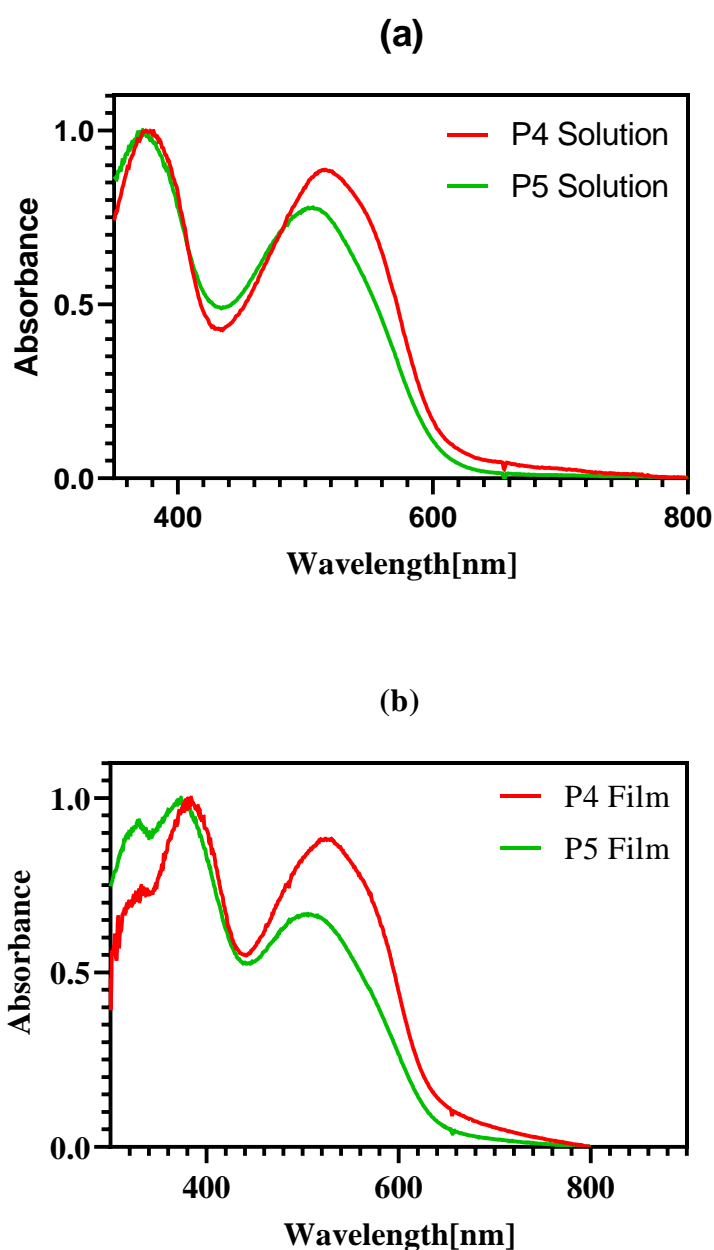


Figure 3.3: The UV-visible wavelengths of **P4** and **P5** (a) in chloroform solutions (b) in thin films.

3.2.3.2 Electrochemical properties of the polymers

Analysis using cyclic voltammetry (CV) was conducted by drop-casting polymeric films onto platinum electrodes from chloroform solutions. Acetonitrile was used as a solvent and tetrabutylammonium perchlorate as an electrolyte. The oxidation potential onsets were used to determine the HOMO levels of the prepared polymers, and the onsets of the reduction potential were used to calculate the LUMO levels. The data shown in Table 3.3 represent a comparison of HOMO and LUMO levels for polymers **P4** and **P5** with fluorinated benzothiadiazole flanked by furan units as acceptors, with analogous polymers **PFO-DFFBT** and **PCDTBT-F** with thiophene instead of furan. The HOMO/ LUMO levels of **P4** and **P5** are -5.34/-3.30 eV and -5.35/-3.33 eV respectively. It should be noted that the HOMO levels of **P4** and **P5** are similar, whereas the LUMO level of **P4** is shallower than **P5**, probably due to the slight decrease in the molecular weight of **P4**. The HOMO levels of analogous polymers **PFO-DFFBT** and **PCDTBT-F** at -5.38 eV and -5.54 eV, respectively, are deeper than those of **P4** and **P5** due to the thiophene being more electron donating than furan. This caused more delocalisation, which led to a reduction in the HOMO level, as discussed in the last chapter. Furthermore, the LUMO levels of **P4** and **P5** are also shallower than analogous polymers **PFO-DFFBT** and **PCDTBT-F** due to the low molecular weights of **P4** and **P5**.

The electrochemical band gaps for **P4** and **P5** are 2.04 eV and 2.02 eV with errors average (+/- 0.07 and +/- 0.09) respectively: the band gap for **P4** was measured to be the same as that of the analogous polymer **PFO-DFFBT** with a band gap of 2.05 eV. However, the electrochemical band gap for **P5** was found to be slightly wider than that of the analogous polymer **PCDTBT-F** at 1.96 eV. Thus, a slight difference between the electrochemical and optical band gaps was caused by the interfacial energy barrier created during the reduction/oxidation reactions between the electrode and polymeric thin film. The HOMO levels of **P1** and **P3** were estimated to be -5.31 eV and the HOMO levels of **P4** and **P5** deeper due to the influence of the fluorinated benzothiadiazole rather than alkoxy group in which fluorine atoms cause benzothiadiazole to have more electron accepting properties. The electrochemical band gaps of **P1** and **P3** were estimated to be 1.92 eV and 2.24 eV whereas **P4** and **P5** were 2.04 eV and 2.02 eV respectively.

Table 3.3: Cyclic voltammetry for **P4**, **P5**, **PFO-DFFBT** and **PCDTBT-F**.

Polymer	HOMO (eV) ^a	LUMO (eV) ^b	Eg (eV) ^c
P4	-5.34	-3.30	2.04 (+/- 0.07)
PFO-DFFBT ²⁰	-5.38	-3.49	2.05
P5	-5.35	-3.33	2.02 (+/- 0.09)
PCDTBT-F ¹⁰	-5.54	-3.58	1.96

^a HOMO level of the polymer calculated from the oxidation potential onset, ^b LUMO level of the polymer calculated from the reduction potential onset, ^c electrochemical band gap.

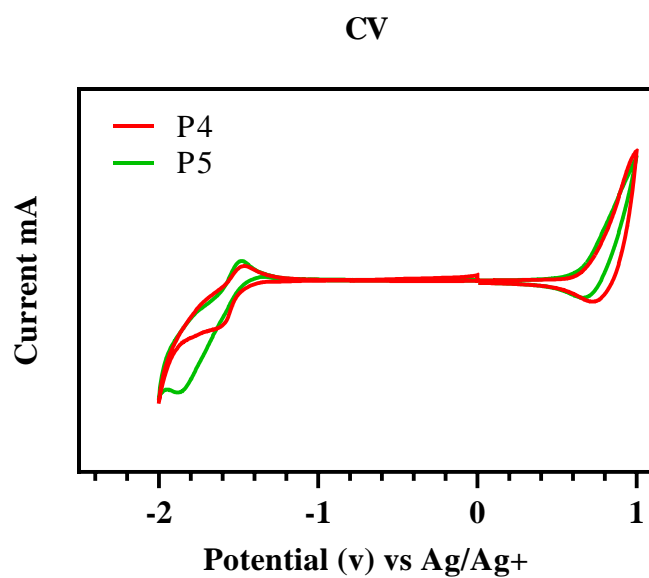


Figure 3.4: Cyclic voltammetry curves for **P4** and **P5**.

3.2.3.3 Thermal Gravimetric Analysis (TGA)

TGA was employed to analyse the thermal stability of synthesised polymers **P4** and **P5**. The polymers **P4** and **P5** presented degradation points at 429 °C and 412 °C, respectively, evidencing good thermal stability at temperatures in excess of 400 °C. A slight difference in the Td was recorded between **P4** and **P5**, which can be attributed to the structures of the polymers and their Mw. The onset decomposition Td of analogous polymers **PFO-DFFBT** and **PCDTBT-F** was measured as 417 °C and 409 °C, and so the Td for **P4** is higher than the Td of **PFO-DFFBT** by 12 °C, and the Td of **P5** is higher than the Td of **PCDTBT-F** by 3 °C. In other words, there is only a slight difference between the thermal stability when the thiophene units flanking the benzothiadiazole are exchanged with furan units. The Td of **P1** and **P3** was measured as 340 °C and 328 °C respectively. This is a significantly lower temperature tolerance prior to decomposition than **P4** and **P5**: 89 °C and 84 °C respectively. It is clear then that the alkoxy side chains are key determinants of thermal stability – the polymers with alkoxy side chains started to decompose before analogous polymers without alkoxy side-chains **P1** and **P3**²². A final conclusion which can be reached on the basis of this data is that the introduction of fluorine instead of alkoxy side chains in the backbone of the polymer slightly increases the degree of stability towards thermal degradation and Td^{13,23}.

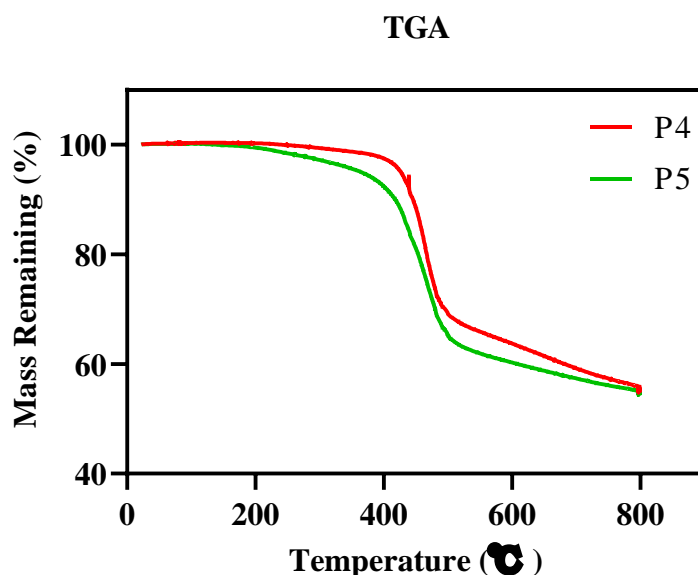


Figure 3.5: TGA curves for **P4** and **P5**.

3.2.3.4 Powder X-ray diffraction (XRD) analysis

Powder X-ray diffraction (XRD) analysis was conducted on **P4** and **P5**. The data from this analysis (see figure 3.5) reveals that both polymers display peaks at 2Θ values of 6 and 6.25 respectively. This corresponds to distances of $\sim 14.7 \text{ \AA}$ for **P4** and $\sim 14.1 \text{ \AA}$ for **P5**. Previous studies have found that the 2Θ value is connected to the distance between the main chains of the polymer, where the alkyl chains on the fluorene unit are interdigitatively self-organised^{24,25}. There is a wide angle broad peak at 2Θ values at 20 and 20.13 for **P4** and **P5**, respectively, which corresponds to a π - π stacking of 4.43 \AA and 4.40 \AA distance²⁶. Analogous polymers **PFO-DFFBT** and **PCDTBT-F** display peaks at 2Θ values of 25.32 and 23.33, respectively, which corresponds a π - π stacking of 3.51 \AA and 3.80 \AA distance, smaller than the distances for **P4** and **P5**^{18,20}.

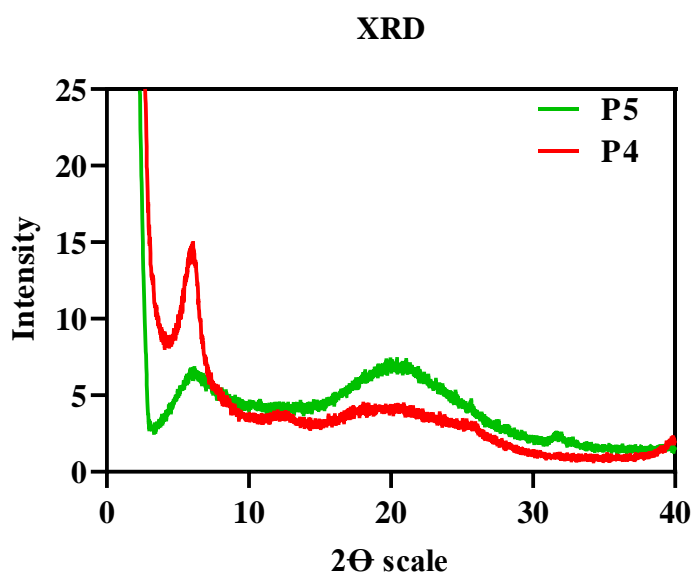


Figure 3.6: Powder X-Ray diffraction curves for **P4** and **P5**.

3.3 Conclusion

In summary, benzothiadiazole with fluorine atoms at the 5,6-positions flanked by furan as an acceptor were synthesised and copolymerised with two donors: firstly with fluorene to afford poly[9,9-dioctyl-9H-fluorene-2,7-diyl-*alt*-(5,6-difluoro-4,7-di-2-furanyl-2,1,3-benzothiadiazole)-5,5-diyl] (**P4**); and secondly with carbazole to afford poly[9-(heptadecan-9-yl)-9H-carbazole-2,7-diyl-*alt*-(5,6-difluoro-4,7-di-2-furanyl-2,1,3-benzothiadiazole)-5,5-diyl] (**P5**) *via* direct hetero arylation (DHA). Analysis was conducted to measure the

molecular weight, optical properties, electrochemical band gap, HOMO and LUMO levels, thermal stability and X-ray diffraction curves using GPC, UV, CV, TGA and the XRD. It was found that the molecular weights of **P4** and **P5** were nearly the same and very low – (2800 Da) and (2900 Da) respectively. This can be explained by the fluorine atoms that were incorporated into the benzothiadiazide unit, leading to strong π - π staking and the polymer chains' aggregation. Therefore, the precipitation of the polymer occurred quickly and limited the molecular weight of the polymers. The optical band gaps of **P4** and **P5** were similar at 1.91 eV and 1.92 eV, perhaps due to the similarity in their molecular weight. **P4** had an estimated electrochemical band gap 2.04 eV, slightly higher than **P5** at 2.02 eV. The HOMO level of **P5** at -5.35 eV was slightly deeper than HOMO level of **P4** at -5.34 eV, a difference of 0.01 eV, which is very small, whereas The LUMO level of **P4** at -3.30 eV was slightly shallower than LUMO level of **P5** at -3.33 eV, a difference of 0.03 eV, possibly due to the slight lowering in the molecular weight of **P4**. In addition, thermal gravimetric analysis (TGA) showed that **P4** and **P5** have good thermal stability above 400°C, and even when exposed to high temperatures above 800°C.

Comparing these findings with those for analogous polymers **PFO-DFFBT** and **PCDTBT-F**, their molecular weight was larger than that of **P4** and **P5** due to the decrease of electronegativity of sulfur in the thiophene ring compared to oxygen in the furan ring that led to a decrease of the π - π staking of the compounds with thiophene. This caused the precipitation of the polymer to take more time to occur, affording polymers with higher molecular weight than the compounds with furan, as mentioned above in the GPC analysis. The optical band gap of **PFO-DFFBT** (1.91 eV) was the same as the optical band gap of **P4** (1.91 eV), and the optical band gap of **PCDTBT-F** (1.96 eV) was slightly larger than the optical band gap of **P5** by 0.04 eV, possibly due to the increase of intramolecular charge transfer along the backbone of **P5**. On the other hand, the estimated electrochemical band gap of **PFO-DFFBT** (2.05 eV) was similar to the electrochemical band gap of **P4** (2.04 eV) whereas the electrochemical band gap of **P5** was larger than that of analogous polymer **PCDTBT-F** (1.96 eV) by about 0.06 eV. The HOMO levels of **P4** and **P5** were -5.34 eV and -5.35 eV, respectively, shallower than those for **PFO-DFFBT** and **PCDTBT-F**, which were estimated at -5.38 eV and -5.54 eV respectively. This is due to the increase of donating in the thiophene, which increased the delocalisation that led to a reduction in the HOMO level. The LUMO levels of **P4** and **P5** were estimated at -3.30 eV and -3.33 eV, respectively, shallower

than those of analogous polymers **PFO-DFFBT** and **PCDTBT-F**, which were estimated at -3.49 eV and -3.58 eV, respectively, due to their lower molecular weight.

As a general conclusion, it can be said that no difference was witnessed in the optical or electrical band gaps of the polymers when exchanging thiophene units by furan units flanked with benzothiadiazole with fluorine atoms substituents. On the other hand, by comparing **P4** and **P5** with **P1** and **P3** in the last chapter, we found that the molecular weight of **P4** and **P5** was smaller than **P1** and **P3** by about 4 and 3.6 times respectively. As we mentioned above, the strong π - π stacking and the aggregation of polymer chains was due to incorporation of fluorine atoms. Therefore, the precipitation of the polymer occurred quickly and limited the molecular weight of the products. The bandgaps of these polymers were smaller than analogous polymers in the last chapter due to increased conjugation, which led to increased intramolecular charge transfer along the backbone of the polymer chains and a decreased band gap. Moreover, the stability of these polymers was higher than the analogous polymers in the last chapter, which could be due to changing the alkyl chains with fluorine atoms, because the alkoxy group easily breaks, leading to degradation by loss of alkoxy side chains compared to fluorine substitutions, which provide more stable materials.

3.4 References

- (1) Boudreault, P.-L. T.; Najari, A.; Leclerc, M. Processable low-bandgap polymers for photovoltaic applications†. *Chemistry of Materials* **2010**, *23* (3), 456.
- (2) Wang, E.; Wang, L.; Lan, L.; Luo, C.; Zhuang, W.; Peng, J.; Cao, Y. High-performance polymer heterojunction solar cells of a polysilafluorene derivative. *Applied Physics Letters* **2008**, *92* (3), 23.
- (3) Dennler, G.; Scharber, M. C.; Brabec, C. Polymer-fullerene bulk-heterojunction solar cells. *Advanced Materials* **2009**, *21* (13), 1323.
- (4) Kim, J.; Lee, K. J. S. JY Kim, K. Lee, NE Coates, D. Moses, T.-Q. Nguyen, M. Dante, and AJ Heeger, *Science* **2007**, *317*, 222.
- (5) Park, S. H.; Roy, A.; Beaupré, S.; Cho, S.; Coates, N.; Moon, J. S.; Moses, D.; Leclerc, M.; Lee, K.; Heeger, A. Bulk heterojunction solar cells with internal quantum efficiency approaching 100%. *Nature Photonics* **2009**, *3* (5), 297.
- (6) Amb, C. M.; Chen, S.; Graham, K. R.; Subbiah, J.; Small, C. E.; So, F.; Reynolds, J. Dithienogermole as a fused electron donor in bulk heterojunction solar cells. *Journal of the American Chemical Society* **2011**, *133* (26), 10062.
- (7) Zhou, H.; Yang, L.; You, W. Rational design of high performance conjugated polymers for organic solar cells. *Macromolecules* **2012**, *45* (2), 607.
- (8) Zhang, Q. T.; Tour, J. Alternating donor/acceptor repeat units in polythiophenes. Intramolecular charge transfer for reducing band gaps in fully substituted conjugated polymers. *Journal of the American Chemical Society* **1998**, *120* (22), 5355.
- (9) Zhou, H.; Yang, L.; Stoneking, S.; You, W. A weak donor– strong acceptor strategy to design ideal polymers for organic solar cells. *ACS Applied Materials & Interfaces* **2010**, *2* (5), 1377.
- (10) Umeyama, T.; Watanabe, Y.; Douvogianni, E.; Imahori, H. Effect of fluorine substitution on photovoltaic properties of benzothiadiazole–carbazole alternating copolymers. *The Journal of Physical Chemistry C* **2013**, *117* (41), 21148.
- (11) Zhang, Y.; Chien, S.-C.; Chen, K.-S.; Yip, H.-L.; Sun, Y.; Davies, J. A.; Chen, F.-C.; Jen, A. Increased open circuit voltage in fluorinated benzothiadiazole-based alternating conjugated polymers. *Chemical Communications* **2011**, *47* (39), 11026.
- (12) You, J.; Dou, L.; Yoshimura, K.; Kato, T.; Ohya, K.; Moriarty, T.; Emery, K.; Chen, C.-C.; Gao, J.; Li, G. A polymer tandem solar cell with 10.6% power conversion efficiency. *Nature Communications* **2013**, *4*, 1446.

- (13) Li, Z.; Lu, J.; Tse, S.-C.; Zhou, J.; Du, X.; Tao, Y.; Ding, J. Synthesis and applications of difluorobenzothiadiazole based conjugated polymers for organic photovoltaics. *Journal of Materials Chemistry* **2011**, *21* (9), 3226.
- (14) Albrecht, S.; Janietz, S.; Schindler, W.; Frisch, J.; Kurpiers, J.; Kniepert, J.; Inal, S.; Pingel, P.; Fostiropoulos, K.; Koch, N. Fluorinated copolymer PCPDTBT with enhanced open-circuit voltage and reduced recombination for highly efficient polymer solar cells. *Journal of the American Chemical Society* **2012**, *134* (36), 14932.
- (15) Zhou, H.; Yang, L.; Stuart, A. C.; Price, S. C.; Liu, S.; You, W. Development of fluorinated benzothiadiazole as a structural unit for a polymer solar cell of 7% efficiency. *Angewandte Chemie International Edition* **2011**, *50* (13), 2995.
- (16) Min, J.; Zhang, Z.-G.; Zhang, S.; Li, Y. Conjugated side-chain-isolated D–A copolymers based on benzo [1, 2-b: 4, 5-b'] dithiophene-alt-dithienylbenzotriazole: synthesis and photovoltaic properties. *Chemistry of Materials* **2012**, *24* (16), 3247.
- (17) Fei, Z.; Shahid, M.; Yaacobi-Gross, N.; Rossbauer, S.; Zhong, H.; Watkins, S. E.; Anthopoulos, T. D.; Heeney, M. Thiophene fluorination to enhance photovoltaic performance in low band gap donor–acceptor polymers. *Chemical Communications* **2012**, *48* (90), 11130.
- (18) Kim, J.; Yun, M. H.; Kim, G.-H.; Lee, J.; Lee, S. M.; Ko, S.-J.; Kim, Y.; Dutta, G. K.; Moon, M.; Park, S. Y. Synthesis of PCDTBT-based fluorinated polymers for high open-circuit voltage in organic photovoltaics: towards an understanding of relationships between polymer energy levels engineering and ideal morphology control. *ACS Applied Materials & Interfaces* **2014**, *6* (10), 7523.
- (19) Cheng, Y.-J.; Yang, S.-H.; Hsu, C.-S. Synthesis of conjugated polymers for organic solar cell applications. *Chemical Reviews* **2009**, *109* (11), 5868.
- (20) Cartwright, L.; Iraqi, A.; Zhang, Y.; Wang, T.; Lidzey, D. Impact of fluorine substitution upon the photovoltaic properties of benzothiadiazole-fluorene alternate copolymers. *RSC Advances* **2015**, *5* (57), 46386.
- (21) Morin, P.-O.; Bura, T.; Sun, B.; Gorelsky, S. I.; Li, Y.; Leclerc, M. Conjugated polymers a la carte from time-controlled direct (hetero) arylation polymerization. *ACS Macro Letters* **2014**, *4* (1), 21.
- (22) Li, W.; Qin, R.; Zhou, Y.; Andersson, M.; Li, F.; Zhang, C.; Li, B.; Liu, Z.; Bo, Z.; Zhang, F. Tailoring side chains of low band gap polymers for high efficiency polymer solar cells. *Polymer* **2010**, *51* (14), 3031.

- (23) Iyer, A.; Bjorgaard, J.; Anderson, T.; Köse, M. Quinoxaline-based semiconducting polymers: effect of fluorination on the photophysical, thermal, and charge transport properties. *Macromolecules* **2012**, *45* (16), 6380.
- (24) Chen, S.; Su, A.; Chen, S. Noncrystalline Phases in Poly (9, 9-di-n-octyl-2, 7-fluorene). *The Journal of Physical Chemistry B* **2005**, *109* (20), 10067.
- (25) Grell, M.; Bradley, D.; Ungar, G.; Hill, J.; Whitehead, K. Interplay of physical structure and photophysics for a liquid crystalline polyfluorene. *Macromolecules* **1999**, *32* (18), 5810.
- (26) Blouin, N.; Michaud, A.; Gendron, D.; Wakim, S.; Blair, E.; Neagu-Plesu, R.; Belletete, M.; Durocher, G.; Tao, Y.; Leclerc, M. Toward a rational design of poly (2, 7-carbazole) derivatives for solar cells. *Journal of the American Chemical Society* **2008**, *130* (2), 732.

Chapter 4:-

Design and synthesis of A-D-A polymers with narrow bandgaps for photovoltaic applications

Chapter 4 - Design and synthesis of A-D_A polymers with narrow bandgaps for photovoltaic applications.

4.1 Introduction

Processable solutions of conjugated polymers have attracted significant scientific attention due to their potential application in the next generation of cheap, flexible and printed electronics^{1,2}. One such application of these is in polymer solar cells (PSCs), a vital area of investigation in organic electronics. In PSCs, irradiation from the sun generates the electricity on a blend of an n-type polymer donor and p-type polymer acceptor that are sandwiched between two electrodes³⁻⁶. Of all the polymers which have previously been studied for this application, fullerene (or n-type organic semiconductors, n-OSs) devices are most capable of offering special stable morphology to thermal and mechanical stress for practical applications in flexible devices⁷⁻¹⁰. Model polymer acceptors of this type have also been shown to harvest strong light, provide suitable energy levels, and have high affinity and mobility of electrons¹¹⁻²¹. Further improvement of polymer solar cells (PSCs) requires a new design approach, such as acceptor-donor-acceptor, to improve the polymer acceptors and their desirable properties²².

In this chapter, we report the manufacture and analysis of three novel polymers **P6**, **P7** and **P8** of acceptor-donor-acceptor (A-D-A) type consisting of IDIC-C16 as the key building block. The linking units in **P6**, **P7** and **P8** were benzothiadiazole flanked by thiophene (**M6**), bithiophene (**M7**) and fluorene (**M8**) respectively. Zhan *et al.* were the first to report IDIC with a fused aromatic ring (ID) as the donor and dicyanovinylindan-1-one (IC) as the acceptor group to synthesise their polymer (**PZ1**)²³. (**PZ1**) has highly planar structure, high electron affinity and increased absorption of light, caused by its good intermolecular charge transfer. These characteristics render it a promising n-OS acceptor. The molecular backbones of **IDIC-C16** and **IDIC** are similar, but **IDIC-C16** (shown in Scheme 4.1) has long alkyl chains in order to improve the solubility of the afforded polymer. Incorporation of **IDIC-C16** as a construction block is likely to maintain the features of the n-OS acceptor²⁴⁻²⁶ and to illustrate the extra advantages of conjugated polymers. These include good film forming properties for processing solution over a large area, further electron-transporting channels through a long range π electron delocalisation to decrease carrier recombination²⁷, and adjustment of the photophysical properties conferred by the linked building blocks.

The synthesised polymers **P6**, **P7** and **P8** were analysed using GPC, NMR and UV-vis absorption spectroscopy, TGA, CV and XRD and compared with polymer **PZ1**.

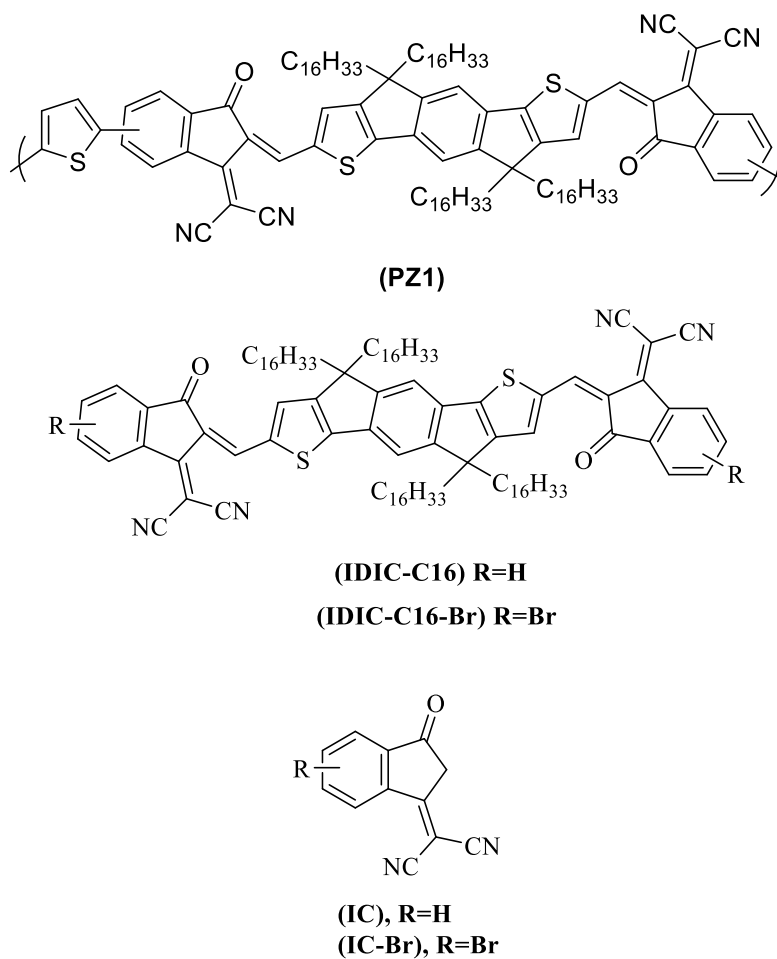
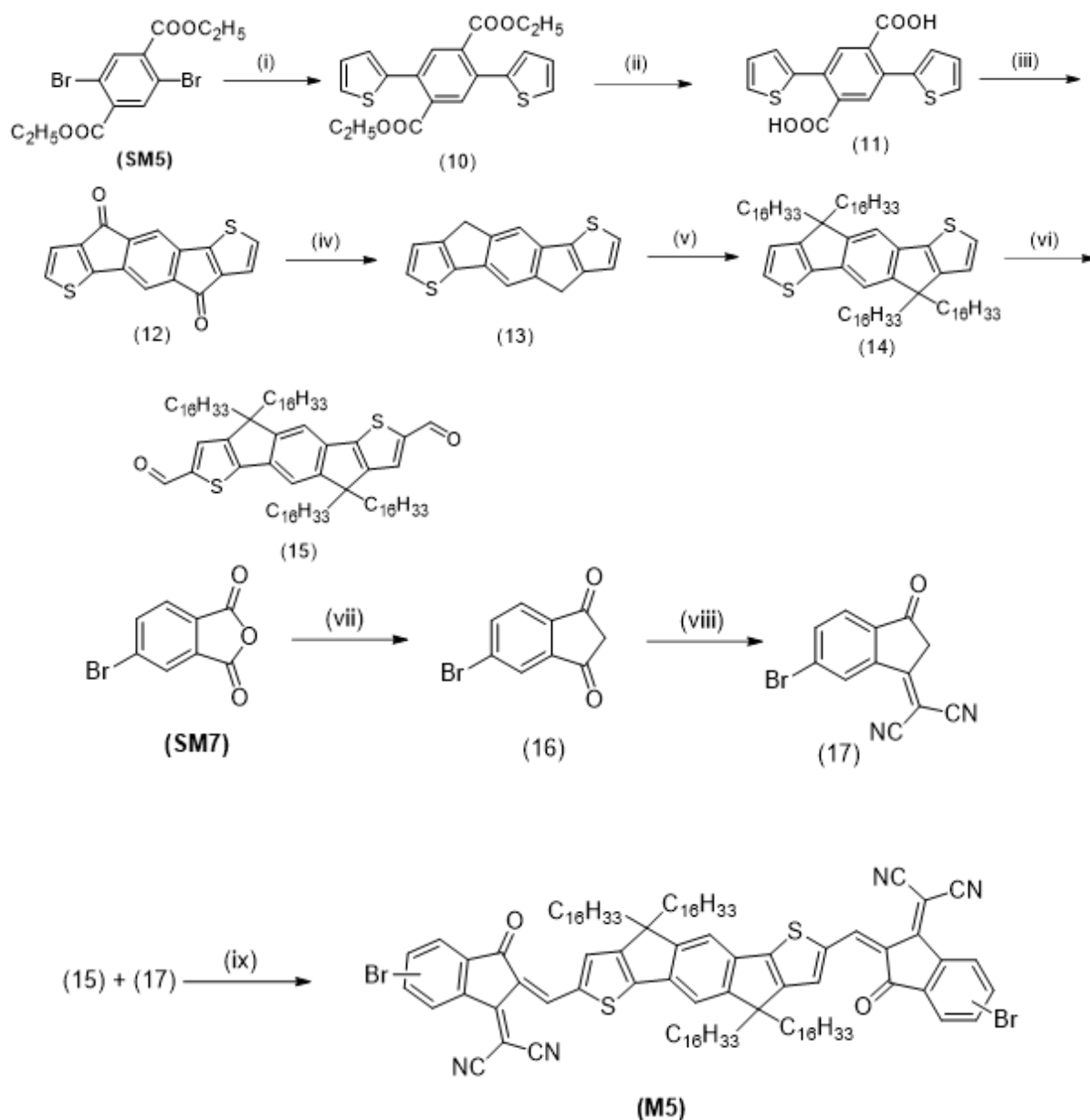


Figure 4.1: The structures of **IDIC-C16**, **IDIC-Br**, **PZ1** and **IC**, **IC-Br**.

4.2 Results and discussion

4.2.1 Synthesis of monomers

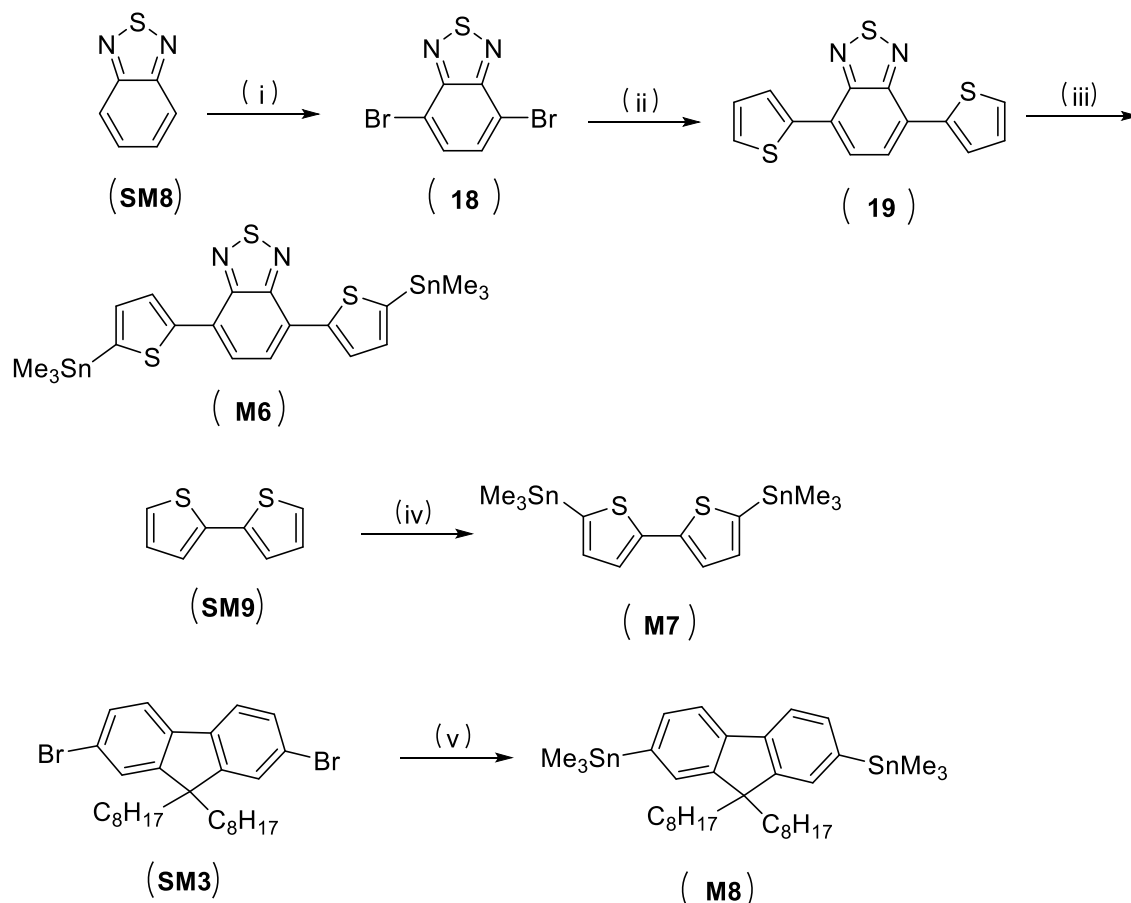
The methods of synthesising the acceptors and donors presented in this chapter are shown in the schemes below.



(i) 2-(Tributylstannyl) thiophene (SM6), Pd(PPh₃)₂Cl₂, dry THF, 85 °C for 15h. (ii) Ethanol and a solution of sodium hydroxide, reflux for 15 h, HCl. (iii) dry DCM, oxalyl chloride, dry DMF, r.t overnight, dry DCM, AlCl₃ at 0 °C, r.t overnight. (iv) Hydrazine monohydrate, KOH, diethylene glycol at 180 °C for 24 h, HCl. (v) Sodium tert-butoxide, anhydrous DMSO, 80 °C for 90 mins, 1-bromohexadecane, 90 °C overnight. (vi) dry DMF, 1,2-

dichloroethane, 0 °C, POCl₃ dropwise, 150 °C overnight. (vii) acetic anhydride, Et₃N, ethyl acetoacetate, r.t for 24 h. (viii) malononitrile, ethanol, anhydrous sodium acetate, 50 °C for 1 h. (ix) dry chloroform, pyridine, 65 °C overnight.

Scheme 4.1: Synthesis of M5.



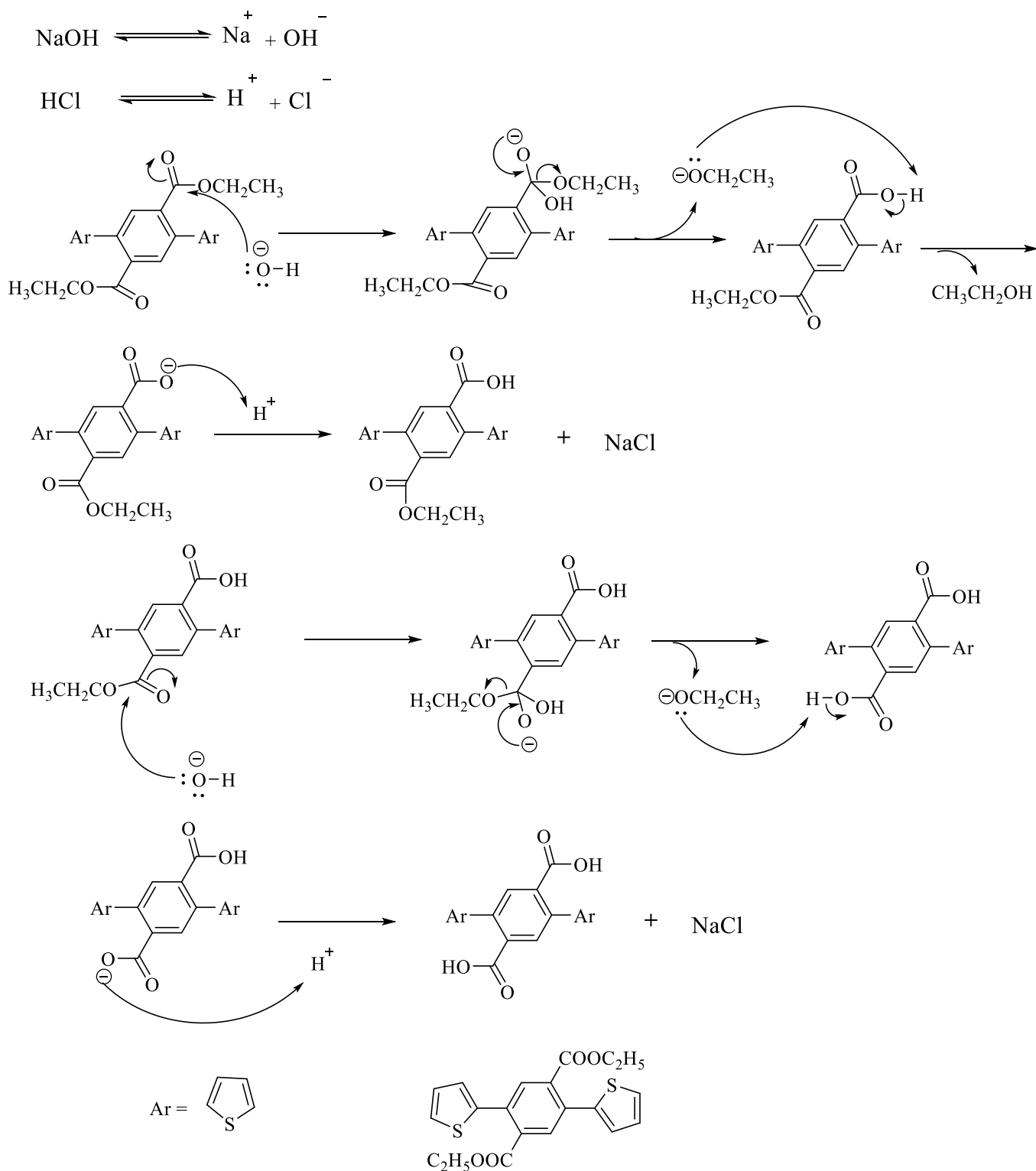
(i) hydrobromic acid, Br₂, hydrobromic acid, reflux for 3 h. (ii) tributyl-2-thienyl-stannane, Palladium (II) acetate, tri-*o*-tolyl-phosphine, dry THF, 75 °C for 24 h. (iii) 2, 2, 6, 6-Tetramethylpiperdine, dry THF, -78 °C and *n*-BuLi, Me₃SnCl, r.t overnight. (iv) dry THF, -78 °C and *n*-BuLi dropwise for 1 h, r.t for 2 h, -78 °C and Me₃SnCl, r.t overnight. (v) dry THF, -78 °C *n*-Buli, 40 °C for 2 h, Me₃SnCl, r.t for 2h.

Scheme 4.2: Synthesis of M6, M7 and M8.

The method used to synthesise product (10) was the Stille-coupling reaction between (SM5) with 2-(tributylstannyl) thiophene in the presence of Pd(PPh₃)₂Cl₂ in dry THF at 85 °C under argon for 15 hours. This process afforded a white solid after washing with methanol in yield

(83%). The proposed mechanism of this reaction is the same as that shown in Scheme 2.8 in Chapter (2)²⁸. The purity and the structure of the product (**10**) was confirmed by, ¹H NMR, ¹³C NMR, elemental analysis and mass spectrometry. The elemental analysis confirmed the structure of the product. The mass spectrum show the main integer mass at 386 (M⁺) which is in agreement with the proposed structure.

Compound (**11**) was found as an off-white solid in a high yield (99%) after hydrolysis of ester (**10**) using ethanol as a solvent in the presence of a solution of sodium hydroxide following the proposed mechanism shown below. The purity and the structure of the product (**11**) was confirmed by, ¹H NMR, ¹³C NMR, elemental analysis and mass spectrometry. The elemental analysis confirmed the structure of the product. The mass spectrum show the main integer mass at 330 (M⁺) which is in agreement with the proposed structure.



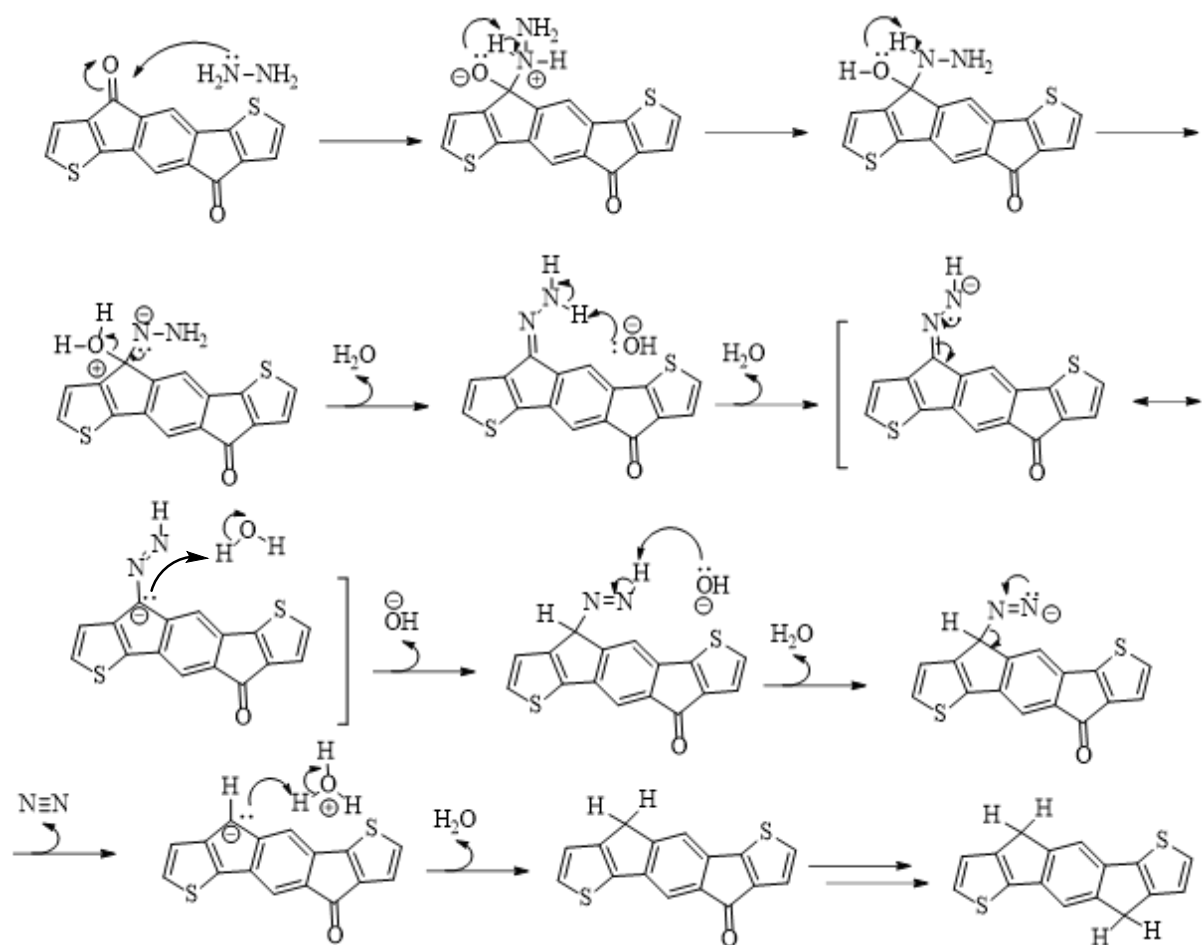
Scheme 4.3: Mechanism for the hydrolysis of ester for compound (11).

The diketone precursor (12) was obtained as a blue solid in a high yield (91%) by Friedel-Crafts reactions. This was done through the reacting of compound (11) with oxalyl chloride and dry DMF dissolved in dry DCM and stirred overnight. The solid, the diacid dichloride,

was then dissolved in dry DCM with AlCl_3 at $0\text{ }^\circ\text{C}$ and stirred at r.t overnight. The purity and the structure of the product (**12**) was confirmed by, ^1H NMR, ^{13}C NMR, elemental analysis and mass spectrometry. The elemental analysis confirmed the structure of the product. The mass spectrum show the main integer mass at 294 (M^+) which is in agreement with the proposed structure.

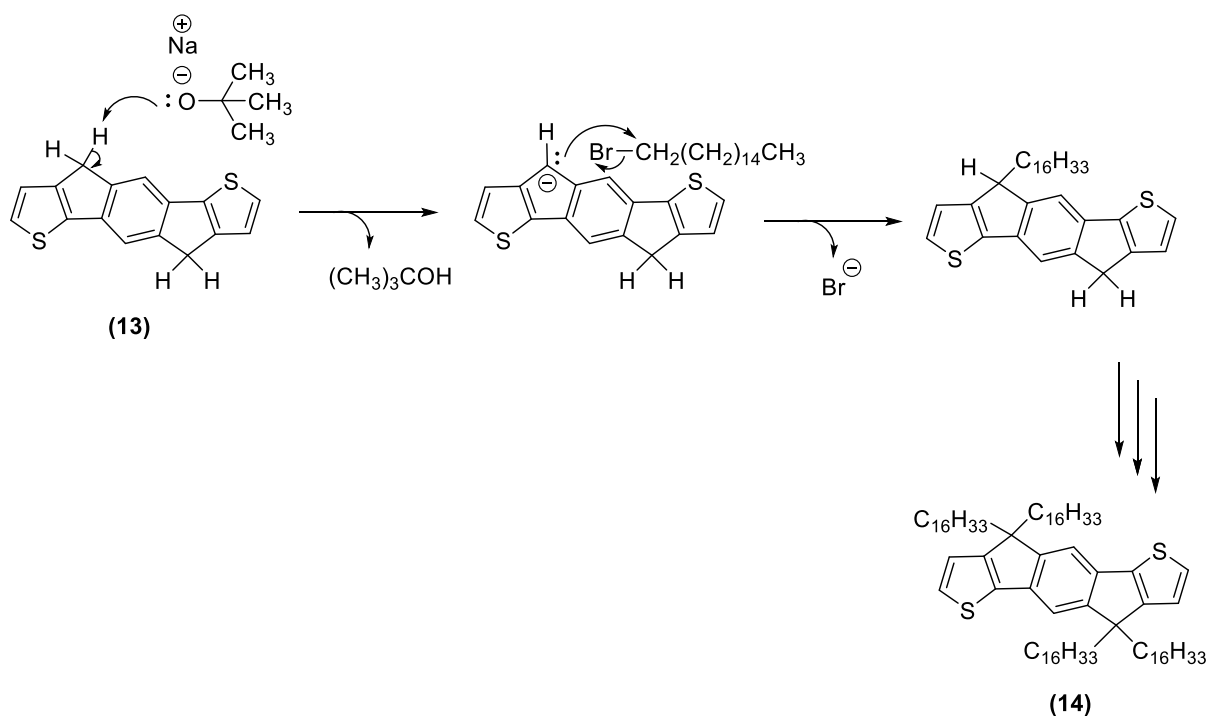
By reduction of compound (**12**) using hydrazine monohydrate in diethylene glycol with potassium hydroxide base, afforded compound (**13**) as a black solid in yield (86%). The mass spectrum show the main integer mass at 266 (M^+) which is in agreement with the proposed structure.

There are a few steps in the mechanism of this reaction, as shown in Scheme 4.3. In the first stage, the carbonyl group of (**12**) was attacked by the hydrazine monohydrate molecule, which acted as a nucleophile to produce an intermediate compound. This intermediate compound was protonated two times. A water molecule was then lost to produce a hydrazone intermediate. After that, hydroxide ion deprotonated the hydrazine intermediate to form a resonance-stabilised intermediate that was protonated and deprotonated before forming a diimide anion intermediate. The leftover of nitrogen gas formed a carbanion intermediate, which was protonated to afford compound (**13**).



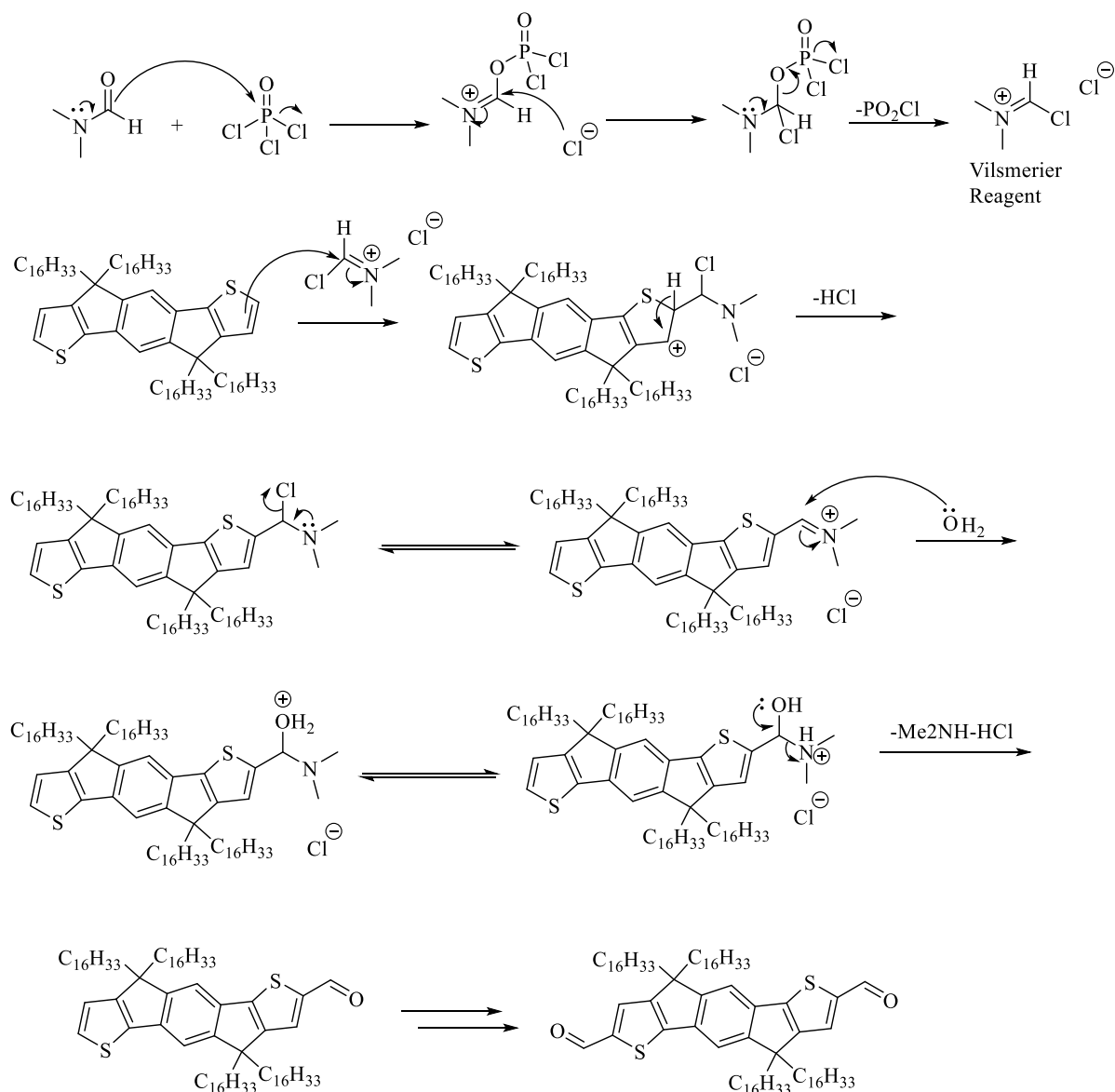
Scheme 4.4: The mechanism of reduction reaction of compound **(12)** to afford **(13)**.

The next step to synthesise the target monomer was alkylation of compound **(13)** using sodium tert-butoxide, which is a strong base, in anhydrous DMSO followed by reaction with 1-bromohexadecane. Through this process, compound **(14)** was afforded as a white to yellow solid in yield (28%). The mechanism of the reaction to afford compound **(14)** followed the bimolecular nucleophilic substitution (S_N2), as shown in Scheme 4.5. below. Initially, the protons in the rings attached between benzene and thiophenes were deprotonated by the base ($(\text{CH}_3)_3\text{CONa}$) to generate the carbanion ion nucleophile, which attacked 1-bromohexadecane to give the desired product **(14)**. The purity and the structure of the product **(14)** was confirmed by, ^1H NMR, ^{13}C NMR, elemental analysis and mass spectrometry. The elemental analysis confirmed the structure of the product. The mass spectrum show the main integer mass at 1163 (M^+) which is in agreement with the proposed structure.



Scheme 4.5: The mechanism of alkylation reaction *via* nucleophilic substitution to afford compound **(14)**.

The method used to synthesise product **(15)** was the Vilsmeier–Haack reaction²⁹. In this reaction, Vilsmeier reagent was obtained by reacting DMF with phosphorous oxychloride (POCl_3). The iminium ion was attacked by the aromatic ring, which was electron rich with loss of aromaticity. The aromaticity was restored *via* a deprotonation stage, and the chlorine ion released to form additional iminium intermediate. The final product **(15)** was afforded by aqueous work-up as a brown solid in yield (85%). The mass spectrum show the main integer mass at 1221 (M^+) which is in agreement with the proposed structure.



Scheme 4.6: The suggested mechanism of synthesis of compound (15).

5-Bromo-1,3-indanedione (**16**) was yielded as a brown solid in yield (85%) through the reaction of 4-bromophthalic anhydride (**SM7**) with acetic anhydride, triethylamine and ethyl acetoacetate at r.t for 24 h. Following this, compound (**16**) and malononitrile were dissolved in ethanol and anhydrous sodium acetate was added. The temperature was raised to 50 °C for one hour then water added, acetified, and recrystallised using a combination of acetic acid and methanol at a 1 to 1 ratio to yield product (**17**) as a black solid in yield (80%). The purity and the structure of these products (**16** and **17**) was confirmed by, ^1H NMR, ^{13}C NMR, elemental analysis and mass spectrometry. The elemental analysis confirmed the structures of the products. The mass spectrum show the main integer mass at 224 (M^+) for compound (**16**) and 272 for compound (**17**) which are in agreement with the proposed structures.

(**M5**) was obtained as a blue soils in a high yield (90%) by reacted of compounds (**15**) and (**17**) in dry chloroform in presence of pyridine. The purity and the structure of (**M5**) was confirmed by, ^1H NMR, ^{13}C NMR, elemental analysis and mass spectrometry. The elemental analysis confirmed the structure of the product. The mass spectrum show the main integer mass at 1729 (M^+) which is in agreement with the proposed structure. The ^1H NMR gave different environments as expected in the aromatic region also the peak in the aldehyde region disappeared which mean the product of (**M5**) obtained. In addition, ^1H NMR gave different peaks as expected in aliphatic area as shown in Figure 4.2.

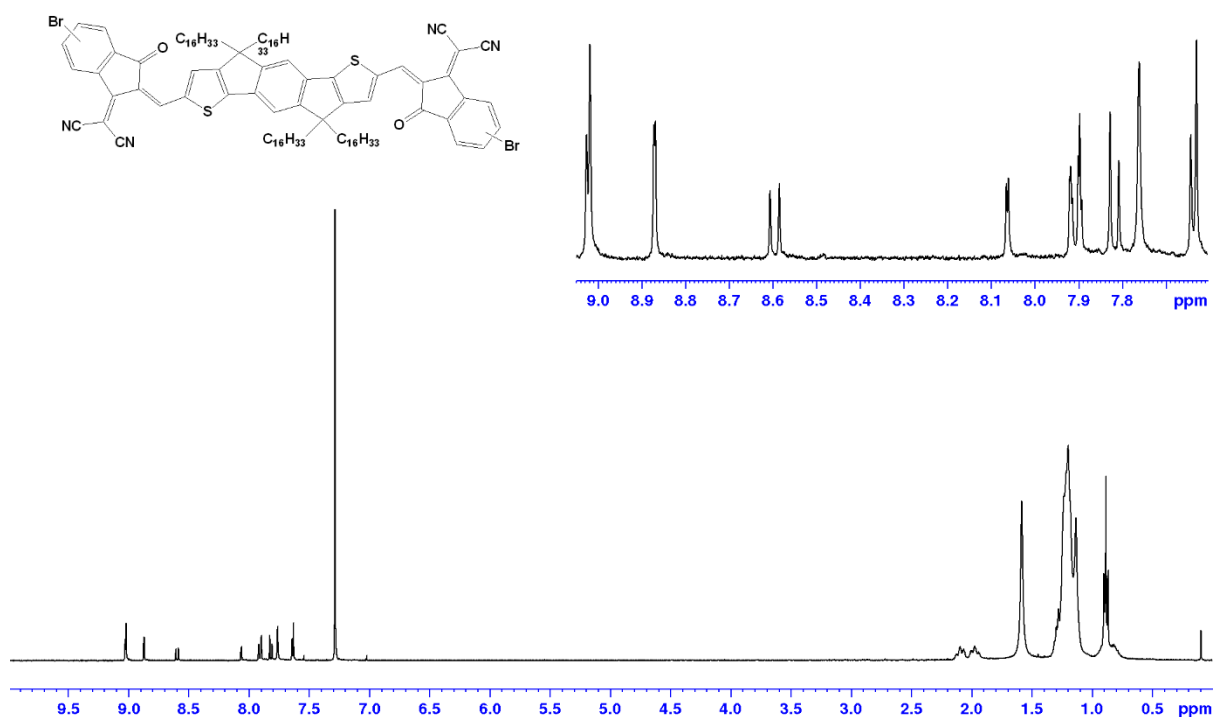


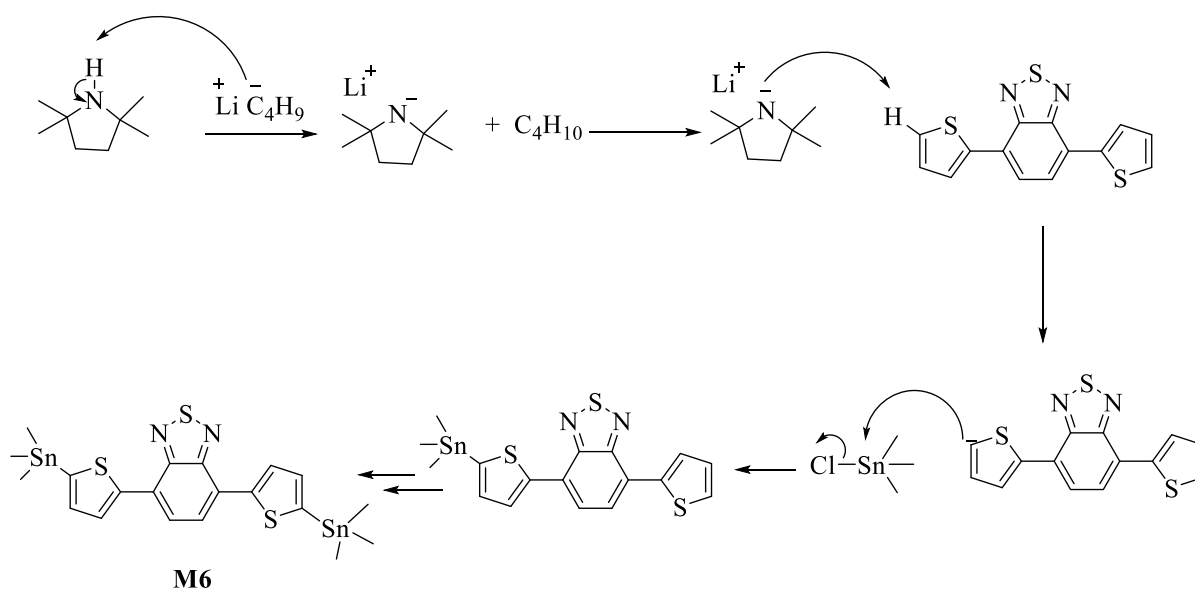
Figure 4.2. ^1H -NMR spectrum of compound (**M5**) in CDCl_3 .

To synthesise (**M6**), brominating of benzo[*c*][1,2,5]thiadiazole **SM8** at the 4, 7 positions occurred using bromine in the presence of hydrobromic acid with reflux to obtain 4,7-dibromobenzo[*c*][1,2,5]thiadiazole (**18**) as white needles in yield (70%). This occurred after it had been washed with water and chloroform had been used to recrystallise it. See Scheme 2.6 for a representation of the reaction mechanism.

Stille coupling reaction of compound (**18**) with tributyl-2-thienyl-stannane followed using palladium (II) acetate and tri-*o*-tolyl-phosphine as catalyst in dry THF kept at 75 °C for 24

hours. This formed 4,7-di (thiophene-2-yl)benzo[c] thiadiazole (**19**) as orange needles after precipitation using methanol in yield (93%). See Scheme 2.8 for a representation of the Stille coupling mechanism.

The final step to afford (**M6**) was to react 2, 2, 6, 6-tetramethylpiperdine with n-BuLi to yield lithium 2,2,6,6- tetramethylpiperdine. This was used to deprotonate compound (**19**) at thionyl – positions. 4,7-Bis(5-(trimethylstannyl) thiophene -2-yl)benzo[c][1, 2, 5] thiadiazole. (**M6**) was produced as an organic solid in yield (66%) by metalation of compound (**19**) using trimethyltin chloride (Me_3SnCl). The product (**M6**) was synthesised *via* a nucleophilic aromatic substitution ($\text{S}_{\text{N}}2$), as shown in scheme 4.7. below. The purity and the structure of all products were confirmed by, ^1H NMR, ^{13}C NMR, elemental analysis and mass spectrometry. The elemental analysis confirmed the structures of the products. The mass spectrum show the main integers' mass which they are in agreement with the proposed structures.



Scheme 4.7: The mechanism of synthesis of (**M6**).

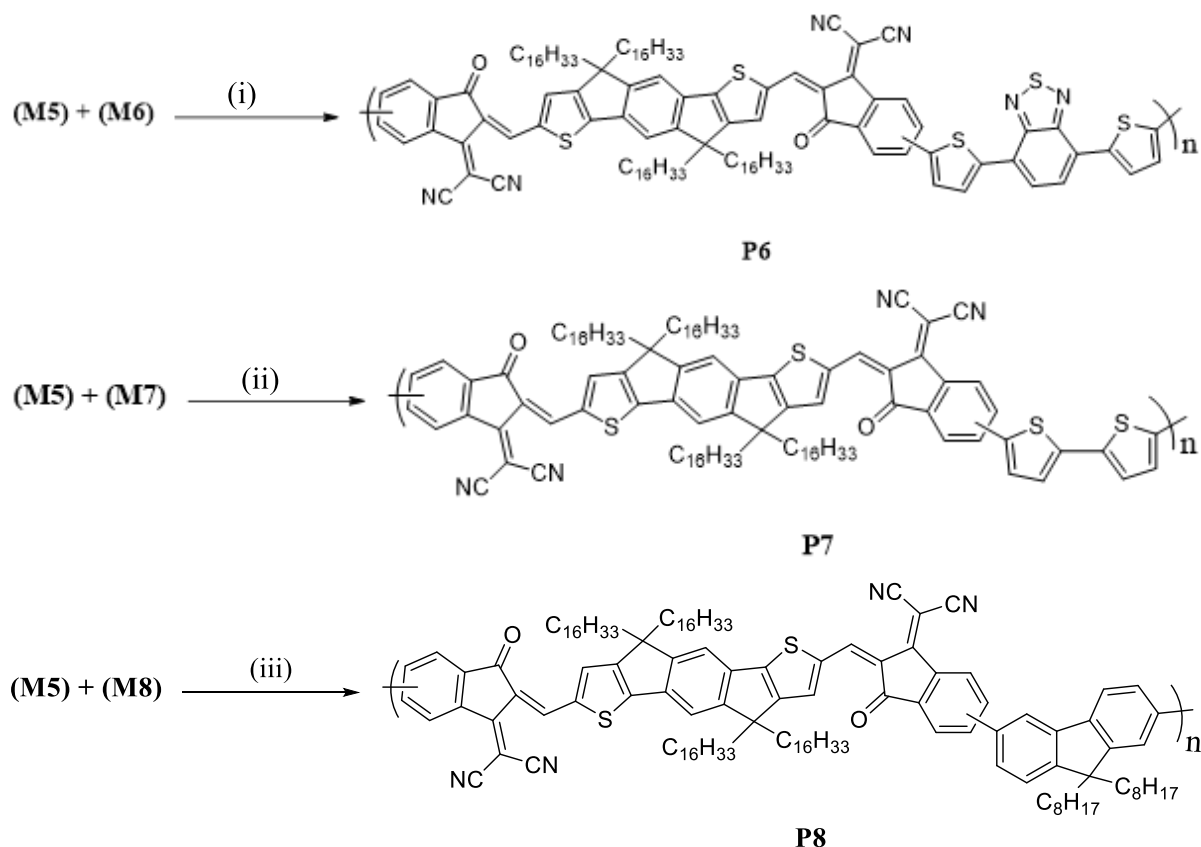
Reaction of bithiophene (**SM9**) with n-butyl lithium (2.5 M in hexane) in dry THF at (-78 °C), followed by addition of tributyltin chloride was done to obtain 5,5' –bis (trimethyl stannyl) -2,2' – bithiophene (**M7**) as a white solid in yield (62%) after it had been washed with methanol. See scheme 2.7 for the reaction mechanism. In addition, 2,7-bis(trimethyltin)-9,9-dioctylfluorene (**M8**) was obtained *via* the reaction of 2,7-dibromo-9,9-dioctyl-9H-fluorene

(**SM3**) with n-butyl lithium (2.5 M in hexane) in dry THF at (-78 °C) followed by the addition of tributyltin chloride, the product obtained as a white solid in yield (67%) and following the mechanism shown in scheme 2.7. The purity and the structures of the products (**M7** and **M8**) was confirmed by, ¹H NMR, ¹³C NMR, elemental analysis and mass spectrometry. The elemental analysis confirmed the structures of the products. The mass spectrum show the main integers' mass at 492 and 716 (M⁺) for **M7** and **M8**, which are in agreement with the proposed structures.

4.2.2 Synthesis of polymers

Three monomers were reacted with **IDIC-C16-Br (M5)**: 4,7-bis(5-(trimethylstannyl)thiophene -2-yl)benzo[c][1, 2, 5] thiadiazole (**M6**); 5,5' -bis (trimethyl stannyl)-2,2' -bithiophene (**M7**); and 2,7-bis(trimethyltin)-9,9-dioctylfluorene (**M8**). These reactions yielded **P6**, **P7** and **P8**, respectively, through Stille cross coupling reactions in the presence of tris(dibenzylideneacetone)dipalladium(0) as a catalyst and tri-o-tolyl phosphine as a ligand in a sealed tube under argon, as suggested in the literature³⁰. Dry toluene was used in these polymerisations as a solvent. The polymerisation reactions occurred for 72, 6 and 24 hours for **P6**, **P7** and **P8**, respectively, measured from the beginning of the reaction until precipitation formed in the sealed tubes. Soxhlet was then used to extract the polymers from different solvents: methanol, acetone, hexane, toluene and chloroform, after removal of the remaining catalysts by washing these with NH₄OH solution. Chloroform was collected and reduced in volume to approximately 10 ml for the subsequent steps.

The next stage involved precipitation of the polymers to yield them as powders through the addition of the polymer solutions drop-wise into methanol. When the polymers were in common organic solvents, their solubility was very high. Following this, the polymers' chemical structures were confirmed using ¹H NMR, and identification of the number average molecular weight and the weight average molecular weight was done using GPC. Scheme 4.8. illustrates the method of synthesis of **P6**, **P7** and **P8**.



(i), (ii) and (iii) Tris(dibenzylideneacetone)dipalladium(0), tri-*o*-tolyl phosphine, 6 ml of dry toluene, refluxed at 120 °C for 72, 6, 24 h .

Scheme 4.8: Synthetic routes to **P6**, **P7** and **P8**.

4.2.3 Analysis of polymers' properties

4.2.3.1 GPC analysis

It is helpful to note that the backbone of all polymers have the ICID-C16 alternate repeat units, which themselves are composed of alternating acceptor–donor–acceptor units. In **P6**, the IDIC-C16 units alternate with different donor-acceptor-donor units where the donors are thiophene rings and the acceptor is benzothiadiazole. As a result, **P6** is composed of different alternating donor and acceptor units. In **P7**, the IDIC-C16 units alternate with bithiophene donor units, while in **P8**, they alternate with fluorene donor units. Gel permeation chromatography (GPC) was conducted using polystyrene standards and chloroform as the eluent at 40 °C. According to the data presented in the table below, **P8** was measured as having the highest values of M_n and M_w compared to **P6** and **P7**: approximately three times higher than **P6** in terms of M_w . This is attributed to the large alkyl chains in the 9- positions

on fluorene repeat units, which increase the solubility of the polymer, retarding the precipitation of the polymer. This caused an increase of the Mn and Mw of the polymer. It can be said that **P7** has almost the same Mn and Mw as **P8**. On the other hand, **P6** has the lowest values of Mn and Mw compared to all polymers. This was potentially caused by the existence of benzothiadiazole and thiophene units. These have no substituents that could help increase the solubility of the final polymer. As a result, the polymer precipitated more rapidly during the polymerisation reaction, which limited the values of Mn and Mw. A comparative analysis of the Mn and Mw in **PZ1** (see figure 4.1), a similar polymer which was synthesised by Zhang *et al.*, shows values larger than those obtained for **P6**, **P7** and **P8**.

Table 4.1: GPC data for **P6**, **P7**, **P8** and their analogous polymer **PZ1**.

Polymer	Soxhlet fraction	Mn(Da)^a	Mw(Da)^a	PDI^b
P6	Chloroform	7400	12300	1.66
P7	Chloroform	12400	35400	2.85
P8	Chloroform	13000	38700	2.97
PZ1²²		33700	73900	2.19

^a Detected by differential refractive index (DRI) of the toluene, hexane and chloroform fractions of the polymer. ^b is the polydispersity index.

4.2.3.2 Optical properties of the polymers

Chloroform was used as a solvent to study the absorption behaviour of polymers in both solution and thin film. Table 4.2. illustrates the absorption maxima values of solution, film and absorption maxima onset values of thin film for the prepared polymers. The absorption maxima onset of the polymers' thin films were used to calculate their optical band gaps.

Table 4.2: UV-visible data for **P6**, **P7** and **P8**.

Polymer	λ_{max} solution (nm)	λ_{max} film (nm)	λ_{max} onset film (nm)	$E_{\text{g opt}}$ (eV)
P6	700	710	800	1.55 (+/- 0.03)
P7	703	716	805	1.54 (+/- 0.04)
P8	685	685	750	1.65 (+/- 0.06)
PZ1 ²²	700	700	800	1.55

Table 4.2. and Figure 4.3. (a), (b) show that the solution and thin films of **P6** and **P7** have minimally varying absorption maxima peaks at 700, 710 nm and 703, 716 nm respectively. In addition, the absorption peaks of **P7** are red-shifted by only 3 and 6 nm compared to **P6**. **P8** shows absorption maxima peaks of 685 nm, blue-shifted by about 15, 25 nm and 18, 31 nm, respectively, compared to **P6** and **P7**. It can be concluded that the addition of thiophene units into the backbone of **P6** and **P7** increases the planarity and the rigidity, causing absorption maxima of **P6** and **P7** to be more red-shifted than **P8**. This may be due to the incorporation of bithiophene units, which enhances the electronic delocalisation along the backbone of polymer. This increases the conjugation and consequently raises the rate of the intramolecular charge transfer along the polymer backbone.

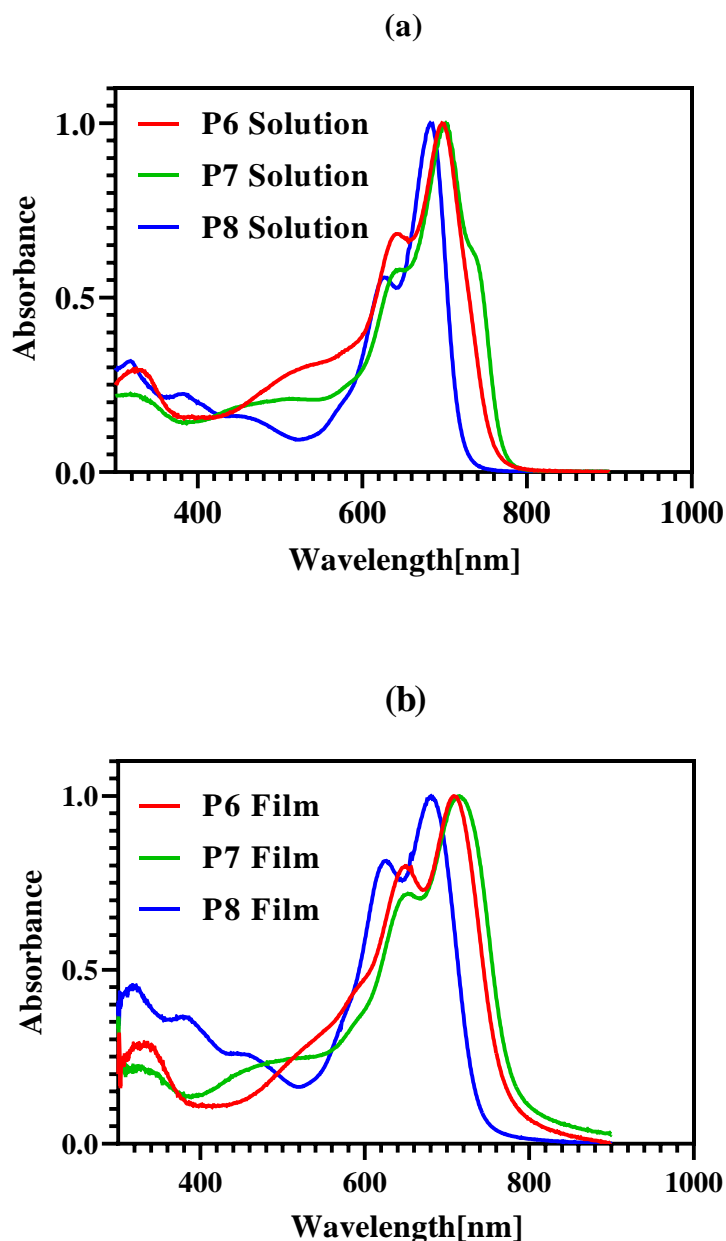


Figure 4.3: The UV-visible of **P6**, **P7** and **P8** (a) in chloroform solutions (b) in thin films.

The absorption bands of all polymers form two distinct groupings for both solutions and thin films. When the bands are formed into shorter wavelengths, this shows the π - π^* transitions from the monomer repeat units. On the other hand, when the bands form into longer wavelengths, this is when intramolecular charge transfer (ICT) occurs. The synthesised polymers **P6**, **P7** and **P8** were found to have optical band gaps of 1.55 eV, 1.54 eV and 1.65 eV with errors average (+/- 0.03, +/- 0.04, +/- 0.06), respectively, while the analogous polymer **PZ1** that has thiophene as the linking unit presents a band gap of 1.55 eV²². The band gaps of **P6** and **P7** are lower than that of **P8** by 0.1 eV and 0.11 eV, respectively,

possibly increasing the delocalisation property caused by thiophene flanking benzothiadiazole in **P6** and bithiophene in **P7**, which increased the ICT and reduced the optical band gap. Clearly the band gaps of **P6** and **P7** are the same as that of **PZ1**, possible due to the thiophene rings and the acceptor being benzothiadiazole linked to **IDIC-C16** in **P6**, the bithiophene units linked to **IDIC-C16** in **P7**, and thiophene units linked to **IDIC-C16** in **PZ1** that have quite similar absorption spectra. The band gap of **P8** is wider than those of **P6**, **P7** and **PZ1** because the fluorene which is linked to **IDIC-C16** in **P8**, is not as good an electron donor as the thiophene and bithiophene, and also causes steric hindrance, which does not lead to as planar polymers as when thiophene or bithiophene are present as repeat units. In addition, one of the reasons for the increase in the optical bandgap is the twisting of the polymer backbone when we have fluorene repeat units. These units twist the backbone of polymers out of conjugation more than thiophene units because fluorene has six member rings whereas thiophene has only a five-member ring.

4.2.3.3 Electrochemical properties of the polymers

Cyclic voltammetry was used to measure HOMO and LUMO energy levels (vs vacuum) of the polymers. This was done with drop-cast polymer films that had tetrabutylammonium perchlorate as the electrolyte material and were in acetonitrile. The HOMO levels of the prepared polymers were determined from the onsets of the oxidation potential whereas the onsets of the reduction potential were applied to calculate the LUMO levels in each polymer. The data presented in table 4.3. below indicate the results of HOMO levels and LUMO levels for synthesised polymers **P6**, **P7**, **P8** and the analogous polymer **PZ1**. The HOMO levels of **P6**, **P7** and **P8** are identical at -5.36 eV. The HOMO level for analogous polymer **PZ1** is equal to -5.74 eV, deeper than those of **P6**, **P7** and **P8**. This could be attributed to an increase of intramolecular charge transfer along the polymer backbone in these polymers.

Table 4.3: Cyclic voltammetry results for **P6**, **P7**, **P8** and **PZ1**.

Polymer	HOMO (eV) ^a	LUMO (eV) ^b	Eg(eV) ^c
P6	-5.36	-3.78	1.58 (+/- 0.07)
P7	-5.36	-3.58	1.78 (+/- 0.09)
P8	-5.36	-3.54	1.82 (+/- 0.10)
PZ1 ²²	-5.74	-3.86	1.88

^aHOMO level of the polymer determined from the onset of the oxidation potential, ^b LUMO level of the polymer determined from the onset of the reduction potential, ^c electrochemical band gap.

The LUMO levels of **P6**, **P7** and **P8** were also compared to those of their analogous polymer **PZ1** with -3.78, -3.58, -3.54 and -3.86 eV respectively. The LUMO level of **P7** and **P8** are similar to each other. However, the LUMO level of **P6** is deeper than **P7** and **P8** due to the strong acceptor, benzothiadiazole, which is on the backbone of the polymer. It is also clear that the LUMO levels of synthesised polymers **P6**, **P7** and **P8** are shallower than the LUMO level of **PZ1** due to the higher molecular weight of **PZ1**. In addition, both the HOMO and LUMO levels of **PZ1** are deeper than those we synthesised in this work. The electrochemical band gaps for **P6**, **P7**, **P8** and **PZ1** are 1.58, 1.78, 1.82 eV with errors average (+/- 0.07, +/- 0.09, +/- 0.10) respectively, and 1.88 eV for **PZ1**. The electrochemical band gap of **P6** is smaller than those of **P7** and **P8** by 0.2 eV and 0.24 eV respectively. The electrochemical band gaps of the synthesised polymers are wider than that of **PZ1** as with their optical band gaps. This is likely due to the interfacial energy barrier between the electrodes used in this system and the polymeric thin film through the reactions of reduction/oxidation.

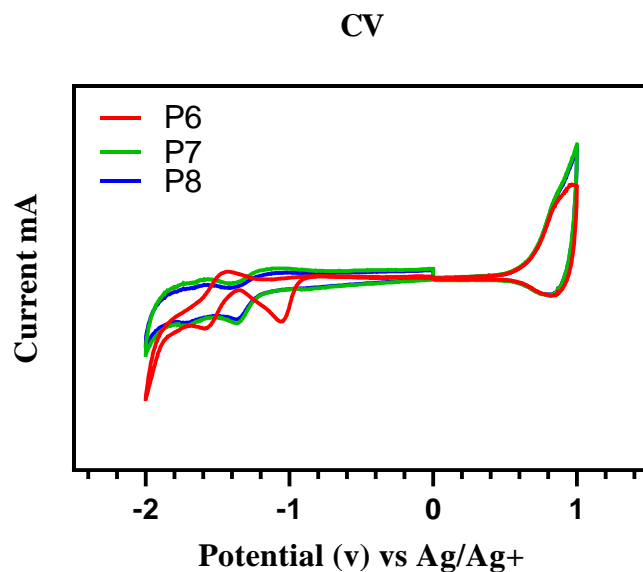


Figure 4.4: Cyclic voltammetry curves for **P6**, **P7** and **P8**.

4.2.3.4 Thermal Gravimetric Analysis (TGA)

Thermogravimetric analysis was used to measure the thermal stability of the polymers. In order to determine the temperature of the onset of decomposition (T_d), the polymers prepared were exposed to temperatures ramped up from room temperature to 800 °C at a heating rate of 10 °C / min under a nitrogen atmosphere. **P6** evidenced two decomposition phases. The first one occurred at 182 °C as a result of loss of alkyl chains attached to the donor unit in the polymer. The second decomposition phase indicated further polymer degradation at 408 °C. **P7** and **P8** showed one decomposition phase each, at 407 °C and 403 °C respectively. All polymers **P6**, **P7** and **P8** degraded until 43%, 46% and 43% of the mass remained respectively. It is hypothesised that during decomposition a burnt layer of significant thickness was created on the polymer, which insulated the polymer against the heat flux because of its minimal conductivity. This method would thus delay the polymer from thermally decomposing. In general, these polymers possess very good thermal stability for requirements of organic solar cells, which are above 400 °C. In comparison, the T_d of **PZI**²² was 386 °C, which also evidences very good thermal stability but is lower than the polymers synthesised in this work due to the decreased rigidity of **PZI**.

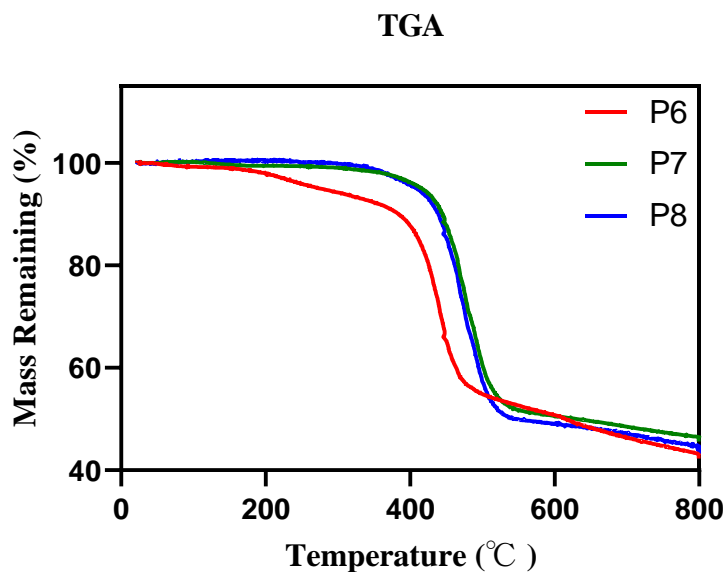


Figure 4.5: TGA curves for **P6**, **P7** and **P8**.

4.2.3.5 Polymers' XRD

The morphology of the synthesised polymers **P6**, **P7** and **P8** was investigated using powder X-ray diffraction. As shown in figure 4.5., a wide-angle broad peak can be seen at 2θ value at 19.88° for **P6**. This value is linked to a π - π stacking of 4.46 \AA distance. In addition, **P7** has a wide-angle broad peak at 2θ value at 20.27° , which corresponds to 4.38 \AA . **P8** also has a wide peak at 2θ value of 20.53 , which coincides to π - π a stacking distance of 4.32 \AA . Generally, the synthesised polymers in this work show an amorphous structure in the solid state because of the steric hindrance that results from the long alkyl chains' introduction to the backbone of the polymers, which has a major role in disturbing the π - π staking in the solid state.

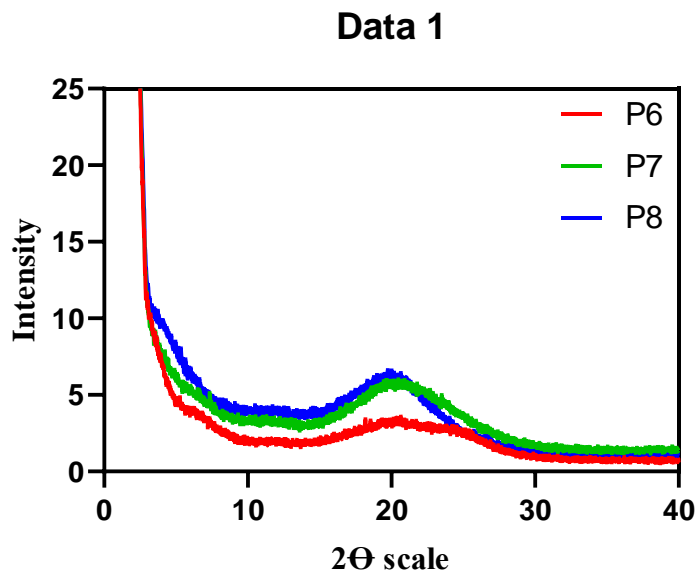


Figure 4.6: Powder X-Ray diffraction curves for **P6**, **P7** and **P8**.

4.3 Conclusion

In this study, we have synthesised three novel polymers **P6**, **P7** and **P8** comprised of acceptor–donor-acceptor (A-D-A) low-energy band gap units through a Stille cross coupling reaction procedure. Three monomers were used to react with **IDIC-C16-Br (M5)**: 4,7-bis(5-(trimethylstannyl)thien-2-yl)benzo[c][1,2,5] thiadiazole (**M6**); 5,5'–bis (trimethyl stannyl)-2,2' – bithiophene (**M7**); and 2,7-bis(trimethyltin)-9,9-dioctylfluorene (**M8**) to obtain **P6**, **P7** and **P8** respectively.

The characterisations of the polymers were analysed *via* GPC, UV-vis absorption, cyclic voltammetry, TGA and XRD. GPC determined the molecular weight of **P6**, **P7** and **P8** as $M_n = 7400$ Da, 12400 Da and 13000 Da, and $M_w = 12300$ Da, 35400 Da and 38700 Da respectively. The GPC revealed that the weight- and number-average molecular weights (M_w , M_n) of **P6** with benzothiadiazole flanked by thiophene (D-A-D) as a monomer was lower than M_w and M_n of **P7** with bithiophene as a monomer and **P8** with fluorene as monomer. This can be attributed to the presence of benzothiadiazole units without any substituents between thiophene rings. This could have limited the solubility of the polymer and caused precipitation to occur more quickly, as well as limiting the values of M_n and M_w . On the other hand, M_w and M_n of **P8** was the highest of all polymers we synthesised. This can be attributed to the large alkyl chains in the 9- position in fluorene repeat units, which increased the polymer's solubility and caused an increase of the M_n and M_w of this polymer.

In terms of optical band gaps, those of **P6** and **P7** were less than that of **P8** by 0.1 eV and 0.11 eV, respectively, indicating a higher electronic delocalisation caused by the presence of thiophene flanking benzothiadiazole units in **P6** and bithiophene in **P7**, which increased the ICT and reduced the optical band gap. In addition, the band gap of **P8** was wider than those of **P6**, **P7** and **PZ1**, because the fluorene which is linked to **IDIC-C16** in **P8**, is not as good an electron donor as the thiophene and bithiophene, and also because of the steric hindrance, which does not lead to planar polymers, as is the case for thiophene or bithiophene repeat units. In addition, one of the reasons for increasing the optical bandgap is the twisting of the polymer backbone when we have fluorene repeat units, which twist the polymer chains out of conjugation.

The electrochemical band gaps for **P6**, **P7**, **P8** and **PZ1** were 1.58, 1.78, 1.82 and 1.88 eV respectively. The band gap of **P6** was smaller than that of **P7** and **P8** as well as the analogous polymer **PZ1**. The electrochemical band gaps of the synthesised polymers and **PZ1** were found to be as high as their optical band gaps. This was caused by interfacial energy barriers between the electrodes used and the polymeric thin film through the reactions of reduction/oxidation.

The Td of **P6**, **P7** and **P8** were determined by TGA and were 408°C, 407°C and 403°C, respectively. These results evidence very good thermal stability. The Td of **PZ1** was lower at 386 °C (still showing good thermal stability) due to its comparatively lesser rigidity.

4.4 References

- (1) Li, C.; Liu, M.; Pschirer, N. G.; Baumgarten, M.; Mullen, K. Polyphenylene-based materials for organic photovoltaics. *Chemical Reviews* **2010**, *110* (11), 6817.
- (2) Wu, J.-S.; Cheng, S.-W.; Cheng, Y.-J.; Hsu, C.-S. Donor–acceptor conjugated polymers based on multifused ladder-type arenes for organic solar cells. *Chemical Society Reviews* **2015**, *44* (5), 1113.
- (3) Yu, G.; Heeger, A. Charge separation and photovoltaic conversion in polymer composites with internal donor/acceptor heterojunctions. *Journal of Applied Physics* **1995**, *78* (7), 4510.
- (4) Halls, J.; Walsh, C.; Greenham, N.; Marseglia, E.; Friend, R.; Moratti, S.; Holmes, A. Efficient photodiodes from interpenetrating polymer networks. *Nature* **1995**.
- (5) Jenekhe, S. A.; Yi, S. Efficient photovoltaic cells from semiconducting polymer heterojunctions. *Applied Physics Letters* **2000**, *77* (17), 2635.
- (6) Facchetti, A. Polymer donor–polymer acceptor (all-polymer) solar cells. *Materials Today* **2013**, *16* (4), 123.
- (7) Kim, T.; Kim, J.-H.; Kang, T. E.; Lee, C.; Kang, H.; Shin, M.; Wang, C.; Ma, B.; Jeong, U.; Kim, T. Flexible, highly efficient all-polymer solar cells. *Nature Communications* **2015**, *6*, 8547.
- (8) Zhou, E.; Cong, J.; Wei, Q.; Tajima, K.; Yang, C.; Hashimoto, K. All-polymer solar cells from perylene diimide based copolymers: material design and phase separation control. *Angewandte Chemie International Edition* **2011**, *50* (12), 2799.
- (9) Ye, L.; Jiao, X.; Zhou, M.; Zhang, S.; Yao, H.; Zhao, W.; Xia, A.; Ade, H.; Hou, J. Manipulating Aggregation and Molecular Orientation in All-Polymer Photovoltaic Cells. *Advanced Materials* **2015**, *27* (39), 6046.
- (10) Benten, H.; Mori, D.; Ohkita, H.; Ito, S. Recent research progress of polymer donor/polymer acceptor blend solar cells. *Journal of Materials Chemistry A* **2016**, *4* (15), 5340.
- (11) Yu, R.; Zhang, S.; Yao, H.; Guo, B.; Li, S.; Zhang, H.; Zhang, M.; Hou, J. Two Well-Miscible Acceptors Work as One for Efficient Fullerene-Free Organic Solar Cells. *Advanced Materials* **2017**, *29* (26), 1700437.
- (12) Fan, B.; Ying, L.; Wang, Z.; He, B.; Jiang, X.-F.; Huang, F.; Cao, Y. Optimisation of processing solvent and molecular weight for the production of green-solvent-

- processed all-polymer solar cells with a power conversion efficiency over 9%. *Energy & Environmental Science* **2017**, *10* (5), 1243.
- (13) Chen, S.; An, Y.; Dutta, G. K.; Kim, Y.; Zhang, Z. G.; Li, Y.; Yang, C. Synergetic Effect of Molecular Weight and Fluorine in All-Polymer Solar Cells with Enhanced Performance. *Advanced Functional Materials* **2017**, *27* (2), 1603564.
- (14) Yan, H.; Chen, Z.; Zheng, Y.; Newman, C.; Quinn, J. R.; Dötz, F.; Kastler, M.; Facchetti, A. A high-mobility electron-transporting polymer for printed transistors. *Nature* **2009**, *457* (7230), 679.
- (15) Jung, J. W.; Jo, J. W.; Chueh, C. C.; Liu, F.; Jo, W. H.; Russell, T. P.; Jen, A. Fluoro-Substituted n-Type Conjugated Polymers for Additive-Free All-Polymer Bulk Heterojunction Solar Cells with High Power Conversion Efficiency of 6.71%. *Advanced Materials* **2015**, *27* (21), 3310.
- (16) Guo, X.; Facchetti, A.; Marks, T. Imide-and amide-functionalized polymer semiconductors. *Chemical Reviews* **2014**, *114* (18), 8943.
- (17) Zhou, E.; Nakano, M.; Izawa, S.; Cong, J.; Osaka, I.; Takimiya, K.; Tajima, K. All-polymer solar cell with high near-infrared response based on a Naphthodithiophene Diimide (NDTI) copolymer. *ACS Macro Letters* **2014**, *3* (9), 872.
- (18) Guo, Y.; Li, Y.; Awartani, O.; Han, H.; Zhao, J.; Ade, H.; Yan, H.; Zhao, D. Improved Performance of All-Polymer Solar Cells Enabled by Naphthodiperylenetetraimide-Based Polymer Acceptor. *Advanced Materials* **2017**, *29* (26), 1700309.
- (19) Dou, C.; Long, X.; Ding, Z.; Xie, Z.; Liu, J.; Wang, L. An Electron-Deficient Building Block Based on the B←N Unit: An Electron Acceptor for All-Polymer Solar Cells. *Angewandte Chemie International Edition* **2016**, *55* (4), 1436.
- (20) Gao, L.; Zhang, Z. G.; Bin, H.; Xue, L.; Yang, Y.; Wang, C.; Liu, F.; Russell, T. P.; Li, Y. High-Efficiency Nonfullerene Polymer Solar Cells with Medium Bandgap Polymer Donor and Narrow Bandgap Organic Semiconductor Acceptor. *Advanced Materials* **2016**, *28* (37), 8288.
- (21) Kang, H.; Lee, W.; Oh, J.; Kim, T.; Lee, C.; Kim, B. From fullerene–polymer to all-polymer solar cells: The importance of molecular packing, orientation, and morphology control. *Accounts of Chemical Research* **2016**, *49* (11), 2424.
- (22) Zhang, Z. G.; Yang, Y.; Yao, J.; Xue, L.; Chen, S.; Li, X.; Morrison, W.; Yang, C.; Li, Y. Constructing a Strongly Absorbing Low-Bandgap Polymer Acceptor for High-

- Performance All-Polymer Solar Cells. *Angewandte Chemie International Edition* **2017**, *56* (43), 13503.
- (23) Lin, Y.; He, Q.; Zhao, F.; Huo, L.; Mai, J.; Lu, X.; Su, C.-J.; Li, T.; Wang, J.; Zhu, J. A facile planar fused-ring electron acceptor for as-cast polymer solar cells with 8.71% efficiency. *Journal of the American Chemical Society* **2016**, *138* (9), 2973.
- (24) Holliday, S.; Ashraf, R. S.; Wadsworth, A.; Baran, D.; Yousaf, S. A.; Nielsen, C. B.; Tan, C.-H.; Dimitrov, S. D.; Shang, Z.; Gasparini, N. High-efficiency and air-stable P3HT-based polymer solar cells with a new non-fullerene acceptor. *Nature Communications* **2016**, *7*, 11585.
- (25) Nielsen, C. B.; Holliday, S.; Chen, H.-Y.; Cryer, S. J.; McCulloch, I. Non-fullerene electron acceptors for use in organic solar cells. *Accounts of Chemical Research* **2015**, *48* (11), 2803.
- (26) Liu, J.; Chen, S.; Qian, D.; Gautam, B.; Yang, G.; Zhao, J.; Bergqvist, J.; Zhang, F.; Ma, W.; Ade, H. Fast charge separation in a non-fullerene organic solar cell with a small driving force. *Nature Energy* **2016**, *1* (7), 16089.
- (27) Cheng, C.; Geng, H.; Yi, Y.; Shuai, Z. Super-exchange-induced high performance charge transport in donor-acceptor copolymers. *Journal of Materials Chemistry C* **2017**, *5* (13), 3247.
- (28) Santos, L. S.; Rosso, G. B.; Pilli, R. A.; Eberlin, M. The mechanism of the Stille reaction Investigated by electrospray ionization mass spectrometry. *The Journal of Organic Chemistry* **2007**, *72* (15), 5809.
- (29) Vilsmeier, A.; Haack, A. Über die Einwirkung von Halogenphosphor auf Alkylformanilide. Eine neue Methode zur Darstellung sekundärer und tertiärer p-Alkylamino-benzaldehyde. *Berichte der Deutschen Chemischen Gesellschaft (A and B Series)* **1927**, *60* (1), 119.
- (30) Carsten, B.; He, F.; Son, H. J.; Xu, T.; Yu, L. Stille polycondensation for synthesis of functional materials. *Chemical Reviews* **2011**, *111* (3), 1493.

Chapter 5:-
Conclusions and future work

Chapter 5 - Conclusions and future work.

5.1 Conclusions

In this thesis, a number of new conjugated polymers were synthesised and characterised. In the second and third chapters we have presented our synthesis and analysis of donor-acceptor conjugated polymers. The fourth chapter presented the synthesis and analysis of acceptor-donor-acceptor conjugated polymers. Three novel D-A polymers were synthesised in the second chapter. The structure of polymer **P1** consisted of alternating fluorene units flanked by furan units and benzothiadiazole units, with octyloxy chains at their 5,6- positions. Polymer **P2** consisted of alternating fluorene units flanked by bifuran units and benzothiadiazole units, with octyloxy chains at their 5,6- positions: **P1** and **P3** have the same acceptor units as **P3** but contained carbazole instead of fluorene. The properties of the new polymers were compared with analogous polymers with thiophene rings (see figure 2.1). Furan moieties were added to the benzothiadiazole monomers in order to extend π -delocalisation of the electronic structures in **P2**. Two new D-A polymers were synthesised in the third chapter. Their structures consisted of alternating fluorene units flanked by furan units and benzothiadiazole units, with fluorine substituents at the 5,6- positions of the benzothiadiazole units. **P4** and **P5** have the same acceptor as polymer **P4** but carbazole was used instead of fluorene. These were compared with **P1** and **P3** also with analogous polymers (see figure 3.1). In the fourth chapter, **P6**, **P7** and **P8** were prepared and analysed as novel polymers of acceptor-donor-acceptor (A-D-A) consisting of IDIC-C16 as the key building block. The linking units in **P6**, **P7** and **P8** were benzothiadiazole flanked by thiophene (**M6**), bithiophene (**M7**) and fluorene (**M8**) respectively. These were then compared with the prepared polymer **PZI** introduced by Zhan *et al.* (see figure 4.1).

In summary, this thesis has presented the following key innovations: extending the conjugated system by flanking extra furan units next to acceptor and donor moieties; adding fluorine atoms to benzothiadiazole units; and incorporating alkoxy chains to the backbone of the polymers to increase the solubility of common organic solvents for easy characterisation. The synthesised compounds were characterised and their structures analysed using ^1H NMR, ^{13}C NMR, mass spectroscopy and elemental analysis. To be more specific, in chapter 2, three novel (D-A) conjugated polymers were synthesised – **P1**, **P2** and **P3** – *via* Suzuki coupling, direct arylation and Suzuki coupling respectively. Polymer **P1** was synthesised through

copolymerisation of benzothiadiazole with alkoxy substituents flanked by furan ring **M1** as an acceptor, the same acceptor used for all polymers described in this chapter, and fluorene as a donor *via* the Suzuki coupling procedure. Polymer **P2** was afforded *via* direct arylation between the acceptor **M1** and fluorene flanked by furan as a donor. Polymer **P3** was synthesised in the same manner as **P1** except that the donor was carbazole instead of fluorene. In terms of the findings, GPC determined the molecular weight (M_n) of **P1**, **P2** and **P3** as 11500 Da, 16400 Da and 10500 Da respectively. According to the results of GPC, **P2** revealed the highest M_n value among these prepared polymers due to the incorporation of an extra furan unit flanked with the acceptor units, which led to a decrease in the steric hindrance between the groups linked to the acceptor and donor units through the reaction.

The optical properties of these polymers were investigated in two states: as solutions and as films. The results show the onset of absorbance maxima values (616 nm, 642 nm and 607 nm) for **P1**, **P2** and **P3** respectively. The optical band gaps calculated from the onset of absorbance maxima for **P1**, **P2** and **P3** were 2.01 eV, 1.93 eV and 2.04 eV respectively. It is clear from the band gap of **P2** that the extension of the backbone of the polymer with the additional furan narrowed the optical band gap compared to **P1** and **P3**. This can be attributed to the higher molecular weight caused by the introduction of an extra furan in the former, which then led to an increase in the electronic delocalisation along the backbone of polymer, increasing the conjugation, and consequently increasing the ICT along the polymer backbone. Further to this, thermal gravimetric analysis (TGA) showed that **P1** and **P3** possessed good thermal stability above 300°C whereas **P2** only maintained stability at 200°C; less than **P1** and **P3** but still good. Powder XRD studies of **P1**, **P2** and **P3** showed broad peaks, which is indicative of amorphous shapes that could have been caused by the steric hindrance resulting from the alkoxy chains attached to the backbone of the polymers. A comparison between **P1**, **P2** and **P3** with analogous polymers **PFDTBT-8**, **PFDT2BT-8** and **PCDTBT-8** with thiophene units instead of furan units showed that the optical properties and electrical properties of **P1**, **P2** and **P3** had a similar or slightly wider bandgap than analogous polymers. Moreover, the M_n and M_w of **PFDTBT-8**, **PFDT2BT-8** and **PCDTBT-8** were higher than those of **P1**, **P2** and **P3**. This is believed to be due to the increase in the electronegativity of oxygen present in the furan ring, which increased the π - π staking and led to the precipitation of the polymer being more rapid than with thiophene-based polymers, preventing the increase of M_n and M_w .

In chapter 3, two new (D-A) conjugated polymers **P4** and **P5** were designed and synthesised *via* direct arylation. The acceptor was benzothiadiazole with fluorine atoms at the 5,6-positions flanked by furan **M4** for both polymers. The donors were fluorene and carbzole for **P4** and **P5** respectively. The molecular weights (Mn) of **P4** and **P5** were very low – (2800 Da) and (2900 Da) respectively – compared to **P1** and **P3**. This can be attributed to the presence of fluorine atoms instead of alkoxy side chains in the benzothiadiazole unit, leading to strong π - π staking and the aggregation of polymer chains. Therefore, the precipitation of the polymer occurred quickly and limited the molecular weight of the product. The optical band gaps of **P4** and **P5** were similar at 1.91 eV and 1.92 eV, respectively, perhaps due to the similarity in their molecular weight. The cyclic voltammetry showed that the bandgaps of **P4** and **P5** were 2.04 eV and 2.02 eV respectively. Finally, TGA showed that **P4** and **P5** had good thermal stability above 400°C.

In addition, a comparison of **P4** and **P5** with analogous polymers **PFO-DFFBT** and **PCDTBT-F** and **P1** and **P3** with an alkoxy group instead of fluorine atoms showed that the molecular weights of analogous polymers **PFO-DFFBT** and **PCDTBT-F** were larger than those of **P4** and **P5**. The reason for this is possibly due to the decrease of electronegativity of sulfur in the thiophene ring compared to the oxygen in the furan ring, which led to a decrease in the π - π staking of the compounds of thiophene. This then would have caused the precipitation of the polymer to take more time to occur, increasing the molecular weight compared to the polymers with furan rings. Moreover, the molecular weights Mn of **P4** and **P5** were smaller than those of **P1** and **P3** due to the exchange of the alkoxy group with fluorine substituents on their benzothiadiazole repeat units. This exchange disturbed the π - π stacking and controlled the aggregation, resulting in a higher molecular weight. Another finding is that the optical and electrical bandgaps of **P4** and **P5** were narrower than those for **P1** and **P3** due to the two fluorine atoms attached at the 5,6-positions of the benzothiadiazide units, providing stronger electron accepting properties and higher ICT on the backbone of the resulting polymers. In addition, the stability of these polymers was higher than the analogous polymers in the last chapter, which could be due to the changing the alkyl chains by fluorine atoms, because the alkoxy groups on the benzothiadiazole units could easily break, leading to degradation and loss of alkoxy side chains compared to fluorine substitutions.

In chapter 4, three novel polymers (**P6**, **P7** and **P8**) that have alternating acceptor-donor-acceptor units (A-D-A) with low-energy band gaps were prepared *via* a Stille cross coupling reaction procedure. The monomer **IDIC-C16-Br** (**M5**) was reacted with three different

monomers: benzothiadiazole flanked by thiophene, bithiophene and fluorene respectively. The molecular weights M_n of **P6**, **P7** and **P8** were 7400 Da, 12400 Da and 13000 Da respectively. It is clear that **P8** had the highest molecular weight due to the large alkyl chains linked in the 9-positions of the fluorene units, which increased the solubility and prevented precipitation from occurring during the polymerisation reaction. This then led to a high molecular weight – **P6** had the lowest molecular weight value among this family of polymers. The optical bandgaps of **P6**, **P7** and **P8** were 1.55 eV, 1.54 eV and 1.65 eV, respectively, and that of the analogous polymer **PZI** was 1.55 eV. The electrochemical bandgaps of **P6**, **P7** and **P8** were 1.58 eV, 1.78 eV and 1.82 eV, respectively, and that of **PZI** was 1.88 eV. These polymers all showed good thermal stability above 400°C.

To conclude, the synthesised polymers based on alkoxy functionalised benzothiadiazole units flanked with furan groups, fluorinated benzothiadiazole flanked with furan units as an acceptor, and fluorene flanked by furan and carbazole in (D-A) polymers showed good optical and electrochemical properties, good thermal stability and showed amorphous structures. Exchange of thiophene units by furan units in acceptors or donors did not allow the narrowing of the band gap. Furthermore, polymers containing furan displayed similar electronic and optical properties relative to their thiophene analogues. It should be mentioned that conjugated polymers (D-A-D) possessed significantly reduced band gaps than the (D-A) polymers prepared in this work.

5.2 Future work

In this thesis, a number of furan-based D-A conjugated polymers were synthesised with low energy bandgaps. Further polymers with much reduced band gaps were also prepared and presented good optical and electrochemical properties that should enable them to act as good electron donors when blended with PC₇₁BM, as well as other non-fullerene acceptors, for application in BHJ solar cells. We anticipate that the furan-based polymers should have better performance than their thienyl analogues described in the literature, in view of their higher fluorescence efficiency. Future work should hence include the investigation of the photovoltaic properties of the polymers prepared in this thesis using both fullerenes and non-fullerene acceptors with adequate HOMO and LUMO energy levels. We also propose to prepare other polymers using monomer (**M1**) as an acceptor with different donors, such as pyrene and bithiophene, to obtain novel polymers with low band gaps. It might also be worthwhile extending the conjugation system of the benzothiadiazole-based acceptor to

achieve better results in terms of bandgap narrowing. Figure 5.1 below shows suggested polymers.

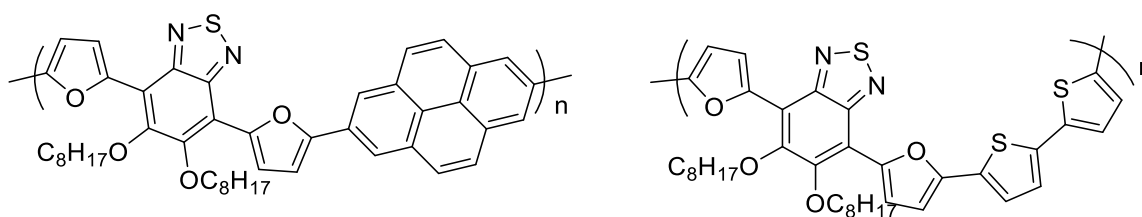


Figure 5.1: Chemical structure of suggested conjugated polymers.

We noticed that the fluorinated benzothiadiazole acceptor narrowed the bandgaps of polymers **P4** and **P5**, we have presented in this work, but this has also decreased the molecular weights of the resulting polymers in view of increased π - π stacking between polymer chains, which caused their aggregation. Therefore, the precipitation of the polymer occurred quickly and limited the molecular weights of the products prepared. In the future, we will incorporate alkyl-solubilising chains in the 3-positions of the furan moieties in monomer (**M4**) and copolymerise this with fluorene or carbazole to increase the solubility and increase the molecular weight of the resulting polymers. The molecular structures of these suggested polymers are shown in figure 5.2.

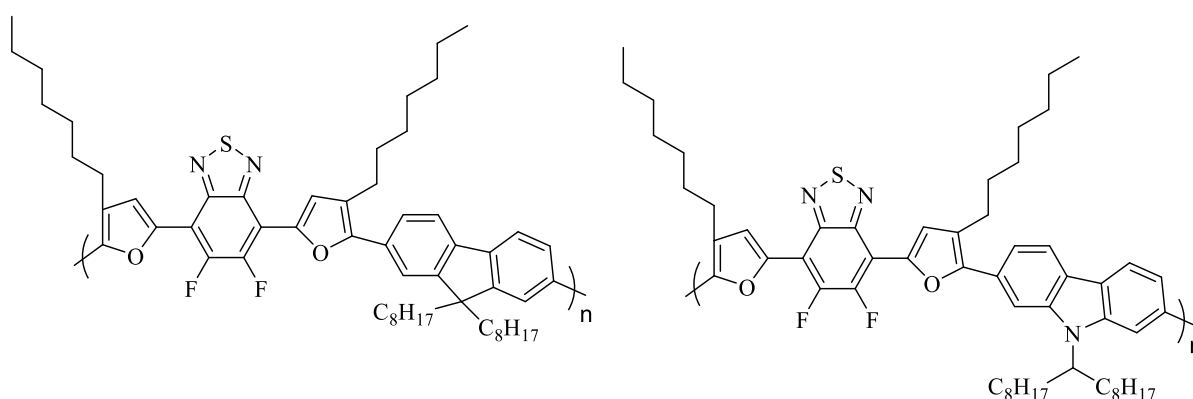


Figure 5.2: Chemical structure of suggested conjugated polymers.

Finally, we synthesised excellent A-D-A conjugated polymers with narrow bandgaps between 1.54 to 1.65 eV, which will be ideal electron acceptors to other electron donating polymers, such as PBDB-T¹, in BHJ solar cells. Future should include an investigation of the photovoltaic properties of polymers **P6**, **P7** and **P8** as electron acceptors to PBDB-T, as well as to other electron donating polymers in BHJ solar cells. Further work could also include the preparation of analogous polymers to **P6**, **P7** and **P8** with different donors that will use

furan units instead of thiophene units and carbazole instead of fluorene units. The properties of these materials will then be compared to their thienyl analogues. The molecular structures of these suggested polymers are shown in figure 5.3.

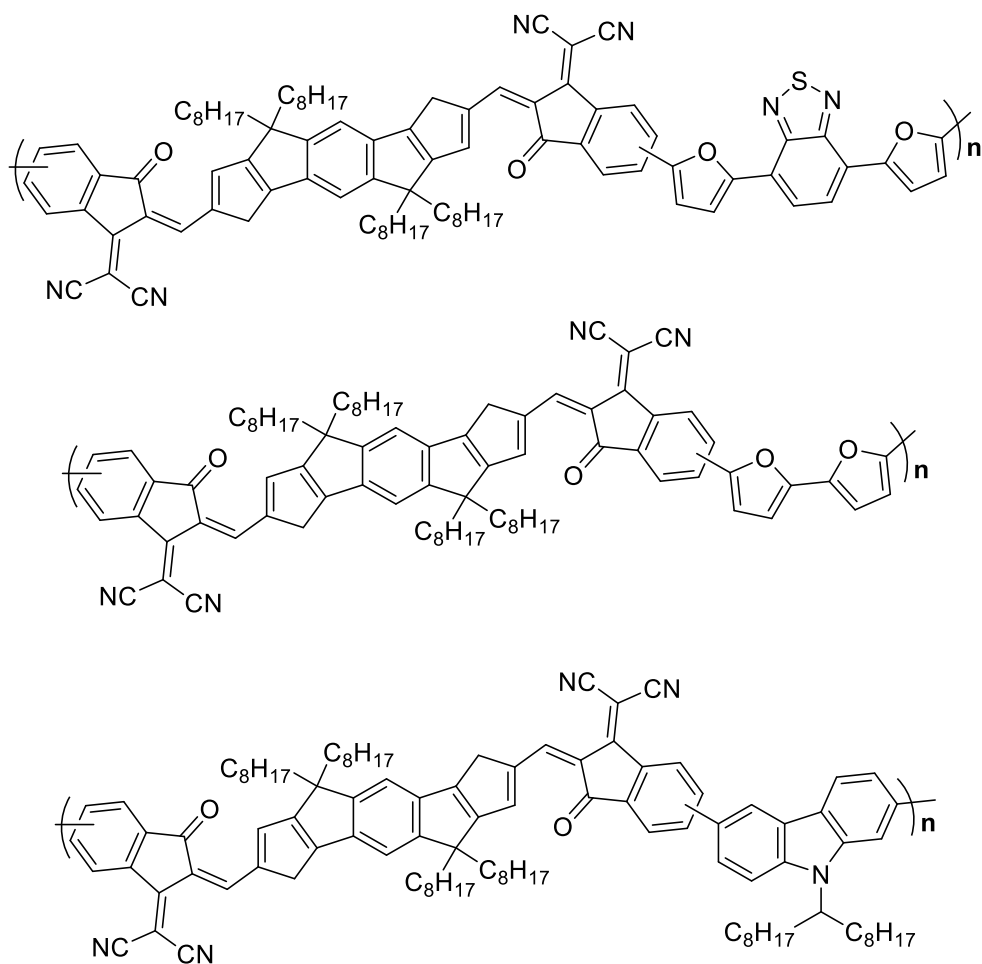


Figure 5.3: Chemical structure of suggested conjugated polymers.

Reference

- (1) Zhang, Z. G.; Yang, Y.; Yao, J.; Xue, L.; Chen, S.; Li, X.; Morrison, W.; Yang, C.; Li, Y. Constructing a Strongly Absorbing Low-Bandgap Polymer Acceptor for High-Performance All-Polymer Solar Cells. *Angewandte Chemie International Edition* **2017**, 56 (43), 13503.

Chapter 6:- Experimental

Chapter 6 - Experimental.

6.1 Materials

The chemicals applied in this research were bought from Sigma–Aldrich, Fisher Scientific and Alfa Aesar and were used without purification unless otherwise stated. The internal chemical store at the University of Sheffield sold us the common solvents used in the experiments. Dry solvents (chloroform, dichloromethane, toluene, THF and DMF) were purchased from Grubbs services and were used without modification.

The following were bought and used without purifying them: Catechol (**SM1**), furan (**SM2**), 2,7-dibromo-9,9-dioctyl-9*H*-fluorene (**SM3**), 9,9-dioctyl-2,7-bis(4,4,5,5-tetramethyl-1,3,2-dioxaborolan-2-yl)-9*H*-fluorene (**SM4**), diethyl 2,5-dibromoterephthalate (**SM5**), 2-(tributylstannyl) thiophene (**SM6**), 4-bromophthalic anhydride (**SM7**), benzo[*c*][1,2,5]thiadiazole (**SM8**), 2,2'-bithiophene (**SM9**) and 2,7-dibromo-9-(heptadecan-9-yl)-9*H*-carbazole (**SM10**).

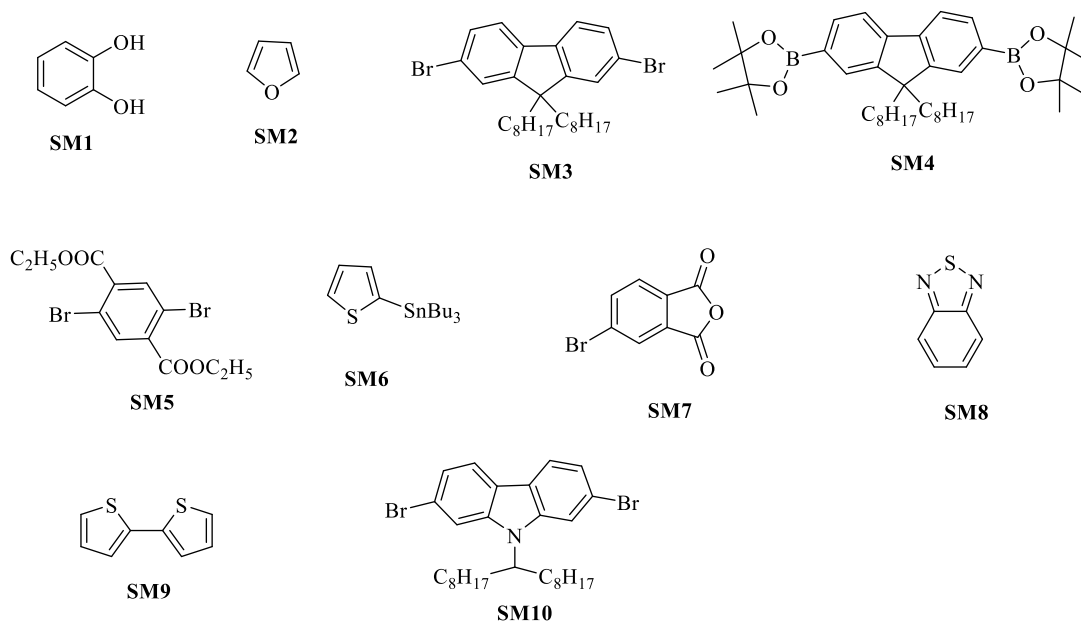
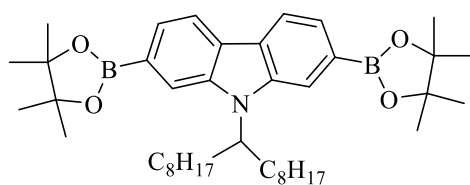


Figure 6.1: Commercially purchased materials.

9-(heptadecan-9-yl)-2,7-bis(4,4,5,5-tetramethyl-1,3,2-dioxaborolan-2-yl)-9*H*-carbazole (**SM11**), 5,6-difluorobenzo[*c*][1,2,5]thiadiazole (**SM12**) shown below were prepared by the Iraqi group.



SM11

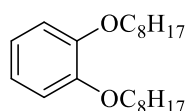


SM12

Figure 6.2: Materials synthesised by the Iraqi group.

6.2 Synthesis of monomers and polymers for chapter 2

6.2.1 1, 2-Bis (octyloxy) benzene (2) ¹

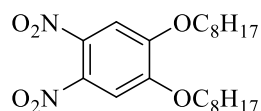


Dry DMF (25ml) was added to a mixture of 1-bromooctane (16.41 mL, 18.35 g, 95.01 mmol), potassium carbonate (19.00 g, 137.45 mmol) and catechol (5.00 g, 45.41 mmol). The mixture was then stirred under argon overnight at 100 °C. The organic layer was separated by adding water (200 mL). Then, the organic layer was extracted with DCM (3× 100 mL) and washed with water (5×200 mL) to remove excess DMF. The sample was dried with MgSO₄ and the solvent was eliminated under reduced pressure. The crude product was purified by recrystallisation from methanol to obtain 1,2-bis(octyloxy)benzene (**2**) as white needle crystals (9.92g, 66% yield).

¹H NMR (400 MHz, CDCl₃): (δH/ppm) 6.90 (s, 4H); 4.00 (t, *J*= 7.0 Hz, 4H); 1.87 – 1.31 (m, 24H); 0.91 (t, *J*= 7.0 Hz, 6H). ¹³C NMR (CDCl₃): (δC/ppm) 149.3, 121.0, 114.1, 69.3, 31.9, 29.4, 29.4, 29.3, 26.1, 22.7, 14.1. EI-MS (m/z) [M]⁺ calculated for C₂₂H₃₈O₂, 334.29; found 334. Elemental analysis calculated for C₂₂H₃₈O₂; C, 78.99; H, 11.45 % found C, 78.90; H, 11.03%.

M.P. 24 – 26 °C in close agreement with reported value in the literature (25 – 26 °C)¹.

6.2.2 1,2-Dinitro-4,5-bis(octyloxy)benzene (**3**)²

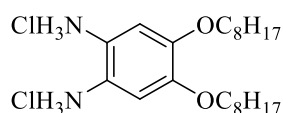


A solution containing acetic acid (160 mL), DCM (160 mL) and 1,2-bis(octyloxy)benzene (**2**) (10.00 g, 29.9 mmol) was cooled to 10 °C, before the dropwise addition of 65% nitric acid (20 mL). Cooling of the mixture to 10 °C occurred again after it had been stirred at room temperature for an hour. Then, fuming nitric acid (50 mL, 100%) was added dropwise. The reaction mixture was stirred at room temperature for 40 hours, before being poured over ice-water. The organic layer was extracted using DCM (3×300 mL) and washed with water (3×400 mL), saturated NaHCO₃ (2×300 mL) and saturated NaCl solutions (2×300 mL). The organic layer was dried over MgSO₄ and reduced pressure was used to remove the solvent. Purification of the crude product was achieved *via* recrystallisation from ethanol to obtain 1,2-dinitro-4,5-bis(octyloxy)benzene (**3**) as yellow crystals (8.17 g, 64% yield).

¹H NMR (CDCl₃): (δH/ppm) 7.31 (s, 2H); 4.12 (t, *J* = 6.5 Hz, 4H); 1.94 – 1.82 (m, 4H); 1.54 – 1.20 (m, 20H); 0.91(t, *J* = 7.0 Hz, 6H). ¹³C NMR (CDCl₃): (δC/ppm) 151.8, 136.4, 107.9, 70.2, 31.8, 29.2, 28.7, 25.8, 22.7, 14.1. EI-MS (m/z) [M]⁺ calculated for C₂₂H₃₆N₂O₆, 424.26; found 424.3. Elemental analysis calculated for C₂₂H₃₆N₂O₆; C, 62.24; H, 8.55; N, 6.60 % found C, 62.31; H, 8.43; N, 6.56 %.

M.P. 87 – 89 °C in close agreement with reported value in the literature (87 – 87.5 °C)².

6.2.3 4,5-Bis(octyloxy)benzene-1,2-diammonium chloride (**4**)³



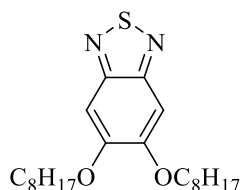
4,5-Bis(octyloxy)benzene-1,2-diammonium chloride (**4**) was prepared using the procedure specified in Helgesen *et al.*'s work³.

A solution containing 1,2-dinitro-4,5-bis(octyloxy)benzene (**3**) (4.00 g, 9.42 mmol), tin (II) chloride, Sn(II)Cl₂ (14.30 g, 75.42 mmol), conc. HCl (40 mL) and ethanol (100 mL) was

heated to 85 °C overnight. When this mixture was then left to cool to room temperature, it was observed that a white precipitate had formed. The precipitate was collected *via* filtration and washed with both water and ethanol. Lastly, the precipitate was dried under N₂, and this yielded a white powder (3.31g, 85% yield) that was used without modification in the next reaction.

No further characterisation was conducted due to the instability of the product.

6.2.4 5,6-Bis(octyloxy)benzo[c][1,2,5]thiadiazole (**5**)⁴

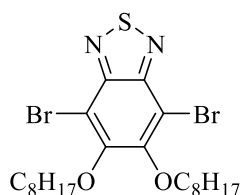


A solution was prepared that contained triethylamine (18.5 mL, 13.43 g, 132.73 mmol) and 4,5-bis(octyloxy)benzene-1,2-diammonium chloride (**4**) (8.33 g, 19.040 mmol) in dry DCM (217 mL). Then a second solution containing thionyl chloride (2.6 mL, 4.26 g, 35.84 mmol) in dry DCM (53.7 mL) was added dropwise to the first solution. After the addition was complete, the combined solutions were heated to reflux overnight. The aqueous phase was washed using water and then extracted with DCM (3×150 mL). Combination and drying of the organic phases with MgSO₄ occurred and then the solvent was removed under lower pressure. Finally, the crude product was purified by recrystallisation from ethanol to obtain 5,6-bis(octyloxy)benzo[c][1,2,5]thiadiazole (**5**) as a brown solid (5.20 g, 70% yield).

¹H NMR (CDCl₃): (δH/ppm) 7.15 (s, 2H); 4.11 (t, *J* = 7.0 Hz, 4H); 1.98 -1.87 (m, 4H); 1.59 - 1.27 (m, 20H); 0.91 (t, *J* = 7.0 Hz, 6H). ¹³C NMR (CDCl₃): (δC/ppm) 154.2, 151.4, 98.4, 69.1, 31.2, 29.7, 29.3, 28.7, 26.0, 22.7, 14.1. EI-MS (*m/z*) [*M*]⁺ calculated for C₂₂H₃₆N₂O₂S, 392.25; found 392. Elemental analysis calculated for C₂₂H₃₆N₂O₂S + (0.05 H₂O); C, 67.15; H, 9.25; N, 7.12; S, 8.15 % found C, 66.62; H, 8.64; N, 7.13; S, 8.78 %.

M.P. 96 – 98 °C in close agreement with reported value in the literature (97.1 – 97.5 °C)⁴.

6.2.5 4,7-Dibromo-5,6-bis(octyloxy)benzo[c][1,2,5]thiadiazole (6)⁴

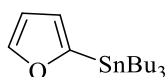


Bromine (4.58 mL, 14.34 g, 88.84 mmol) was added to a solution of 5,6 bis(octyloxy)benzo[c][1,2,5]thiadiazole (**5**) (5.00 g, 12.7mmol), acetic acid (100 mL) and DCM (250 mL). This mixture was then stirred in the dark at room temperature for 48h. Once the reaction had completed, the mixture was poured over water (400 mL). The organic phase was extracted with DCM (3 × 200 mL) and washed with water, (3×200 mL) saturated NaHCO₃ (3×200 mL) and 1M Na₂S₂O₃. The organic phase was then dried over MgSO₄ and the solvent was eliminated under reduced pressure. Finally, purification of the product was done *via* recrystallisation from ethanol to obtain 4,7-dibromo-5,6-bis(octyloxy)benzo [c][1,2,5]thiadiazole (5.88 g, 84 % yield).

¹H NMR (CDCl₃): (δH/ppm) 4.18 (t, *J* = 7.0 Hz, 4H); 1.95 –1.86 (m, 4H); 1.58 - 1.31 (m, 20H); 0.92 (t, *J* = 7.0 Hz, 6H). ¹³C NMR (CDCl₃): (δC/ppm) 154.5, 150.4, 106.3, 75.2, 31.8, 30.3, 29.4, 29.3, 26.0, 22.7, 14.1. EI-MS (*m/z*) [*M*]⁺ calculated for C₂₂H₃₆N₂O₂S, 550.07; found 550. Elemental analysis calculated for C₂₂H₃₄Br₂N₂O₂S; C, 48.01; H, 6.23; N, 5.09; Br, 29.04; S, 5.82 % found C, 48.02; H, 6.21; N, 5.03; Br, 29.19; S, 6.21 %.

M.P. 44 – 46 °C in close agreement with reported value in the literature (44.5 – 45.6 °C)⁴.

6.2.6 Tributyl(furan-2-yl)stannane (7)⁵

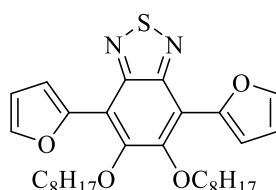


n-BuLi (2.5M in hexane) (2.68 g, 16.76 mL, 41.9 mmol) was added dropwise to a solution of furan (3.00 g, 3.21 mL, 41.9 mmol) in dry THF (20 mL) at –78 °C under an inert argon atmosphere and then stirred for 2 hours. Following this, the temperature of the solution was

increased to 40 °C and Bu₃SnCl (13.64 g, 11.37 mL, 41.9 mmol) was added dropwise to the reaction mixture before being stirred for 2 hours under argon. Then the solution was warmed to room temperature and stirred overnight. Ethyl acetate (50 mL ×3) and saturated NaCl (50 mL ×3) were added to the solution to extract the product from the organic phase, which was then dried with MgSO₄. The solvent was then eliminated under lower pressure, with the final product being a yellow liquid (13.87 g, 93%).

¹H NMR (CDCl₃): (δH/ppm) 7.75 (d, *J* = 1.0 Hz, 1H); 6.58 (d, *J* = 3.0 Hz, 1H); 6.44 (dd, *J* = 2.0 and 3.0 Hz, 1H); 1.67 (m, 6H); 1.40 (m, 6H); 1.16 (m, 6H); 0.96 (m, 9H). ¹³C NMR (CDCl₃): (δC/ppm) 160.8, 146.9, 121.1, 109.0, 29.3, 29.1, 29.0, 28.9, 27.9, 27.5, 27.4, 27.2, 13.7, 13.7, 10.2, 10.0. EI-MS (m/z) [M]⁺ calculated for C₁₆H₃₀OSn, 358.13; found 357.8. Elemental analysis calculated for C₁₆H₃₀OSn + (5 C₄H₈O₂); C, 54.21; H, 8.85% found C, 55.08; H, 9.22%.

6.2.7 5,6 Bis(octyloxy)-4,7-di(furan-2-yl)benzo [c][1,2,5]thiadiazole. (8)⁶

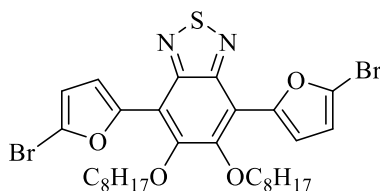


A solution was prepared that contained 4,7-dibromo-5,6-bis(octyloxy)benzo [c][1,2,5]thiadiazole (**6**) (1.00 g, 1.816 mmol) and tributyl(furan-2-yl) stannane (**7**) (2.60 g, 2.3 mL, 7.267 mmol). A second catalytic solution was also prepared that contained Pd(OAc)₂ (28.50 mg, 0.13 mmol) and tri(*o*-tolyl)phosphine (77.00 mg, 0.25 mmol) in 10 mL dry toluene. The catalytic solution was then added to the first solution, after which the reaction mixture was degassed and then heated at 115°C for 48 hours whilst being stirred. Purification of the crude product was done using column chromatography (eluent with petroleum ether / DCM, gradient 4/1). The product was obtained as a dark brown liquid (0.90 g, 95%).

¹H NMR (CDCl₃): (δH/ppm) 7.72 (d, *J* = 1.0 Hz, 2H); 7.43 (d, *J* = 3.5 Hz, 2H); 6.67 (dd, *J* = 1.5 and 3.0 Hz, 2H); 4.12 (m, 4H); 1.92-1.83 (m, 4H); 1.40-1.25 (m, 20H); 0.94-0.87 (m, 6H). ¹³C NMR (CDCl₃): (δC/ppm) 152.6, 150.1, 147.6, 142.9, 115.0, 114.5, 113.8, 74.9,

31.8, 30.4, 29.5, 29.3, 26.1, 22.7, 14.1. EI-MS (m/z) $[M]^+$ calculated for $C_{30}H_{40}N_2O_4S$, 524.27; found 524. Elemental analysis calculated for $C_{30}H_{40}N_2O_4S + (0.03 CH_2Cl_2)$; C, 66.15; H, 7.44; N, 5.09; S, 5.83 % found C, 66.84; H, 6.87; N, 5.17; S, 5.55 %.

6.2.8 4, 7- Bis (5-bromofuran-2-yl)-5, 6-bis (octyloxy)benzo[c][1,2,5] thiadiazole. (M1)⁶

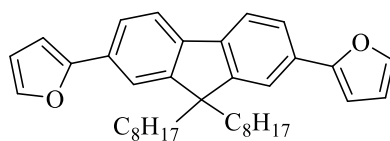


A solution was prepared that contained 5,6-bis(octyloxy)-4,7-di (furan-2-yl) benzo[c] [1, 2, 5] thiadiazole (**8**) (0.85 g, 1.62 mmol), dry chloroform (41.6 mL) and glacial acetic acid (41.6 mL) and (NBS) (0.58 g, 3.2 mmol). Stirring of the reaction mixture occurred in the dark at 60 °C for 24 hours, and then the crude product was washed with water (3×300 mL) for removal of the acetic acid. At this point, the organic solvent was concentrated to precipitate the product using cold methanol. The product was obtained as an orange solid (0.63 g, 60%).

¹H NMR (CDCl₃): (δH/ppm) 7.50 (d, *J*= 3.0 Hz, 2H); 6.58 (d, *J*= 3.0 Hz, 2H); 4.15(t, *J*= 7.0 Hz, 4H); 1.98 -1.91 (m, 4H); 1.40 -1.26 (m, 20H); 0.92 -0.89 (t, *J*= 7.0 Hz, 6H).
¹³CNMR(CDCl₃): (δC/ppm)152.7, 149.6, 149.6, 122.9, 116.5, 113.7, 113.5, 75.2, 31.9, 31.3, 29.7, 29.3, 26.1, 22.7, 14.1. EI-MS (m/z) $[M]^+$ calculated for $C_{30}H_{38}Br_2N_2O_4S$, 682.09; found 682. Elemental analysis calculated for $C_{30}H_{38}Br_2N_2O_4S$; C, 52.79; H, 5.61; N, 4.10; Br,23.41; S, 4.70 % found C, 54.65; H, 6.18; N, 3.71; Br, 23.14; S, 3.71 %.

M.P. 90 – 93 °C.

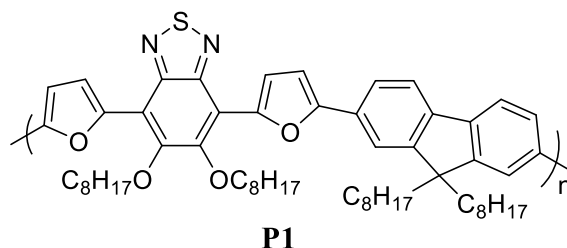
6.2.9 2,7-Bis(furan-2-yl)-9,9-dioctyl-9H-fluorene (M2)⁷



2,7-Dibromo-9,9-dioctyl-9H-fluorene (1.00 g, 1.82 mmol) (**SM3**), Palladium(II) acetate (28.00 mg, 0.13 mmol, 7% equiv) and tri(o-tolyl)phosphine(77.00 mg, 0.25 mmol, 14% equiv) were degassed under argon and dissolved with 50 mL of dry toluene. Tributyl(furan-2-yl) stannane (**7**) (1.95 g, 5.47 mmol, 1.7mL) was added to the solution, then the reaction mixture was degassed under argon and heated to reflux at 115 °C whilst being stirred for 24 hours. Cooling of the mixture then occurred and 100mL each of water and chloroform were added to extract it. The organic layer was separated, washed with water (3× 100 mL), dried with MgSO₄, and the solvent then evaporated. The crude was purified using column chromatography with eluent petroleum ether / DCM (9:1) to produce a dark yellow to green oil (0.57g, 60%).

¹H NMR (CDCl₃): (δH/ppm) 7.71(m, J= 0.7, 2H); 7.68 (d, J= 1.0 Hz, 2H); 7.66(s, 2H); 7.53 (d, J= 1.0 Hz, 2H); 6.73 (d, J= 3.5 Hz, 2H); 6.53 (m,2H); 2.00 (m, 4H); 1.30-1.00 (m, 24H); 0.80 (t, J= 7.0 Hz, 6H). ¹³C NMR (CDCl₃): (δC/ppm) 154.7, 151.6, 141.8, 140.3, 129.8, 123.0, 119.9, 118.1, 111.9, 105.0, 55.3, 40.5, 31.8, 30.0, 29.2, 23.8, 22.6, 14.1. EI-MS (m/z) [M]⁺ calculated for C₃₇H₄₆O₂, 522.35; found 522. Elemental analysis calculated for C₃₇H₄₆O₂ + (0.5 DCM) ; C, 79.69; H, 8.38 % found C, 79.83; H, 7.95 %.

6.2.10 Poly[9,9-dioctyl-9H-fluorene-2,7-diyl-*alt*-(5,6-bis(octyloxy)-4,7-di-2-furanyl-2,1,3-benzothiadiazole)-5,5-diyl] (P1)



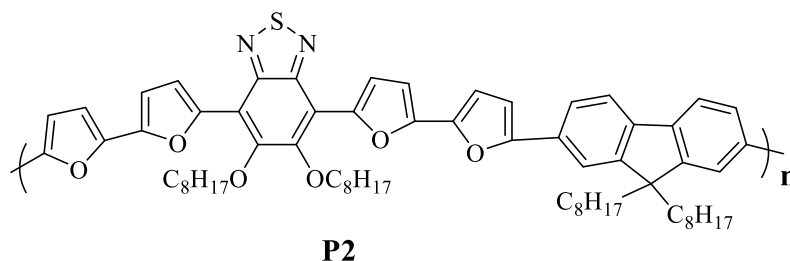
4,7-Bis (5-bromofuran-2-yl)-5,6-bis(octyloxy)benzo[c][1,2,5]thiadiazole (100.00 mg, 0.15 mmol, 1 equiv) (**M1**) and 9,9-dioctyl-2,7-bis(4,4,5,5-tetramethyl-1,3,2-dioxaborolan-2-yl)-

9H-fluorene (90.00 mg, 0.14 mmol, 1 equiv) (**SM4**) were dissolved in dry THF (4 mL). A saturated solution of NaHCO₃ (1 mL) was degassed then added to the reaction mixture. Tri-*o*-tolylphosphine (11.50 mg, 0.4 mmol, 0.1 equiv.) and Pd(OAc)₂ (8.60 mg, 0.038 mmol, 0.14 equiv.) were then added. After this, the reaction mixture was degassed and heated to 90 °C under reflux and the mixture was stirred and became viscous. It was then left to stir at this temperature for 2 hours and 40 minutes. Cooling of the mixture to room temperature then occurred and bromobenzene (150.00 mg, 0.1 mL, 0.9 mmol) was added. The mixture was degassed and stirred whilst being heated to 90 °C under reflux for 1 hour. The mixture was then cooled to room temperature and phenyl boronic acid (50.00 mg, 0.4 mmol) was added. The mixture was then degassed and stirred whilst being heated to 90 °C under reflux for a further 1 hour. Cooling of the mixture to room temperature was then done and 250 mL of chloroform was added. This was then transferred to 500 mL flask. Then 50 mL of ammonium hydroxide solution was added to the mixture and the solution was stirred vigorously for 3 hours. The organic layer and aqueous layer were then separated. The organic layer was washed with deionised water (20 mL × 3). The amount of solvent CHCl₃ in the organic layer was reduced to approximately 40 mL and then the organic layer was added to 200 mL of stirred methanol dropwise and left stirring overnight to form a precipitate, which was then filtrated. The crude product was then purified using the Soxhelt extraction method with different solvents; methanol, acetone, hexane, toluene and chloroform. The toluene, hexane and chloroform fractions were then concentrated and precipitated in methanol and the precipitates (polymer) were filtered. The polymer was obtained as a dark red solid (103.80 mg, 77 %).

GPC (toluene fraction): Mw = 29700 g mol⁻¹, Mn = 11500 g mol⁻¹, PDI = 2.57;

¹H NMR (CDCl₃): (δH/ppm) 8.25 – 7.48 (m, 2H), 7.08 (s, 2H), 4.26 (br,4H), 2.28 – 1.77 (br, 8H), 1.41 – 1.22 (br, 16H), 1.20 – 0.98 (br, 24H), 0.95 – 0.68 (br, 16H). Calculated elemental analysis (%): C, 77.59; H, 8.83; N, 3.07; S, 3.51. Found: C, 73.51; H, 8.06; N, 2.67; S, 3.19.

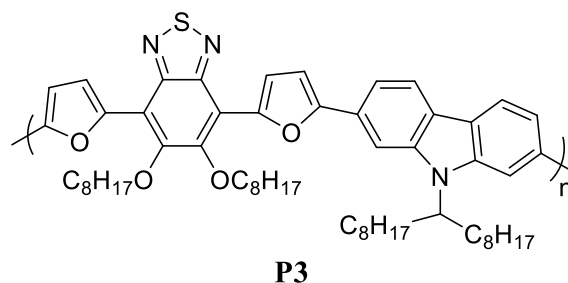
6.2.11 Poly[9,9-dioctyl-9H-fluorene-2,7-diyl-*alt*-(5,6-bis(octyloxy)-4,7-di(2,2'-bifuran-5-yl)benzo[c][1,2,5] thiadiazole)-5,5-diyl] (P2)



2,7-Bis(furan-2-yl)-9,9-dioctyl-9H-fluorene (80.00 mg, 0.146 mmol) (**M2**) was added to 4,7-bis(5-bromofuran-2-yl)-5,6-bis(octyloxy)benzo[c][1,2,5] thiadiazole (100.00 mg, 0.146 mmol) (**M1**) in a polymerisation tube. Then PdCl₂(MeCN)₂ (2.70 mg , 0.104 mmol), P(*o*-OMePh)₃ (3.60 mg, 0.102 mmol), Cs₂CO₃(142.70 mg, 0.438 mmol) and pivalic acid (14.91 mg, 0.146 mmol) were added to the polymerisation tube and degassed under argon. To this mixture was added 1 mL of dry THF, and the mixture was then degassed and stirred under argon at 120°C in an oil bath. After 45 minutes, the mixture changed from orange to dark brown and after one day changed to red. After 72 hours, cooling of the mixture to room temperature occurred and the polymer was dissolved in 250 mL of chloroform, then 50 mL of ammonium hydroxide was added. It was then stirred for 24 hours and extracted with water to separate the organic layer. The solvent was reduced in volume to approximately 20 mL and then precipitated in 200 mL of cold methanol and the mixture stirred for 3 hours. The polymer was filtered through a membrane and the solids extracted using the Soxhelt method, starting with methanol and followed by acetone, hexane and toluene. The fraction of hexane was concentrated then precipitated using methanol, and the precipitate that formed was filtered using a membrane. The fraction of toluene after precipitation afforded the polymer as a red powder (125.11 mg, 82 %).

GPC (hexane fraction): M_w = 35500 g mol⁻¹, M_n = 16400 g mol⁻¹, PDI = 2.16; ¹H NMR (CDCl₃): (δH/ppm) 8.17 – 7.37 (m, 10H), 6.98 (m, 2H), 6.6 (d, *J*=3.44 Hz, 2H), 4.20 (br, 4H), 2.28 – 1.77 (br, 8H), 1.41 – 1.22 (br, 16H), 1.20 – 0.98 (br, 24H), 0.95 – 0.68 (br, 16H). Calculated elemental analysis (%): C, 76.97; H, 8.10; N, 2.68; S, 3.07. Found: C, 76.38; H, 7.33; N, 2.65; S, 3.17.

6.2.12 Poly[9-(heptadecan-9-yl)-9H-carbazole-2,7-diyl-*alt*-(5,6-bis(octyloxy)-4,7-di-2-furanyl-2,1,3-benzothiadiazole)-5,5-diyl] (P3)

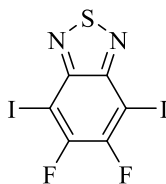


4,7-Bis(5-bromofuran-2-yl)-5,6-bis(octyloxy)benzo[*c*][1,2,5]thiadiazole (100.00 mg, 0.15 mmol, 1 equiv) (**M1**) and 9-(heptadecan-9-yl)-2,7-bis(4,4,5,5-tetramethyl-1,3,2-dioxaborolan-2-yl)-9H-carbazole (96.00 mg, 0.15 mmol, 1equiv.) (**SM11**) were dissolved in dry THF (4 mL). A saturated solution of NaHCO₃ (1 mL) was then degassed and added to the reaction mixture. Tri-*o*-tolyphosphine (6.00 mg, 0.02 mmol) and Pd(OAc)₂ (2.00 mg, 0.01 mmol) were added and then the reaction mixture was degassed and heated to 90 °C under reflux. The mixture was stirred until it became viscous, and it was left under heating and stirring for 5 hours. Cooling of the mixture occurred and bromobenzene (150.00 mg, 0.1 mL, 0.9 mmol) was added, then the mixture was degassed and stirred whilst being heated to 90 °C under reflux for 1 hour. Cooling of the mixture occurred and phenyl bronic acid (47.00 mg, 0.4 mmol) was added. Then the mixture was degassed and stirred whilst being heated to 90 °C under reflux for 1 hour. After this, the mixture was cooled to room temperature and dissolved in 250 mL of chloroform. It was then transferred to a 500mL flask. Then 50 mL of ammonium hydroxide solution was added to the mixture and the solution was stirred vigorously for 3 hours. The organic layer and aqueous layer were separated. The organic layer was then washed with deionised water (20 mL × 3). The volume of the organic layer was reduced to approximately 20 mL and then added dropwise to 200 mL of methanol under stirring and left overnight to form a precipitate. The precipitate was then filtered using a membrane. The crude product was purified using the Soxhelt extraction method with different fractions: methanol, acetone, hexane, toluene and chloroform. The chloroform fractions were concentrated and precipitated in methanol then the precipitates were filtered. The polymer from the chloroform fraction was obtained as a dark red powder (77.40 mg, 56 %).

GPC (chloroform fraction): $M_w = 25800 \text{ g mol}^{-1}$, $M_n = 10500 \text{ g mol}^{-1}$, PDI = 2.44; $^1\text{H NMR}$ (CDCl_3): ($\delta\text{H/ppm}$) 8.43 – 7.37 (br, 8H), 7.12 – 6.98 (br, 2H), 4.93 – 4.57 (br, 1H) 4.45 – 3.94 (br, 4H), 2.64 – 2.26 (br, 2H), 2.19 – 1.80 (br, 5H), 1.75 – 1.53 (br, 4H), 1.38 – 1.00 (br, 40H), 0.92 – 0.70 (d, $J=0.10 \text{ Hz}$, 13H). Calculated elemental analysis (%): C, 67.33; H, 8.79; N, 4.53; S, 3.45. Found: C, 68.72; H, 7.82; N, 4.18; S, 3.01.

6.3 Synthesis of monomers and polymers for chapter 3

6.3.1 5,6-Difluoro-4,7-diiodobenzo[c][1,2,5]thiadiazole (9).⁸

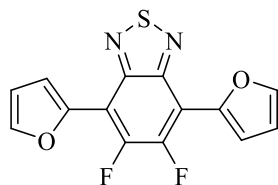


5,6-Difluorobenzo[c][1,2,5]thiadiazole (**SM12**) (2.67 g, 15 mmol), I_2 (15.00 g, 60 mmol) and fuming H_2SO_4 were reacted together in one flask and stirred at 60°C for 24 hours. Cooling of the mixture then occurred and after this it was poured into a crushed ice. CHCl_3 was added and then washed with deionised water (3 x 250 mL) using a separation funnel. Treatment of the mixture with both 1.0 M NaOH solution and saturated solution of NaHCO_3 was done in order to force the removal of any excess iodine. Separation and drying of the organic layer was done over MgSO_4 , and then the solvent was evaporated in vacuo. Cream- yellow coloured crystals were yielded (4.46 g, 100.5 mmol, 70%).

$^{19}\text{F NMR}$ (CDCl_3) δ (ppm): -105. $^{13}\text{C NMR}$ (CDCl_3): ($\delta\text{C/ppm}$) 155.7, 153.1, 150.3, 142.0, 128.1, 116.9. EI-MS (m/z) $[\text{M}]^+$ calculated for $\text{C}_6\text{F}_2\text{I}_2\text{N}_2\text{S}$, 423.78; found 423. Elemental analysis calculated for $\text{C}_6\text{F}_2\text{I}_2\text{N}_2\text{S}$; C, 17.00; N, 6.61; I, 59.87; S, 7.56 % found C, 17.00; N, 6.63; I, 59.77; S, 7.72 %.

M.P. $202 - 206^\circ\text{C}$.

6.3.2 5,6-Difluoro-4,7-di(furan-2-yl)benzo[c][1, 2, 5] thiadiazole(M4)⁹.

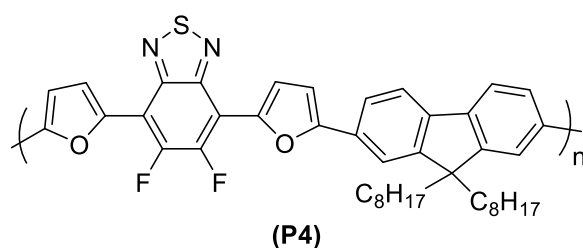


A mixture of 5,6-difluoro-4,7-diiodobenzo[c][1,2,5]thiadiazole (**9**) (2.00 g, 4.7 mmol), tributyl(furan-2-yl)stannane (**7**) (6.74 g, 5.94 mL, 0.01887 mol), Pd(OAc)₂ (0.07 g, 0.329 mmol) and tri-*o*-tolyl phosphine (0.15 g, 0.658 mmol) was degassed under argon then dissolved using dry THF (40 mL). The reaction mixture was heated to reflux at 70 °C overnight under argon. The solvent was evaporated and then the crude was washed using methanol and filtrated to yield an orange solid (1.34 g, 93 %).

¹H NMR (CDCl₃): 7.75 (d, *J* = 2.0 Hz, 2H), 7.58 (d, *J* = 3.5 Hz, 2H), 6.69 (dd, *J* = 2.0 and 4.0 Hz, 2H). ¹³C NMR (CDCl₃): (δC/ppm) 150.7, 150.5, 147.7, 145.5, 144.2, 115.2, 112.1. EIMS (m/z) [M]⁺ calculated for C₁₄H₆F₂N₂O₂S, 304.1; found 304. Elemental analysis calculated for C₁₄H₆F₂N₂O₂S + (0.1 CH₃OH and 0.45 H₂O); C, 53.66; H, 2.33; N, 8.88; S, 10.54 % found C, 53.79; H, 2.21; N, 8.73; S, 9.86 %.

M.P. 180 – 183 °C.

6.3.3 Poly[9,9-dioctyl-9H-fluorene-2,7-diyl-*alt*-(5,6-difluoro-4,7-di-2-furanyl-2,1,3-benzothiadiazole)-5,5-diyl] (P4)

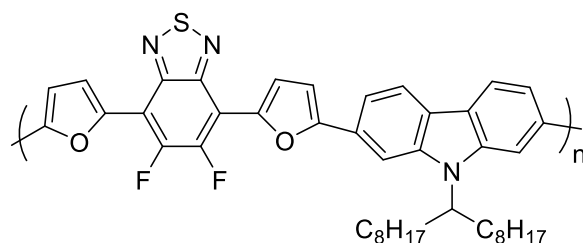


5,6-Difluoro-4,7-di(furan-2-yl)benzo[c][1, 2, 5] thiadiazole (**M4**) (100.00 mg, 0.33 mmol, 1 equiv), 2,7-dibromo-9,9-dioctyl-9H-fluorene (**SM3**) (160.00 mg, 0.30 mmol, 1 equiv), tris(dibenzylideneacetone)dipalladium(0) (19.23 mg, 0.02 mmol), tris(2-methoxyphenyl) phosphine (14.80 mg, 0.04 mmol), caesium carbonate (293.00 mg, 0.9 mmol, 3 equiv) and pivalic acid (30.00 mg, 0.3 mmol) were degassed under argon then dissolved using 1 mL of

dry toluene and heated to reflux at 120 °C for 24 hours. The colour of the reaction mixture changed to orange then dark red. The mixture was then cooled to room temperature and dissolved in 250 mL of chloroform. This was then transferred to a 500 mL round flask and 50 mL of ammonium hydroxide was added before being stirred overnight. Following this, the organic layer was separated and the volume reduced to approximately 20 mL. This was then precipitated in 200 mL of methanol and the precipitate was filtered to obtain the crude polymer as a dark red solid. The crude was transferred to a thimble and then extracted using the Soxhelt method with methanol, acetone, hexane then chloroform. The solvent in the chloroform fraction was reduced to 20 mL then precipitated using 200 mL of methanol and filtered using a membrane to obtain the polymer as a dark red powder (160.40 mg, 77 %).

GPC (chloroform fraction): $M_w = 6400 \text{ g mol}^{-1}$, $M_n = 2800 \text{ g mol}^{-1}$, PDI = 2.29; $^1\text{H NMR}$ (CDCl_3): ($\delta\text{H/ppm}$) 8.11 – 7.52 (m, 8H), 7.05 (s, 2H), 2.16 (s, 4H), 1.38 – 0.96 (br, 20H), 0.93 – 0.69 (s, 10H). Calculated elemental analysis (%): C, 74.54; H, 6.69; N, 4.04; S, 4.63. found: C, 71.95; H, 6.27; N, 3.73; S, 4.32.

6.3.4 Poly[9-(heptadecan-9-yl)-9H-carbazole-2,7-diyl-*alt*-(5,6-difluoro-4,7-di-2-furanyl-2,1,3-benzothiadiazole)-5,5-diyl] (P5)



(P5)

5,6-Difluoro-4,7-di(furan-2-yl)benzo[c][1,2,5] thiadiazole (**M4**) (100 mg, 0.33 mmol, 1 equiv), 2,7-dibromo-9-(heptadecan-9-yl)-9H-carbazole (**SM10**) (160 mg, 0.3 mmol, 1 equiv), tris(dibenzylideneacetone)dipalladium(0) (19.23 mg, 0.02 mmol), tris(2-methoxyphenyl) phosphine (14.80 mg, 0.04 mmol), caesium carbonate (293.00 mg, 0.9 mmol, 3 equiv) and pivalic acid (30.00 mg, 0.3 mmol) were degassed under argon then dissolved using 1 mL of dry toluene. This was then heated to reflux for 3 days. After 30 min the colour of the mixture changed to orange, then purple. The polymer was then dissolved in 250 mL of chloroform and then transferred to a 500 mL round flask. 50 mL of ammonium hydroxide was added and

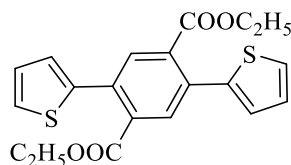
it was stirred overnight. After this, the organic layer was separated and the volume reduced to approximately 20 mL. This was then precipitated in 200 mL of methanol and a membrane was used to filter it to obtain the crude polymer as a purple solid. The crude was transferred to a thimble then extracted using the Soxhelt method with different solvents: methanol, acetone, hexane then chloroform. The solvent in the chloroform fraction was reduced to 20 mL then precipitated into 200 mL of methanol. This was then filtered using a membrane to obtain the polymer as a purple powder (161.70 mg, 76 %).

GPC (chloroform fraction): $M_w = 6500 \text{ g mol}^{-1}$, $M_n = 2900 \text{ g mol}^{-1}$, PDI = 2.24;

$^1\text{H NMR}$ (CDCl_3): ($\delta\text{H/ppm}$) 8.30 – 7.7.40 (m, 8H), 7.08 (s, 2H), 4.77 (s, 1H), 2.13 (s, 4H), 1.40 – 0.94 (br, 20H), 0.90 – 0.69 (s, 10H). Calculated elemental analysis (%): C, 72.96; H, 6.69; N, 5.94; S, 4.53. Found: C, 71.56; H, 6.42; N, 5.48; S, 4.01.

6.4 Synthesis of monomers and polymers for chapter 4

6.4.1 2,5- Dithien-2-yl terephthalic acid diethyl ester (10)¹⁰

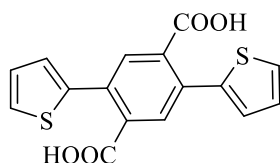


Diethyl 2,5-dibromoterephthalate (**SM5**) (8.60 g, 22.6 mmol) and $\text{Pd}(\text{PPh}_3)_2 \text{Cl}_2$ (0.79 g, 1.13 mmol) were dissolved in dry THF (30 mL). 2-(tributylstannyl)thiophene (**SM6**) (21.6 mL, 25.38 g, 67.8 mmol) was then added before the reaction mixture was degassed and stirred at 85 °C under argon for 15 hours. Cooling of the mixture to room temperature occurred and then potassium fluoride aqueous solution (10 wt%, 100 mL) was treated with it for 2 hours. Extraction of the product with DCM was done three times (3×100 mL). The combined organic phase was also washed with water three times and then dried over MgSO_4 . Following the filtering process, removal of the solvent under lower pressure was done. The product was finally washed using methanol to obtain a white solid (7.19g, 83%).

^1H NMR (CDCl_3): ($\delta\text{H/ppm}$) 7.83 (s, 2H), 7.40 (dd, $J= 1.5$ and 5.0 Hz, 2H), 7.10 (m, 4H), 4.24 (q, $J= 8.0$ Hz, 4H), 1.15 (t, $J= 7.0$ Hz, 6H). ^{13}C NMR (CDCl_3): ($\delta\text{C/ppm}$) 167.7, 140.6, 134.3, 133.5, 131.9, 127.6, 127.0, 126.5, 61.9, 14.1. EI-MS (m/z) $[\text{M}]^+$ calculated for $\text{C}_{20}\text{H}_{18}\text{O}_4\text{S}_2$, 386.06; found 386. Elemental analysis calculated for $\text{C}_{20}\text{H}_{18}\text{O}_4\text{S}_2$; C, 62.16; H, 4.69; S, 16.59 % found C, 62.06; H, 4.73; S, 16.50 %.

M.P. 110 – 113 °C.

6.4.2 2,5-Di(thien-2-yl)terephthalic acid (**11**)¹¹

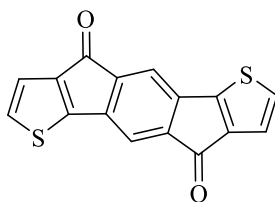


2,5- Dithien-2-yl terephthalic acid diethyl ester (**10**) (5.00 g, 12.9 mol) was dissolved in 300 mL of ethanol and then a solution of sodium hydroxide (7.05 g NaOH in 50 mL water) was added. The mixture was heated at reflux for 15 h then evaporated it under lower pressure. To the remainder of the water, concentrated hydrochloric acid was added. The precipitate formed was filtrated, washed using water, and then dried in vacuo to afford a product as an off-white solid (4.20 g, 99%).

^1H NMR (DMSO-d_6): ($\delta\text{H/ppm}$) 13.48 (s, 2 H, COOH), 7.71 (s, 2H, Ar-H), 7.70 (dd, 2H, $J= 1.0$ and 5.0 Hz, Ar-H) 7.26 (dd, 2H, $J= 1.0$ and 4.0 Hz, Ar-H) 7.17 (m, 2H, Ar-H). ^{13}C NMR (CDCl_3): ($\delta\text{C/ppm}$) 169.3, 140.4, 135.3, 131.9, 130.8, 128.6, 128.1, 127.6. EI-MS (m/z) $[\text{M}]^+$ calculated for $\text{C}_{16}\text{H}_{10}\text{O}_4\text{S}_2$, 330.37; found 330. Elemental analysis calculated for $\text{C}_{16}\text{H}_{10}\text{O}_4\text{S}_2 + (\text{H}_2\text{O})$; C, 54.74; H, 3.53; S, 18.26 % found C, 54.39; H, 3.20; S, 17.99 %.

M.P. 320 – 324 °C.

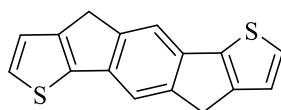
6.4.3 4, 9-Dihydro-s-indaceno [1, 2-b: 5, 6-b']-dithiophene-4, 9-dione (**12**)¹²



2,5-Di(thien-2-yl)terephthalic acid (**11**) (4.00 g, 12.1 mmol) was suspended in dry DCM (200 mL), followed by the addition of oxalyl chloride (5.50 g, 3.67 mL, 43.56 mmol). To this mixture dry DMF (1.8 mL) was added dropwise at room temperature. This mixture was stirred overnight. The solvent was eliminated under lower pressure to yield crude acid dichloride (yellow solid). This solid was dissolved in dry DCM (150 mL) and added to a mixture of AlCl₃ (7.5 g, 56.25 mmol) with dry DCM 225 mL at 0 °C. The entire reaction mixture was then left for approximately one hour in ice at 0 °C. Following this, it was stirred at room temperature overnight. The mixture was added to ice-cold hydrochloric acid (50 mL) and water (300 mL), which formed blue precipitate. The precipitate was collected using filtration and washed with 2M HCl solution and water then dried in an oven. The product was yielded as a blue solid (3.23g, 91%).

El-MS (m/z) [M]⁺ calculated for C₁₆H₆O₂S₂, 294.31; found 294. Elemental analysis calculated for C₁₆H₆O₂S₂ + (2H₂O); C, 58.33; H, 3.03; S, 19.46 % found C, 57.73; H, 2.43; S, 19.49 %.

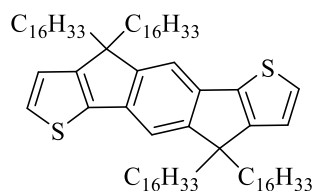
6.4.4 4,9-Dihydro-s-indaceno[1,2-b:5,6-b']-dithiophene (**13**)¹³



4, 9-Dihydro-s-indaceno [1, 2-b: 5, 6-b']-dithiophene-4, 9-dione (**12**) (2.50 g, 8.49 mmol), hydrazine monohydrate (8.01 g, 7.77 ml, 160 mmol) and potassium hydroxide (8.98 g, 160 mmol) were dissolved in 67 mL of diethylene glycol and heated to reflux at 180 °C for 24 hours before being poured into ice containing HCl. The precipitate collected and washed with water. It then dried at reduced pressure to yield 4,9-dihydro-s-indaceno[1,2-b:5,6-b']-dithiophene (**12**) as a black solid (1.84 g, 86%).

¹H NMR (CDCl₃): (δH/ppm) 7.72 (s, 2H, Ar-H); 7.55 (d, 2H, *J*= 5.0 Hz, Ar-H); 7.22 (d, 2H, *J*= 5.0 Hz, Ar-H); 3.77 (s, 4H, CH₂). ¹³C NMR (CDCl₃): (δC/ppm) 147.8, 145.7, 142.7, 135.9, 128.0, 123.7, 116.3, 33.7,. El-MS (m/z) [M]⁺ calculated for C₁₆H₁₀S₂, 266.02; found 266. Elemental analysis calculated for C₁₆H₁₀S₂ + (1.8 diethylene glycol and 0.05 H₂O); C, 62.12; H, 5.56; S, 16.92 % found C, 61.39; H, 3.79; S, 15.16 %.

6.4.5 4,9-Dihydro-4,4,9,9-tetrahexadecyl-s-indaceno[1,2-b:5,6-b']-dithiophene (14)¹¹

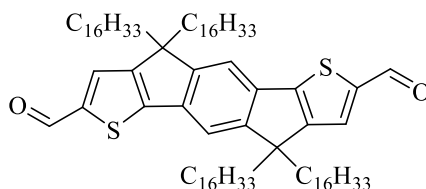


Sodium tert-butoxide (3.60 g, 37.5 mmol) was added to a suspension of 4,9-dihydro-s-indaceno[1,2-b:5,6-b']-dithiophene (**13**) (0.40 g, 1.5 mmol) in anhydrous DMSO (15 mL) then degassed and heated at 80 °C for 90 minutes under argon. 1- Bromohexadecane (11.45 mL, 11.44 g, 37.5 mmol) was added dropwise slowly (one drop every 5 minutes) then it was degassed and the temperature increased to 90 °C overnight before being poured into ice-water. The precipitate was collected using filtration and washed with water and methanol to give crude as a black solid. This was then purified using column chromatography and eluted with petroleum ether to yield a white to yellow solid (0.48 g, 28%).

¹H NMR (CDCl₃): (δH/ppm) 7.29 (s, 2H), 7.27 (d, *J*= 5.0 Hz, 2H), 6.97 (d, *J*= 5.0 Hz, 2H), 1.81-2.04 (m, 4H), 1.81-1.92 (m, 4H), 1.02 (m, 104H), 0.75-0.98 (m, 20H).¹³C NMR (CDCl₃): (δC/ppm) 155.1, 153.2, 141.7, 135.6, 126.1, 121.7, 113.1, 53.7, 39.1, 32.0, 30.0, 29.7, 29.7, 29.6, 29.6, 29.5, 29.4, 24.2, 22.7, 14.1. EI-MS (m/z) [M]⁺ calculated for C₈₀H₁₃₈S₂, 1163.02; found 1163. Elemental analysis calculated for C₈₀H₁₃₈S₂ + (1.3 H₂O); C, 80.90; H, 11.95; S, 5.40 % found C, 81.52; H, 11.29; S, 4.81 %.

M.P. 80 – 83 °C.

6.4.6 4,4,9,9-Tetrahexadecyl-4,9-dihydro-s-indaceno[1,2-b:5,6-b'] dithiophene-2,7-dicarbaldehyde (15)¹⁴



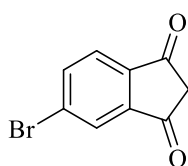
4,9-Dihydro-4,4,9,9-tetrahexadecyl-s-indaceno[1,2-b:5,6-b']-dithiophene (**14**) (0.50 g, 0.4 mmol) was dissolved in dry DMF (40 mL) and 1,2-dichloroethane (50 mL, 62.50 g, 631.57 mmol) was added then degassed under argon. The solution was cooled to 0 °C and stirred

while phosphorus oxychloride (POCl₃) (1.2 mL, 1.97 g, 12.85 mmol) was added dropwise. We stirred the reaction mixture for one hour at room temperature and overnight at 105 °C. Then we cooled the mixture to room temperature and poured it into ice-water. The solution of NaOH 1M was added and extracted with DCM (150 mL × 3). The solvent was reduced then the product was precipitated using methanol, and finally filtered to yield a brown solid (0.45 g, 85%).

¹H NMR (DMSO-d₆): 9.93(s, 2H, CHO), 7.66(s, 2H, Ar-H), 7.47 (s, 2H, Ar-H), 2.08-2.01 (m, 4H, CH₂), 1.86-1.94 (m, 4H, CH₂), 1.10-1.31 (m, 104H, CH₂), 0.78-0.89 (m, 20H, CH₂ and CH₃). ¹³C NMR (CDCl₃): (δC/ppm) 183.0, 156.1, 155.2, 151.4, 136.5, 130.4, 115.0, 54.3, 38.9, 31.9, 29.9, 29.7, 29.7, 29.6, 29.5, 29.4, 29.3, 24.3, 22.7, 14.1. EI-MS (m/z) [M]⁺ calculated for C₈₂H₁₃₈O₂S₂, 1219.01; found 1221. Elemental analysis calculated for C₈₂H₁₃₈O₂S₂; C, 80.72; H, 11.40; S, 5.26 % found C, 80.28; H, 11.37; S, 4.79 %.

M.P. 89 – 93 °C.

6.4.7 5-Bromo-1,3-indanedione (**16**)¹⁵



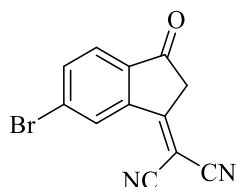
4-Bromophthalic anhydride (**SM7**) (3.00 g, 13.23 mmol) was added to a solution of acetic anhydride (7.2 mL, 7.78 g, 76.21 mmol) and triethylamine (3.9 mL, 2.83 g, 27.97 mmol) forming an orange suspension. To this reaction mixture, ethyl acetoacetate (1.9 mL, 1.94 g, 14.91 mmol) was added rapidly and the mixture stirred at room temperature for 24 hours. Ice (5.10 g) and conc. HCl (4.8 mL) were added followed by 5 M HCl (21 mL). The reaction mixture was stirred at 85 °C for 20 minutes then cooled it to room temperature. After that, the crude of the reaction was extracted using DCM (150 mL × 3). The extract was washed using brine and dried using sodium sulphate. The organic solvent was eliminated until the product was finally obtained as a brown solid (2.52 g, 85 %).

¹H NMR (CDCl₃): (δH/ppm) 8.14 (d, *J*= 2.0 Hz, 1H) 7.98 (dd, *J*= 2.0 and 2.0 Hz, 1H) 7.86 (s, 1H) 3.28 (s, 2H). ¹³C NMR (CDCl₃): (δC/ppm) 196.2, 195.9, 144.5, 141.8, 138.8, 131.3, 126.4, 124.6, 45.0. EI-MS (m/z) [M]⁺ calculated for C₉H₅BrO₂, 223.95; found 224. Elemental

analysis calculated for $C_9H_5BrO_2 + (0.1 DCM \text{ and } 0.1 H_2O)$; C, 46.44; H, 2.31; Br, 33.95 % found C, 49.50; H, 2.82; Br, 30.90 %.

M.P. 142 – 144 °C.

6.4.8 2-(6-Bromo-2,3-dihydro-3-oxo-1-inden-1-ylidene)-propanedinitrile (**17**)¹⁶

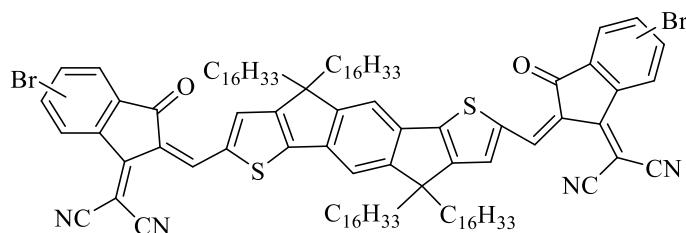


A mixture of 5-bromo-1,3-indanedione (**16**) (0.50 g, 2.22 mmol) and malononitrile (0.29 g, 4.44 mmol) was dissolved in absolute ethanol (30 mL). Anhydrous sodium acetate (0.24 g, 2.9 mmol) was added while being stirred. The temperature was increased to 50 °C for an hour and then cooled to room temperature. The mixture was poured into water (130 mL) and acidified with the addition of hydrochloric acid. The precipitate was filtered and recrystallised using a mixture of acetic acid and methanol in a 1:1 ratio. The yield was a black solid (0.48 g, 80%).

¹H NMR ($CDCl_3$): ($\delta H/ppm$) 8.79 (d, $J = 1.0$ Hz, 1H), 8.13 (d, $J = 2.0$ Hz, 1H), 7.99 (m, 2H), 7.86 (d, $J = 8.0$, 1H). ¹³C NMR ($CDCl_3$): ($\delta C/ppm$) 193.7, 193.4, 143.7, 141.7, 131.8, 131.6, 128.9, 128.0, 127.1, 125.8, 112.1, 111.7. EI-MS (m/z) [M]⁺ calculated for $C_{12}H_5BrN_2O$, 271.96; found 272. Elemental analysis calculated for $C_{12}H_5BrN_2O$; C, 52.78; H, 1.85; N, 10.26; Br, 29.26 % found C, 50.21; H, 2.17; N, 8.2; Br, 32.15 %.

M.P. 180 - 182 °C.

6.4.9 2-Bis[(6-bromo-2,3-dihydro-3-oxo-1-inden-1-ylidene)-propanedinitrile]-4,4,9,9-tetrahexadecyl-4,9-dihydro-s-indaceno[1,2-b:5,6-b'] dithiophene-2,7-diethylene. IDIC-C16-Br (**M5**)¹⁷

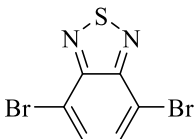


4,4,9,9-Tetrahexadecyl-4,9-dihydro-s-indaceno[1,2-b:5,6-b']-dithiophene-2,7-dicarbaldehyde (**15**) (0.10 g, 0.08 mmol) and 2-(6-bromo-2,3-dihydro-3-oxo-1-inden-1-ylidene)-propanedinitrile (**17**) (0.16 g, 0.57 mmol) were dissolved in 10 mL of dry chloroform. (0.1 mL, 0.10 g, 1.26 mmol) of pyridine was added under argon, degassed and stirred at 65 °C to reflux overnight. After this, poured the reaction mixture into 20 mL of methanol and the blue precipitate was filtered. The yield was a blue solid (0.12 g, 90 %).

¹H NMR (CDCl₃): (δH/ppm) 9.02 (m, 2H), 8.87 (m, 1H), 7.78- 8.57 (m, 5H), 7.76 (s, 1H), 7.63 (m, 2H), 2.16-1.91 (m, 10H), 1.33-1.08 (br,125H). ¹³C NMR (CDCl₃): (δC/ppm) 178.7, 187.3, 160.4, 158.2, 156.9, 144.0, 141.6, 141.1, 140.3, 139.8, 138.3, 137.9, 136.6, 131.7, 127.5, 126.1, 124.7, 123.0, 122.5, 121.8, 119.9, 116.3, 114.6, 54.8, 39.0, 33.50, 31.9, 30.1, 29.7, 29.6, 29.4, 29.3, 23.0, 14.0. EI-MS (m/z) [M]⁺ calculated for C₁₀₈H₁₅₂Br₂N₄O₂S₂, 1726.91; found 1729. Elemental analysis calculated for C₁₀₈H₁₅₂Br₂N₄O₂S₂; C, 73.58; H, 8.39; N, 3.24; Br, 9.24; S, 3.71 % found C, 72.28; H, 7.64; N, 3.58; Br, 10.92; S, 3.15 %.

M.P. 130 – 133 °C.

6.4.10 4,7-Dibromobenzo[c][1,2,5]thiadiazol (**18**)¹⁸

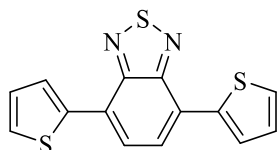


Benzo[c][1,2,5]thiadiazole **SM8** (5.10 g, 37.5 mmol) was dissolved with hydrobromic acid (8 mL, 45 %) and heated to reflux. Then bromine (18.00 g, 5.8 mL, 112.5 mmol) was added dropwise to the mixture. After completing bromine addition, we added an additional amount of hydrobromic acid (8 mL, 45 %) and then heated the mixture under reflux for 3 more hours. Following this, we filtered the mixture, washed it with water and recrystallised it from chloroform to obtain white needles as a final product (7.72 g, 70%).

¹H NMR (CDCl₃): (δH/ppm) 7.74 (s,2H). ¹³C NMR (CDCl₃): (δC/ppm) 153.0, 132.4, 113.9. EI-MS (m/z) [M]⁺ calculated for C₆H₂Br₂N₂S, 291.83; found 293. Elemental analysis calculated for C₆H₂Br₂N₂S; C, 24.52; H, 0.69; N, 9.35; Br, 54.36; S, 10.91 % found C, 24.62; H, 0.67; N, 9.47; Br, 49.81; S, 11.21 %.

M.P. 185 – 187 °C.

6.4.11 4,7-Di (thiophene-2-yl)benzo[c] thiadiazole (**19**)¹⁹

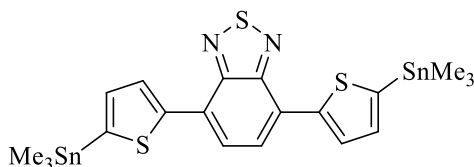


4,7-Dibromobenzo[c][1,2,5]thiadiazole (**18**) (2.00 g, 6.8 mmol), 2-tributylstannyl thiophene (5.59 g, 4.9 mL, 14.97 mmol), Palladium (II) acetate (0.11 g, 0.476 mmol) and tri-*o*-tolylphosphine (0.21 g, 0.69 mmol) were added together in a 2-neck round flask, degassed and then dissolved using dry THF (40 mL). We heated the reaction mixture to reflux for a day under argon. After this, we cooled the mixture to room temperature and removed the solvent. The crude was precipitated using methanol then filtered to yield orange solid needles (1.90 g, 93%).

¹H NMR (CDCl₃): (δH/ppm) 8.14 (d, *J*= 3.5 Hz, 2H), 7.90 (s, 2H), 7.48 (d, *J*= 5.0 Hz, 2H), 7.24 (dd, *J*= 4.0 and 5.0 Hz, 2H). ¹³C NMR (CDCl₃): (δC/ppm) 153.5, 139.3, 128.1, 127.6, 126.8, 126.0, 125.6. EI-MS (*m/z*) [*M*]⁺ calculated for C₁₄H₈N₂S₃, 299.98; found 299. Elemental analysis calculated for C₁₄H₈N₂S₃; C, 55.97; H, 2.68; N, 9.33; S, 32.02 % found C, 55.86; H, 2.81; N, 9.28; S, 32.35 %.

M.P. 122 – 124 °C

6.4.12 4,7-bis(5-(trimethylstannyl)thien-2-yl)benzo[c][1,2,5] thiadiazole (**M6**)²⁰



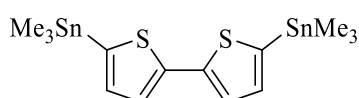
2, 2, 6, 6-Tetramethylpiperidine (0.29 mL, 0.24 g, 1.73 mmol, 2.6 eq) was mixed with dry THF (4 mL) under argon. We cooled the solution to -78 °C and *n*-BuLi (0.69 mL, 2.5 M solution in hexane, 1.73 mmol, and 2.6 eq) was quickly added to the mixture before it was stirred at -78 °C for 30 min. We then warmed the solution to room temperature, after which

we stirred it for 10 min to produce lithium 2, 2, 6, 6-tetramethylpiperidide (LTMP). After that we cooled the solution to $-78\text{ }^{\circ}\text{C}$ and 4, 7-di (thiophene-2-yl) benzo[c] [1, 2, 5] thiadiazole (**19**) (0.20 g, 0.67 mmol) in 3 mL of dry THF was added dropwise. At this time, the colour of solution changed to purple. The solution was then stirred at $-78\text{ }^{\circ}\text{C}$ for 45 min. Trimethyltin chloride (1.66 mL, 1.0 M solution in THF, 1.66 mmol, 2.5eq) was then added dropwise and the colour of the reaction mixture changed from purple to orange. After this we warmed the solution to room temperature and it was stirred overnight. After an addition of 20 mL brine to the solution, the solution was extracted into DCM (30 mL \times 3). The organic phases were combined and washed with brine (60 mL \times 3) and dried by magnesium sulphate. MgSO_4 was filtered using filter paper and the solvent was eliminated in vacuo. We then recrystallised the crude product from ethanol to yield the pure product as an orange solid (0.28g, 66%).

^1H NMR (CDCl_3): ($\delta\text{H/ppm}$) 8.20 (d, $J= 3.0$ Hz, 2H), 7.89 (s, 2H), 7.32 (d, $J= 4.0$ Hz, 2H), 0.46 (s, 18H). ^{13}C NMR (CDCl_3): ($\delta\text{C/ppm}$) 152.8, 145.2, 140.6, 136.4, 128.6, 126.3, -8.0. EI-MS (m/z) $[\text{M}]^+$ calculated for $\text{C}_{20}\text{H}_{24}\text{N}_2\text{S}_3\text{Sn}_2$, 627.91; found 625. Elemental analysis calculated for $\text{C}_{20}\text{H}_{24}\text{N}_2\text{S}_3\text{Sn}_2$; C, 38.37; H, 3.86; N, 4.47; S, 15.36 % found C, 38.95; H, 3.86; N, 4.78; S, 17.16 %.

M.P. $158 - 160\text{ }^{\circ}\text{C}$.

6.4.13 5,5' -Bis (trimethyl stannyl)-2,2' - bithiophene.(M7)⁵

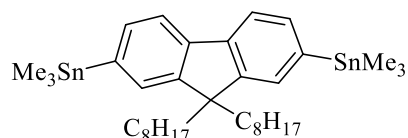


2,2'-Bithiophene (**SM9**) (0.50 g, 3.00 mmol) was dissolved in 15 mL of dry THF and degassed under argon before being cooled to $-78\text{ }^{\circ}\text{C}$. $n\text{-BuLi}$ (2.5 M in hexane) (0.69 mL , 0.48 g, 7.5 mmol) was then added dropwise whilst being stirred for 1 h at $-78\text{ }^{\circ}\text{C}$. We increased the temperature of the reaction to room temperature and stirred it for 2 h. Trimethyltin chloride (1.51 mL, 1.49 g 7.5 mmol) was added dropwise after the reaction mixture was cooled to $-78\text{ }^{\circ}\text{C}$ again. Finally, we stirred the mixture under argon at room temperature overnight. The solvent was reduced in pressure and the solid was washed using methanol and finally filtered to yield a white solid product (0.09 g, 62%).

^1H NMR (CDCl_3): ($\delta\text{H/ppm}$) 7.29 (d, $J= 3.0$ Hz, 2H), 7.10 (d, $J= 3.0$ Hz, 2H), 0.40 (s, 18H). ^{13}C NMR (CDCl_3): ($\delta\text{C/ppm}$) 143.0, 137.1, 135.9, 124.89, 1.0. EI-MS (m/z) [M] $^+$ calculated for $\text{C}_{14}\text{H}_{22}\text{S}_2\text{Sn}_2$, 493.29; found 492. Elemental analysis calculated for $\text{C}_{14}\text{H}_{22}\text{S}_2\text{Sn}_2$; C, 34.19; H, 4.51; S, 13.04 % found C, 34.08; H, 4.61; S, 12.76 %.

M.P. 90 – 93 °C.

6.4.14 2,7-Bis(trimethyltin)-9,9-dioctylfluorene (M8)⁵

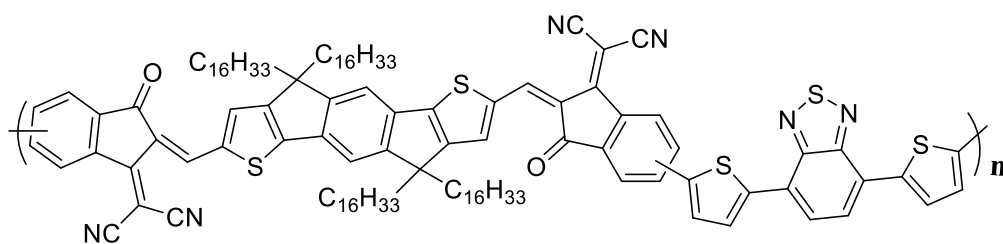


Dry THF 15 mL was added to degassed 2,7-dibromo-9,9-dioctyl-9*H*-fluorene (**SM3**) (0.20 g, 0.36 mmol) and cooled to – 78 °C. After that, we added *n*-Buli (2.5 M in hexane, 0.09 mL, 0.06 g, 1.00 mmol) to the reaction mixture in a dropwise fashion and left it to warm to -40 °C whilst it was stirred for 2 hours. Trimethyltin chloride (1 M in THF, 0.20 mL, 0.20 g, 1.0 mmol) was then added rapidly. We removed the cooling bath to allow the reaction mixture to reach room temperature, after which we stirred the reaction for 2 hours. We then poured the reaction into brine and extracted it using diethyl ether (5×70 mL). We washed the extracted layer with water and dried it using MgSO_4 before removing the solvent. The thick crude was then washed with methanol through basic alumina, which afforded a white solid (0.17 g, 67%).

^1H NMR (CDCl_3): ($\delta\text{H/ppm}$) 7.68 (d, $J= 7.0$ Hz, 2H), 7.45 (d, $J= 7.0$ Hz, 2H), 7.39 (s, 2H), 1.96 (m, 4H), 1.22 – 0.82 (m, 24 H), 0.85 (m, 6H), 0.34 (s, 18 H). ^{13}C NMR (CDCl_3): ($\delta\text{C/ppm}$) 150.1, 141.3, 140.8, 134.1, 130.2, 119.2, 54.9, 40.0, 31.8, 29.9, 29.2, 29.1, 23.7, 22.6, 14.1, 1.0. EI-MS (m/z) [M] $^+$ calculated for $\text{C}_{35}\text{H}_{58}\text{Sn}_2$, 718.26; found 716. Elemental analysis calculated for $\text{C}_{35}\text{H}_{58}\text{Sn}_2$; C, 58.69; H, 8.16 % found C, 59.36; H, 8.11 %.

M.P. 45 – 47 °C.

6.4.15 Polymer 6 (P6)

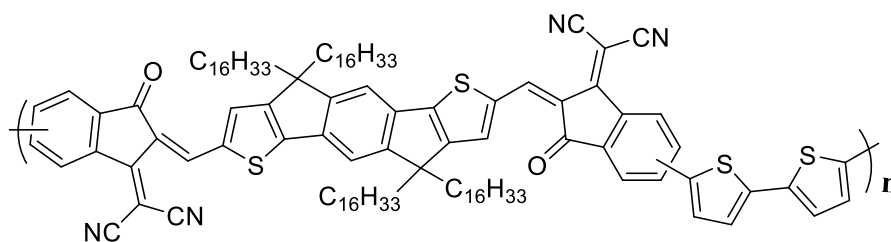


P6

IDIC-C16-Br (**M5**) (120.00 mg, 0.069 mmol), 4,7-bis(5-(trimethylstannyl)thien-2-yl)benzo[*c*][1,2,5] thiadiazole (40.00 mg, 0.069 mmol) (**M6**), tris(dibenzylideneacetone) dipalladium(0) (3.60 mg, 0.004 mmol) and tri-*o*-tolyl phosphine (4.80 mg, 0.016 mmol) were added in a two-neck flask and this was then degassed under argon. We added dry toluene (6 mL) to the mixture then the solution was degassed and stirred under heating to reflux at 110°C for 72 hours. We then cooled the reaction and chloroform (250 mL) added. Then 50 mL of ammonium hydroxide was added and we stirred the mixture overnight at room temperature. The two layers were then separated and the volume of the organic phase was concentrated to approximately 20 mL, then precipitated into 200 mL of methanol. The precipitate was filtered and a Soxhlet extraction with different solvents (methanol, acetone, hexane and chloroform) was undertaken. The solvent in the chloroform fraction was reduced to 20 mL then precipitated into 200 mL of methanol. Then the polymer was filtered and yielded as a blue powder (96.2 mg, 76 %).

GPC (chloroform fraction): $M_w = 12300 \text{ g mol}^{-1}$, $M_n = 7400 \text{ g mol}^{-1}$, PDI = 1.66; $^1\text{H NMR}$ (CDCl_3): ($\delta\text{H/ppm}$) 9.26 – 8.49 (br, 3H), 8.34 – 7.34 (br, 13H), 5.54 – 5.09 (m, 2H), 2.46 – 0.46 (m, 132H). Calculated elemental analysis (%): C, 77.04; H, 8.19; N, 4.49; S, 8.57. found: C, 76.79; H, 8.06; N, 4.24; S, 7.73.

6.4.16 Polymer 7 (P7)

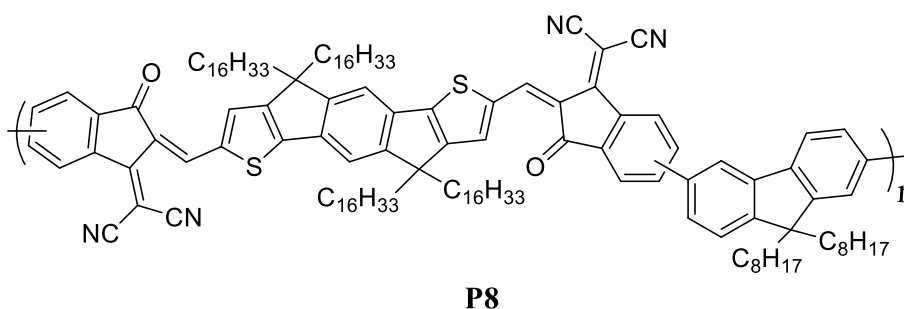


P7

IDIC-C16-Br (**M5**) (120.00 mg, 0.06941 mmol), 5,5'-bis(trimethyl stannyl)-2,2'-bithiophene (**M7**) (34.00 mg, 0.06941 mmol), tris(dibenzylideneacetone)dipalladium(0) (3.60 mg, 0.004 mmol) and tri-*o*-tolyl phosphine (4.80 mg, 0.016 mmol) were mixed in a two-neck round-bottom flask and then degassed under argon. We added dry toluene (6 mL) to the mixture and the system was degassed again under argon then heated at 110°C to reflux for 6 hours. We then cooled the reaction to room temperature and dissolved it in chloroform (250 mL). Then 50 mL of ammonium hydroxide was added and we stirred it overnight at room temperature. We separated the two layers using a separation funnel and the volume of the organic phase was reduced to approximately (20 mL) then precipitated into 200 mL of methanol. The precipitate was filtered, then subjected to a Soxhlet extraction with different organic solvents (methanol, acetone, hexane and chloroform). The chloroform fraction was reduced to 20 mL volume, then precipitated into 200 mL of methanol. The polymer was filtered using a membrane to afford the product as a purple powder (97.90 mg, 83 %).

GPC (chloroform fraction): $M_w = 35400 \text{ g mol}^{-1}$, $M_n = 12400 \text{ g mol}^{-1}$, PDI = 2.85; $^1\text{H NMR}$ (CDCl_3): ($\delta\text{H/ppm}$) 9.15 – 8.50 (d, $J = 0.29 \text{ Hz}$, 4H), 8.19 – 7.33 (m, 10H), 2.35 – 0.55 (m, 132H). Calculated elemental analysis (%): C, 78.84; H, 8.71; N, 3.23; S, 7.38. found: C, 78.10; H, 8.48; N, 3.19; S, 6.77.

6.4.17 Polymer 8 (P8)



IDIC-C16-Br (**M5**) (120 mg, 0.06941 mmol), 2,7-bis(trimethyltin)-9,9-dioctylfluorene (**M8**) (50 mg, 0.06941 mmol), tris(dibenzylideneacetone) dipalladium(0) (3.60 mg, 0.004 mmol) and tri-*o*-tolyl phosphine (4.80 mg, 0.016 mmol) were mixed together in two-neck flask and degassed under argon. We then added dry toluene (6 mL) and the mixture was degassed then heated to reflux for 24 hours. The reaction mixture was cooled to room temperature and chloroform (250 mL) added. 50 mL of ammonium hydroxide was then added and we stirred the mixture overnight at room temperature. The two layers were separated and the organic phase was reduced to approximately (20 mL) then precipitated into 200 mL of methanol. The precipitate was filtered and subjected to a Soxhlet extraction with different organic solvents (methanol, acetone, hexane and chloroform in succession). The chloroform fraction was concentrated then precipitated into methanol and finally filtered using a membrane to yield the polymer as a green solid (57.23, 43 %).

GPC (chloroform fraction): $M_w = 38700 \text{ g mol}^{-1}$, $M_n = 13000 \text{ g mol}^{-1}$, PDI = 2.97;

$^1\text{H NMR}$ (CDCl_3): ($\delta\text{H/ppm}$) 9.07 (d, $J = 0.1 \text{ Hz}$, 2H), 8.84 (s, 1H), 8.28 (s, 1H), 8.19-8.02 (m, 2H), 7.98-7.58 (m, 10H), 5.32 (s, 1H), 2.19-1.97 (br, 6H), 1.68-1.53 (br, 12H), 1.34-1.53 (br, 122H), 0.94-0.75 (m, 26H). Calculated elemental analysis (%): C, 82.68; H, 9.56; N, 2.86; S, 3.27. Found: C, 80.35; H, 8.99; N, 2.83; S, 3.15.

6.5 References

- (1) Zhang, D. M.; Tessier, C. A.; Youngs, W. J. Synthesis of tris(2,5-dialkynylthieno)cyclotriynes, tris(4,5-dialkoxyphenyl)cyclotriynes, and tetrakis(4,5-dialkoxyphenyl)cyclotetraynes with long-chain alkyl substituents, and the nickel and cobalt complexes of tris 4,5-(didodecyloxy)phenyl cyclotriyne. *Chemistry of Materials* **1999**, *11* (11), 3050.
- (2) Sessler, J. L.; Callaway, W. B.; Dudek, S. P.; Date, R. W.; Bruce, D. W. Synthesis and characterization of a discotic uranium-containing liquid crystal. *Inorganic Chemistry* **2004**, *43* (21), 6650.
- (3) Helgesen, M.; Gevorgyan, S. A.; Krebs, F. C.; Janssen, R. Substituted 2, 1, 3-benzothiadiazole-and thiophene-based polymers for solar cells– Introducing a new thermocleavable precursor. *Chemistry of Materials* **2009**, *21* (19), 4669.
- (4) Bouffard, J.; Swager, T. M. Fluorescent conjugated polymers that incorporate substituted 2,1,3-benzooxadiazole and 2,1,3-benzothiadiazole units. *Macromolecules* **2008**, *41* (15), 5559.
- (5) Zhen, S.; Lu, B.; Xu, J.; Zhang, S.; Li, Y. Poly (mono-, bi-or trifuran): effect of oligomer chain length on the electropolymerization performances and polymer properties. *RSC Advances* **2014**, *4* (27), 14001.
- (6) Zhou, E.; Yamakawa, S.; Zhang, Y.; Tajima, K.; Yang, C.; Hashimoto, K. Indolo [3, 2-b] carbazole-based alternating donor–acceptor copolymers: synthesis, properties and photovoltaic application. *Journal of Materials Chemistry* **2009**, *19* (41), 7730.
- (7) Güneş, A.; Cihaner, A.; Önal, A. Synthesis and electro-optical properties of new conjugated hybrid polymers based on furan and fluorene units. *Electrochimica Acta* **2013**, *89*, 339.
- (8) Wang, N.; Chen, Z.; Wei, W.; Jiang, Z. Fluorinated benzothiadiazole-based conjugated polymers for high-performance polymer solar cells without any processing additives or post-treatments. *Journal of the American Chemical Society* **2013**, *135* (45), 17060.
- (9) Uddin, M. A.; Lee, T. H.; Xu, S.; Park, S. Y.; Kim, T.; Song, S.; Nguyen, T. L.; Ko, S.-j.; Hwang, S.; Kim, J. Interplay of intramolecular noncovalent coulomb interactions for semicrystalline photovoltaic polymers. *Chemistry of Materials* **2015**, *27* (17), 5997.

- (10) Liu, J.; Li, K.; Liu, B. Far-red/near-infrared conjugated polymer nanoparticles for long-term in situ monitoring of liver tumor growth. *Advanced Science* **2015**, *2* (5), 1500008.
- (11) Zhang, W.; Smith, J.; Watkins, S. E.; Gysel, R.; McGehee, M.; Salleo, A.; Kirkpatrick, J.; Ashraf, S.; Anthopoulos, T.; Heeney, M. Indacenodithiophene semiconducting polymers for high-performance, air-stable transistors. *Journal of the American Chemical Society* **2010**, *132* (33), 11437.
- (12) Guo, Y.; Li, Y.; Awartani, O.; Han, H.; Zhao, J.; Ade, H.; Yan, H.; Zhao, D. Improved Performance of All-Polymer Solar Cells Enabled by Naphthodiperylenetetraimide-Based Polymer Acceptor. *Advanced Materials* **2017**, *29* (26), 1700309.
- (13) Li, Y.; Tatum, W. K.; Onorato, J. W.; Barajas, S. D.; Yang, Y. Y.; Luscombe, C. An indacenodithiophene-based semiconducting polymer with high ductility for stretchable organic electronics. *Polymer Chemistry* **2017**, *8* (34), 5185.
- (14) Chen, W.; Zhang, Q. Recent progress in non-fullerene small molecule acceptors in organic solar cells (OSCs). *Journal of Materials Chemistry C* **2017**, *5* (6), 1275.
- (15) Wilbuer, J.; Schnakenburg, G.; Esser, B. Syntheses, Structures and Optoelectronic Properties of Spiroconjugated Cyclic Ketones. *European Journal of Organic Chemistry* **2016**, *2016* (14), 2404.
- (16) Cui, Y.; Ren, H.; Yu, J.; Wang, Z.; Qian, G. An indanone-based alkoxy silane dye with second order nonlinear optical properties. *Dyes and Pigments* **2009**, *81* (1), 53.
- (17) Zhang, Z. G.; Yang, Y.; Yao, J.; Xue, L.; Chen, S.; Li, X.; Morrison, W.; Yang, C.; Li, Y. Constructing a Strongly Absorbing Low-Bandgap Polymer Acceptor for High-Performance All-Polymer Solar Cells. *Angewandte Chemie International Edition* **2017**, *56* (43), 13503.
- (18) Hacioglu, S. O.; Ataoglu, E.; Hizalan, G.; Depci, T.; Cirpan, A.; Toppare, L. J. P., Sulfur, Silicon, Elements, t. R. Thiadiazoloquinoline and benzodithiophene bearing polymers for electrochromic and organic photovoltaic applications. *Phosphorus, Sulfur, and Silicon and the Related Elements* **2019**, *1*.
- (19) Giannopoulos, P.; Raptis, D.; Theodosiou, K.; Andreopoulou, A. K.; Anastasopoulos, C.; Dokouzis, A.; Leftheriotis, G.; Lianos, P.; Kallitsis, J. Organic dyes end-capped with perfluorophenyl anchors: Synthesis, electrochemical properties and assessment of sensitization capacity of titania photoanodes. *Dyes and Pigments* **2018**, *148*, 167.

- (20) Fu, B.; Baltazar, J.; Hu, Z.; Chien, A.-T.; Kumar, S.; Henderson, C. L.; Collard, D. M.; Reichmanis, E. High charge carrier mobility, low band gap donor–acceptor benzothiadiazole-oligothiophene based polymeric semiconductors. *Chemistry of Materials* **2012**, *24* (21), 4123.